NOTE TO USERS

Dynamic instability analysis of tapered composite plates using Ritz and finite element methods

Weiguang Liu

A Thesis

in

The Department

of

Mechanical and Industrial Engineering

Presented in Partial Fulfillment of the Requirements

for the Degree of Master of Applied Science at

Concordia University

Montreal, Quebec, Canada

July 2005

Your file Votre référence
ISBN: 0-494-10266-7
Our file Notre référence
ISBN: 0-494-10266-7

ABSTRACT

Dynamic instability analysis of tapered composite plates using Ritz and finite element methods

Weiguang Liu

Tapered composite plates are widely used in civil, mechanical and aerospace structures such as robot arms, wing structures, helicopter yoke and turbine blade where the plate structure needs to be stiff at one location and flexible at another location. By terminating some plies at discrete locations, different types of ply drop-off can be obtained depending on the application. In the present work, the instability of tapered laminates under dynamic loading conditions is considered. Because of the complicated mechanical behavior of the tapered composite plate and the complexity of the analysis, no exact solution is available at present and therefore, Ritz method and finite element method have been used for the calculation of the dynamic instability regions. Solutions based on classical laminated plate theory have been developed first for vibration and buckling of uniform and tapered composite plates without in-plane forces. The effects on the laminate stiffness of the composite plates caused by the taper angle have been considered. Different configurations of tapered plates have been investigated. Then, based on the formulations for free vibration and buckling, the formulation for the dynamic instability analysis has been developed using Finite Element Method and Ritz method for both uniform-thickness and tapered composite plates based on classical

laminated plate theory. The efficiency and accuracy of the developed formulation are established in comparison with available solutions for uniform-thickness laminates. The dynamic instability regions that serve as a measure of the degree of instability of the laminates are determined considering different boundary conditions, the tapered composite plate configurations, and the in-plane loading patterns. The NCT301 graphite-epoxy composite material is considered in the numerical study.

ACKNOWLEDGMENTS

I would like to express my sincere thanks to my supervisor, Dr.Rajamohan Ganesan, whose expertise, understanding, and patience, added considerably to my graduate experience in Concordia University. I appreciate his vast knowledge and skill in his research areas, and his assistance in writing this thesis, which made me improve greatly in my research ability.

Here, I would also like to express my heartfelt appreciation to my wife Chunyan Miao. Without her support and encouragement, this work would not have been possible.

TABLE OF CONTENTS

List of Figures

List of Tables

Nomenclature

α	Taper angle of the tapered beam
θ	Orientation angle of ply
ε_{ij}	Strain corresponding to coordinate system x y z
σ_{ij}	Stress corresponding to coordinate system x y z
S_{ij}	Coefficient of compliance matrix
C_{ij}	Coefficient of stiffness matrix
$\varepsilon_{ij}^{'}$	Strain corresponding to coordinate system $x'y'z'$
$\sigma_{ij}^{'}$	Stress corresponding to coordinate system $x'y'z'$
$\{\varepsilon\}_{123}$	Strain vector corresponding to coordinate system x y z
$\{\sigma\}_{123}$	Stress vector corresponding to coordinate system x y z
$[T]_{\sigma}$	Stress transformation matrix
$[T]_{\varepsilon}$	Strain transformation matrix
$[\ ]^{-1}$	Inverse of the matrix
$[\ ]^{T}$	Transverse of the matrix
S_{ij}'	Coefficient of the transformed ply compliance matrix
C_{ij}'	Coefficient of the transformed ply stiffness matrix
Q_{ij}'	Coefficient of the reduced ply stiffness matrix
$[A]$	Extensional stiffness matrix

$[B]$ Coupling stiffness matrix

$[D]$ Bending stiffness matrix

A_{ij} Coefficients of stretching stiffness matrix of composite plate

B_{ij} Coefficients of bending-stretching coupling matrix of composite plate

D_{ij} Coefficients of bending stiffness matrix of composite plate

w Displacement in z direction

w_x Slope in the x direction

w_y Slope in the y direction

a Length of the plate

b Width of the plate

h Height of the plate

ρ Density

ρ_r Density of the resin

E_1 Modulus of elasticity in fiber direction

E_2 Modulus of elasticity in transverse direction

ν_{21} Poisson ratio of ply

G_{23} Out-of-plane shear modulus

G_{12} In-plane shear modulus

E Modulus of elasticity of resin

ν Poisson ratio of resin

G Shear modulus of resin

u Displacement in x direction

v Displacement in y direction

z_k Coordinate of the top surface of the k^{th} layer of composite plate

U Strain energy

T Kinetic energy

t Time variable

ω Natural frequency

$\{P\}$ Vector of the nodal forces of the structural system

$\{Q\}$ Vector of the nodal displacements of the structural system

$[K]$ Stiffness matrix of the structural system

$[M]$ Mass matrix of the structural system

W Potential energy

$[N]$ Incremental stiffness matrix of the structural system

N_{xb} Buckling force

N_{cr} Critical buckling load

α_0 Static parameter

α_1 Dynamic parameter

θ Parametric resonance frequency

$\theta/2\omega$ Parameter ratio

F_x In-plane dynamic buckling loading

Chapter 1

Introduction, Literature Survey and Scope of the Thesis

1.1 Dynamic instability and vibration analysis in mechanical design

Periodic dynamic loading may cause dynamic instability of a structure through parametric vibration. The plate structures consisting of individual rectangular component plates are rigidly connected together at their edges to form structures of arbitrary cross-section and frequently subjected to in-plane stress systems. When the stress system is time-dependent, the dynamic instability of the plate structure must be considered in the design process.

The vibrations may not threaten the structure or its normal operation, but they can bring about fatigue failure if they continue to act. If the in-plane stress system makes the mechanical structure work in the dynamic instability regions, the mechanical component will reach the state of parametric resonance. The resonance will decrease the life time of the structure and causes unpredictable failures. Therefore, the study of the formation of parametric vibrations and the method for the prevention of their occurrence are necessary in the various areas of mechanical design.

In the case of a free vibration, during vibration, there are no externally applied forces, but an external force may have caused an initial displacement or velocity in the system. After the external force is removed, the body will continue to vibrate because of the action of elasticity and mass. Undamped natural frequency is a frequency of the structural system when it undergoes a free vibration without friction. Similarly, if the frequency of exciting force gets close to the frequency band of the natural frequencies of the structure, the mechanical component will reach severe vibration due to resonance. The resonance will also decrease the life time of the structure and causes unpredictable failures. Therefore, vibration analysis in mechanical design is as important and necessary in the various areas of mechanical design as that of dynamic instability analysis.

1.2 Buckling analysis in mechanical design

A simple way to describe the buckling phenomenon is to use an example of a plate subjected to uniformly distributed compressive in-plane forces around the edges. Under such forces, the plate will be slightly shortened but remain straight with no bending. If a small out-of-plane load is applied, the plate will be bent infinitesimally but will return to its original straight form when the small in-plane load disappears. If the uniformly distributed compressive in-plane forces are gradually increased, a condition will be reached in which small in-plane loads will cause a deflection which remains when the in-plane loads disappear. Such an unstable phenomenon is called buckling and the critical

forces are called buckling loads. Buckling usually occurs when the compressive stresses are well below the material stress limit.

Buckling can happen to structures in many forms, such as columns, truss members, components of thin-walled beams and plate girders, walls, arches and shell roofs. In aerospace structures, minimum-weight design is an important criterion so that the structures are made of skins and thin members. The instability due to buckling can lead to a catastrophic failure of a structure and it must be considered when one designs a mechanical structure.

1.3 Composite materials and structures

The increased use of composites in aerospace, land, and marine applications has resulted in ever-growing research in the design of structures made of fiber-reinforced composite materials. The composite materials refer to materials created by synthetic assembly of two or more organic or inorganic materials, such that the specific characteristics and properties such as high strength, high stiffness, high modulus and low weight can be obtained. In many mechanical structures, composite materials took the place of previously used aluminum alloys and other metallic materials, and they also achieved quite good mechanical properties with low specific weight. Furthermore, fiber composite materials provide the unique opportunity to simultaneously optimize structure configuration, material make-up, fabrication process and structural integrity.

Fiber reinforced composite materials are the engineering materials which are most commonly used in modern industries and composite plate is one of the most widely used structural elements. They are made by stacking together many plies of fiber-reinforced layers in different orientations to achieve the desired properties. In fibrous composite materials, the fibers provide virtually all strength and stiffness. The purpose of the matrix is to bind the reinforcements together and keep them in proper orientation, transfer and distribute the load to and between them. These stacked layers are permanently bonded together under heat and pressure using a hot press or autoclave. Some specific applications of composite plates need to be stiff at one end and flexible at the other end. Such plates can be made by dropping off some plies at discrete locations to reduce the stiffness of the plates. This results in a tapered shape, which is to be discussed in this thesis work.

1.4 Finite element method

As one of the powerful numerical methods for solving the mathematical problems of engineering, the finite element method has been increasingly used in many engineering areas with the rapid development of computers. Its application ranges from static analysis of a simple component to a complicated fluid flowing system. Most importantly, the finite element method has now become a predominant structural analysis and design tool which is used routinely by structural engineers.

For analysis of complex structures such as tapered composite plates, the finite

element method is one of the efficient and powerful tools. The speed of convergence and accuracy of the results obtained by finite element method are strongly dependent on the element types which are chosen for the analysis. In conventional finite element method, a plate element is modeled using four nodes where each node has three degrees of freedom. In conventional finite element method, the plates should be divided into a large number of elements to achieve an accurate result. With the rapid development of computers, it is not difficult for dividing a large number of elements of the plate to obtain an acceptable accuracy. In this thesis work, the finite element method is used to analyze deflection, vibration, buckling and instability of the plates.

1.5 Literature survey

In this section, a comprehensive literature survey is presented on the instability and vibration of composite plates, and on the application of the finite element method to composite plates. Important works done on the dynamic instability and vibration analysis of uniform and thickness-tapered composite plates by finite element methodologies have been chronicled. The majority of works done on the dynamic instability analysis of plates are limited to homogeneous material and uniform composite plates. The works on the dynamic instability analysis of composite plates are presented, though the quantity of such works is of course very limited.

1.5.1 Dynamic instability analysis of composite plates

A number of researchers have investigated the dynamic instability of isotropic thin plates due to periodic in-plane stress systems. A comprehensive study of dynamic instability problems has been given in the text of Bolotin [1] for elastic systems, such as rods, plates and shells, under periodically varying loads. The dynamic instability of rectangular plates has been studied by Hutt and Salam [2] using the finite element method (FEM) and by Krajcinovic and Herrmann [3] using an integral equation technique. Duffield and Willems [4] have studied the behavior of stiffened rectangular plates. The dynamic stability of skew stiffened plates has been investigated by Merritt and Willems [5] and of annular plates by Tani and Nakamura [6].

The increasing application of fiber-reinforced composite laminated materials to primary components in advanced structures such as spacecraft, high speed aircraft, naval vessels and other transportation vehicles has stimulated a renewed interest in problems involving dynamic instability. Birman [7] has considered unsymmetrically laminated cross-ply rectangular plates under a harmonically varying biaxial stress system. In this work damping is neglected and the four edges are assumed to be simple supported so that the problem is governed by a set of uncoupled Mathieu equations. The principal dynamic instability region (DIR) is determined analytically. Srinivasan and Chellapandi [8] have analyzed thin laminated plates under harmonically varying biaxial stress systems by using the semi-analytical finite strip method. Damping is again neglected and the four edges are assumed to be clamped. A set of coupled Mathieu equations is obtained and Hill's method of infinite determinants is applied to determine the DIRs. The above-mentioned studies [2-8] are based in the context of the use of classical laminated plate

theory (CLPT). When considering composite laminated plates, however, it is well known that through-thickness shearing effect can be significant in some cases and hence that it is desirable to base the analysis on the use of a shear deformation plate theory (SDPT) rather than on the use of the CLPT. Bert and Birman [9] have used the first-order SDPT in an analysis of the dynamic instability of anti-symmetric angle-ply laminates in which both the through-thickness shear effect and rotary inertia are included. Damping is neglected and the four edges are assumed to be simple supported with no in-plane displacements perpendicular to the edge and no tangential stress. As with the earlier work of Birman [7], this allows for a closed-form solution and leads to uncoupled Mathieu equations. For a uniaxial stress system, the principle DIRs are determined and the effects of the aspect ratio, thickness-to-length ratio, numbers of layers, and magnitudes of the shear correction factors are studied. Chen and Yang [10] have also used the first-order SDPT to study the dynamic instability of anti-symmetric angle-ply plates using the Galerkin FEM. The plates are assumed to be subjected to the combination of a periodic bending stress and a periodic uniaxial in-plane stress system. Damping is not included and the effects of various parameters and boundary conditions on the DIR are studied. Moorthy [11] have carried out a similar investigation using the FEM based on the first-order SDPT. In this study, both symmetric cross-ply laminates and anti-symmetric angle-ply laminates are considered. Damping is included and the dynamic load is a uniaxial in-plane stress system. Two methods are used to determine the DIRs, namely Hill's method of infinite determinants and an analytical method, and mainly the principal DIRs are considered. The effects of damping, thickness-to-length ratio, anisotropy, boundary conditions, number of layers and lamination angles are investigated. Aditi and Adrian

[12] have analyzed the instability of isotropic and cross-ply composite plates using FEM based on CLPT, first-order SDPT and the higher order theory (HOT). Damping is neglected in this study. The DIRs are determined with periodic in-plane stress system under the boundary conditions of one of the short edges fixed and both the short edges fixed. Wang and Dawe [13] have determined the DIRs of composite laminated rectangular plates and prismatic plate structures using B-spline finite strip method.

Although a limited amount of work has been conducted on analyzing the dynamic instability of some categories of plates, it appears that no studies are available in the open literature on the dynamic instability of tapered composite plates subjected to combined in-plane stress systems. The present thesis focuses on the topic by describing the development of a reliable, efficient, accurate and versatile procedure for predicting DIRs of rectangular tapered composite plates.

1.5.2 Vibration and buckling analysis of composite structures

Vibration analysis of composite laminates has been done by some researchers. At the same time, the works on vibration analysis of composite plates or shells have concentrated on uniform laminates. Study on the vibration analysis of tapered laminated plates has been scarce in spite of their applicability in important mechanical structures.

Nigam [14] used hierarchical finite element method to investigate the static and dynamic response of uniform and tapered laminated composite beams. Zabihollah [15] extended Nigam's work to tapered composite beams based on a higher-order finite

element. He presented the vibration and buckling analysis of uniform and tapered composite beams using conventional and advanced finite element method based on the classical laminate theory and the first-order shear deformation theory. Chen [16] studied the vibration of uniform and tapered beams with and without axial force using hierarchical finite element method.

Reddy [17] used virtual work principles, and variational methods to study the static and dynamic response of laminated composite plates based on the classical and first-order shear deformation theories of laminated plates. Whitney [18] derived the foundation in the theory of uniform laminated anisotropic plates and beams, including the problems of bending under transverse load, stability, and free-vibration. Noor [19] studied the free vibration of simply supported symmetric laminated plate based on classical laminate theory, which neglects the effects of the rotary inertia and shearing deformation. Reddy and Khdeir [20] dealt with the free vibration behavior of cross-ply composite laminates under various boundary conditions considering the shear deformation laminate theory.

Khdeir and Reddy [21] used various plate theories to study the buckling of laminated plates, and different boundary conditions are considered. Bertholet [22], in his text book, has used classical method and Ritz method to analyze the vibration and buckling of laminate and sandwich beams and plates. Kollar and Springer [23] also studied more details about vibration and buckling analysis of composite laminated plates. But no researcher has investigated tapered composite plates.

1.5.3 The finite element analysis

The finite element method is an efficient tool for the analysis of mechanical structures. The standard finite element method is to divide the domain of interest into a number of smaller sub-domains called Finite Elements. The solution is then approximated by locally admissible polynomial functions. Various procedures have been developed to obtain more accuracy and rapid convergence of solutions. The most common procedure is to increase the number of elements while keeping the degrees of freedom of each element fixed.

Research works have been carried out using conventional FEM to study the vibration of beams and plates. Reddy [24], Zienkiewicz [25] and Cook [26] investigated the vibration of beams and plates made of conventional materials. In refs. [27,28,29], similar works have been applied on the dynamic analysis of Timoshenko beams. Also, some researchers extended their study to tapered beams. Thomas and Dokumaci [30] treated the dynamic analysis of tapered beams by using an internal node element considering the total deflection and bending slope as the co-ordinates at the two terminal nodes and two internal nodes giving eight degrees of freedom to the element. Thomas and Abbas [31] used four degrees of freedom per node and two nodes at the ends to obtain stiffness and mass matrices for tapered beams based on the Euler-Bernoulli beam element. In this kind of model, the deflection, rotation, curvature and gradient of curvature are considered as degrees of freedom. Cleghorn and Tabarrok [32] presented a

finite element model for free vibration of lineary-tapered Timoshenko beams.

Some research works have been carried out on the dynamic analysis of composite beams or plates using conventional FEM. Shi *et al* [33] considered a finite element model for higher order plate theories for the vibration analysis of composite beams and plates. Ramtekkar *et al* [34] presented a mixed finite element formulation to calculate the natural frequencies of laminated beams. Rao and Ganesan [35] studied the natural frequencies of tapered composite beams considering the shear deformation. However there are only few research works on the finite element dynamic analysis of tapered composite plate configurations.

1.6 Objectives of the thesis

The objectives of the present thesis are, (1) to derive the formulations for the mechanical behavior of tapered laminated plates considering the effect on the stiffness of plies caused by the taper angle; (2) to analyze the tapered composite plates for free vibration and buckling using the finite element method based on the Classical Laminated Plate Theory (CLPT) and Ritz method; and, (3) to conduct a detailed instability analysis of tapered composite plates with dynamic in-plate forces.

The formulations using Ritz method and the finite element method are developed. The formulations are analyzed for their performance in the vibration and buckling analyses of uniform and tapered composite plates. These formulations are then used to

analyze for the instability regions of tapered composite plates subjected to dynamic in-plane forces. A detailed parametric study on the instability of tapered composite plates is conducted.

1.7 Layout of the thesis

The present chapter provided a brief introduction and literature survey on the finite element method and the instability analysis of uniform and tapered composite plates.

Chapter 2 provides the formulation of off-axis behavior of an arbitrary oblique ply in a tapered composite plate. Then the formulations of elastic behavior of different tapered composite configurations are developed considering the effect on the stiffness of plies due to the taper angle.

In Chapter 3, formulations based on Ritz method and the finite element method are developed and applied to the deflection analysis of tapered composite plate configurations based on the classical laminated plate theory. The effect on the stiffness of plies due to the taper angle is considered. Then a detailed comparison is made between the Ritz solutions and the finite element solutions.

In Chapter 4, the vibration analysis of uniform and tapered composite plates is developed by using finite element method and Ritz method. Then a detailed comparison is made between the solutions obtained using Ritz method and the finite element

formulation for the tapered composite plate configurations. For the uniform composite plate, the results are compared with the results given in ref. [12].

In Chapter 5, the buckling analysis of uniform and tapered composite plates is developed by using finite element method and Ritz method. Then a detailed comparison is made between the solutions obtained using Ritz method and the finite element formulation for the tapered composite plate configurations. For the uniform composite plate, the results are compared with the results given in ref. [12].

In Chapter 6, the instability analysis of uniform and tapered composite plates is developed by using both the finite element method and Ritz method. Comparisons are made between the solutions obtained using Ritz method and the finite element formulation for the tapered composite plate configurations. For the uniform composite plate, the instability region results are compared with the results given in ref. [12]. A parametric study on the dynamic instability of tapered laminates is presented.

Chapter 7 brings the thesis to its end by providing an overall conclusion of the present work and some recommendations for future work.

Chapter 2

Mechanical Behavior of Tapered Laminated Plates

2.1 Introduction

Laminated plates are extensively used in aerospace, mechanical, and automotive structures, where saving in weight without reduction in strength is of paramount importance. The tapered composite laminated plates are used in many structures, such as turbine blades, wing structures, helicopter blades, and robot arms. To investigate and analyze the static and dynamic performance, we must study the mechanical behavior of the tapered laminated plates first. Since most laminated composite plates are composed of a number of layers, it is possible to construct variable thickness composite structures and adjust the taper angle to achieve the desired performance of the structures. In this chapter, the mechanical behavior of tapered laminated plates is considered and the effect of taper angle is determined.

2.2 Stiffness and Compliance Matrices

The stiffness constants C_{ij} or the compliance constants S_{ij} can be used to

describe the elastic behavior of the composite materials. According to Hooke's law, these matrices for a material can be written based on the linear elasticity relations as in the following equations [22]:

$$\begin{Bmatrix} \varepsilon_{11} \\ \varepsilon_{22} \\ \varepsilon_{33} \\ \gamma_{23} \\ \gamma_{13} \\ \gamma_{12} \end{Bmatrix} = \begin{bmatrix} S_{11} & S_{12} & S_{13} & S_{14} & S_{15} & S_{16} \\ S_{12} & S_{22} & S_{23} & S_{24} & S_{25} & S_{26} \\ S_{13} & S_{23} & S_{33} & S_{34} & S_{35} & S_{36} \\ S_{14} & S_{24} & S_{34} & S_{44} & S_{45} & S_{46} \\ S_{15} & S_{25} & S_{35} & S_{45} & S_{55} & S_{56} \\ S_{16} & S_{26} & S_{36} & S_{46} & S_{56} & S_{66} \end{bmatrix} \cdot \begin{Bmatrix} \sigma_{11} \\ \sigma_{22} \\ \sigma_{33} \\ \tau_{23} \\ \tau_{13} \\ \tau_{12} \end{Bmatrix} \tag{2.1}$$

where, ε_{ij} and σ_{ij} are the strain and stress components in the material coordinate system (1, 2, 3). S_{ij} is the corresponding compliance coefficient. We can also write the equation in a condensed form:

$$\{\varepsilon\}_{123} = [S]_{123}\{\sigma\}_{123} \tag{2.2}$$

The stresses are given by

$$\begin{Bmatrix} \sigma_{11} \\ \sigma_{22} \\ \sigma_{33} \\ \tau_{23} \\ \tau_{13} \\ \tau_{12} \end{Bmatrix} = \begin{bmatrix} C_{11} & C_{12} & C_{13} & C_{14} & C_{15} & C_{16} \\ C_{12} & C_{22} & C_{23} & C_{24} & C_{25} & C_{26} \\ C_{13} & C_{23} & C_{33} & C_{34} & C_{35} & C_{36} \\ C_{14} & C_{24} & C_{34} & C_{44} & C_{45} & C_{46} \\ C_{15} & C_{25} & C_{35} & C_{45} & C_{55} & C_{56} \\ C_{16} & C_{26} & C_{36} & C_{46} & C_{56} & C_{66} \end{bmatrix} \cdot \begin{Bmatrix} \varepsilon_{11} \\ \varepsilon_{22} \\ \varepsilon_{33} \\ \gamma_{23} \\ \gamma_{13} \\ \gamma_{12} \end{Bmatrix} \tag{2.3}$$

where, C_{ij} is the corresponding stiffness coefficient. This equation can also be written in a condensed form:

$$\{\sigma\}_{123} = [C]_{123}\{\varepsilon\}_{123} \tag{2.4}$$

where,

$$[C]_{123} = \begin{bmatrix} C_{11} & C_{12} & C_{13} & C_{14} & C_{15} & C_{16} \\ C_{12} & C_{22} & C_{23} & C_{24} & C_{25} & C_{26} \\ C_{13} & C_{23} & C_{33} & C_{34} & C_{35} & C_{36} \\ C_{14} & C_{24} & C_{34} & C_{44} & C_{45} & C_{46} \\ C_{15} & C_{25} & C_{35} & C_{45} & C_{55} & C_{56} \\ C_{16} & C_{26} & C_{36} & C_{46} & C_{56} & C_{66} \end{bmatrix} \tag{2.5}$$

The matrix $[C]_{123}$ is called as the stiffness matrix.

Further

$$[S]_{123} = \begin{bmatrix} S_{11} & S_{12} & S_{13} & S_{14} & S_{15} & S_{16} \\ S_{12} & S_{22} & S_{23} & S_{24} & S_{25} & S_{26} \\ S_{13} & S_{23} & S_{33} & S_{34} & S_{35} & S_{36} \\ S_{14} & S_{24} & S_{34} & S_{44} & S_{45} & S_{46} \\ S_{15} & S_{25} & S_{35} & S_{45} & S_{55} & S_{56} \\ S_{16} & S_{26} & S_{36} & S_{46} & S_{56} & S_{66} \end{bmatrix} \tag{2.6}$$

The matrix $[S]_{123}$ is called as the compliance matrix.

The relation between stiffness matrix and compliance matrix is expressed as:

$$[S]_{123} = [C]_{123}^{-1} \tag{2.7}$$

The elastic behavior of an orthotropic composite material can be described by introducing either the stiffness constants C_{ij} or the compliance constants S_{ij}. By taking into account the fact that the value of some stiffness and compliance coefficients is zero for orthotropic ply, Hooke's law is written in the matrix form:

$$\begin{Bmatrix} \sigma_{11} \\ \sigma_{22} \\ \sigma_{33} \\ \tau_{23} \\ \tau_{13} \\ \tau_{12} \end{Bmatrix} = \begin{bmatrix} C_{11} & C_{12} & C_{13} & 0 & 0 & 0 \\ C_{12} & C_{22} & C_{23} & 0 & 0 & 0 \\ C_{13} & C_{23} & C_{33} & 0 & 0 & 0 \\ 0 & 0 & 0 & C_{44} & 0 & 0 \\ 0 & 0 & 0 & 0 & C_{55} & 0 \\ 0 & 0 & 0 & 0 & 0 & C_{66} \end{bmatrix} \cdot \begin{Bmatrix} \varepsilon_{11} \\ \varepsilon_{22} \\ \varepsilon_{33} \\ \gamma_{23} \\ \gamma_{13} \\ \gamma_{12} \end{Bmatrix} \tag{2.8}$$

The elastic behavior of the orthotropic composite material can be characterized by two groups of nine independent coefficients respectively.

2.3 Off-Axis Behavior of Composite Materials

The linear elastic relation can be written as the equations (2.1) and (2.3). At the same time, the elastic behavior of a unidirectional composite material can be described by introducing either the stiffness constants C_{ij} or the compliance constants S_{ij}, the

equations can be obtained as the equations (2.8) and (2.9). The principal directions of the composite materials are written in the coordinate system (1, 2, 3) as in the following Figure 2.1. The transformation equations are used to obtain the stiffness matrix $[C]$ and compliance matrix $[S]$, written in the coordinate system (x', y', z'). There is a rotation of angle θ between coordinate system (1,2,3) and coordinate system (x', y', z') in the plane $1O2$ and $x'Oy'$.

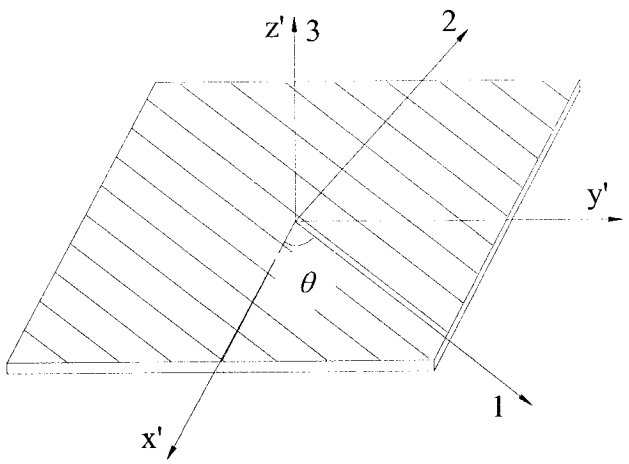

Figure 2.1 The principal directions (1, 2, 3) and the reference system (x', y', z')

The principle directions of a lamina are set in the system (1,2,3), and the reference system (1',2',3) is equivalent to system (x', y', z') of the laminate. According to the reference system, we can get the stiffness matrix $[C]_{x'y'z'}$ and the compliance matrix $[S]_{x'y'z'}$ respectively:

$$\{\sigma\}_{x'y'z'} = [C]_{x'y'z'} \cdot \{\varepsilon\}_{x'y'z'} \tag{2.10}$$

$$[T]_{\sigma} \cdot \{\sigma\}_{123} = [C]_{x'y'z'} \cdot [T]_{\varepsilon} \cdot \{\varepsilon\}_{123} \tag{2.11}$$

$$\{\sigma\}_{123} = [T]_{\sigma}^{-1} \cdot [C]_{x'y'z'} \cdot [T]_{\varepsilon} \cdot \{\varepsilon\}_{123} \tag{2.12}$$

$$[C]_{123} = [T]_{\sigma}^{-1} \cdot [C]_{x'y'z'} \cdot [T]_{\varepsilon} \tag{2.13}$$

$$[C]_{x'y'z'} = [T]_{\sigma} \cdot [C]_{123} \cdot [T]_{\varepsilon}^{-1} \tag{2.14}$$

$$\{\varepsilon\}_{x'y'z'} = [S]_{x'y'z'} \cdot \{\sigma\}_{x'y'z'} \tag{2.15}$$

$$\{\varepsilon\}_{123} = [S]_{123} \cdot \{\sigma\}_{123} \tag{2.16}$$

$$[T]_{\varepsilon} \cdot \{\varepsilon\}_{123} = [S]_{x'y'z'} \cdot [T]_{\sigma} \cdot \{\sigma\}_{123} \tag{2.17}$$

$$[S]_{123} = [T]_{\varepsilon}^{-1} \cdot [S]_{x'y'z'} \cdot [T]_{\sigma} \tag{2.18}$$

$$[S]_{x'y'z'} = [T]_{\varepsilon} \cdot [S]_{123} \cdot [T]_{\sigma}^{-1} \tag{2.19}$$

Matrices $[T]_{\sigma}$ and $[T]_{\varepsilon}$ are the transformation matrix for stresses and the transformation matrix for strains respectively, and they have the form as follow:

$$[T]_{\sigma} = \begin{bmatrix} l_1^2 & l_2^2 & l_3^2 & 2 \cdot l_2 \cdot l_3 & 2 \cdot l_1 \cdot l_3 & 2 \cdot l_1 l_2 \\ m_1^2 & m_2^2 & m_3^2 & 2 \cdot m_2 \cdot m_3 & 2 \cdot m_1 \cdot m_3 & 2 \cdot m_1 \cdot m_2 \\ n_1^2 & n_2^2 & n_3^2 & 2 \cdot n_2 \cdot n_3 & 2 \cdot n_1 \cdot n_3 & 2 \cdot n_1 \cdot n_2 \\ m_1 \cdot n_1 & m_2 \cdot n_2 & m_3 \cdot n_3 & m_3 \cdot n_2 + m_2 \cdot n_3 & m_3 \cdot n_1 + m_1 \cdot n_3 & m_2 \cdot n_1 + m_1 \cdot n_2 \\ l_1 \cdot n_1 & l_2 \cdot n_2 & l_3 \cdot n_3 & l_3 \cdot n_2 + l_2 \cdot n_3 & l_3 \cdot n_1 + l_1 \cdot n_3 & l_2 \cdot n_1 + l_1 \cdot n_2 \\ l_1 \cdot m_1 & l_2 \cdot m_2 & l_3 \cdot m_3 & l_3 \cdot m_2 + l_2 \cdot m_3 & l_3 \cdot m_1 + l_1 \cdot m_3 & l_2 \cdot m_1 + l_1 \cdot m_2 \end{bmatrix} \tag{2.20}$$

$$[T]_{\varepsilon} = \begin{bmatrix} l_1^2 & l_2^2 & l_3^2 & l_2 \cdot l_3 & l_1 \cdot l_3 & l_1 l_2 \\ m_1^2 & m_2^2 & m_3^2 & m_2 \cdot m_3 & m_1 \cdot m_3 & m_1 \cdot m_2 \\ n_1^2 & n_2^2 & n_3^2 & n_2 \cdot n_3 & n_1 \cdot n_3 & n_1 \cdot n_2 \\ 2 \cdot m_1 \cdot n_1 & 2 \cdot m_2 \cdot n_2 & 2 \cdot m_3 \cdot n_3 & m_3 \cdot n_2 + m_2 \cdot n_3 & m_3 \cdot n_1 + m_1 \cdot n_3 & m_2 \cdot n_1 + m_1 \cdot n_2 \\ 2 \cdot l_1 \cdot n_1 & 2 \cdot l_2 \cdot n_2 & 2 \cdot l_3 \cdot n_3 & l_3 \cdot n_2 + l_2 \cdot n_3 & l_3 \cdot n_1 + l_1 \cdot n_3 & l_2 \cdot n_1 + l_1 \cdot n_2 \\ 2 \cdot l_1 \cdot m_1 & 2 \cdot l_2 \cdot m_2 & 2 \cdot l_3 \cdot m_3 & l_3 \cdot m_2 + l_2 \cdot m_3 & l_3 \cdot m_1 + l_1 \cdot m_3 & l_2 \cdot m_1 + l_1 \cdot m_2 \end{bmatrix}$$

(2.21)

where l_i, m_i, and n_i are the direction cosines relating the coordinate systems (1, 2, 3) and (x', y', z'). The direction cosines are expressed as follows:

Table 2.1: Direction cosines relating coordinate systems (1, 2, 3) and(x', y', z')

	1	2	3
x'	$l_1 = \cos\alpha_1$	$l_2 = \cos\alpha_2$	$l_3 = \cos\alpha_3$
y'	$m_1 = \cos\beta_1$	$m_2 = \cos\beta_2$	$m_3 = \cos\beta_3$
z'	$n_1 = \cos\gamma_1$	$n_2 = \cos\gamma_2$	$n_3 = \cos\gamma_3$

As it can be seen from Figure 2.1, there is a rotation of angle θ between coordinate system (1,2,3) and coordinate system (x', y', z') in the plane $1O2$ and $x'Oy'$. Therefore, we can see that :

$\alpha_1 = \theta$, $\alpha_2 = 90^0 - \theta$, $\alpha_3 = 90^0$;

$\beta_1 = 90^0 + \theta$, $\beta_2 = \theta$, $\beta_3 = 90^0$;

$\gamma_1 = 90^0$, $\gamma_2 = 90^0$, $\gamma_3 = 0^0$;

and then, we can express the direction cosines in Table 2.2.

Table 2.2: Direction cosines between systems (1, 2, 3) and (x', y', z')

	1	2	3
x'	$l_1 = \cos\theta$	$l_2 = \sin\theta$	$l_3 = 0$
y'	$m_1 = -\sin\theta$	$m_2 = \cos\theta$	$m_3 = 0$
z'	$n_1 = 0$	$n_2 = 0$	$n_3 = 1$

By substituting the results of the direction cosines in the Table (2.2) into the equations (2.20) and (2.21), the equations (2.14) and (2.19) can be used, when a unidirectional composite's fiber direction has an angle θ with the coordinate system (x', y', z') in the plane $1O2$ and $x'Oy'$. Hereafter, the stiffness constants are written as in the following [22].

$$C'_{11} = C_{11}\cos^4\theta + C_{22}\sin^4\theta + 2(C_{12} + 2C_{66})\sin^2\theta\cos^2\theta \tag{2.22}$$

$$C'_{12} = (C_{11} + C_{22} - 4C_{66})\sin^2\theta\cos^2\theta + C_{12}(\sin^4\theta + \cos^4\theta) \tag{2.23}$$

$$C'_{13} = C_{12}\cos^2\theta + C_{23}\sin^2\theta \tag{2.24}$$

$$C'_{14} = 0 \tag{2.25}$$

$$C'_{15} = 0 \tag{2.26}$$

$$C'_{16} = (C_{11} - C_{12} - 2C_{66})\sin\theta\cos^3\theta + (C_{12} - C_{22} + 2C_{66})\sin^3\theta\cos\theta \tag{2.27}$$

$$C'_{22} = C_{11}\sin^4\theta + 2(C_{12} + 2C_{66})\sin^2\theta\cos^2\theta + C_{22}\cos^4\theta \tag{2.28}$$

$$C'_{23} = C_{12}\sin^2\theta + C_{23}\cos^2\theta \tag{2.29}$$

$$C'_{24} = 0 \tag{2.30}$$

$$C'_{25} = 0 \tag{2.31}$$

$$C'_{26} = (C_{11} - C_{12} - 2C_{66})\sin^3\theta\cos\theta + (C_{12} - C_{22} + 2C_{66})\sin\theta\cos^3\theta \tag{2.32}$$

$$C'_{33} = C_{22} \tag{2.33}$$

$$C'_{34} = 0 \tag{2.34}$$

$$C'_{35} = 0 \tag{2.35}$$

$$C'_{36} = (C_{12} + C_{23})\sin\theta\cos\theta \tag{2.36}$$

$$C'_{44} = \frac{C_{22} - C_{23}}{2}\cos^2\theta + C_{66}\sin^2\theta \tag{2.37}$$

$$C'_{45} = (C_{66} - \frac{C_{22} - C_{23}}{2})\sin\theta\cos\theta \tag{2.38}$$

$$C'_{46} = 0 \tag{2.39}$$

$$C'_{55} = \frac{C_{22} - C_{23}}{2}\sin^2\theta + C_{66}\cos^2\theta \tag{2.40}$$

$$C'_{56} = 0 \tag{2.41}$$

$$C_{66} = [C_{11} + C_{22} - 2(C_{12} + C_{66})]\sin^2\theta\cos^2\theta + C_{66}(\sin^4\theta + \cos^4\theta) \tag{2.42}$$

Similarly, the compliance constants can be written as follow:

$$S'_{11} = S_{11}\cos^4\theta + S_{22}\sin^4\theta + (2S_{12} + S_{66})\sin^2\theta\cos^2\theta \tag{2.43}$$

$$S'_{12} = (S_{11} + S_{22} - S_{66})\sin^2\theta\cos^2\theta + S_{12}(\sin^4\theta + \cos^4\theta) \tag{2.44}$$

$$S'_{13} = S_{12}\cos^2\theta + S_{23}\sin^2\theta \tag{2.45}$$

$$S'_{14} = 0 \tag{2.46}$$

$$S'_{15} = 0 \tag{2.47}$$

$$S'_{16} = [2(S_{11} - S_{12}) - 2S_{66}]\sin\theta\cos^3\theta + [2(S_{12} - S_{22}) + S_{66})]\sin^3\theta\cos\theta \quad (2.48)$$

$$S'_{22} = S_{11}\sin^4\theta + (2S_{12} + S_{66})\sin^2\theta\cos^2\theta + S_{22}\cos^4\theta \quad (2.49)$$

$$S'_{23} = S_{12}\sin^2\theta + S_{23}\cos^2\theta \quad (2.50)$$

$$S'_{24} = 0 \quad (2.51)$$

$$S'_{25} = 0 \quad (2.52)$$

$$S'_{26} = [2(S_{11} - S_{12}) - S_{66}]\sin^3\theta\cos\theta + [2(S_{12} - S_{22}) + S_{66}]\sin\theta\cos^3\theta \quad (2.53)$$

$$S'_{33} = S_{22} \quad (2.54)$$

$$S'_{34} = 0 \quad (2.55)$$

$$S'_{35} = 0 \quad (2.56)$$

$$S'_{36} = 2(S_{12} + S_{23})\sin\theta\cos\theta \quad (2.57)$$

$$S'_{44} = 2(S_{22} - S_{23})\cos^2\theta + S_{66}\sin^2\theta \quad (2.58)$$

$$S'_{45} = [s_{66} - 2(S_{22} - S_{23})]\sin\theta\cos\theta \quad (2.59)$$

$$S'_{46} = 0 \quad (2.60)$$

$$S'_{55} = 2(S_{22} - S_{23})\sin^2\theta + S_{66}\cos^2\theta \quad (2.61)$$

$$S'_{56} = 0 \quad (2.62)$$

$$S_{66} = 2[2(S_{11} + S_{22} - 2S_{12}) - S_{66})]\sin^2\theta\cos^2\theta + S_{66}(\sin^4\theta + \cos^4\theta) \quad (2.63)$$

2.4 Elasticity Equations for Plane Stress State

Under plane-stress state, one of the normal stresses and two of out-of-plane shear stresses are zero. We select the normal stress σ_3' to be zero in the z' coordinate direction and the out-of-plane shear stresses, τ_{23}' and τ_{13}', to be zero in $x'-y'$ plane, just as it is shown in Figure 2.1. So the strains can be obtained as [36]:

$$\begin{bmatrix} \varepsilon_{11}' \\ \varepsilon_{22}' \\ \varepsilon_{33}' \\ \gamma_{23}' \\ \gamma_{13}' \\ \gamma_{12}' \end{bmatrix} = \begin{bmatrix} S_{11}' & S_{12}' & S_{13}' & 0 & 0 & S_{16}' \\ S_{12}' & S_{22}' & S_{23}' & 0 & 0 & S_{26}' \\ S_{13}' & S_{23}' & S_{33}' & 0 & 0 & S_{36}' \\ 0 & 0 & 0 & S_{44}' & S_{45}' & 0 \\ 0 & 0 & 0 & S_{45}' & S_{55}' & 0 \\ S_{16}' & S_{26}' & S_{36}' & 0 & 0 & S_{66}' \end{bmatrix} \cdot \begin{bmatrix} \sigma_{11}' \\ \sigma_{22}' \\ 0 \\ 0 \\ 0 \\ \tau_{12}' \end{bmatrix} \tag{2.64}$$

Therefore, from the equation (2.64), we deduce that:

$\gamma_{23}' = 0$, and $\gamma_{13}' = 0$

The relations between stresses and strains given in terms of stiffness constants are written as:

$$\begin{bmatrix} \sigma_{11}' \\ \sigma_{22}' \\ 0 \\ 0 \\ 0 \\ \tau_{12}' \end{bmatrix} = \begin{bmatrix} C_{11}' & C_{12}' & C_{13}' & 0 & 0 & C_{16}' \\ C_{12}' & C_{22}' & C_{23}' & 0 & 0 & C_{26}' \\ C_{13}' & C_{23}' & C_{33}' & 0 & 0 & C_{36}' \\ 0 & 0 & 0 & C_{44}' & C_{45}' & 0 \\ 0 & 0 & 0 & C_{45}' & C_{55}' & 0 \\ C_{16}' & C_{26}' & C_{36}' & 0 & 0 & C_{66}' \end{bmatrix} \cdot \begin{bmatrix} \varepsilon_{11}' \\ \varepsilon_{22}' \\ \varepsilon_{33}' \\ 0 \\ 0 \\ \gamma_{12}' \end{bmatrix} \tag{2.65}$$

We can get the following equations:

$$\sigma_{11}' = C_{11}'\varepsilon_{11}' + C_{12}'\varepsilon_{22}' + C_{13}'\varepsilon_{33}' + C_{16}'\gamma_{12}' \tag{2.66}$$

$$\sigma_{22}' = C_{12}'\varepsilon_{11}' + C_{22}'\varepsilon_{22}' + C_{23}'\varepsilon_{33}' + C_{26}'\gamma_{12}' \tag{2.67}$$

$$0 = C'_{13}\varepsilon'_{11} + C'_{23}\varepsilon'_{22} + C'_{33}\varepsilon'_{33} + C'_{36}\gamma'_{12} \tag{2.68}$$

$$\tau'_{12} = C'_{16}\varepsilon'_{11} + C'_{26}\varepsilon'_{22} + C'_{36}\varepsilon'_{33} + C'_{66}\gamma'_{12} \tag{2.69}$$

From the equation (2. 68), we deduce the following equation:

$$\varepsilon'_{33} = -\frac{1}{C'_{33}}(C'_{13}\varepsilon'_{11} + C'_{23}\varepsilon'_{22} + C'_{36}\gamma'_{12}) \tag{2.70}$$

By substituting equation (2.70) into the other three equations (2.66), (2.67), and (2.69) above, we can get the reduced stiffness matrix:

$$\begin{bmatrix} \sigma'_{11} \\ \sigma'_{22} \\ \tau'_{12} \end{bmatrix} = \begin{bmatrix} Q_{11}' & Q_{12}' & Q_{16}' \\ Q_{12}' & Q_{22}' & Q_{26}' \\ Q_{16} & Q_{26} & Q_{66} \end{bmatrix} \cdot \begin{bmatrix} \varepsilon'_{11} \\ \varepsilon'_{22} \\ \gamma'_{12} \end{bmatrix} \tag{2.71}$$

Here:

$$Q_{ij}' = C_{ij}' - \frac{C_{i3}' \cdot C_{j3}'}{C_{33}'} \tag{2.72}$$

The coefficients Q_{ij}' are called as the transformed reduced stiffness constants for a plane stress state. The matrix

$$[Q'] = \begin{bmatrix} Q_{11}' & Q_{12}' & Q_{16}' \\ Q_{12}' & Q_{22}' & Q_{26}' \\ Q_{16} & Q_{26} & Q_{66} \end{bmatrix} \tag{2. 73}$$

is called as the transformed reduced stiffness matrix.

2.5 Elastic Behavior of Laminated Composite Plate

First, the elastic behavior of uniform laminate is considered and the laminate stiffness matrices are derived following. Then the tapered laminate is considered. This approach is followed here to highlight the effect of taper angle on the laminate stiffness.

2.5.1 Elastic Behavior of the Uniform Laminated Composite Plate

The uniform laminated composite plate is shown in Figure 2.2 given below. In the coordinate system (x, y z), the stress field can be obtained by equation (2.71). In the case of the classical laminate theory, for the $k-th$ layer we get the following equations [22]:

$$\sigma_{xx} = Q'_{11}\varepsilon_{xx} + Q'_{12}\varepsilon_{yy} + Q'_{16}\gamma_{xy} \tag{2.74}$$

$$\sigma_{yy} = Q'_{12}\varepsilon_{xx} + Q'_{22}\varepsilon_{yy} + Q'_{26}\gamma_{xy} \tag{2.75}$$

$$\tau_{xy} = Q'_{16}\varepsilon_{xx} + Q'_{26}\varepsilon_{yy} + Q'_{66}\gamma_{xy} \tag{2.76}$$

$$\tau_{yz} = 0 \tag{2.77}$$

$$\tau_{xz} = 0 \tag{2.78}$$

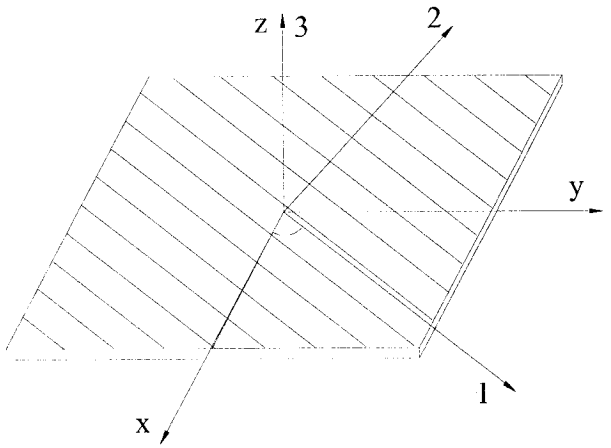

Figure 2.2 Uniform laminated composite plate in (x, y, z) coordinate system

The stresses in the $k-th$ layer are written as following:

$$\begin{bmatrix} \sigma_{xx} \\ \sigma_{yy} \\ \tau_{xy} \end{bmatrix}_k = [Q']_k \begin{bmatrix} \varepsilon_{xx} \\ \varepsilon_{yy} \\ \gamma_{xy} \end{bmatrix} \tag{2.79}$$

where $[Q']_k$ is the reduced stiffness matrix of the $k-th$ layer introduced by the equation (2.71). According to the classical laminates theory, the following equation can be obtained:

$$\begin{bmatrix} \varepsilon_{xx} \\ \varepsilon_{yy} \\ \gamma_{xy} \end{bmatrix}_k = \begin{bmatrix} \varepsilon^0{}_{xx} \\ \varepsilon^0{}_{yy} \\ \gamma^0{}_{xy} \end{bmatrix} + z \begin{bmatrix} k_x \\ k_y \\ k_{xy} \end{bmatrix} \tag{2.80}$$

We can also write the equation as:

$$[\varepsilon] = [\varepsilon_m] + [\varepsilon_f] \tag{2.81}$$

Here:

$[\varepsilon_m] = \begin{bmatrix} \varepsilon^0{}_{xx} \\ \varepsilon^0{}_{yy} \\ \gamma^0{}_{xy} \end{bmatrix}$ is called as the in-plane strain matrix. And

$$[\varepsilon_f] = \begin{bmatrix} \varepsilon^f{}_{xx} \\ \varepsilon^f{}_{yy} \\ \gamma^f{}_{xy} \end{bmatrix} = z \begin{bmatrix} k_x \\ k_y \\ k_{xy} \end{bmatrix}$$ is called as the flexural strain matrix.

By substituting the equation (2.79) into the equation (2.71), the stresses in the $k-th$ layer are expressed as follows:

$$\begin{bmatrix} \sigma_{xx} \\ \sigma_{yy} \\ \tau_{xy} \end{bmatrix}_k = \begin{bmatrix} Q_{11}' & Q_{12}' & Q_{16}' \\ Q_{12}' & Q_{22}' & Q_{26}' \\ Q_{16}' & Q_{26}' & Q_{66}' \end{bmatrix}_k \cdot \begin{bmatrix} \varepsilon^0{}_{xx} \\ \varepsilon^0{}_{yy} \\ \gamma^0{}_{xy} \end{bmatrix} + z \begin{bmatrix} Q_{11}' & Q_{12}' & Q_{16}' \\ Q_{12}' & Q_{22}' & Q_{26}' \\ Q_{16}' & Q_{26}' & Q_{66}' \end{bmatrix}_k \begin{bmatrix} k_x \\ k_y \\ k_{xy} \end{bmatrix} \tag{2.82}$$

The in-plane resultants of the laminate can be written as in the following:

$$[N(x,y)] = \begin{bmatrix} N_x \\ N_y \\ N_{xy} \end{bmatrix} = \int_{-h/2}^{h/2} \begin{bmatrix} \sigma_{xx} \\ \sigma_{yy} \\ \tau_{xy} \end{bmatrix} dz \tag{2.83}$$

where h is the thickness of the laminate.

By substituting the equation (2.80) into the equation (2.82), we obtain the following equation:

$$[N(x,y)] = \sum_{k=1}^{n} \int_{h_{k-1}}^{h_k} [[Q']_k [\varepsilon_m(x,y)] + z \cdot [Q']_k [k(x,y)]] dz \tag{2.84}$$

where, $k(x,y) = \begin{bmatrix} k_x \\ k_y \\ k_{xy} \end{bmatrix}$

From the equation (2.83), we can obtain the following equation:

$$[N(x,y)] = \sum_{k=1}^{n} [[Q']_k [\varepsilon_m(x,y)] \int_{h_{k-1}}^{h_k} dz] + \sum_{k=1}^{n} [[Q']_k [k(x,y)] \int_{h_{k-1}}^{h_k} z dz]$$

$$= \{\sum_{k=1}^{n} (h_k - h_{k-1})[Q']_k\}[\varepsilon_m(x,y)] + \{\frac{1}{2}\sum_{k=1}^{n} ({h_k}^2 - {h_{k-1}}^2)[Q']_k\}[k(x,y)] \tag{2.85}$$

This expression can be written in the following form:

$$[N(x,y)] = [A][\varepsilon_m(x,y)] + [B][k(x,y)] \tag{2.86}$$

So we can obtain the following matrices:

$$[A] = \sum_{k=1}^{n} (h_k - h_{k-1})[Q']_k \tag{2.87}$$

$$A_{ij} = \sum_{k=1}^{n} (h_k - h_{k-1})(Q'_{ij})_k \tag{2. 88}$$

$$[B] = \frac{1}{2}\sum_{k=1}^{n} ({h_k}^2 - {h_{k-1}}^2)[Q']_k \tag{2.89}$$

$$B_{ij} = \frac{1}{2}\sum_{k=1}^{n} ({h_k}^2 - {h_{k-1}}^2)(Q'_{ij})_k \tag{2.90}$$

The resultant bending moments and twisting moment of the laminate are defined by the following equation:

$$[M(x,y)]=\begin{bmatrix} M_x \\ M_y \\ M_{xy} \end{bmatrix}=\int_{-h/2}^{h/2} z\begin{bmatrix} \sigma_{xx} \\ \sigma_{yy} \\ \tau_{xy} \end{bmatrix}dz \tag{2.91}$$

By substituting the equation (2.82) into the equation (2.91), we obtain the following equation:

$$[M(x,y)]=\sum_{k=1}^{n}\int_{h_{k-1}}^{h_k}[z[Q']_k[\varepsilon_m(x,y]+z^2[Q']_k[k(x,y)]]dz \tag{2.92}$$

Hence, we can write $[M(x,y)]$ as follows:

$$[M(x,y)]=[\frac{1}{2}\sum_{k=1}^{n}({h_k}^2-{h_{k-1}}^2)[Q']_k][[\varepsilon_m(x,y)]+[\frac{1}{3}\sum_{k=1}^{n}({h_k}^3-{h_{k-1}}^3)[Q']_k][[k(x,y)] \tag{2.93}$$

This expression can be written in the following form:

$$[M(x,y)]=[B][[\varepsilon_m(x,y)]+[D][[k(x,y)] \tag{2.94}$$

We can get the new matrix:

$$[D]=\frac{1}{3}\sum_{k=1}^{n}({h_k}^3-{h_{k-1}}^3)[Q']_k \tag{2.95}$$

$$D_{ij} = \frac{1}{3}\sum_{k=1}^{n}({h_k}^3 - {h_{k-1}}^3)(Q'_{ij})_k \tag{2.96}$$

For the mechanical behavior of a laminate, the constitutive equation of a laminated plate can be written as follows:

$$\begin{bmatrix} N_x \\ N_y \\ N_{xy} \\ M_x \\ M_y \\ M_{xy} \end{bmatrix} = \begin{bmatrix} A_{11} & A_{12} & A_{16} & B_{11} & B_{12} & B_{16} \\ A_{12} & A_{22} & A_{26} & B_{12} & B_{22} & B_{26} \\ A_{16} & A_{26} & A_{66} & B_{16} & B_{26} & B_{66} \\ B_{11} & B_{12} & B_{16} & D_{11} & D_{12} & D_{16} \\ B_{12} & B_{22} & B_{26} & D_{12} & D_{22} & D_{26} \\ B_{16} & B_{26} & B_{66} & D_{16} & D_{26} & D_{66} \end{bmatrix} \begin{bmatrix} {\varepsilon^0}_{xx} \\ {\varepsilon^0}_{yy} \\ {\gamma^0}_{xy} \\ k_x \\ k_y \\ k_{xy} \end{bmatrix} \tag{2.97}$$

By introducing the thickness e_k and the z coordinate z_k of the center of the $k-th$ layer, the expressions (2.88), (2.90), and (2.96) can also be written as follows:

$$A_{ij} = \sum_{k=1}^{n}(Q'_{ij})_k e_k \tag{2.98}$$

$$B_{ij} = \sum_{k=1}^{n}(Q'_{ij})_k e_k z_k \tag{2.99}$$

$$D_{ij} = \sum_{k=1}^{n}(Q'_{ij})_k ({e_k z_k}^2 + \frac{{e_k}^3}{12}) \tag{2.100}$$

Matrix $[A]$ is called as the stretching matrix or the extensional stiffness matrix.

Matrix $[B]$ is called as the coupling stiffness matrix.

Matrix $[D]$ is called as the bending stiffness matrix.

2.5.2 Elastic Behavior of the Tapered Laminated Composite Plate

Tapered composite laminates can be made using different configurations. Four such configurations are shown in Fig 2.7, Fig 2.8, Fig 2.9, and Fig 2.10, and they are called as configurations A, B, C, and D respectively.

We consider that the tapered laminate layers below the mid-plane have a positive oblique angle, α and the others above the mid-plane have a negative oblique angle α. It can be seen in Figure 2.3 given below.

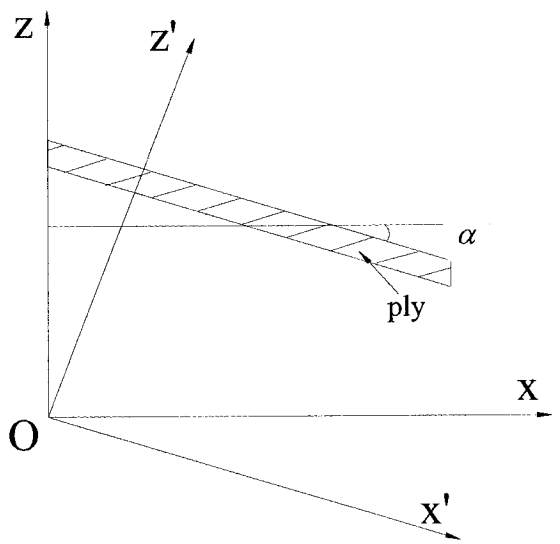

Figure 2.3 A ply in the tapered laminate with oblique angle $-\alpha$.

From the Table 2.3, we can obtain the stress transformation relations between the two coordinate systems, (x', y', z'), and (x, y, z).

For transformation from (x', y', z') to (x, y, z):

$\alpha_1 = \alpha$, $\alpha_2 = 90^0$, $\alpha_3 = 90^0 - \alpha$;

$\beta_1 = 90^0$, $\beta_2 = 0$, $\beta_3 = 90^0$;

$\gamma_1 = 90^0 + \alpha$, $\gamma_2 = 90^0$, $\gamma_3 = \alpha$;

The direction cosines are given in the Table 2.3.

Table 2.3: Direction cosines for a ply in the tapered laminate

	x	y	z
x'	$l_1' = \cos\alpha$	$l_2' = 0$	$l_3' = \sin\alpha$
y'	$m_1' = 0$	$m_2' = 1$	$m_3' = 0$
z'	$n_1' = -\sin\alpha$	$n_2' = 0$	$n_3' = \cos\alpha$

The matrices, $\left[T_\sigma'\right]$ and $\left[T_\varepsilon'\right]$, have the form:

$$\left[T_\sigma'\right] = \begin{bmatrix} l_1'^2 & l_2'^2 & l_3'^2 & 2l_2'l_3' & 2l_1'l_3' & 2l_1'l_2' \\ m_1'^2 & m_2'^2 & m_3'^2 & 2m_2'm_3' & 2m_1'm_3' & 2m_1'm_2' \\ n_1'^2 & n_2'^2 & n_3'^2 & 2n_2'n_3' & 2n_1'n_3' & 2\cdot n_1'n_2' \\ m_1'n_1' & m_2'n_2' & m_3'n_3' & m_3'n_2' + m_2'n_3' & m_3'n_1' + m_1'n_3' & m_2'n_1' + m_1'n_2' \\ l_1'n_1' & l_2'n_2' & l_3'n_3' & l_3'n_2' + l_2'n_3' & l_3'n_1' + l_1'n_3' & l_2'n_1' + l_1'n_2' \\ l_1m_1 & l_2m_2 & l_3m_3 & l_3m_2 + l_2m_3 & l_3m_1 + l_1m_3 & l_2m_1 + l_1m_2 \end{bmatrix} \tag{2.101}$$

$$\left[T_{\varepsilon}{}'\right]=\begin{bmatrix} l_1'^2 & l_2'^2 & l_3'^2 & l_2' l_3' & l_1' l_3' & l_1' l_2' \\ m_1'^2 & m_2'^2 & m_3'^2 & m_2' m_3' & m_1' m_3' & m_1' m_2' \\ n_1'^2 & n_2'^2 & n_3'^2 & n_2' n_3' & n_1' n_3' & n_1' n_2' \\ 2m_1' n_1' & 2m_2' n_2' & 2m_3' n_3' & m_3' n_2' + m_2' n_3' & m_3' n_1' + m_1' n_3' & m_2' n_1' + m_1' n_2' \\ 2l_1' n_1' & 2l_2' n_2' & 2l_3' n_3' & l_3' n_2' + l_2' n_3' & l_3' n_1' + l_1' n_3' & l_2' n_1' + l_1' n_2' \\ 2l_1' m_1' & 2l_2' m_2' & 2l_3' m_3' & l_3' m_2' + l_2' m_3' & l_3' m_1' + l_1' m_3' & l_2' m_1' + l_1' m_2' \end{bmatrix} \tag{2.102}$$

By considering the equations (2.14) and (2.19), we can get the following equations:

$$[C]_{xyz}=\left[T_{\sigma}{}'\right]\cdot[C]_{x'y'z'}\left[T_{\varepsilon}{}'\right]^{-1}=\left[T_{\sigma}{}'\right]\cdot[T_{\sigma}]\cdot[C]_{123}\cdot[T_{\varepsilon}]^{-1}\cdot\left[T_{\varepsilon}{}'\right]^{-1} \tag{2.103}$$

and

$$[S]_{xyz}=\left[T_{\varepsilon}{}'\right]\cdot[S]_{x'y'z'}\cdot\left[T_{\sigma}{}'\right]^{-1}=\left[T_{\varepsilon}{}'\right]\cdot[T_{\varepsilon}]\cdot[S]_{123}\cdot[T_{\sigma}]^{-1}\cdot\left[T_{\sigma}{}'\right]^{-1} \tag{2.104}$$

The state of the stress and strain corresponds to the plane stress state. The stresses in the $k-$th layer are expressed by means of the stiffness coefficients Q_{ij} as follows:

$$\begin{bmatrix}\sigma_{xx}\\ \sigma_{yy}\\ \tau_{xy}\end{bmatrix}=\begin{bmatrix}Q_{11} & Q_{12} & Q_{16}\\ Q_{12} & Q_{22} & Q_{26}\\ Q_{16} & Q_{26} & Q_{66}\end{bmatrix}\cdot\begin{bmatrix}\varepsilon_{xx}\\ \varepsilon_{yy}\\ \gamma_{xy}\end{bmatrix} \tag{2.105}$$

By considering plane stress assumption for the ply in tapered laminate, we can not calculate the stiffness coefficient using equation (2.72), because the stiffness matrix and compliance matrix of the ply with taper angle do not have the same forms as that

of the ply with no taper angle which are shown in equations (2.64) and (2.65). For plane stress assumption, $\sigma_{zz}=\tau_{yz}=\tau_{xz}=0$, and we have the following stress-strain relationship:

$$\begin{Bmatrix}\varepsilon_{xx}\\ \varepsilon_{yy}\\ \varepsilon_{zz}\\ \gamma_{yz}\\ \gamma_{xz}\\ \gamma_{xy}\end{Bmatrix}=\begin{bmatrix}\bar{\bar{S}}_{11} & \bar{\bar{S}}_{12} & \bar{\bar{S}}_{13} & \bar{\bar{S}}_{14} & \bar{\bar{S}}_{15} & \bar{\bar{S}}_{16}\\ \bar{\bar{S}}_{12} & \bar{\bar{S}}_{22} & \bar{\bar{S}}_{23} & \bar{\bar{S}}_{24} & \bar{\bar{S}}_{25} & \bar{\bar{S}}_{26}\\ \bar{\bar{S}}_{13} & \bar{\bar{S}}_{23} & \bar{\bar{S}}_{33} & \bar{\bar{S}}_{34} & \bar{\bar{S}}_{35} & \bar{\bar{S}}_{36}\\ \bar{\bar{S}}_{14} & \bar{\bar{S}}_{24} & \bar{\bar{S}}_{34} & \bar{\bar{S}}_{44} & \bar{\bar{S}}_{45} & \bar{\bar{S}}_{46}\\ \bar{\bar{S}}_{15} & \bar{\bar{S}}_{25} & \bar{\bar{S}}_{35} & \bar{\bar{S}}_{45} & \bar{\bar{S}}_{55} & \bar{\bar{S}}_{56}\\ \bar{\bar{S}}_{16} & \bar{\bar{S}}_{26} & \bar{\bar{S}}_{36} & \bar{\bar{S}}_{46} & \bar{\bar{S}}_{56} & \bar{\bar{S}}_{66}\end{bmatrix}\cdot\begin{Bmatrix}\sigma_{xx}\\ \sigma_{yy}\\ 0\\ 0\\ 0\\ \tau_{xy}\end{Bmatrix} \tag{2.106}$$

Condensing out ε_{zz}, γ_{yz} and γ_{xz}, the reduced equation is:

$$\begin{Bmatrix}\varepsilon_{xx}\\ \varepsilon_{yy}\\ \gamma_{xy}\end{Bmatrix}=\begin{bmatrix}\bar{\bar{S}}_{11} & \bar{\bar{S}}_{12} & \bar{\bar{S}}_{16}\\ \bar{\bar{S}}_{12} & \bar{\bar{S}}_{22} & \bar{\bar{S}}_{26}\\ \bar{\bar{S}}_{16} & \bar{\bar{S}}_{26} & \bar{\bar{S}}_{66}\end{bmatrix}\cdot\begin{Bmatrix}\sigma_{xx}\\ \sigma_{yy}\\ \tau_{xy}\end{Bmatrix} \tag{2.107}$$

By inverting the reduced stiffness matrix, we can get the reduced compliance matrix as below:

$$\begin{bmatrix}Q_{11} & Q_{12} & Q_{16}\\ Q_{12} & Q_{22} & Q_{26}\\ Q_{16} & Q_{26} & Q_{66}\end{bmatrix}=\begin{bmatrix}\bar{\bar{S}}_{11} & \bar{\bar{S}}_{12} & \bar{\bar{S}}_{16}\\ \bar{\bar{S}}_{12} & \bar{\bar{S}}_{22} & \bar{\bar{S}}_{26}\\ \bar{\bar{S}}_{16} & \bar{\bar{S}}_{26} & \bar{\bar{S}}_{66}\end{bmatrix}^{-1} \tag{2.108}$$

By using the results for the uniform laminated composite plate, we can write the following equations:

The stretching stiffness matrix:

$$[A]=\sum_{k=1}^{n}(h_k-h_{k-1})\cdot[Q_k] \tag{2.109}$$

The coupling stiffness matrix:

$$[B]=\sum_{k=1}^{n}\frac{1}{2}\cdot(h_k{}^2-h_{k-1}{}^2)\cdot[Q_k] \tag{2.110}$$

The bending stiffness matrix:

$$[D]=\sum_{k=1}^{n}\frac{1}{3}\cdot(h_k{}^3-h_{k-1}{}^3)\cdot[Q_k] \tag{2.111}$$

From Figure 2.4, for the $k-th$ ply above the mid-plane in the tapered composite laminate, if the oblique angle is $-\alpha$, the equations for h_k and h_{k-1} can be written as follows:

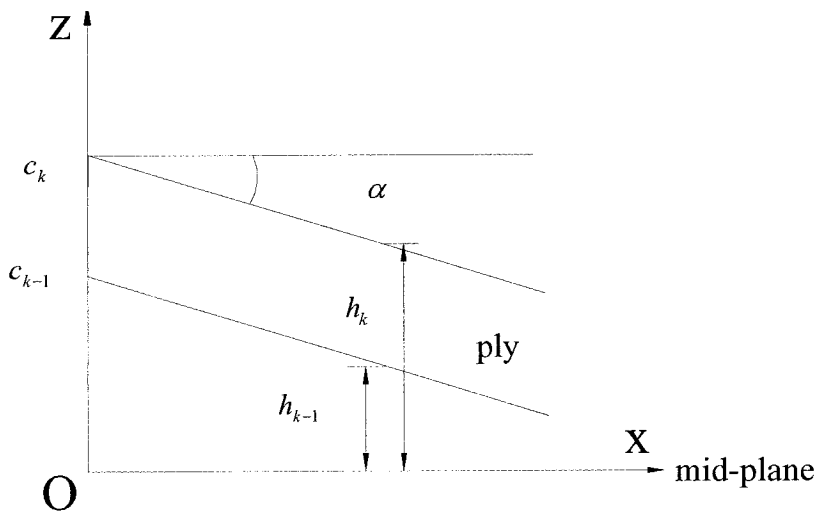

Figure 2.4 $k-th$ layer with oblique angle $-\alpha$

$$h_k = \tan(-\alpha)\cdot x + c_k \tag{2.112}$$

$$h_{k-1} = \tan(-\alpha)\cdot x + c_{k-1} \tag{2.113}$$

So we can obtain the following matrices for the tapered composite laminated plate:

$$[A] = \sum_{k=1}^{n}[(\tan(-\alpha)\cdot x + c_k) - (\tan(-\alpha)\cdot x + c_{k-1})]\cdot[Q_k] \tag{2.114}$$

$$[B] = \sum_{k=1}^{n}\frac{1}{2}\cdot[(\tan(-\alpha)\cdot x + c_k)^2 - (\tan(-\alpha)\cdot x + c_{k-1})^2]\cdot[Q_k] \tag{2.115}$$

$$[D] = \sum_{k=1}^{n}\frac{1}{3}\cdot[(\tan(-\alpha)\cdot x + c_k)^3 - (\tan(-\alpha)\cdot x + c_{k-1})^3]\cdot[Q_k] \tag{2.116}$$

2.5.3 The Reduced Stiffness Matrix for Isotropic Materials

The tapered laminated composite plate has resin pocket. Because resin is isotropic material, the reduced stiffness matrix is written for the behavior of the resin inside the tapered laminates [40].

$$Q = \begin{bmatrix} Q_{11} & Q_{12} & 0 \\ Q_{12} & Q_{22} & 0 \\ 0 & 0 & Q_{66} \end{bmatrix} \tag{2.117}$$

Here:

$$Q_{11} = \frac{E}{1-\nu^2} \tag{2.118}$$

$$Q_{22} = \frac{E}{1-\nu^2} \tag{2.119}$$

$$Q_{12} = \frac{\nu \cdot E}{1-\nu^2} \tag{2.120}$$

$$Q_{66} = \frac{E}{2(1+\nu)} \tag{2.121}$$

The stiffness matrix for the resin is written as in the following:

$$Q = \begin{bmatrix} \frac{E}{1-\nu^2} & \frac{\nu E}{1-\nu^2} & 0 \\ \frac{\nu E}{1-\nu^2} & \frac{E}{1-\nu^2} & 0 \\ 0 & 0 & \frac{E}{2(1+\nu)} \end{bmatrix} = \frac{E}{1-\nu^2}\begin{bmatrix} 1 & \nu & 0 \\ \nu & 1 & 0 \\ 0 & 0 & \frac{1-\nu}{2} \end{bmatrix} \tag{2.122}$$

In Figure 2.5, by considering the taper angle of the resin pocket inside the tapered laminate, we can determine the elastic behavior of the resin pocket as follows:

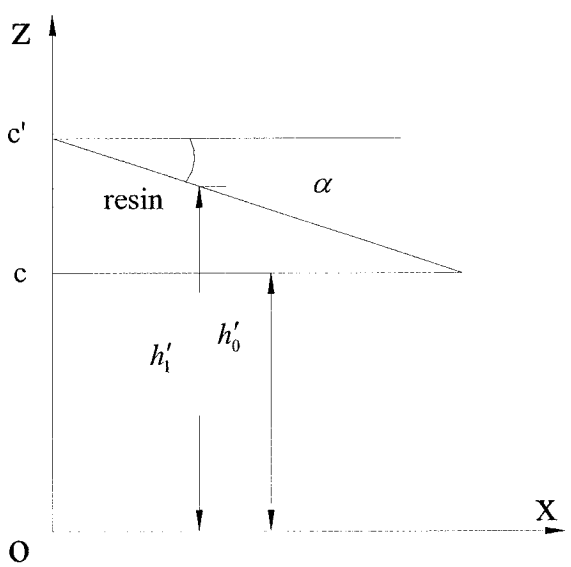

Figure 2.5 Resin pocket with one side having a taper angle

According to equations (2.109), (2.110), and (2.111), we can obtain the following equations for hypothetical one layer of resin pocket from Figure 2.5.

$$[A] = \int_{h_0'}^{h_1'} [Q] \cdot dz = [Q] \cdot (h_1' - h_0') \tag{2.123}$$

$$[B] = \int_{h_0'}^{h_1'} [Q] \cdot z \cdot dz = \frac{1}{2} \cdot [Q] \cdot (h_1' - h_0')^2 \tag{2.124}$$

$$[D] = \int_{h_0'}^{h_1'} [Q] \cdot z^2 \cdot dz = \frac{1}{3} \cdot [Q] \cdot (h_1' - h_0')^3 \tag{2.125}$$

As can be seen from the Figure 2.5,

$h_0' = c$, and $h_1' = \tan(-\alpha) \cdot x + c'$;

Therefore, considering the resin inside the tapered composite plate, the stretching stiffness matrix, the coupling stiffness matrix, and the bending stiffness matrix of the tapered composite laminate are written as the following:

$$[A] = \sum_{k=1}^{n} [(\tan(-\alpha) \cdot x + c_k) - (\tan(-\alpha) \cdot x + c_{k-1})] \cdot [Q_k] + \sum_{k=1}^{m} [Q] \cdot (h_{m-1}' - h_m') \tag{2.126}$$

$$[B] = \sum_{k=1}^{n} \frac{1}{2} \cdot [(\tan(-\alpha) \cdot x + c_k)^2 - (\tan(-\alpha) \cdot x + c_{k-1})^2] \cdot [Q_k] + \frac{1}{2} \cdot \sum_{k=1}^{m} [Q] \cdot (h_{m-1}'^2 - h_m'^2) \tag{2.127}$$

$$[D]=\sum_{k=1}^{n}\frac{1}{3}\cdot[(\tan(-\alpha)\cdot x+c_k)^3-(\tan(-\alpha)\cdot x+c_{k-1})^3]\cdot[Q_k]+\frac{1}{3}\cdot\sum_{k=1}^{m}[Q]\cdot(h'^{3}_{m-1}-h'^{3}_{m}) \tag{2.128}$$

2.6 Example Applications

2.6.1 Example Calculation for Elastic Behavior of a Uniform Laminated Composite Plate

A uniform rectangular laminated plate is made up of graphite/epoxy composite material with symmetric cross-ply arrangement. The laminate is made of eight identical plies each with the mechanical properties as follow.

$E_1=134.4\times10^9\,Pa$; $E_2=E_3=10.34\times10^9\,Pa$; $G_{12}=G_{13}=4.999\times10^9\,Pa$; $G_{23}=1.999\times10^9\,Pa$; $\nu_{12}=\nu_{13}=\nu_{23}=0.33$. The plate has a length $L=127$ mm and a width $b=12.7$ mm. Two different plate thicknesses, $h=1.016$ mm and $h=10.16$ mm resulting in the two cases $L/h=125$ and $L/h=12.5$ are considered. The uniform plate has configuration $[(90/0)_2]_S$ at the left and right ends respectively (Figure 2.6). According to the direction cosines for the plies that have an angle of 90^0, we can obtain the direction cosines given in Table 2.4:

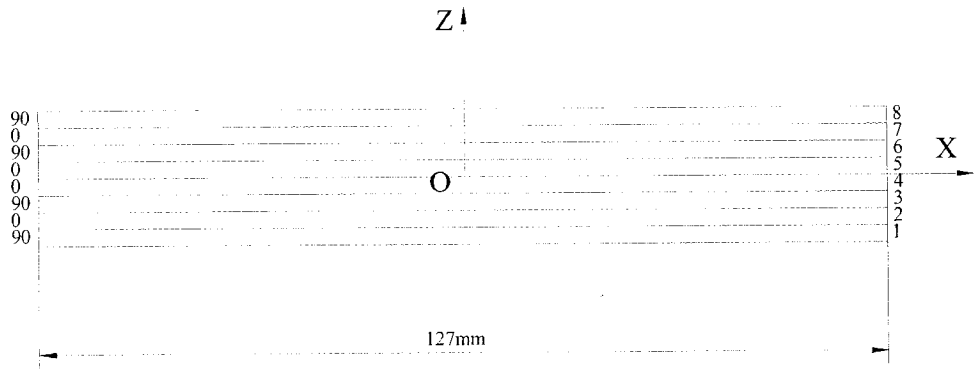

Figure 2.6 Uniform Composite Laminate

Table 2.4: Direction Cosines of the Composite ply with 90^0 *Orientation Angle*

	1	2	3
x'	$l_1 = 0$	$l_2 = 1$	$l_3 = 0$
y'	$m_1 = -1$	$m_2 = 0$	$m_3 = 0$
z'	$n_1 = 0$	$n_2 = 0$	$n_3 = 1$

By using the equation (2.14), we get the following:

$$[C']_{90} = [T_\sigma] \cdot [C]_0 \cdot [T_\varepsilon]^{-1} \qquad (2.129)$$

By considering the equations (2.72) and (2.73), we can obtain the following reduced stiffness matrix of the layer that has the 90^0 orientation angle:

$$[Q']_{90} = \begin{bmatrix} Q_{11}' & Q_{12}' & 0 \\ Q_{12}' & Q_{22}' & 0 \\ 0 & 0 & Q_{66}' \end{bmatrix}_{90} \tag{2.130}$$

The stretching stiffness matrix is written as:

$$[A] = \sum_{k=1}^{8} (h_k - h_{k-1})[Q']_k = (h_1 - h_0)[Q']_{90} + (h_2 - h_1)[Q]_0 + (h_3 - h_2)[Q']_{90} + (h_4 - h_3)[Q]_0 + (h_5 - h_4)[Q]_0 + (h_6 - h_5)[Q']_{90} + (h_7 - h_6)[Q]_0 + (h_8 - h_7)[Q']_{90} \tag{2.131}$$

The coupling stiffness matrix: Because the laminated plate is made up of the graphite/epoxy with symmetric cross-ply, we can obtain the following result:

$$[B] = \frac{1}{2}\sum_{k=1}^{n} (h_k^{\,2} - h_{k-1}^{\,2})[Q']_k = [0] \tag{2.132}$$

The bending stiffness matrix:

$$[D] = \frac{1}{3}\sum_{k=1}^{8} (h_k^{\,3} - h_{k-1}^{\,3})[Q']_k = \frac{1}{3}(h_1^{\,3} - h_0^{\,3})[Q']_{90} + \frac{1}{3}(h_2^{\,3} - h_1^{\,3})[Q]_0 + \frac{1}{3}(h_3^{\,3} - h_2^{\,3})[Q']_{90} + \frac{1}{3}(h_4^{\,3} - h_3^{\,3})[Q]_0 + \frac{1}{3}(h_5^{\,3} - h_4^{\,3})[Q]_0 + \frac{1}{3}(h_6^{\,3} - h_5^{\,3})[Q']_{90} + \frac{1}{3}(h_7^{\,3} - h_6^{\,3})[Q]_0 + \frac{1}{3}(h_8^{\,3} - h_7^{\,3})[Q']_{90} \tag{2.133}$$

For the laminate with $L/h = 125$, we can express the mechanical behavior of this uniform laminated plate as:

$$[A]=\begin{bmatrix}7.4149 & 0.3496 & 0.0000\\ 0.3496 & 7.4149 & 0.0000\\ 0.0000 & 0.0000 & 0.5079\end{bmatrix}\times 10^{6}\,Nm^{-1}$$

$$[B]=\begin{bmatrix}0.0000 & 0.0000 & 0.0000\\ 0.0000 & 0.0000 & 0.0000\\ 0.0000 & 0.0000 & 0.0000\end{bmatrix}N$$

$$[D]=\begin{bmatrix}8.4286 & 0.3007 & 0.0000\\ 0.3007 & 4.3283 & 0.0000\\ 0.0000 & 0.0000 & 0.4369\end{bmatrix}Nm$$

For this kind of uniform laminate, A_{16}, A_{26}, A_{61} and A_{62} are zeros because of the 0/90 configuration, and all the B_{ij} are zero because of symmetry. D_{16}, D_{26}, D_{61} and D_{62} are also zeros because of the 0/90 configuration.

For the laminate with $L/h=12.5$, we can express the mechanical behavior of this uniform laminated plate as:

$$[A]=\begin{bmatrix}7.4149 & 0.3496 & 0.0000\\ 0.3496 & 7.4149 & 0.0000\\ 0.0000 & 0.0000 & 0.5079\end{bmatrix}\times 10^{8}\,Nm^{-1}$$

$$[B]=\begin{bmatrix}0.0000 & 0.0000 & 0.0000\\ 0.0000 & 0.0000 & 0.0000\\ 0.0000 & 0.0000 & 0.0000\end{bmatrix}N$$

$$[D]=\begin{bmatrix} 8.4286 & 0.3007 & 0.0000 \\ 0.3007 & 4.3283 & 0.0000 \\ 0.0000 & 0.0000 & 0.4369 \end{bmatrix} \times 10^3 Nm$$

Similarly, for this uniform laminate, A_{16}, A_{26}, A_{61} and A_{62} are zeros because of the 0/90 configuration, and all the B_{ij} are zero because of symmetry. D_{16}, D_{26}, D_{61} and D_{62} are also zeros because of the 0/90 configuration.

2.6.2 Example Calculation for Elastic Behavior of Tapered Composite Plate

Four configurations A, B, C, and D of the tapered composite laminates as shown in Figure 2.7, Figure 2.8, Figure 2.9 and Figure 2.10 respectively are considered. The laminates are made up of the NCT301 graphite/epoxy material with symmetric cross-ply arrangement. The laminates have twelve plies in the left side and six plies in the right side. For configuration A, B and C, the tapered plates have ply configurations $[(0/90)_3]_S$ at the left end and $[0/90/0]_S$ at the right end respectively. For configuration D, the tapered plates have ply configurations $[0/resin/90/0/0/90]_S$ at the left end and $[0/90/0]_S$ at the right end respectively. The ply has the following mechanical properties:

Elastic Modulus: $E_1 = 113.9\times10^9 Pa; E_2 = E_3 = 7.9\times10^9 Pa;$

Shear Modulus: $G_{12} = G_{13} = 3.1\times10^9 Pa;\ G_{23} = 2.8\times10^9 Pa;$

Poisson's Ratio: $\nu_{12} = 0.28$; $\nu_{23} = 0.40$; $\nu_{21} = 0.02$.

These plates have the length $a = 240$ mm and the width $b = 240$ mm.

The properties of the epoxy resin making up the resin pocket of the tapered composite laminates are written as follows:

Elastic Modulus: $E = 3.93 \times 10^9 Pa$, Shear Modulus: $G = 1.034 \times 10^9 Pa$, and Poisson's Ratio: $\nu = 0.37$.

According to the direction cosines of the plies that have an orientation angle of 90^0, we can obtain the following Table 2.5 of the direction cosines:

Table 2.5 Direction cosines of the plies that have an orientation angle of 90^0

	1	2	3
x'	$l_1 = 0$	$l_2 = 1$	$l_3 = 0$
y'	$m_1 = -1$	$m_2 = 0$	$m_3 = 0$
z'	$n_1 = 0$	$n_2 = 0$	$n_3 = 1$

We use the procedure explained in example 1. By considering the equations (2.14), (2.129), (2.72) and (2.73), we can obtain the following reduced stiffness matrix of the layer that has the 90^0 orientation angle:

$$[Q']_{90} = \begin{bmatrix} Q_{11}' & Q_{12}' & 0 \\ Q_{12}' & Q_{22}' & 0 \\ 0 & 0 & Q_{66}' \end{bmatrix}_{90} \tag{2.134}$$

By considering the taper angle α, we get the direction cosines for the plies that have a taper angle of α in Table 2.6:

Table 2.6 Direction cosines for the plies that have a taper angle of α

	x'	y'	z'
x	$l_1' = \cos\alpha$	$l_2' = 0$	$l_3' = \sin\alpha$
y	$m_1' = 0$	$m_2' = 1$	$m_3' = 0$
z	$n_1' = -\sin\alpha$	$n_2' = 0$	$n_3' = \cos\alpha$

We can get the following equations about the stiffness matrix and compliance matrix of the plies that have a 90^0 orientation angle and a taper angle of α.

$$[C]_{xyz} = T_\sigma' \cdot [C]_{x'y'z'} T_\varepsilon'^{-1} = T_\alpha' \cdot T_\alpha \cdot [C]_{123} \cdot T_\varepsilon^{-1} \cdot T_\varepsilon'^{-1} \tag{2.135}$$

$$[S]_{xyz} = T_\varepsilon' \cdot [S]_{x'y'z'} \cdot T_\alpha'^{-1} = T_\varepsilon' \cdot T_\varepsilon \cdot [S]_{123} \cdot T_\alpha^{-1} \cdot T_\alpha^{-1} \tag{2.136}$$

We can also obtain the reduced stiffness matrix and stiffness coefficients using equation (2.108). By using the equations (2.126), (2.127) and (2.128), we can obtain the mechanical behavior of the four kinds of tapered composite plate models.

$$[A]=\sum_{k=1}^{n}[(\tan(-\alpha)\cdot x+c_k)-(\tan(-\alpha)\cdot x+c_{k-1})]\cdot[Q_k]+\sum_{k=1}^{m}[Q]\cdot(h'_{m-1}-h'_m)$$

(2.137)

$$[B]=\sum_{k=1}^{n}\frac{1}{2}\cdot[(\tan(-\alpha)\cdot x+c_k)^2-(\tan(-\alpha)\cdot x+c_{k-1})^2]\cdot[Q_k]+\frac{1}{2}\cdot\sum_{k=1}^{m}[Q]\cdot(h'^{\,2}_{m-1}-h'^{\,2}_m)$$

(2.138)

$$[D]=\sum_{k=1}^{n}\frac{1}{3}\cdot[(\tan(-\alpha)\cdot x+c_k)^3-(\tan(-\alpha)\cdot x+c_{k-1})^3]\cdot[Q_k]+\frac{1}{3}\cdot\sum_{k=1}^{m}[Q]\cdot(h'^{\,3}_{m-1}-h'^{\,3}_m)$$

(2.139)

At first, we set the coordinate point O at the center of the tapered composite plate and the following results can be obtained:

1. Taper Configuration A:

By using the equation (2.139) given above, we can obtain the following stiffness coefficients of the taper configuration A.

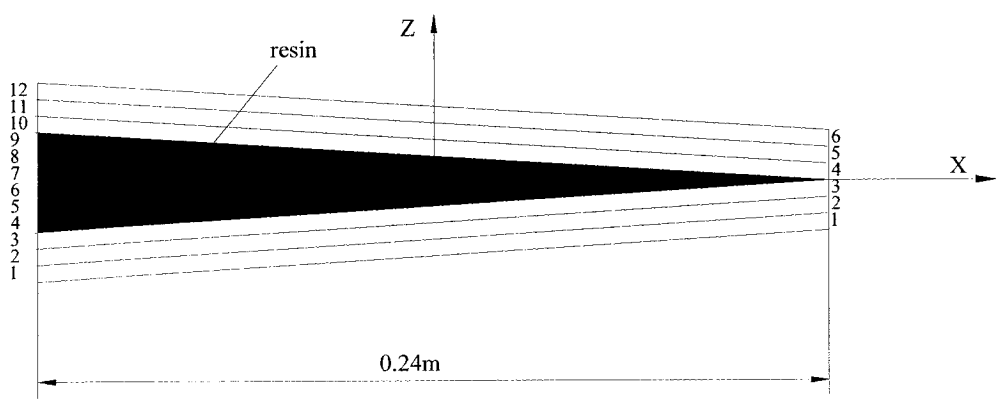

Figure 2.7 Taper Configuration A

The stiffness coefficients for Configuration A $(-0.12m \le x \le 0.12m)$ of the laminate (see Figure 2.7) are computed as follows (unit: Nm):

$$D_{11}(x) = -15.5814x^3 + 200.2225x^2 - 94.0874x + 12.5442$$

$$D_{12}(x) = -5.7651x^3 + 7.5550x^2 - 2.8792x + 0.3518$$

$$D_{21}(x) = -5.7651x^3 + 7.5550x^2 - 2.8792x + 0.3518$$

$$D_{22}(x) = -15.5814x^3 + 112.7107x^2 - 52.0818x + 6.3365$$

$$D_{66}(x) = -4.9081x^3 + 9.4047x^2 - 3.8781x + 0.4850$$

$$D_{16}(x) = 0;\ D_{26}(x) = 0;\ D_{61}(x) = 0;\ D_{62}(x) = 0$$

2. Taper Configuration B:

By considering the equation (2.139), we can obtain the following results for the mechanical behavior of the taper configuration B.

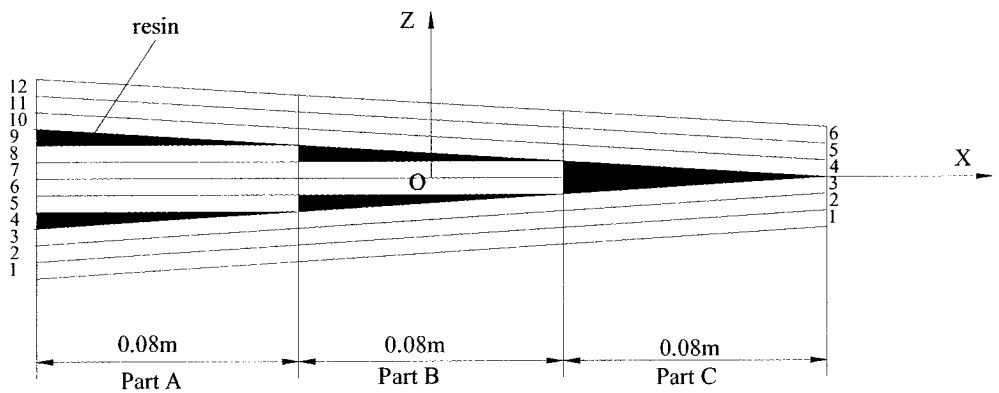

Figure 2.8 Taper Configuration B

The stiffness coefficients for the part A $(-0.12m \le x \le -0.04m)$ of the laminate (see Figure 2.8) are computed as follows (unit: Nm):

$$D_{11}(x) = -15.5814x^3 + 200.2225x^2 - 94.0874x + 13.8988$$

$$D_{12}(x) = -5.7651x^3 + 7.5550x^2 - 2.8792x + 0.3594$$

$$D_{21}(x) = -5.7651x^3 + 7.5550x^2 - 2.8792x + 0.3594$$

$$D_{22}(x) = -15.5814x^3 + 112.7107x^2 - 52.0818x + 6.5708$$

$$D_{66}(x) = -4.9081x^3 + 9.4047x^2 - 3.8781x + 0.5084$$

$$D_{16}(x) = 0;\ D_{26}(x) = 0;\ D_{61}(x) = 0;\ D_{62}(x) = 0$$

The stiffness coefficients for the part B $(-0.04m \le x \le 0.04m)$ of the laminate (see Figure 2.8) are computed as follows (unit: Nm):

$$D_{11}(x) = -15.5814x^3 + 200.2225x^2 - 94.0874x + 12.5501$$

$$D_{12}(x) = -5.7651x^3 + 7.5550x^2 - 2.8792x + 0.3528$$

$$D_{21}(x) = -5.7651x^3 + 7.5550x^2 - 2.8792x + 0.3528$$

$$D_{22}(x) = -15.5814x^3 + 112.7107x^2 - 52.0818x + 6.5292$$

$$D_{66}(x) = -4.9081x^3 + 9.4047x^2 - 3.8781x + 0.4880$$

$$D_{16}(x) = 0;\ D_{26}(x) = 0;\ D_{61}(x) = 0;\ D_{62}(x) = 0$$

The stiffness coefficients for the part C $(0.04m \le x \le 0.12m)$ of the laminate (see

Figure 2.8) are computed as follows (unit: Nm):

$$D_{11}(x) = -15.5814x^3 + 200.2225x^2 - 94.0874x + 12.5442$$

$$D_{12}(x) = -5.7651x^3 + 7.5550x^2 - 2.8792x + 0.3518$$

$$D_{21}(x) = -5.7651x^3 + 7.5550x^2 - 2.8792x + 0.3518$$

$$D_{22}(x) = -15.5814x^3 + 112.7107x^2 - 52.0818x + 6.3365$$

$$D_{66}(x) = -4.9081x^3 + 9.4047x^2 - 3.8781x + 0.4850$$

$$D_{16}(x) = 0;\ D_{26}(x) = 0;\ D_{61}(x) = 0;\ D_{62}(x) = 0$$

3. Taper Configuration C:

By considering the equation (2.139), we can obtain the following results for the mechanical behavior of the taper configuration C.

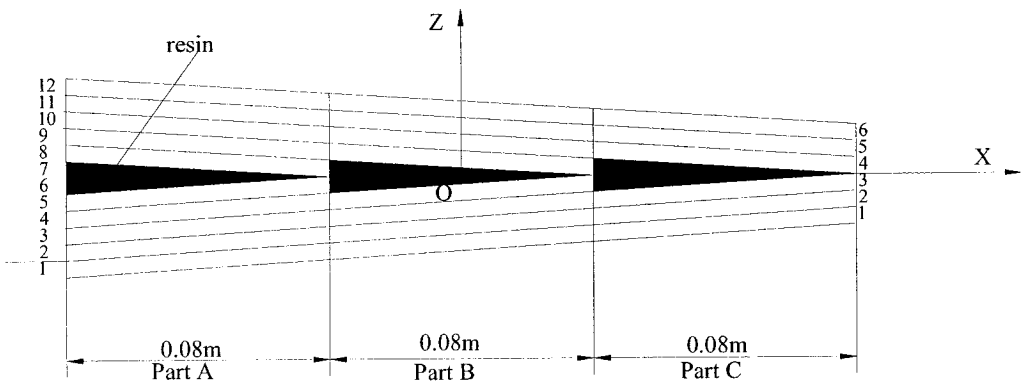

Figure 2.9 Taper Configuration C

The stiffness coefficients for the part A $(-0.12m \le x \le -0.04m)$ of the laminate (see

Figure 2.9) are computed as follows (unit: Nm):

$$D_{11}(x) = -15.5814x^3 + 293.3213x^2 - 94.5328x + 12.6116$$

$$D_{12}(x) = -5.7651x^3 + 8.4409x^2 - 2.9501x + 0.3551$$

$$D_{21}(x) = -5.7651x^3 + 8.4409x^2 - 2.9501x + 0.3551$$

$$D_{22}(x) = -15.5814x^3 + 205.8095x^2 - 66.5321x + 6.9642$$

$$D_{66}(x) = -4.9081x^3 + 12.1407x^2 - 4.0970x + 0.4925$$

$$D_{16}(x) = 0;\ D_{26}(x) = 0;\ D_{61}(x) = 0;\ D_{62}(x) = 0$$

The stiffness coefficients for the part B $(-0.04m \le x \le 0.04m)$ of the laminate (see Figure 2.9) are computed as follows (unit: Nm):

$$D_{11}(x) = -15.5814x^3 + 203.0065x^2 - 94.5328x + 12.5635$$

$$D_{12}(x) = -5.7651x^3 + 7.9979x^2 - 2.9501x + 0.3549$$

$$D_{21}(x) = -5.7651x^3 + 7.9979x^2 - 2.9501x + 0.3549$$

$$D_{22}(x) = -15.5814x^3 + 203.0255x^2 - 66.5321x + 6.9627$$

$$D_{66}(x) = -4.9081x^3 + 10.7727x^2 - 4.0970x + 0.4945$$

$$D_{16}(x) = 0;\ D_{26}(x) = 0;\ D_{61}(x) = 0;\ D_{62}(x) = 0$$

The stiffness coefficients for the part C $(0.04m \le x \le 0.12m)$ of the laminate (see Figure 2.9) are computed as follows (unit: Nm):

$$D_{11}(x) = -15.5814x^3 + 200.2225x^2 - 94.0874x + 12.5442$$

$$D_{12}(x) = -5.7651x^3 + 7.5550x^2 - 2.8792x + 0.3518$$

$$D_{21}(x) = -5.7651x^3 + 7.5550x^2 - 2.8792x + 0.3518$$

$$D_{22}(x) = -15.5814x^3 + 112.7107x^2 - 52.0818x + 6.3365$$

$$D_{66}(x) = -4.9081x^3 + 9.4047x^2 - 3.8781x + 0.4850$$

$$D_{16}(x) = 0;\ D_{26}(x) = 0;\ D_{61}(x) = 0;\ D_{62}(x) = 0$$

4. Taper Configuration D:

By considering the equation (2.139), we can obtain the following results for the mechanical behavior of the taper configuration D.

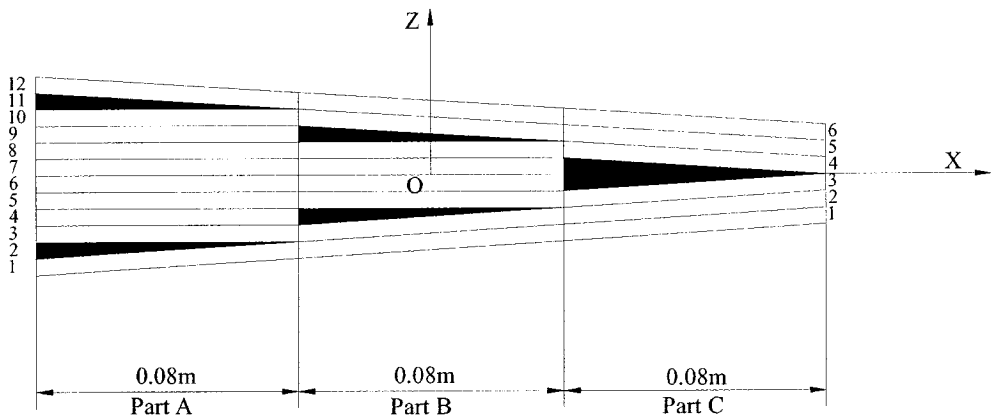

Figure 2.10 Taper Configuration D

The stiffness coefficients for the part A $(-0.12m \le x \le -0.04m)$ of the laminate (see Figure 2.10) are computed as follows (unit: Nm):

$$D_{11}(x) = -15.5814x^3 + 107.1332x^2 - 63.8534x + 15.2575$$

$$D_{12}(x) = -5.7651x^3 + 6.6692x^2 - 2.5249x + 0.3750$$

$$D_{21}(x) = -5.7651x^3 + 6.6692x^2 - 2.5249x + 0.3750$$

$$D_{22}(x) = -15.5814x^3 + 19.6119x^2 - 7.8398x + 8.4894$$

$$D_{66}(x) = -4.9081x^3 + 6.6687x^2 - 2.7838x + 0.5565$$

$$D_{16}(x) = 0;\ D_{26}(x) = 0;\ D_{61}(x) = 0;\ D_{62}(x) = 0$$

The stiffness coefficients for the part B $(-0.04m \le x \le 0.04m)$ of the laminate (see Figure 2.10) are computed as follows (unit: Nm):

$$D_{11}(x) = -15.5814x^3 + 109.9172x^2 - 65.1897x + 11.5388$$

$$D_{12}(x) = -5.7651x^3 + 7.1121x^2 - 2.7375x + 0.3478$$

$$D_{21}(x) = -5.7651x^3 + 7.1121x^2 - 2.7375x + 0.3478$$

$$D_{22}(x) = -15.5814x^3 + 109.9267x^2 - 51.1909x + 6.4980$$

$$D_{66}(x) = -4.9081x^3 + 8.0367x^2 - 3.4404x + 0.4726$$

$$D_{16}(x) = 0;\ D_{26}(x) = 0;\ D_{61}(x) = 0;\ D_{62}(x) = 0$$

The stiffness coefficients for the part C $(0.04m \le x \le 0.12m)$ of the laminate (see Figure 2.10) are computed as follows (unit: Nm):

$$D_{11}(x) = -15.5814x^3 + 200.2225x^2 - 94.0959x + 12.5442$$

$$D_{12}(x) = -5.7651x^3 + 7.5550x^2 - 2.8792x + 0.3518$$

$$D_{21}(x) = -5.7651x^3 + 7.5550x^2 - 2.8792x + 0.3518$$

$$D_{22}(x) = -15.5814x^3 + 112.7107x^2 - 52.0818x + 6.3365$$

$$D_{66}(x) = -4.9081x^3 + 9.4047x^2 - 3.8781x + 0.4850$$

$$D_{16}(x) = 0;\ D_{26}(x) = 0;\ D_{61}(x) = 0;\ D_{62}(x) = 0$$

As we can see from the above results, the four configurations' D_{16}, D_{26}, D_{61} and D_{62} are zeros because of the 0/90 laminate configuration. This is as same as that of the uniform plate. The other terms in D matrix are cubic functions of x because of the tapered configuration.

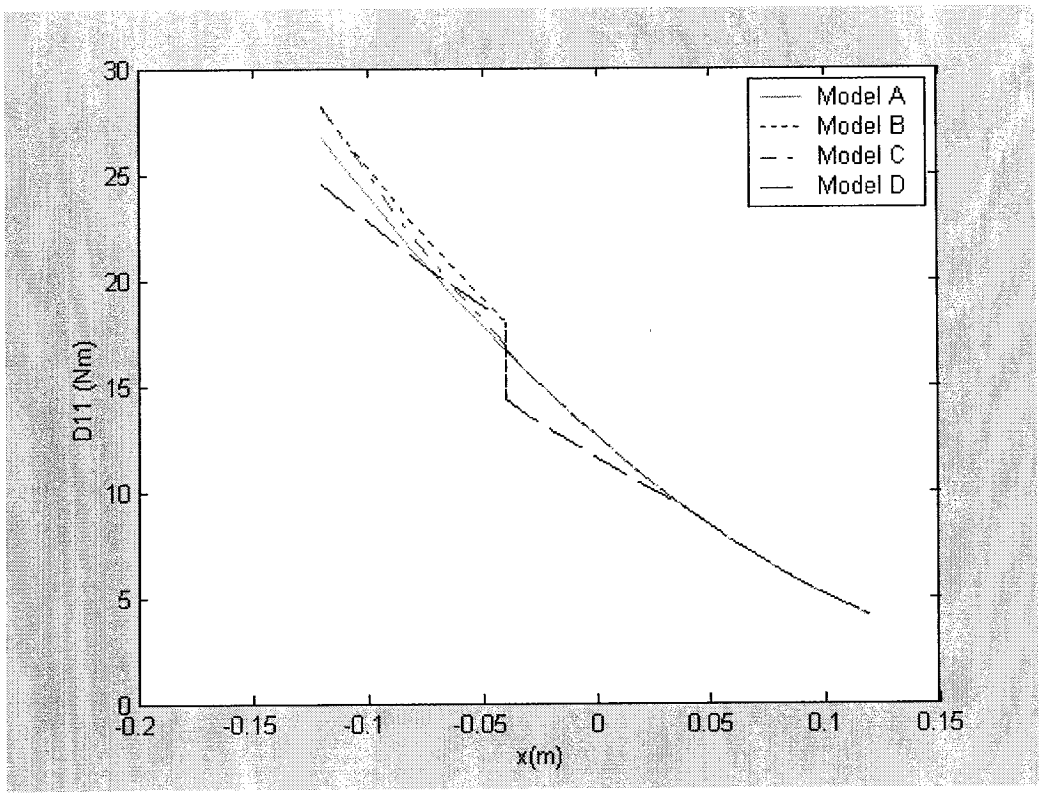

Figure 2.11 Coefficient D_{11} of tapered composite plate

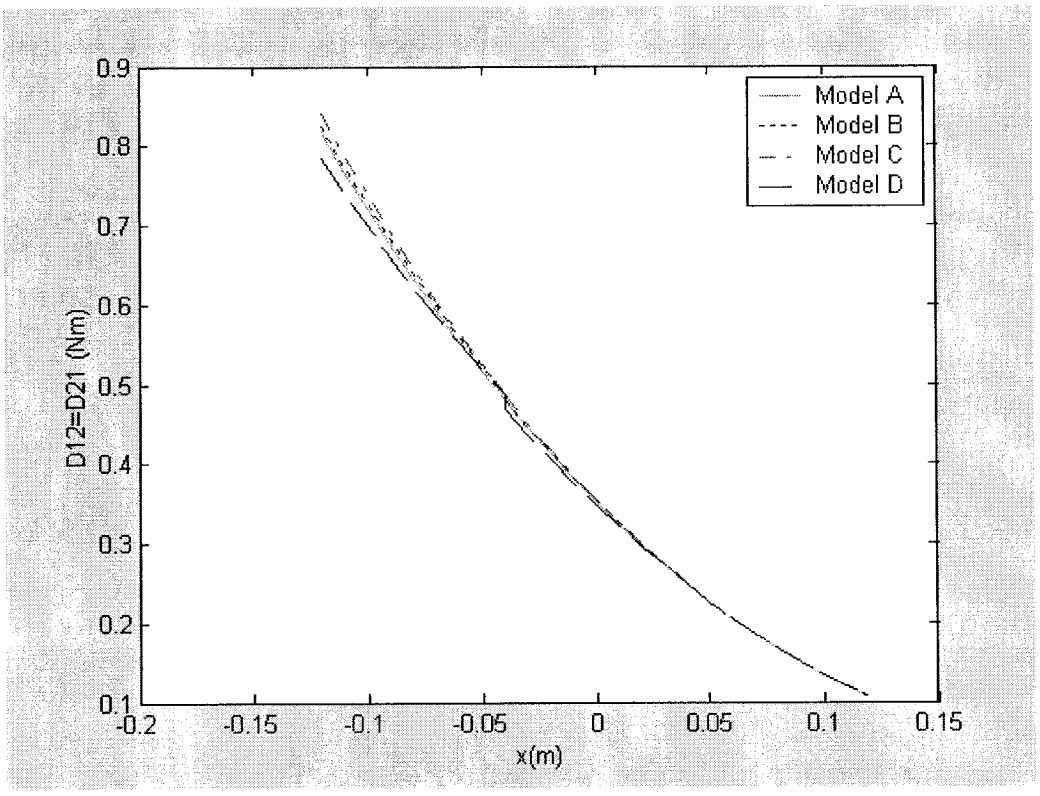

Figure 2.12 Coefficients D_{12} and D_{21} of tapered composite plate

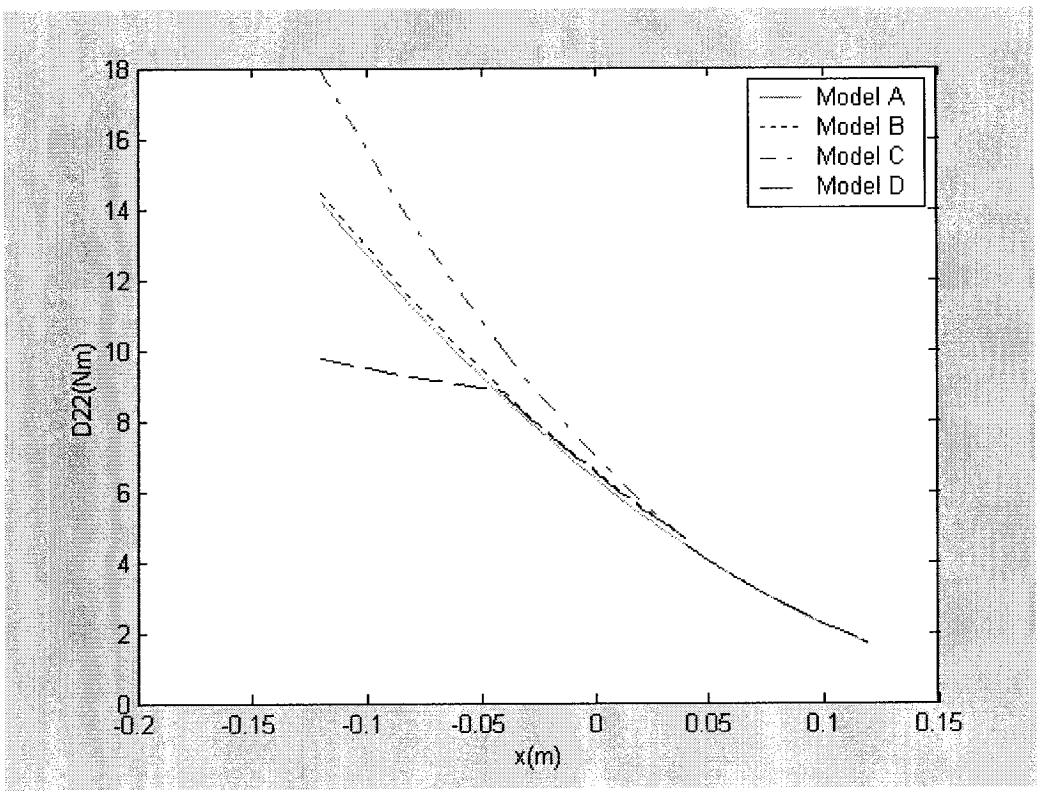

Figure 2.13 Coefficient D_{22} of tapered composite plate

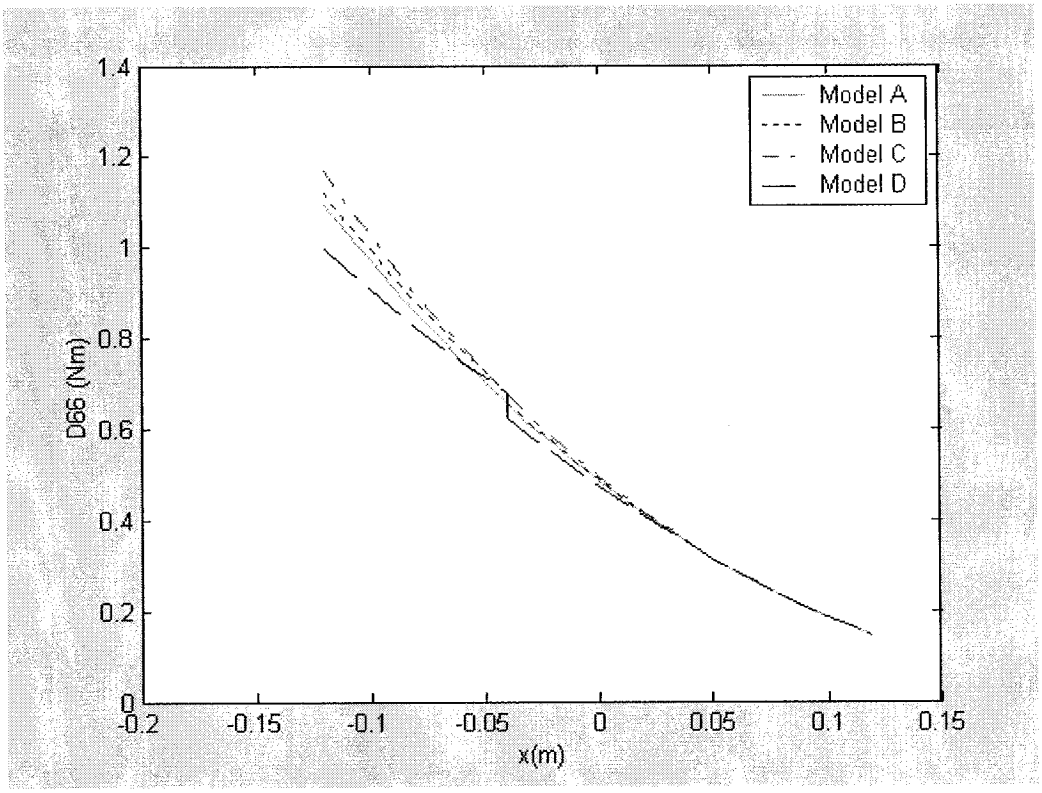

Figure 2.14 Coefficient D_{66} of tapered composite plate

The graphs in Figure 2.11 show the variation of coefficient D_{11} with respect to x for Configuration A, Configuration B, Configuration C and Configuration D. The coefficient D_{11} of Configuration A has a continuous variation with x in all the three parts (Part A, Part B and Part C), because all dropped-off plies are replaced by resin pocket in Configuration A. Whereas the other three configurations have the discontinuous variations through different parts, Part A, Part B and Part C, because the tapered structure of each part is different. All of the four configurations have the same tapered structure in Part C, therefore the D_{11} variations of them have the same trend. In Part B, the three configurations, Configuration A, Configuration B and Configuration C, have almost the same behavior, whereas Configuration D has a little

bit lower performance than others. In Part A, the coefficient D_{11} of all the four configurations has different characteristics: Configuration D has lowest stiffness, and the Configuration B has the highest stiffness, whereas Configuration A and Configuration C have the stiffness between that of Configuration A and Configuration D.

In Figure 2.12, the graphs show the variation of coefficient D_{12} (D_{21} is the same as D_{12}) respect to x for Configuration A, Configuration B, Configuration C and Configuration D. The coefficient D_{12} of Configuration A has a continuous variation with x in all the three parts, due to the same reason as in Figure 2.11, and the others have discontinuous variations with different parts, Parts A, B and C. Just as D_{11} in Figure 2.11, in Part C, the variations of the four configuration s is the same. In Part B, the variations of the four configurations are very close where as Configuration D has a little bit low variation. In Part A, the tendency is almost the same as in Part B.

In Figure 2.13, the D_{22} variation is almost the same as in Figure 2.12, but in Part A, Configuration D has a low performance, because the top and the bottom plies have the 0° orientation.

In Figure 2.14, D_{66} variation has almost the same tendency as D_{12} variation in Figure 2.12.

Next, we set the coordinate point O at the left side of the tapered composite plate, and the following results are obtained:

1. Taper Configuration A:

By using the equation (2.139), we can obtain the following stiffness coefficients of the taper configuration A:

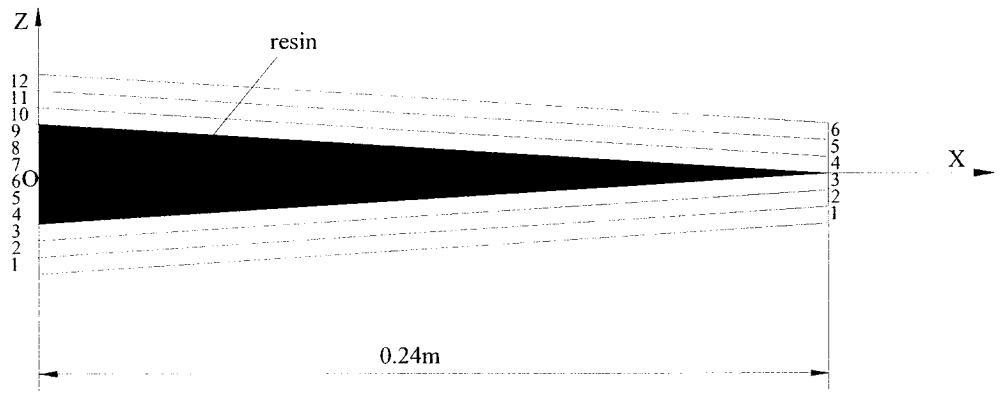

Figure 2.15 Taper configuration A with the coordinate point O at the left side

The stiffness coefficients for Configuration A $(0m \le x \le 0.24m)$ of the laminate (see Figure 2.15) are computed as follows (unit: Nm):

$$D_{11}(x) = -15.5814x^3 + 205.8318x^2 - 142.8139x + 26.7448$$

$$D_{12}(x) = -5.7651x^3 + 9.6304x^2 - 4.9414x + 0.8161$$

$$D_{21}(x) = -5.7651x^3 + 9.6304x^2 - 4.9414x + 0.8161$$

$$D_{22}(x) = -15.5814x^3 + 118.3200x^2 - 79.8055x + 14.2363$$

$$D_{66}(x) = -4.9081x^3 + 11.1717x^2 - 6.3473x + 1.0943$$

$$D_{16}(x) = 0;\ D_{26}(x) = 0;\ D_{61}(x) = 0;\ D_{62}(x) = 0$$

2. Taper Configuration B:

Considering the equation (2.139), we can obtain the following stiffness coefficients of the taper configuration B:

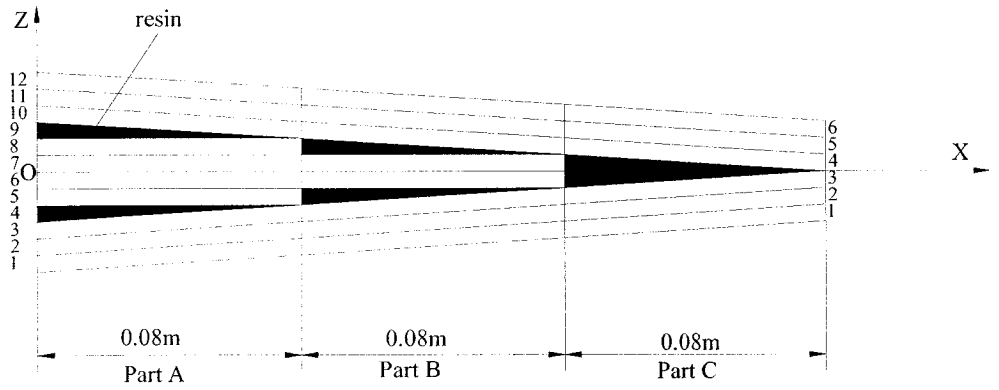

Figure 2.16 Taper configuration B with the coordinate point O at the left side

The stiffness coefficients for the part A $(0m \le x \le 0.08m)$ of the laminate (see Figure 2.16) are computed as follows (unit: Nm):

$$D_{11}(x) = -15.5814x^3 + 205.8318x^2 - 142.8139x + 28.0994$$

$$D_{12}(x) = -5.7651x^3 + 9.6304x^2 - 4.9414x + 0.8237$$

$$D_{21}(x) = -5.7651x^3 + 9.6304x^2 - 4.9414x + 0.8237$$

$$D_{22}(x) = -15.5814x^3 + 118.3200x^2 - 79.8055x + 14.4706$$

$$D_{66}(x) = -4.9081x^3 + 11.1717x^2 - 6.3473x + 1.1177$$

$$D_{16}(x) = 0;\ D_{26}(x) = 0;\ D_{61}(x) = 0; D_{62}(x) = 0$$

The stiffness coefficients for the part B $(0.08m \le x \le 0.16m)$ of the laminate (see Figure 2.16) are computed as follows (unit: Nm):

$$D_{11}(x) = -15.5814x^3 + 205.8318x^2 - 142.8139x + 26.7507$$

$$D_{12}(x) = -5.7651x^3 + 9.6304x^2 - 4.9414x + 0.8170$$

$$D_{21}(x) = -5.7651x^3 + 9.6304x^2 - 4.9414x + 0.8170$$

$$D_{22}(x) = -15.5814x^3 + 118.3200x^2 - 79.8055x + 14.4290$$

$$D_{66}(x) = -4.9081x^3 + 11.1717x^2 - 6.3473x + 1.0972$$

$$D_{16}(x) = 0;\ D_{26}(x) = 0;\ D_{61}(x) = 0;\ D_{62}(x) = 0$$

The stiffness coefficients for the part C $(0.16m \le x \le 0.24m)$ of the laminate (see Figure 2.16) are computed as follows (unit: Nm):

$$D_{11}(x) = -15.5814x^3 + 205.8318x^2 - 142.8139x + 26.7448$$

$$D_{12}(x) = -5.7651x^3 + 9.6304x^2 - 4.9414x + 0.8161$$

$$D_{21}(x) = -5.7651x^3 + 9.6304x^2 - 4.9414x + 0.8161$$

$$D_{22}(x) = -15.5814x^3 + 118.3200x^2 - 79.8055x + 14.2363$$

$$D_{66}(x) = -4.9081x^3 + 11.1717x^2 - 6.3473x + 1.0943$$

$$D_{16}(x) = 0;\ D_{26}(x) = 0;\ D_{61}(x) = 0;\ D_{62}(x) = 0$$

3. Taper Configuration C:

By using the same steps or calculation used for taper configuration B, we can obtain

the following stiffness coefficients of the taper configuration C:

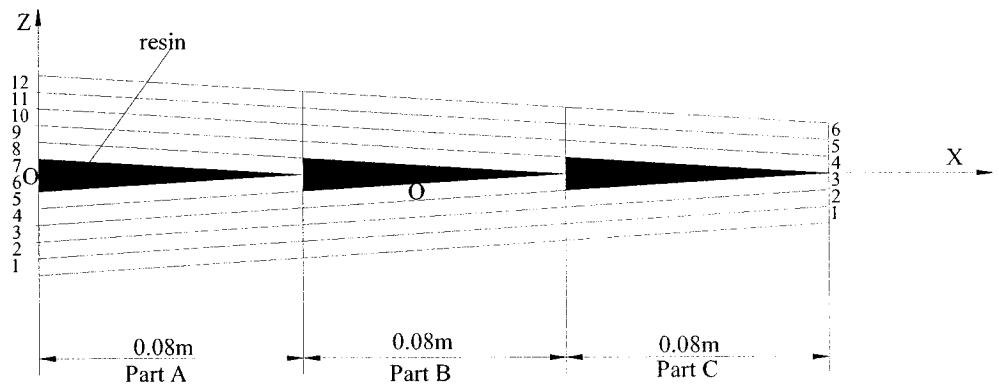

Figure 2.17 Taper configuration C with the coordinate point O at the left side

The stiffness coefficients for the part A $(0m \le x \le 0.08m)$ of the laminate (see Figure 2.17) are computed as follows (unit: Nm):

$$D_{11}(x) = -15.5814x^3 + 298.9306x^2 - 165.6031x + 28.2063$$

$$D_{12}(x) = -5.7651x^3 + 10.5163x^2 - 5.2249x + 0.8407$$

$$D_{21}(x) = -5.7651x^3 + 10.5163x^2 - 5.2249x + 0.8407$$

$$D_{22}(x) = -15.5814x^3 + 211.4188x^2 - 116.5995x + 17.9387$$

$$D_{66}(x) = -4.9081x^3 + 13.9076x^2 - 7.2228x + 1.1702$$

$$D_{16}(x) = 0;\ D_{26}(x) = 0;\ D_{61}(x) = 0;\ D_{62}(x) = 0$$

The stiffness coefficients for the part B $(0.08m \le x \le 0.16m)$ of the laminate (see Figure 2.17) are computed as follows (unit: Nm):

$$D_{11}(x) = -15.5814x^3 + 208.6158x^2 - 143.9275x + 26.8576$$

$$D_{12}(x) = -5.7651x^3 + 10.0734x^2 - 5.1186x + 0.8341$$

$$D_{21}(x) = -5.7651x^3 + 10.0734x^2 - 5.1186x + 0.8341$$

$$D_{22}(x) = -15.5814x^3 + 208.6349x^2 - 115.9314x + 17.8971$$

$$D_{66}(x) = -4.9081x^3 + 12.5396x^2 - 6.8945x + 1.1498$$

$$D_{16}(x) = 0;\ D_{26}(x) = 0;\ D_{61}(x) = 0;\ D_{62}(x) = 0$$

The stiffness coefficients for the part C $(0.16m \le x \le 0.24m)$ of the laminate (see Figure 2.17) are computed as follows (unit: Nm):

$$D_{11}(x) = -15.5814x^3 + 205.8318x^2 - 142.8139x + 26.7448$$

$$D_{12}(x) = -5.7651x^3 + 9.6304x^2 - 4.9414x + 0.8161$$

$$D_{21}(x) = -5.7651x^3 + 9.6304x^2 - 4.9414x + 0.8161$$

$$D_{22}(x) = -15.5814x^3 + 118.3200x^2 - 79.8055x + 14.2363$$

$$D_{66}(x) = -4.9081x^3 + 11.1717x^2 - 6.3473x + 1.0943$$

$$D_{16}(x) = 0;\ D_{26}(x) = 0;\ D_{61}(x) = 0;\ D_{62}(x) = 0$$

4. Taper Configuration D:

By using the equation (1.139), we can obtain the following stiffness coefficients of the taper configuration D:

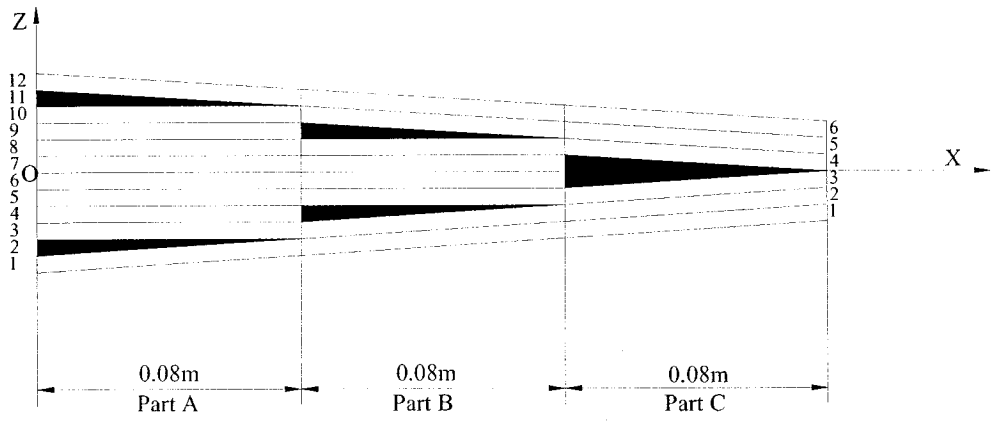

Figure 2.18 Taper configuration D with the coordinate point O at the left side

The stiffness coefficients for the part A $(0m \le x \le 0.08m)$ of the laminate (see Figure 2.18) are computed as follows (unit: Nm):

$$D_{11}(x) = -15.5814x^3 + 112.7425x^2 - 90.2385x + 24.4896$$

$$D_{12}(x) = -5.7651x^3 + 8.7446x^2 - 4.3745x + 0.7840$$

$$D_{21}(x) = -5.7651x^3 + 8.7446x^2 - 4.3745x + 0.7840$$

$$D_{22}(x) = -15.5814x^3 + 25.2212x^2 - 13.2197x + 9.7395$$

$$D_{66}(x) = -4.9081x^3 + 8.4357x^2 - 4.5963x + 0.9951$$

$$D_{16}(x) = 0;\ D_{26}(x) = 0;\ D_{61}(x) = 0;\ D_{62}(x) = 0$$

The stiffness coefficients for the part B $(0.08m \le x \le 0.16m)$ of the laminate (see

Figure 2.18) are computed as follows (unit: Nm):

$$D_{11}(x) = -15.5814x^3 + 115.5265x^2 - 92.2430x + 20.9713$$

$$D_{12}(x) = -5.7651x^3 + 9.1875x^2 - 4.6934x + 0.7887$$

$$D_{21}(x) = -5.7651x^3 + 9.1875x^2 - 4.6934x + 0.7887$$

$$D_{22}(x) = -15.5814x^3 + 115.5360x^2 - 78.2464x + 14.2508$$

$$D_{66}(x) = -4.9081x^3 + 9.8037x^2 - 5.5812x + 1.0097$$

$$D_{16}(x) = 0;\ D_{26}(x) = 0;\ D_{61}(x) = 0;\ D_{62}(x) = 0$$

The stiffness coefficients for the part C $(0.16m \le x \le 0.24m)$ of the laminate (see Figure 2.18) are computed as follows (unit: Nm):

$$D_{11}(x) = -15.5814x^3 + 205.8318x^2 - 142.8139x + 26.7448$$

$$D_{12}(x) = -5.7651x^3 + 9.6304x^2 - 4.9414x + 0.8161$$

$$D_{21}(x) = -5.7651x^3 + 9.6304x^2 - 4.9414x + 0.8161$$

$$D_{22}(x) = -15.5814x^3 + 118.3200x^2 - 79.8055x + 14.2363$$

$$D_{66}(x) = -4.9081x^3 + 11.1717x^2 - 6.3473x + 1.0943$$

$$D_{16}(x) = 0;\ D_{26}(x) = 0;\ D_{61}(x) = 0;\ D_{62}(x) = 0$$

The coefficients D_{16}, D_{26}, D_{61} and D_{62} are zeros because of the 0/90 configuration. This is as same as that of the uniform plate. The other terms in D matrix are cubic functions of x because of the tapered configuration.

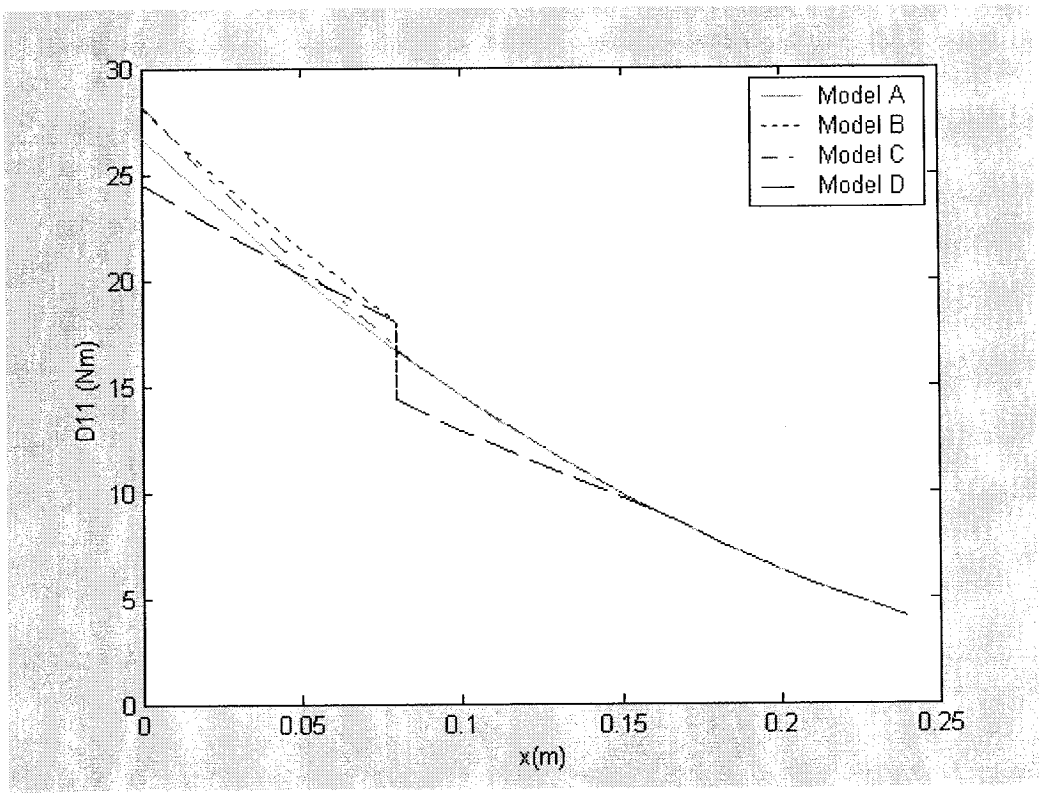

Figure 2.19 Coefficient D_{11} of tapered composite plate

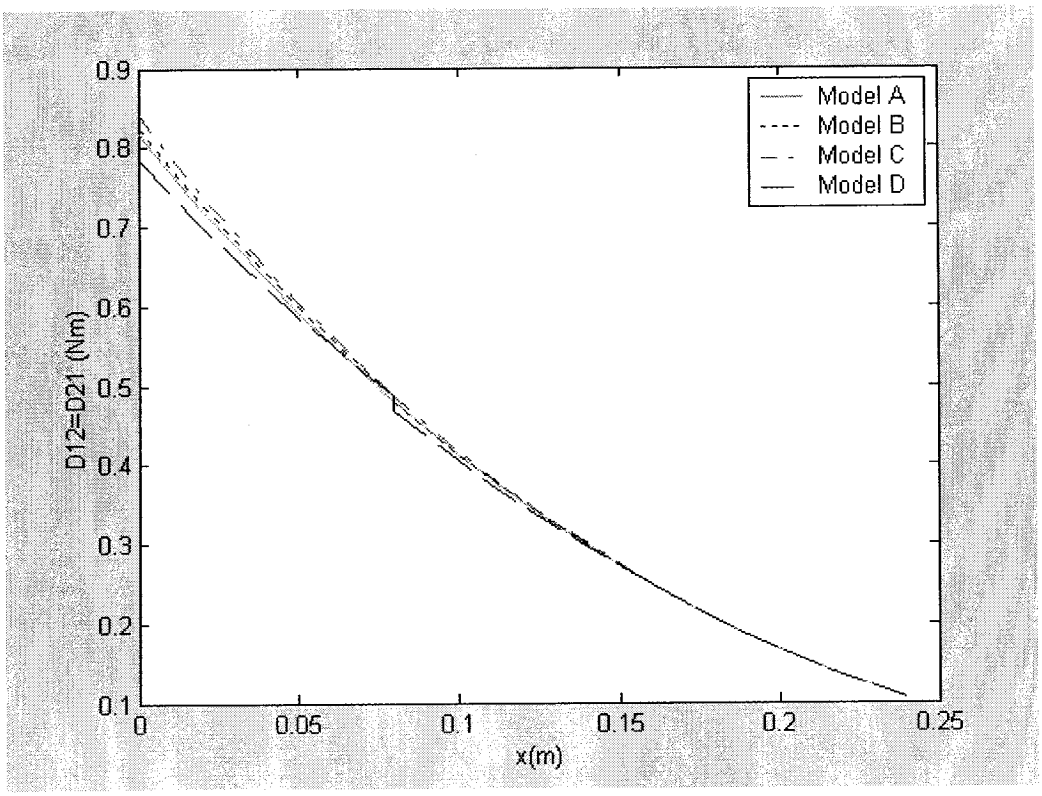

Figure 2.20 Coefficients D_{12} and D_{21} of tapered composite plate

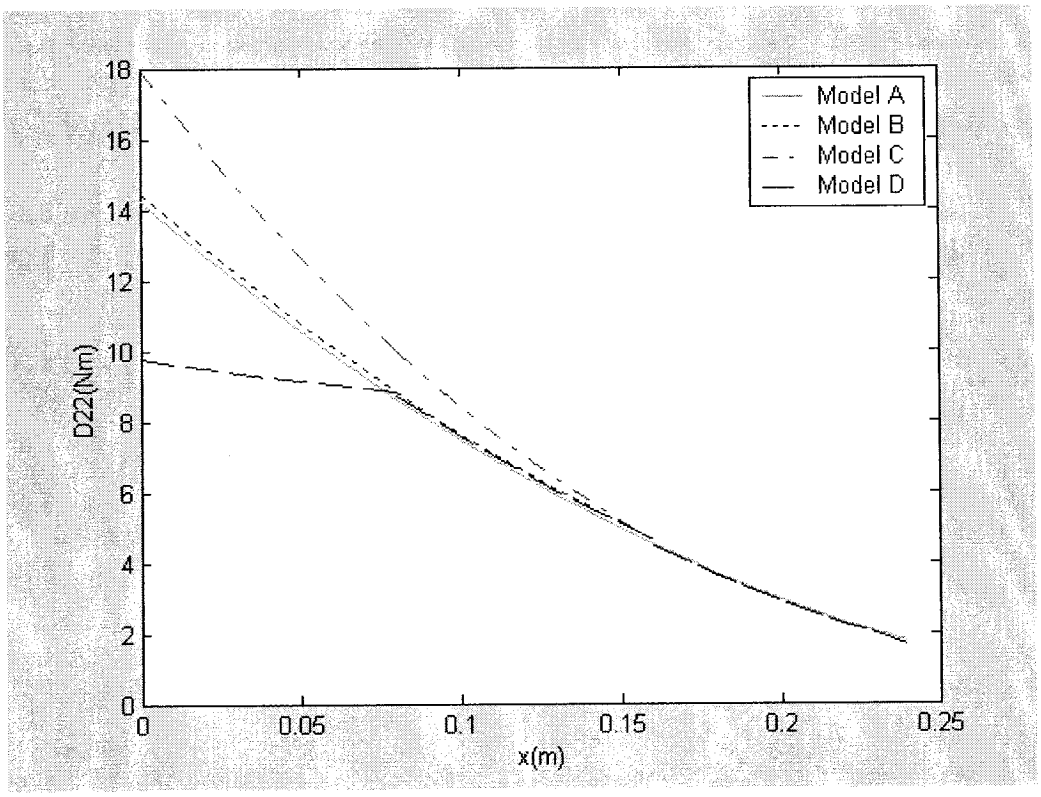

Figure 2.21 Coefficient D_{22} of tapered composite plate

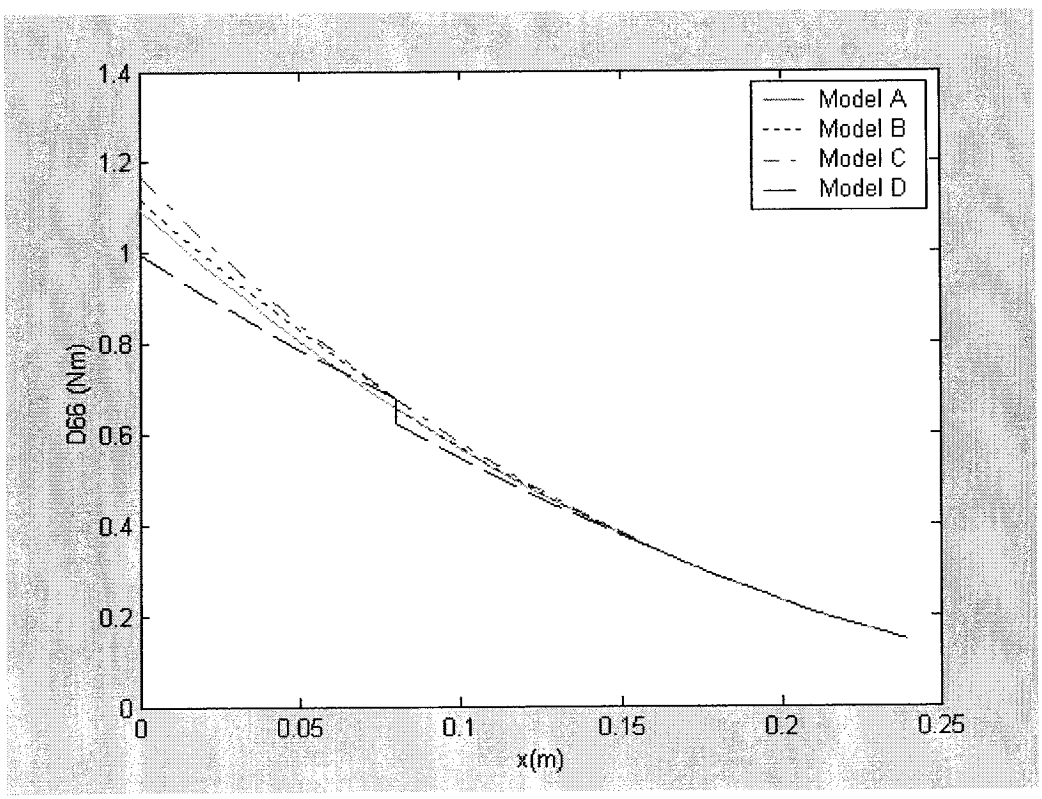

Figure 2.22 Coefficient D_{66} of tapered composite plate

In Figures 2.19, 2.20, 2.21 and 2.22, all the variations the coefficients are the same as in Figures 2.11, 2.12, 2.13 and 2.14 respectively, and the only difference is that the point O of the coordinate system is at the left side of the tapered composite laminates.

2.7 Conclusion

In this chapter, the stiffness and compliance matrices of both the uniform laminated plate and the tapered laminated plate have been determined. By using the derived equations, two example problems involving a uniform laminated plate and a tapered laminated plate have been solved. For the tapered laminated plate, four kinds of taper configurations, Configuration A, Configuration B, Configuration C and Configuration D, have been considered, and their mechanical behavior has been determined taking the resin pocket into consideration. Different coordinate systems were used in the calculation of the stiffness matrices of the tapered laminated plate with the objective of using them in the following chapter in the calculation of the dynamic response using Finite Element Method and Ritz (Energy) Method.

Chapter 3

Deflection Analysis of Tapered Composite Plates Using Finite Element Method and Ritz Method

3.1 Introduction

Composite materials, especially laminated composites are being increasingly used in the aerospace, mechanical and automobile industries. This is mainly because the composite materials exhibit high strength-to-weight and stiffness-to-weight ratios. The response to static loading is an important characteristic of composite laminates, and the accurate prediction of the effect of static loading is the first step in analyzing the effect of dynamic loadings on the composite structures.

By using the results of the preceding chapter, in this chapter, we use Finite Element Method and Ritz Method to analyze the deflections of different tapered composite plate configurations, when uniform loadings are distributed over the tapered composite plates. The maximum deflections of tapered composite plates are computed under different boundary conditions according to the classical laminated plate theory. These two methods give a practical way to predict the static response of the tapered

composite plates, which is an important step in conducting the analysis of dynamic characteristics of the tapered laminated plates in the following chapters.

In this thesis work, we consider that the tapered laminated plate is thin and the deflection is small. For the thin plate's bending with small deflection, we have the following assumptions [37]:

1. The middle plane of the plate remains neutral (undeformed) during bending.
2. Straight lines initially normal to the middle plane of the plate remain straight and normal to the middle surface. This assumption is equivalent to the neglect of the effect of transverse shear deformation.
3. The stresses normal to the middle surface are negligible.

The classical theory of laminates uses a first-order model. In this model the transverse shear strains are zero, therefore:

$$\gamma_{xz} = \gamma_{yz} = 0 \tag{3.1}$$

Hereafter, the displacement field can be written as follow:

$$u(x, y, z) = u_0(x, y) - z\frac{\partial w_0}{\partial x}(x, y) \tag{3.2}$$

$$v(x,y,z) = v_0(x,y) - z\frac{\partial w_0}{\partial y}(x,y) \tag{3.3}$$

$$w(x,y,z) = w_0(x,y) \tag{3.4}$$

where, u, v, and w are displacements in the x, y, and z directions in the coordinate system (x,y,z).

Therefore, the strain field is written as:

$$\varepsilon_{xx} = \frac{\partial u_0}{\partial x} - z\frac{\partial^2 w_0}{\partial x^2} \tag{3.5}$$

$$\varepsilon_{yy} = \frac{\partial v_0}{\partial y} - z\frac{\partial^2 w_0}{\partial y^2} \tag{3.6}$$

$$\gamma_{xy} = (\frac{\partial u_0}{\partial y} + \frac{\partial v_0}{\partial x}) - 2z\frac{\partial^2 w_0}{\partial x \partial y} \tag{3.7}$$

The strain field can also be written in the matrix form as follow:

$$\begin{bmatrix} \varepsilon_{xx} \\ \varepsilon_{yy} \\ \gamma_{xy} \end{bmatrix} = \begin{bmatrix} \varepsilon_{xx}^{\ 0} \\ \varepsilon_{yy}^{\ 0} \\ \gamma_{xy}^{\ 0} \end{bmatrix} + z\begin{bmatrix} k_x \\ k_y \\ k_{xy} \end{bmatrix} \tag{3.8}$$

where,

$\varepsilon_{xx}^{\ 0} = \frac{\partial u_0}{\partial x}(x,y)$, $\varepsilon_{yy}^{\ 0} = \frac{\partial u_0}{\partial x}(x,y)$, $\gamma_{xy}^{\ 0} = \frac{\partial u_0}{\partial y} + \frac{\partial v_0}{\partial x}$, and

$$k_x = -\frac{\partial^2 w_0}{\partial x^2}(x,y),\quad k_y = -\frac{\partial^2 w_0}{\partial y^2}(x,y),\quad k_{xy} = -2\frac{\partial^2 w_0}{\partial x \partial y}(x,y)$$

In the study of laminated plate bending, the most complex analysis is that of laminates made of an arbitrary stacking, presenting stretching-bending, stretching-twisting, and bending-twisting couplings. Here, we study the laminated plate of cross-ply symmetric lay-up configuration which has the following properties: there exists no in-plane stretching bending coupling, that is, $B_{ij} = 0$; there exists no bending-twisting coupling, that is, $D_{16} = D_{26} = 0$.

In Figure 3.1, we consider a rectangular plate subjected to a distributed transverse load $q = q(x,y)$. In the case of cross-ply symmetric laminates, the response can be expressed as:

$$A_{11}\frac{\partial^2 u_0}{\partial x^2} + A_{66}\frac{\partial^2 u_0}{\partial y^2} + (A_{12} + A_{66})\frac{\partial^2 v_0}{\partial x \partial y} = 0 \tag{3.9}$$

$$(A_{12} + A_{66})\frac{\partial^2 u_0}{\partial x \partial y} + A_{66}\frac{\partial^2 v_0}{\partial x^2} + A_{22}\frac{\partial^2 v_0}{\partial y^2} = 0 \tag{3.10}$$

$$D_{11}\frac{\partial^4 w_0}{\partial x^4} + 2(D_{12} + 2D_{66})\frac{\partial^4 w_0}{\partial x^2 \partial y^2} + D_{22}\frac{\partial^4 w_0}{\partial y^4} = q(x,y) \tag{3.11}$$

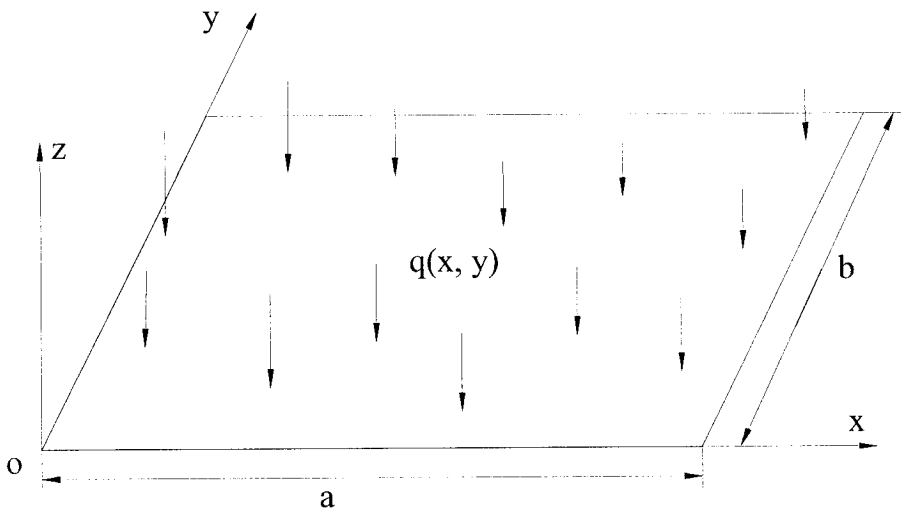

Figure 3.1 Rectangular Plate Subjected to a Distributed Load

In the general case, the transverse load can be expanded as a double Fourier sine series [22]:

$$q(x,y)=\sum_{m=1}^{\infty}\sum_{n=1}^{\infty}q_{mn}\sin\frac{m\pi x}{a}\sin\frac{n\pi y}{b} \tag{3.12}$$

where, the coefficients q_{mn} are given by:

$$q_{mn}=\frac{4}{ab}\int_0^b\int_0^a q(x,y)\sin\frac{m\pi x}{a}\sin\frac{n\pi y}{b}dxdy \tag{3.13}$$

The solutions to the bending problem can be investigated by expressing the displacements in the form of a double Fourier series satisfying different boundary conditions. For example, for the four-side-simple-supported boundary condition, we

can obtain the following equations:

$$u_0(x,y) = \sum_{m=1}^{\infty}\sum_{n=1}^{\infty} A_{mn} \cos\frac{m\pi x}{a} \cos\frac{n\pi y}{b} \tag{3.14}$$

$$v_0(x,y) = \sum_{m=1}^{\infty}\sum_{n=1}^{\infty} B_{mn} \cos\frac{m\pi x}{a} \cos\frac{n\pi y}{b} \tag{3.15}$$

$$w_0(x,y) = \sum_{m=1}^{\infty}\sum_{n=1}^{\infty} C_{mn} \sin\frac{m\pi x}{a} \sin\frac{n\pi y}{b} \tag{3.16}$$

By substituting $u_0(x,y)$ and $v_0(x,y)$ into the equations (3.9) and (3.10), we can get that $A_{mn} = 0$ and $B_{mn} = 0$. The in-plane displacements are identically zero: $u_0 = 0$, $v_0 = 0$.

3.2 Finite Element Analysis for the Deflection of the Tapered Composite Plate

3.2.1 Four-Node 12-D.O.F. Nonconforming Rectangular Element

According to the results above, we can select the Four-Node 12-D.O.F. Nonconforming Rectangular Element [37] to calculate the deflections of the tapered composite plates with different configurations using Finite Element Method. This kind of element is a typical rectangular element with four corner nodal points. It can be seen from Figure 3.2 that the element has length a, width b, and thickness 2h (changing along the x direction for tapered laminated plate configurations). Let us assume that the origin of the Cartesian coordinates is at the nodal point 1 and that

there are three degrees of freedom at each nodal point: deflection w; slope in the x direction, $w_x = \partial w / \partial x$; and slope in the y direction, $w_y = \partial w / \partial y$. Then we can derive the stiffness matrix by assuming the displacement function as a 12-term polynomial.

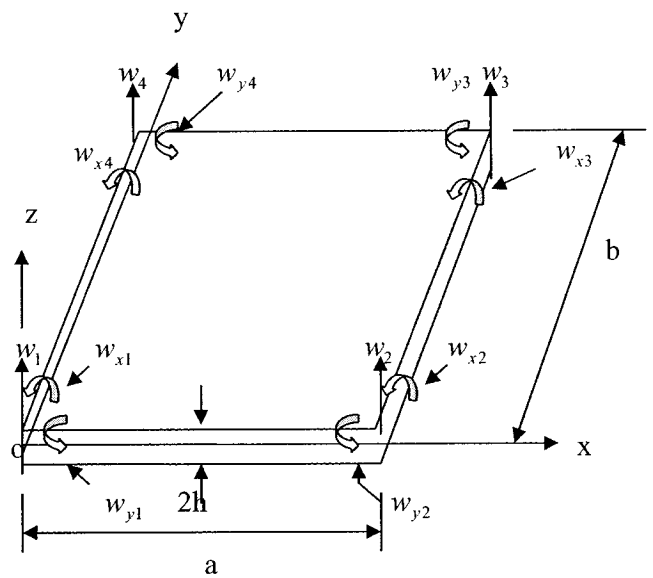

Figure 3.2 Four-node 12-d.o.f. rectangular plate bending element

The displacement function is assumed as

$$w(x,y) = c_1 + c_2 x + c_3 y + c_4 x^2 + c_5 xy + c_6 y^2 + c_7 x^3 + c_8 x^2 y + c_9 xy^2 + c_{10} y^3 + c_{11} x^3 y + c_{12} xy^3 \tag{3.17}$$

For the four nodal points (0, 0), (a, 0), (a, b), and (0, b), we can evaluate the values of the 12 nodal degrees of freedom based on the equation (3.17).

Therefore, the nodal degrees of freedom can be expressed as follow:

$$\begin{Bmatrix} w_1 \\ w_{x1} \\ w_{y1} \\ w_2 \\ w_{x2} \\ w_{y2} \\ w_3 \\ w_{x3} \\ w_{y3} \\ w_4 \\ w_{x4} \\ w_{y4} \end{Bmatrix} = \begin{bmatrix} 1 & 0 & 0 & 0 & 0 & 0 & 0 & 0 & 0 & 0 & 0 & 0 \\ 0 & 1 & 0 & 0 & 0 & 0 & 0 & 0 & 0 & 0 & 0 & 0 \\ 0 & 0 & 1 & 0 & 0 & 0 & 0 & 0 & 0 & 0 & 0 & 0 \\ 1 & a & 0 & a^2 & 0 & 0 & a^3 & 0 & 0 & 0 & 0 & 0 \\ 0 & 1 & 0 & 2a & 0 & 0 & 3a^2 & 0 & 0 & 0 & 0 & 0 \\ 0 & 0 & 1 & 0 & a & 0 & 0 & a^2 & 0 & 0 & a^3 & 0 \\ 1 & a & b & a^2 & ab & b^2 & a^3 & a^2b & ab^2 & b^3 & a^3b & ab^3 \\ 0 & 1 & 0 & 2a & b & 0 & 3a^2 & 2ab & b^2 & 0 & 3a^2b & b^3 \\ 0 & 0 & 1 & 0 & a & 2b & 0 & a^2 & 2ab & 3b^2 & a^3 & 3ab^2 \\ 1 & 0 & b & 0 & 0 & b^2 & 0 & 0 & 0 & b^3 & 0 & 0 \\ 0 & 1 & 0 & 0 & b & 0 & 0 & 0 & b^2 & 0 & 0 & b^3 \\ 0 & 0 & 1 & 0 & 0 & 2b & 0 & 0 & 0 & 3b^2 & 0 & 0 \end{bmatrix} \cdot \begin{Bmatrix} c_1 \\ c_2 \\ c_3 \\ c_4 \\ c_5 \\ c_6 \\ c_7 \\ c_8 \\ c_9 \\ c_{10} \\ c_{11} \\ c_{12} \end{Bmatrix} \tag{3.18}$$

or symbolically,

$$\{q\} = [\alpha] \cdot \{c\} \tag{3.19}$$

And then

$$\{c\} = [\alpha]^{-1} \cdot \{q\} = [\beta] \cdot \{q\} \tag{3.20}$$

The strain field of the laminated plate can be written using equations (3.5), (3.6), and (3.7).

By considering the thin plate and small deflection assumption, we can simplify the equations (3.5), (3.6) and (3.7) as follow:

$$\varepsilon_{xx} = -z\frac{\partial^2 w_0}{\partial x^2} \tag{3.21}$$

$$\varepsilon_{yy} = -z\frac{\partial^2 w_0}{\partial y^2} \tag{3.22}$$

$$\gamma_{xy} = -2z\frac{\partial^2 w_0}{\partial x \partial y} \tag{3.23}$$

By substituting equation (3.17) into (3.21), (3.22), and (3.23), the strain-displacement relations are written as follow:

$$\begin{Bmatrix} \varepsilon_x \\ \varepsilon_y \\ \gamma_{xy} \end{Bmatrix} = -z\begin{Bmatrix} \partial^2 w/\partial x^2 \\ \partial^2 w/\partial y^2 \\ 2\cdot\partial^2/\partial x\partial y \end{Bmatrix} = -z\begin{bmatrix} 0 & 0 & 0 & 2 & 0 & 0 & 6x & 2y & 0 & 0 & 6xy & 0 \\ 0 & 0 & 0 & 0 & 0 & 2 & 0 & 0 & 2x & 6y & 0 & 6xy \\ 0 & 0 & 0 & 0 & 2 & 0 & 0 & 4x & 4y & 0 & 6x^2 & 6y^2 \end{bmatrix} \begin{Bmatrix} c_1 \\ c_2 \\ c_3 \\ c_4 \\ c_5 \\ c_6 \\ c_7 \\ c_8 \\ c_9 \\ c_{10} \\ c_{11} \\ c_{12} \end{Bmatrix}$$

$$= [G_1]\cdot\{c\} = [G_1]\cdot[\beta]\cdot\{q\} = [A_1]\cdot\{q\} \tag{3.24}$$

Hereafter, the element stiffness matrix can be derived by first formulating the strain energy for the element and then performing partial differentiation of the strain energy

with respect to each degree of freedom following Castigliano's theorem [34].

The strain energy in the subject finite element is in the form [34]

$$U = \frac{1}{2}\int_0^a \int_0^b \int_{-h}^{h} \{\varepsilon\}^T \{\sigma\} dz dy dx \tag{3.25}$$

where,

$$\{\varepsilon\} = \begin{Bmatrix} \varepsilon_{xx} \\ \varepsilon_{yy} \\ \gamma_{xy} \end{Bmatrix} \quad \text{and} \quad \{\sigma\} = \begin{Bmatrix} \sigma_{xx} \\ \sigma_{yy} \\ \tau_{xy} \end{Bmatrix}$$

By considering the stress-strain relations for composite laminates and using equation (3.24), we obtain the following:

$$\{\sigma\} = [Q]\{\varepsilon\} = [Q][A_1]\{q\} \tag{3.26}$$

By substituting the equation (3.26) into (3.25), the following equation of strain energy can be obtained:

$$\begin{aligned} U &= \frac{1}{2}\int_0^a \int_0^b \int_{-h}^{h} \{q\}^T [A_1]^T [Q][A_1]\{q\} dx dy dz \\ &= \frac{1}{2}\{q\}^T \left[\int_0^a \int_0^b \int_{-h}^{h} [A_1]^T [Q][A_1] dx dy dz\right]\{q\} \end{aligned} \tag{3.27}$$

Applying Castigliano's first theorem [37],

$$F_i = \frac{\partial U}{\partial q_i} \tag{3.28}$$

By performing partial differentiation of the strain energy with respect to each of the degrees of freedom of the finite element, we obtain:

$$\{F\} = [k]\{q\} \tag{3.29}$$

$\{F\}$: the vector of the nodal forces of the element

$\{q\}$: the vector of nodal displacements of the element

$[k]$: the stiffness matrix of the element

The stiffness matrix of the element can be obtained as:

$$[k] = \sum_{k=1}^{n} \int_0^a \int_0^b \int_{h_{k-1}}^{h_k} [A_1]^T \cdot [Q]_k \cdot [A_1] \cdot dxdydz \tag{3.30}$$

Here, we set $[a] = \frac{1}{z} \cdot [A_1]$. Therefore, we can obtain the following equation:

$$[k] = \sum_{k=1}^{n} \int_0^a \int_0^b \int_{h_{k-1}}^{h_k} z \cdot [a]^T \cdot [Q]_k \cdot z \cdot [a] \cdot dxdydz \tag{3.31}$$

By using the method of calculating material's mechanical behavior as in chapter 2, we can get the following equation:

$$\sum_{k=1}^{n} \int_{h_{k-1}}^{h_k} z^2 \cdot [Q]_k \cdot dz = [D] \tag{3.32}$$

Since the thickness of the tapered composite plate changes in x direction, we can write the mechanical behavior of the tapered composite plate as follow:

$$[D] = [D(x)] \tag{3.33}$$

The mechanical behaviors of the tapered composite plate configurations can be calculated by using the method in chapter 2 of this thesis. Therefore, the stiffness matrix of the element of the tapered composite plate is expressed as:

$$[k] = \int_0^a \int_0^b [a]^T D(x)[a] dxdy \tag{3.34}$$

3.2.2 The Structure Stiffness Matrix and the Treatment of Boundary Condition

For the stiffness equation of the complete structure, we can do the systematic addition of the stiffness matrix of all elements. The system stiffness equation can be expressed as

$$\{P\} = [K] \cdot \{Q_1\} \tag{3.35}$$

$\{P\}$: the vector of the nodal forces of the structural system

$\{Q_1\}$: the vector of nodal displacements of the structural system

$[K]$: the stiffness matrix of the structural system

According to the loads applied to the tapered laminated plate, we can get $\{P\}$.

Using the boundary condition, we can solve the equation (3.35) above and get the result of $\{Q_1\}$.

Calculation of the stiffness matrix of the tapered laminated plate can be done as follow. For example, we can consider the 4×4 mesh to calculate the stiffness matrix of the structural system, and the element numbering is done just as in the following Figure 3.3.

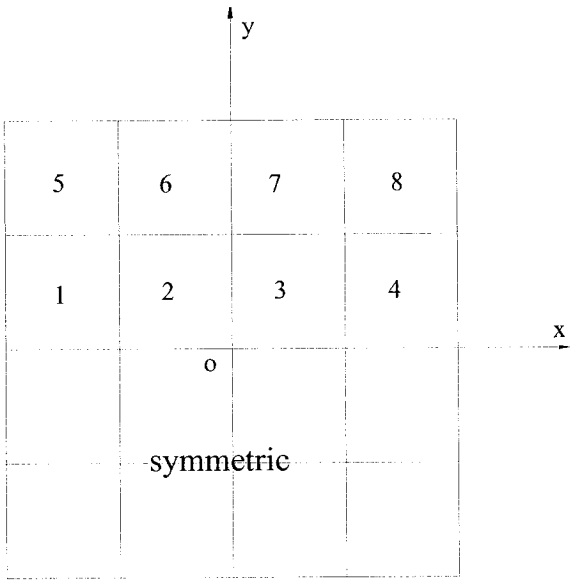

Figure 3.3 The 4×4 *mesh of the plate model*

We can calculate the stiffness matrices $[k]_1$, $[k]_2$, $[k]_3$ and $[k]_4$ for elements 1, 2, 3 and 4 by using equation (3. 34).

If this plate is a tapered plate and the thickness changes in x direction, the stiffness matrices $[k]_1$, $[k]_2$, $[k]_3$ and $[k]_4$ should be different. We can assemble the structure stiffness matrix by using the element stiffness matrices $[k]_1$, $[k]_2$, $[k]_3$, $[k]_4$, $[k]_5$, $[k]_6$, $[k]_7$, and $[k]_8$. Matrices $[k]_5$, $[k]_6$, $[k]_7$, and $[k]_8$ have the same value as matrices $[k]_1$, $[k]_2$, $[k]_3$, $[k]_4$ respectively. We can get the structure stiffness matrix $[K]$ by assembling these matrices.

According to the applied forces on the plate, by considering the elements of the plate, we can get the vector of the nodal forces of the structural system $\{P\}$. Then, by use

of equation (3.35), we will get the vector of the nodal displacements $\{Q_1\}$.

By considering the boundary condition, it is common and efficient practice to formulate the condensed stiffness matrix $[K]'$ instead of the whole stiffness matrix $[K]$ based on the zero-displacement conditions. By use of the condensed stiffness matrix $[K]'$ for different boundary conditions, we can get the displacement results that correspond to different boundary conditions.

In this thesis work, we consider three kinds of boundary conditions as follow:

1. simple support for four edges
2. four edges clamped
3. one edge clamped and other three edges free.

Finally, we can get $\{Q_1\}$ for different boundary conditions. From these, we can get the maximum deflection of the plate and the corresponding boundary condition for the tapered composite plate configuration.

As another example, we can consider the 6×6 mesh to calculate the stiffness matrix of the structural system, and the element numbering is done just as in the following Figure 3.4.

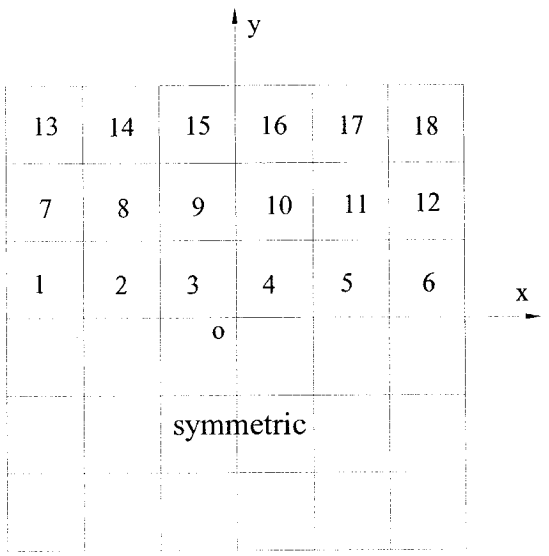

Figure 3.4 The 6×6 mesh of the plate

Similarly, we can calculate the stiffness matrices $[k]_1$, $[k]_2$, $[k]_3$, $[k]_4$, $[k]_5$ and $[k]_6$ that correspond to elements 1, 2, 3, 4, 5 and 6 by using equation (3. 34).

If we consider the tapered composite plate configuration, the thickness of the plate changes in x direction, and therefore matrices $[k]_1$, $[k]_2$, $[k]_3$, $[k]_4$, $[k]_5$ and $[k]_6$ should have different values that correspond to elements, 1, 2, 3, 4, 5, and 6. By using the procedure that was used for the 4×4 mesh, we can assemble the structure stiffness matrix using the element stiffness matrices $[k]_1$, $[k]_2$, $[k]_3$, $[k]_4$, $[k]_5$, $[k]_6$, $[k]_7$, $[k]_8$, $[k]_9$, $[k]_{10}$, $[k]_{11}$, $[k]_{12}$, $[k]_{13}$, $[k]_{14}$, $[k]_{15}$, $[k]_{16}$, $[k]_{17}$, and $[k]_{18}$. Matrices $[k]_1$, $[k]_2$, $[k]_3$, $[k]_4$, $[k]_5$, and $[k]_6$ have the same values as the matrices $[k]_7$, $[k]_8$, $[k]_9$, $[k]_{10}$, $[k]_{11}$ and $[k]_{12}$, and matrices $[k]_{13}$, $[k]_{14}$, $[k]_{15}$,

$[k]_{16}$, $[k]_{17}$, and $[k]_{18}$ respectively. We can get the structure stiffness matrix $[K]$ by assembling these matrices.

As in the case of 4×4 mesh, by considering three kinds of boundary conditions, i.e. simple support for four edges, four edges camped and one edge clamped with other three edges free, we can get the $\{Q_1\}$ for the cases of different boundary conditions. Finally, we can get the maximum deflection of the plate for different tapered composite plate configurations.

3.3 Deflection of the Tapered Composite Plate Based on Ritz Method

The energy theorems can be used to obtain a variational formulation of the governing equations of the laminate. This formulation with associated boundary conditions provides the basis for the development of approximate solutions of the mechanical behavior of laminates [22].

The strain energy of an elastic solid can be written in Cartesian coordinates as follows:

$$U_d = \frac{1}{2}\iiint(\sigma_{xx}\varepsilon_{xx} + \sigma_{yy}\varepsilon_{yy} + \sigma_{zz}\varepsilon_{zz} + \tau_{xz}\gamma_{xz} + \tau_{yz}\gamma_{yz} + \tau_{xy}\gamma_{xy})dxdydz \qquad (3.36)$$

By taking into account the assumptions of the classical theory of laminates, we can obtain that $\sigma_{zz} = 0$, $\gamma_{xz} = \gamma_{yz} = 0$, and the following equation:

$$\begin{bmatrix} \sigma_{xx} \\ \sigma_{yy} \\ \tau_{xy} \end{bmatrix}_k = \begin{bmatrix} Q_{11} & Q_{12} & Q_{16} \\ Q_{12} & Q_{22} & Q_{26} \\ Q_{16} & Q_{26} & Q_{66} \end{bmatrix}_k \cdot \begin{bmatrix} \varepsilon_{xx} \\ \varepsilon_{yy} \\ \gamma_{xy} \end{bmatrix} \tag{3.37}$$

It may be noted that the kinematic assumptions of Euler-Bernoulli beam bending theory and classical laminate theory correspond to the assumption that $\sigma_{zz} = \gamma_{xz} = \gamma_{yz} = 0$. Therefore, the strain energy can be written as:

$$U_d = \frac{1}{2}\iiint (Q^k{}_{11}\varepsilon_{xx}{}^2 + Q^k{}_{22}\varepsilon_{yy}{}^2 + Q^k{}_{66}\gamma_{xy}{}^2 + 2Q^k{}_{12}\varepsilon_{xx}\varepsilon_{yy} + 2Q^k{}_{16}\varepsilon_{xx}\gamma_{xy} + 2Q^k{}_{26}\varepsilon_{yy}\gamma_{xy})dxdydz \tag{3.38}$$

where, the constants $Q^k{}_{11}$, $Q^k{}_{22}$, $Q^k{}_{66}$, $Q^k{}_{12}$, $Q^k{}_{16}$, and $Q^k{}_{26}$ are reduced stiffness constants of the $k-th$ layer of the composite laminate. For cross-ply laminate, $Q^k{}_{16} = Q^k{}_{26} = 0$.

The equation (3.38) can be written as a function of the displacement by substituting the equations (3.21), (3.22) and (3.23) into the preceding expression. In the case of symmetric laminates, the stretching-bending coupling terms B_{ij} are zero. In case of pure bending and orthotropic plates, the strain energy can be written as follow:

$$U_d = \frac{1}{2}\int_0^a \int_0^b [D_{11}(\frac{\partial^2 w_0}{\partial x^2})^2 + 2D_{12}\frac{\partial^2 w_0}{\partial x^2}\frac{\partial^2 w_0}{\partial y^2} + D_{22}(\frac{\partial^2 w_0}{\partial y^2})^2 + 4D_{66}(\frac{\partial^2 w_0}{\partial x \partial y})^2]dxdy + C \tag{3.39}$$

As we can see in Figure 3.1, in the case of transverse loading, the potential energy owed to distributed transverse load $q = q(x, y)$ is written as:

$$W_f = \int_0^a \int_0^b q(x,y) w_0(x,y) dxdy \tag{3.40}$$

The shape function can be written in a double series to satisfy the different boundary conditions as follow:

$$w_0(x,y) = \sum_{m=1}^{M}\sum_{n=1}^{N} A_{mn} X_m(x) Y_n(y) \tag{3.41}$$

Here, the coefficients A_{mn} are determined by the stationary condition.

We can express the potential energy of the structure and its derivative using the following equations [38]:

$$U = U_d - W_f \tag{3.42}$$

$$\frac{\partial U}{\partial A_{mn}} = \frac{\partial (U_d - W_f)}{\partial A_{mn}} = 0 \tag{3.43}$$

where, U_d and W_f are the strain energy and the potential energy owed to the transverse load, obtained by substituting the expression (3.41) for the deflection into equations (3.39) and (3.40) respectively.

By considering different boundary conditions, we can obtain different shape functions for use in equation (3.41). Then, W_f can be obtained considering transverse load $q = q(x, y)$ applied. By substituting U_d and W_f into equation (3.43), a system equation about the A_{mn} will be achieved, thereafter, the solution of the system allows us to find the coefficients A_{mn} and to deduce the transverse displacement at each point (x, y) by using equation (3.41).

The maximum deflection of the tapered composite plate can be obtained by substituting the coefficients A_{mn} into the equations given below for different boundary conditions:

1. When we consider the boundary condition of simple support for four edges of the tapered composite plate, the shape function can be written as [22]

$$w_0(x, y) = \sum_{m=1}^{M} \sum_{n=1}^{N} A_{mn} \cdot \sin \frac{m\pi x}{a} \cdot \sin \frac{n\pi y}{b} \tag{3.44}$$

2. When we consider the boundary condition of four edges clamped for the tapered composite plate, the shape function can be written as [22]

$$w_0(x,y)=\sum_{m=1}^{M}\sum_{n=1}^{N}A_{mn}\cdot\frac{x^2}{a^2}\left(\frac{x}{a}-1\right)^2\left(\frac{x}{a}\right)^{m-1}\cdot\frac{y^2}{b^2}\cdot\left(\frac{y}{b}-1\right)^2\left(\frac{y}{b}\right)^{m-1} \tag{3.45}$$

3. When we consider the boundary condition of one edge clamped and the other three edges free for the tapered composite plate, the shape function can be written as [39]:

$$w(x)=\sum_{n=1}^{N}A_n(1-\cos\frac{\pi x(n-1)}{2a}) \tag{3.46}$$

If the boundary conditions are simple support for four sides and clamped for four sides, we set $x=\frac{a}{2}$, and $y=\frac{b}{2}$, so the maximum deflection can be obtained as follow:

$$w_{\max}(x,y)=\sum_{m=1}^{M}\sum_{n=1}^{N}A_{mn}X_m(\frac{a}{2})Y_n(\frac{b}{2}) \tag{3.47}$$

If the boundary condition is one side clamped and the other three sides free, we set $x=a$, and so the maximum deflection can be obtained as follow:

$$w(x)=\sum_{n=1}^{N}A_n(1-\cos\frac{\pi a(n-1)}{2a}) \tag{3.48}$$

In the following example, for the first two boundary conditions, we set m = n = 2 and m = n = 3 to calculate the maximum deflections of different kinds of tapered

composite plate configurations. And for the third boundary condition, n = 9 is considered.

3.4 The Example for Calculating the Deflections of the Four Tapered Composite Plate Configurations Subjected to Distributed Transverse Loading

In this part, we consider four different kinds of tapered composite plate configurations, Configuration A, Configuration B, Configuration C, and Configuration D, which can be seen in Figure 2.7, Figure 2.8, Figure 2.9, and Figure 2.10 respectively. By using Finite Element Method and Ritz Method, we can get the results of the maximum deflections of the four tapered composite plate configurations which are subjected to distributed transverse loads.

The four tapered composite plate configurations considered here are made up with 12 plies in the left side and 6 plies in the right side, and the composite material is NCT/301 graphite-epoxy. The mechanical properties of NCT/301 are: $E_1 = 113.9$ GPa, $E_2 = E_3 = 7.9$ GPa, $\nu_{12} = 0.28$, $\nu_{23} = 0.4$, $\nu_{13} = 0.02$, $G_{12} = 3.1$ GPa, $G_{13} = 3.1$ GPa, $G_{23} = 2.8$ GPa, $\rho = 1480\ kg/m^3$, $h_0 = 0.138$ mm.

The geometric properties of the tapered composite plates are: the length a is 240 mm and the width b is 240 mm; the thickness changes in x direction from 2.208 mm to 1.104 mm; the laminates for Configuration A, Configuration B and Configuration C

are $[(90/0)_3]_s$ in the left side and $(0/90/0)_s$ in right side. For configuration D, the tapered plate has lay-up configuration $[0/resin/90/0/0/90]_s$ at the left end and $[0/90/0]_s$ at the right end respectively.

3.4.1 Solution Using Finite Element Method

In this example, the problem is solved using 36 finite elements to obtain accurate results of the maximum deflections of the four kinds of tapered composite plate configurations under three kinds of boundary conditions:

1. simple support for the four edges of the tapered composite plate
2. four edges of the tapered composite plate clamped
3. one edge of the tapered composite plate is clamped and the other three edges are free

A distributed load of $2000N/m^2$ is applied on the four kinds of tapered composite plate configurations. By using the results of the mechanical behaviors of the four kinds of tapered plate configurations calculated in the chapter 2, we obtained the results of the maximum deflections given in the Tables 3.1, 3.2, 3.3 and 3.4. The coordinate system used in the finite element analysis is as in Figure 3.5.

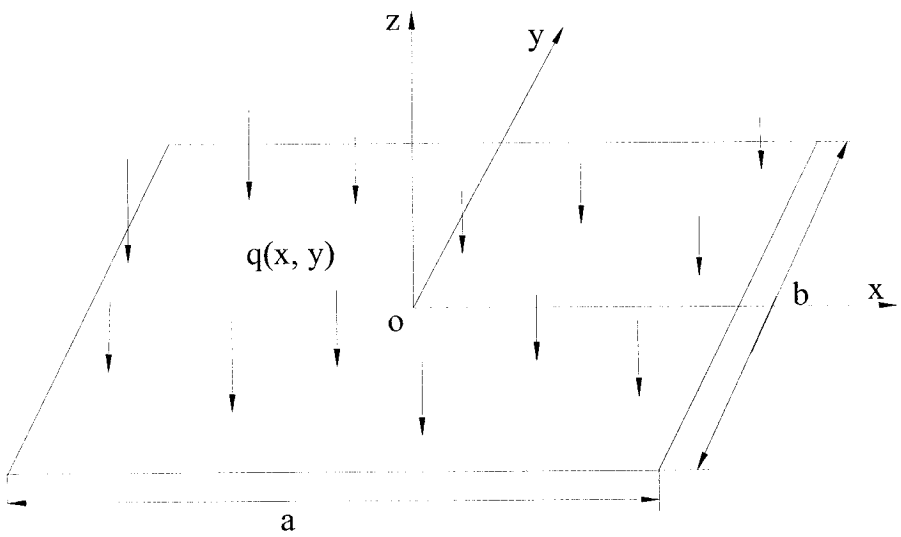

Figure 3.5 Rectangular Plate Subjected to a Distributed Load with Point O at the center of the plate

3.4.2 Solution Using Ritz Method

The problem is also solved using Ritz Method. For the first two boundary conditions, we set m = n = 2 and m = n = 3 to analyze the four different kinds of tapered composite plate configurations for the maximum deflections. For the third boundary condition, n = 9 is considered.

A distributed load of $2000N/m^2$ is applied on the four kinds of tapered composite plates. By using the results of the mechanical behaviors of the four kinds of the tapered plate configurations calculated in the chapter 2, we obtained the results of the maximum deflections given in the Tables 3.1, 3.2, 3.3 and 3.4. The coordinate system used in Ritz Method is the same as in Figure 3.1.

3.4.3 The Results of the Maximum Deflections Calculated Using Finite Element Method and Ritz Method

1. Boundary condition: Four edges of the tapered laminated plate simply supported

For the distributed load of $2000N/m^2$ applied on the tapered composite plates, the results of deflections for four kinds of taper configurations are calculated by using Finite Element Method and Ritz Method (two terms and three terms). In Table 3.1 and Figure 3.6, we can see all the deflection results.

Table 3.1 Deflections (in: $\times 10^{-2}$ m) of Four Taper Configurations Subjected to Uniformly Distributed Loading and with Four Simply Supported Edges

Taper Configuration	Finite Element Solution				Ritz Solution			
	12 elements	24 elements	36 elements	48 elements	5-Terms	4-Terms	3-Terms	2-Terms
A	0.4928	0.4980	0.5002	0.5008	0.5301	0.5301	0.5303	0.5371
B	0.4851	0.4905	0.4927	0.4932	0.5236	0.5236	0.5238	0.5304
C	0.4740	0.4780	0.4807	0.4813	0.5107	0.5107	0.5109	0.5175
D	0.5136	0.5178	0.5206	0.5215	0.5416	0.5416	0.5418	0.5528

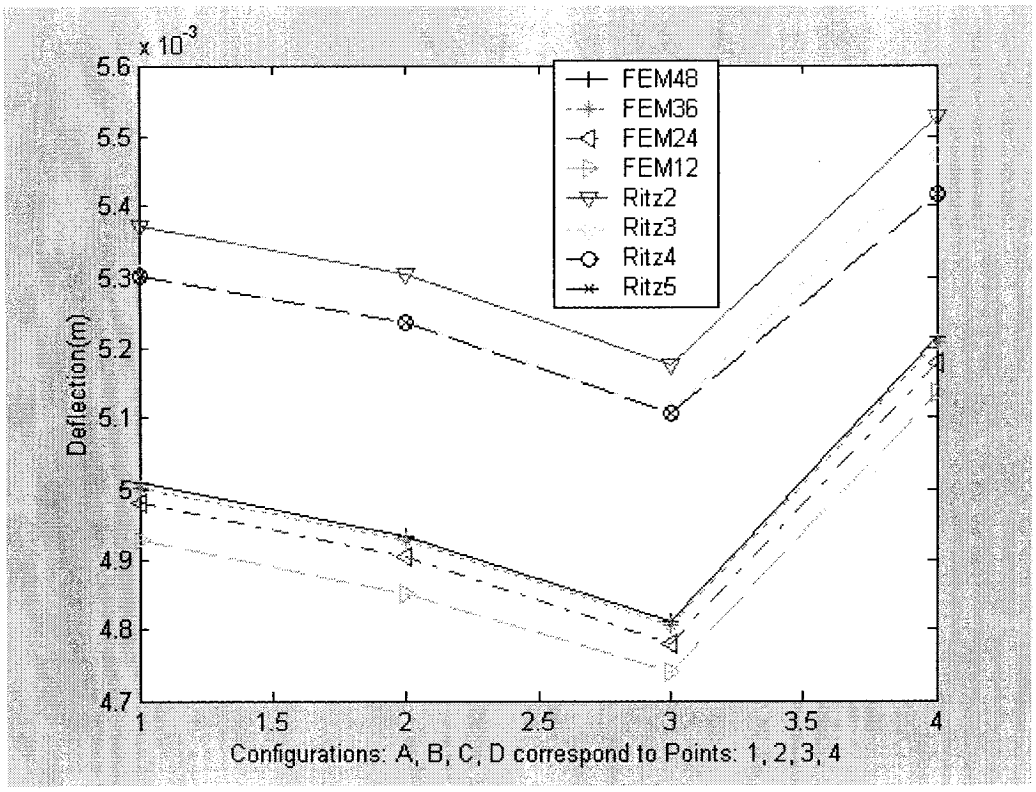

Figure 3.6 Deflections of Four Taper Configurations Subjected to Uniformly Distributed Loading and with Four Simply Supported Edges

In table 3.1, we can see that the results of 36 elements and 48 elements using finite element method are much closer, and the results of 3 terms, 4 terms and 5 terms using Ritz method are also much closer. Therefore, the 36 elements result for finite element method and 3 terms results for Ritz method are used as converged results to be compared below.

The graphs in Figure 3.6 show the deflections of the four taper configurations calculated by Finite Element Method and Ritz Method (two terms and three terms). Both the methods give the same result that the Configuration D has largest deflection due to the position of resin pockets far from the mid-plane, and that the Configuration C has the smallest deflection. The deflections change from small to large in the order of Configuration C, Configuration B, Configuration A, and Configuration D. The results of Finite Element Method are much closer to that of the Ritz Method solution using three terms than the Ritz Method solution using two terms, and the three solutions show the same tendency of deflections with the change in the taper configuration.

2. Boundary Condition: Four Plate Edges Clamped

For the distributed load of $2000N/m^2$ applied on the tapered composite plates, the results of deflections for four kinds of taper configurations are calculated by using Finite Element Method and Ritz Method (three terms). In Table 3.2 and Figure 3.7,

we can see all the deflection results.

Table 3.2 Deflections (in m) of Four Taper Configurations Subjected to Uniformly Distributed Loading and with Four Edges Clamped

Taper Configuration	Finite Element Solution (36 elements)	Ritz 3-terms Solution
A	0.115426×10^{-2}	0.110012×10^{-2}
B	0.112762×10^{-2}	0.106640×10^{-2}
C	0.110397×10^{-2}	0.105877×10^{-2}
D	0.119962×10^{-2}	0.112570×10^{-2}

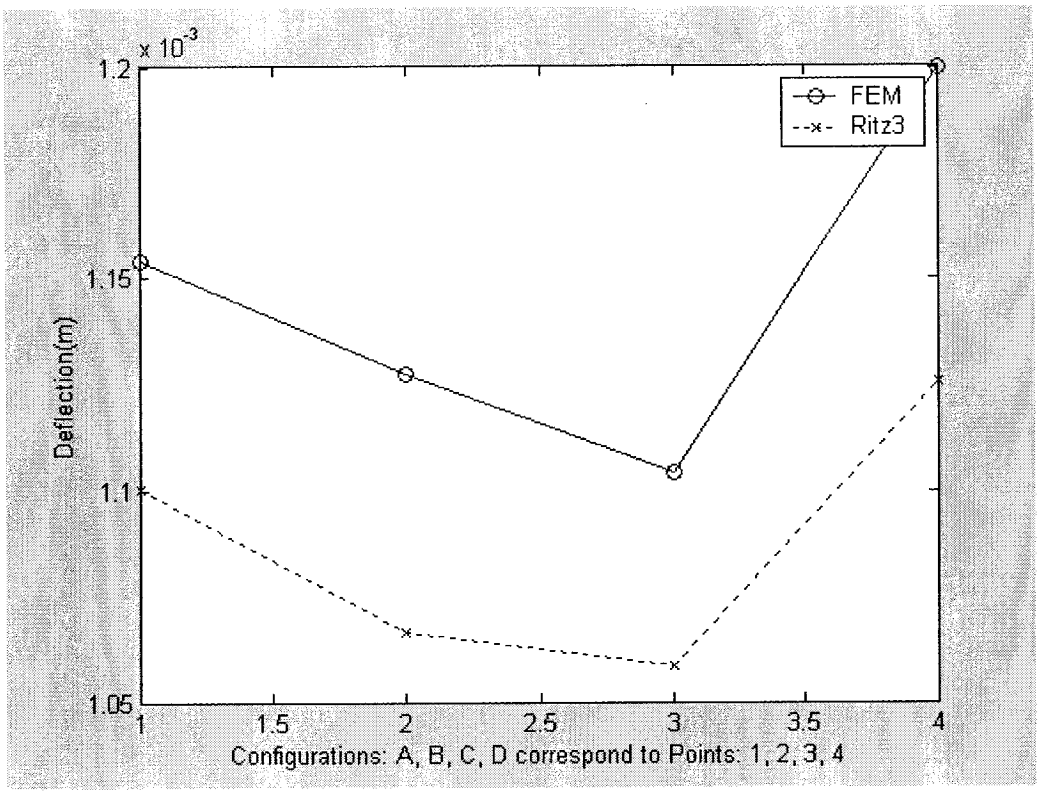

Figure 3.7 Deflections of Four Taper Configurations Subjected to Uniformly Distributed Loading and with Four Edges Clamped

The graphs in Figure 3.7 show the deflections of the four taper configurations calculated by Finite Element Method and Ritz Method (three terms). Both the methods give the same result that the Configuration D has largest deflection due to the position of resin pockets, and that the Configuration C has the smallest deflection. The deflections change from small to large in the order of Configuration C, Configuration B, Configuration A, and Configuration D. The results of Finite Element Method are much closer to that of the Ritz Method solution using three terms, and the two solutions show the same tendency of deflections with the change in the taper configuration. The deflection tendencies are very similar in Figure 3.6 and Figure 3.7.

3. Boundary condition: One Plate Edge Clamped and Three Edges Free

For the distributed load of $2000N/m^2$ applied on the tapered composite plates, in the first step, the results of deflections at the center for four kinds of taper configurations are calculated by using Finite Element Method and Ritz Method (three terms). In Table 3.3 and Figure 3.8, we can see all the deflection results.

Table 3.3 Deflections (in m) at the Center of Four Taper Configurations Subjected to Uniformly Distributed Loading and with One Edge Clamped and Three Edges Free

Taper Configuration	Finite Element Solution (36 elements)	Ritz 9-terms Solution
A	0.134777×10^{-1}	0.117111×10^{-1}
B	0.127684×10^{-1}	0.111051×10^{-1}
C	0.130290×10^{-1}	0.113447×10^{-1}
D	0.140101×10^{-1}	0.121468×10^{-1}

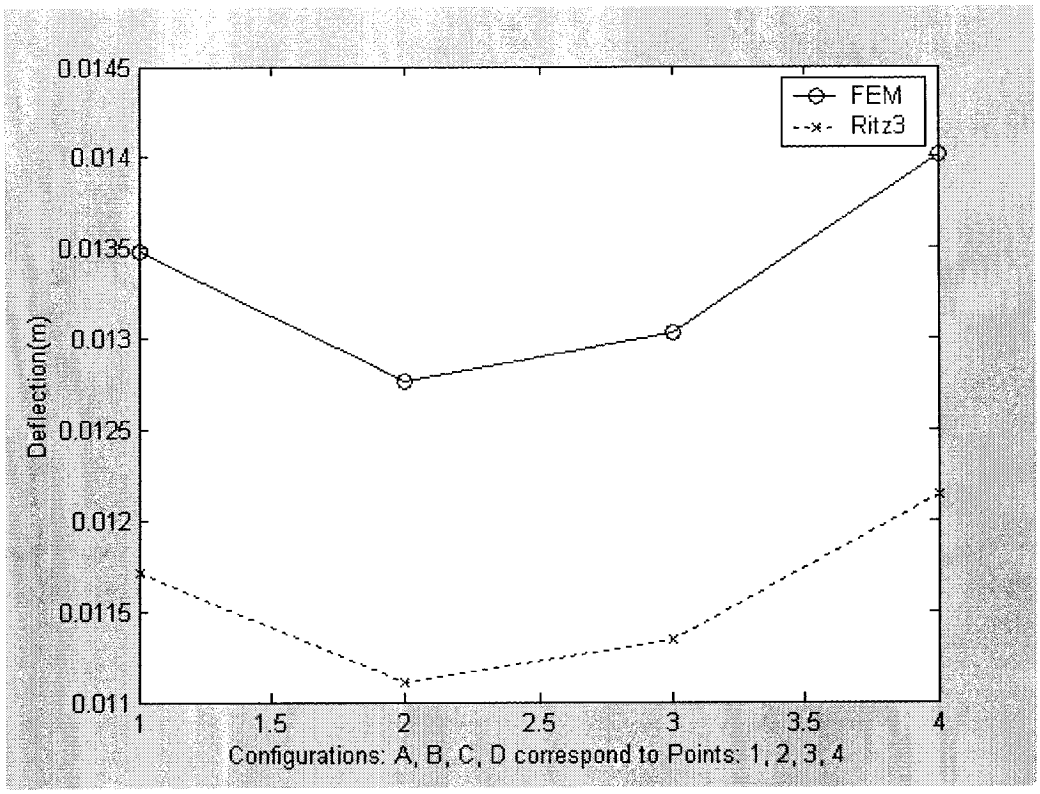

Figure 3.8 Deflections at the Center of Four Taper Configurations Subjected to Uniformly Distributed Loading and with One Edge Clamped and Three Edges Free

The graphs in Figure 3.8 show the deflections at the center of the four taper configurations calculated by Finite Element Method and Ritz Method (three terms). Both the methods give the same result that the Configuration D has largest deflection due to the position of resin pockets, and that Configuration B has the smallest deflection. The deflections change from small to large in the order of Configuration B, Configuration C, Configuration A, and Configuration D. The results of Finite Element Method are much closer to that of the Ritz Method solution using three terms, and the two solutions show the same tendency of deflections with the change in the taper configuration.

In the second step, the results of deflections at the free side for four kinds of taper configurations are calculated by using Finite Element Method and Ritz Method (three terms). In Table 3.4 and Figure 3.9, we can see all the deflection results.

Table 3.4 Deflections (in m) at the Free Edge of Four Taper Configurations Subjected to Uniformly Distributed Loading and with One Edge Clamped and Three Edges Free

Taper Configuration	Finite Element Solution (36 elements)	Ritz 9-terms Solution
A	0.433599×10^{-1}	0.458674×10^{-1}
B	0.415718×10^{-1}	0.443034×10^{-1}
C	0.422972×10^{-1}	0.449774×10^{-1}
D	0.452268×10^{-1}	0.477735×10^{-1}

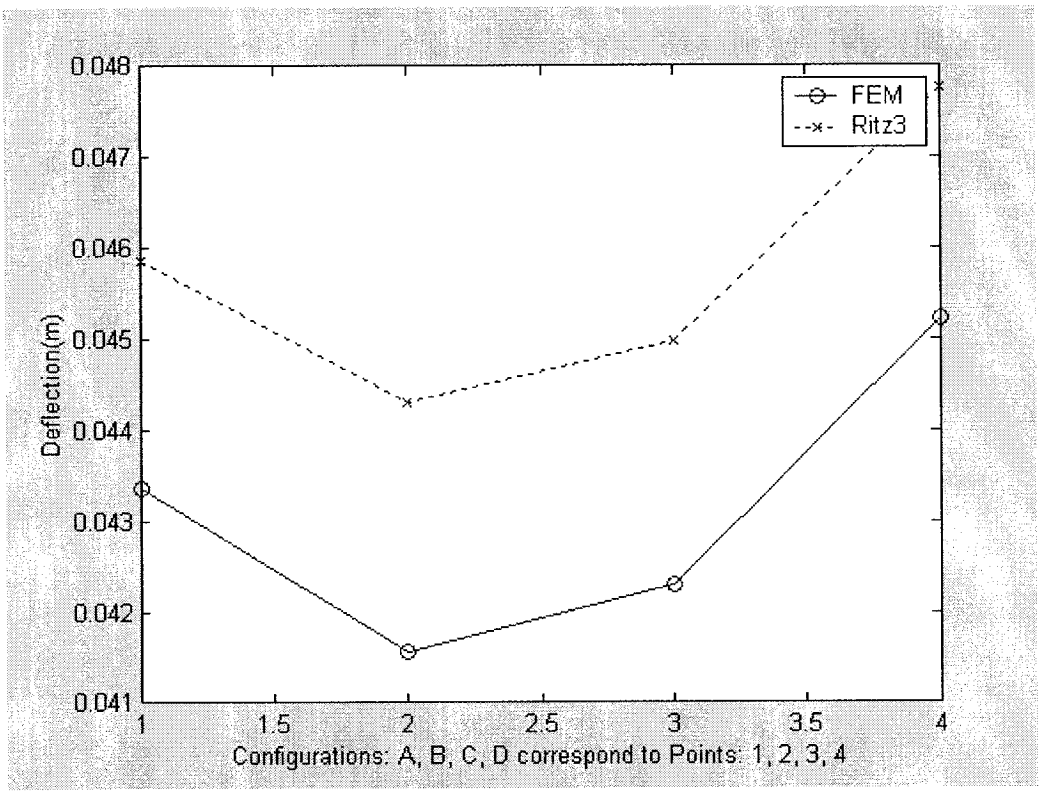

Figure 3.9 Deflections at the Free End Edge of Four Taper Configurations Subjected to Uniformly Distributed Loading and with One Edge Clamped and Three Edges Free

The graphs in Figure 3.9 show the deflections at the center of the four taper configurations calculated by Finite Element Method and Ritz Method (three terms). Both the methods give the same result that the Configuration D has largest deflection due to the position of resin pockets, and that Configuration B has the smallest deflection. The deflections change from small to large in the order of Configuration B, Configuration C, Configuration A, and Configuration D. The results of Finite Element Method are much closer to the Ritz Method solution using three terms, and the two

solutions show the same tendency of deflections with the change in the taper configuration. The tendency is the same as in Figure 3.8 for the deflections at the center of the plates.

3.5 Conclusion

In this chapter, the Finite Element Method and Ritz Method have been used to calculate the deflections of different tapered composite plate configurations. By using these two methods, the example problem involving four tapered composite plate configurations has been solved. For the tapered composite plate, four kinds of taper configurations, Configuration A, Configuration B, Configuration C and Configuration D, have been considered, and their deflections for the distributed load and for different boundary conditions have been determined by using Finite Element Method and Ritz Method, and using the mechanical behavior calculated in Chapter 2. Both the methods yield much closer results for deflection. In the following chapters, the calculation of the dynamic response is performed using the Finite Element Method and Ritz Method.

Chapter 4

Free Vibration Analysis of Uniform and Tapered composite Plates Using Finite Element Method and Ritz Method

4.1 Introduction

Composite plates are widely used in civil, mechanical and aerospace structures. In this chapter, the uniform composite plate configuration and four tapered composite plate configurations are considered. By using the thin plate assumption as in Chapter 3, in this chapter, we calculate the free vibration characteristics using Finite Element Method and Ritz Method. We will derive the formulations based on classical laminate theory for analyses using Finite Element Method and Ritz Method. By using the results of mechanical behavior of tapered composite plate configuration calculated in Chapter 2 and the stiffness matrix of tapered composite plate configuration calculated in Chapter 3, we can determine the free vibration response of uniform and tapered plate configurations. All the results will be used in instability analysis of different kinds of composite plate configurations in the following chapter.

4.2 Finite Element Analysis of the Free Vibration Response of Uniform and Tapered Composite Plates

When a plate undergoes free, undamped vibration, the deflection of the plate has a sinusoidal variation with respect to time t [23],

$$w = w_0 \cdot \sin \omega t \tag{4.1}$$

where, ω is called as the circular frequency.

By considering the symmetric cross-ply laminate analyzed in Chapter 3, the strain energy of the plate structure can be written as follow:

$$U_d = \frac{1}{2}\int_0^a \int_0^b [D_{11}(\frac{\partial^2 w}{\partial x^2})^2 + 2D_{12}\frac{\partial^2 w}{\partial x^2}\frac{\partial^2 w}{\partial y^2} + D_{22}(\frac{\partial^2 w}{\partial y^2})^2 + 4D_{66}(\frac{\partial^2 w}{\partial x \partial y})^2]dxdy \tag{4.2}$$

The kinetic energy of the vibrating plate in bending with small deflection:

$$T = \int_0^a \int_0^b \frac{\rho h}{2}(\dot{w})^2 dxdy = \frac{\rho}{2}\int_0^a \int_0^b h(\dot{w})^2 dxdy \tag{4.3}$$

By substituting the equation (4.1) into the equation (4.2), the strain energy equation is obtained:

$$U_d = U_{d\max} \sin^2 \omega t \tag{4.4}$$

where $U_{d\max}$ is defined as

$$U_{d\max} = \frac{1}{2}\int_0^a \int_0^b [D_{11}(\frac{\partial^2 w_0}{\partial x^2})^2 + 2D_{12}\frac{\partial^2 w_0}{\partial x^2}\frac{\partial^2 w_0}{\partial y^2} + D_{22}(\frac{\partial^2 w_0}{\partial y^2})^2 + 4D_{66}(\frac{\partial^2 w_0}{\partial x \partial y})^2]dxdy \tag{4.5}$$

By substituting the equation (4.1) into the equation (4.3), the kinetic energy equation is obtained:

$$T = \frac{1}{2}\omega^2 \cos^2 \omega t \int_0^b \int_0^a \rho h {w_0}^2 dxdy = T_{\max} \cos^2 \omega t \tag{4.6}$$

where $T_{\max}$ is defined as

$$T_{\max} = \frac{1}{2}\int_0^b \int_0^a \rho h \omega^2 {w_0}^2 dxdy \tag{4.7}$$

If the plate is of the tapered composite plate configuration, we can obtain the thickness of the plate $h = f(x)$ and the load can be expressed as follow:

$$F_i = \frac{\partial U_{d\max}}{\partial q_i} + \frac{d}{dt}(\frac{\partial T_{\max}}{\partial \dot{q}}) \tag{4.8}$$

Therefore, the equation of motion can be written as follow:

$$\{F\} = [k] \cdot \{q\} + [m] \cdot \{\ddot{q}\} \tag{4.9}$$

Because the plate undergoes free vibration, we can obtain a set of eigenvalue equations for free vibration by using the equation (4.9).

$$\{0\} = [[k] - \omega^2 \cdot [m]] \cdot \{q\} \tag{4.10}$$

$\{F\}$: the vector of the nodal forces of the element

$\{q\}$: the vector of nodal displacements of the element

$[k]$: the stiffness matrix of the element

$[m]$: the mass matrix of the element

ω^2: the eigenvalue

ω: the natural frequency

We can use the equation (3.34) to get the stiffness matrix of one element, and then, we can assemble the stiffness matrices of all elements to obtain the stiffness matrix of the whole plate system $[K]$. For Calculating the mass matrix $[m]$, we can use the following steps. Considering the displacement function (3.17), we change this equation to matrix form as follow:

$$w(x, y) = [XY] \cdot \{c\} \tag{4.11}$$

where the matrices $[XY]$ and $\{c\}$ are expressed as follow:

$$[XY] = \begin{bmatrix} 1 & x & y & x^2 & xy & y^2 & x^3 & x^2y & xy^2 & y^3 & x^3y & xy^3 \end{bmatrix}$$

$$\{c\} = \{c_1 \quad c_2 \quad c_3 \quad c_4 \quad c_5 \quad c_6 \quad c_7 \quad c_8 \quad c_9 \quad c_{10} \quad c_{11} \quad c_{12}\}^T$$

The values of the 12 nodal degrees of the freedom can be expressed as the following matrix:

$$\{q\} = \{w_1 \quad w_{x1} \quad w_{y1} \quad w_2 \quad w_{x2} \quad w_{y2} \quad w_3 \quad w_{x3} \quad w_{y3} \quad w_4 \quad w_{x4} \quad w_{y4}\}^T$$

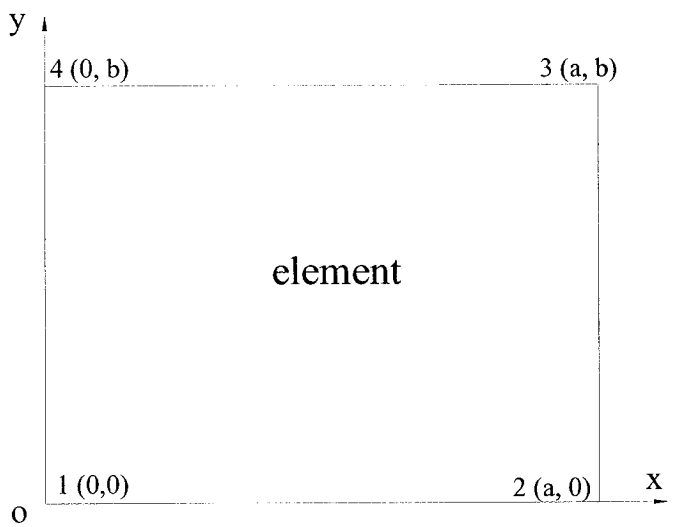

Figure 4.1 The rectangular finite element

The rectangular finite element is taken as in the Figure 4.1, and the equations (3.19) and (3.20) are taken into account. The following equation is obtained:

$$w(x,y) = [XY]\cdot\{c\} = [XY]\cdot[\alpha]^{-1}\cdot\{q\}$$

$$= \sum_{i=1}^{12} f_i(x,y)\cdot q_i \tag{4.12}$$

By substituting the equation (4.12) into equation (4.3), the following equation is obtained:

$$T = \int_0^a \int_0^b \frac{\rho h}{2}(\dot{w})^2\,dxdy = \frac{\rho}{2}\int_0^a \int_0^b h(\dot{w})^2\,dxdy$$

$$= \int_0^a \int_0^b \frac{\rho h}{2}(\sum_{i=1}^{12} f_i(x,y)\cdot\dot{q}_i)^2\,dxdy \tag{4.13}$$

Therefore, we can obtain the following equation:

$$\frac{d}{dt}(\frac{\partial T}{\partial \dot{q}_i}) = \frac{d}{dt}[\int_0^a \int_0^b \rho h(\sum_{i=1}^{12}\sum_{j=1}^{12} f_i(x,y)\cdot f_j(x,y)\cdot\dot{q}_i)dxdy$$

$$= \rho\sum_{i=1}^{12}\sum_{j=1}^{12}[\int_0^a \int_0^b h\cdot f_i(x,y)\cdot f_j(x,y)dxdy\cdot\ddot{q}_i] \tag{4.14}$$

The mass matrix coefficient can be written as follow:

$$m_{ij} = \rho\int_0^a \int_0^b h\cdot f_i(x,y)\cdot f_j(x,y)\cdot dxdy \tag{4.15}$$

For tapered composite plate configurations, the thickness h is the function of x.

When we consider the tapered composite plate configurations, the resin pocket must be taken into account. In Figure 4.2, the top side of the resin pocket (1) has the height

h_{11} in the left and the height h_{10} in the right with the taper angle $-\alpha$, and the bottom side has the height h_{10} without taper angle. The density of the composite is ρ, and the density of resin is ρ_r.

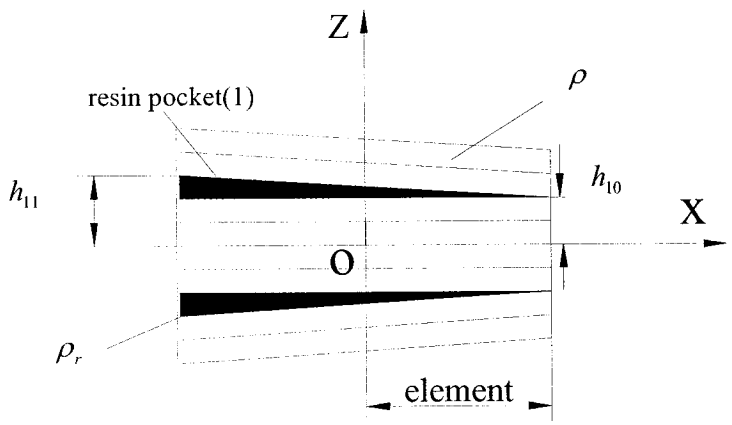

Figure 4.2 Tapered composite plate element with resin pocket

Therefore, the thickness of the resin pocket (1) can be expressed as:

$$h_1' = [\tan(-\alpha)\cdot x + \frac{h_{11}+h_{10}}{2}] - h_{10} \tag{4.16}$$

Similarly, we can write the following equation for resin pocket (n) inside the tapered composite plate configuration:

$$h_n' = [\tan(-\alpha)\cdot x + \frac{h_{n1}+h_{n0}}{2}] - h_{n0} \tag{4.17}$$

Because the resin pocket has the same displacement function as the whole element, we can express the mass matrix coefficient of the resin pocket as follow:

$$m'_{nij} = \rho_r \int_0^a \int_0^b h'_n \cdot f_i(x,y) \cdot f_j(x,y) \cdot dxdy \tag{4.18}$$

Hereafter, the mass matrix coefficient of tapered composite plate configuration element with n resin pockets can be written as follow:

$$m_{ij} = \rho \int_0^a \int_0^b h \cdot f_i(x,y) \cdot f_j(x,y) \cdot dxdy - \sum_{n=1}^{n} (\rho - \rho_r) \int_0^a \int_0^b h'_n f_i(x,y) \cdot f_j(x,y) dxdy \tag{4.19}$$

Thereafter, we can get mass matrix of finite element $[m]$. For the 4×4 mesh and 6×6 mesh, we assemble the mass matrices of all elements, and hence we get the system mass matrix $[M]$ of the composite plate structural system. By using the system stiffness matrix $[K]$, the equation of motion for the plates can now be written as:

$$\{P\} = [K] \cdot \{Q\} + [M] \cdot \{\ddot{Q}\} \tag{4.20}$$

$\{P\}$: the vector of the nodal forces of the structural system

$\{Q\}$: the vector of nodal displacements of the structural system

$[K]$: the stiffness matrix of the structural system

$[M]$: the mass matrix of the structural system

By assuming sinusoidal motion with natural frequency ω, we obtain a set of eigenvalue equations for free vibration,

$$\{0\} = [[K] - \omega^2 \cdot [M]] \cdot \{Q\} \tag{4.21}$$

By solving the equation (4.21) given above, we can get free vibration frequencies. Here, we consider three kinds of boundary conditions, four edges simply supported, four edges clamped and one edge clamped with other three edges free. By considering the boundary conditions, it is common and efficient practice to formulate the condensed stiffness matrix $[K]'$ instead of the whole stiffness matrix $[K]$ based on the zero-displacement conditions. Similarly, we can formulate the condensed mass matrix $[M]'$ instead of the whole mass matrix $[M]$ based on the zero-displacement conditions. By use of the condensed stiffness matrix $[K]'$ and the condensed mass matrix $[M]'$ for different boundary conditions, we can get the vibration frequency results corresponding to different boundary conditions. Finally, we can calculate the frequencies of the free vibration of 1st mode, 2nd mode, 3rd mode, etc for the uniform composite plate configuration and tapered composite plate configurations.

4.3 Ritz Method for Free Vibration of Uniform and Tapered Composite Plates

The determination of natural frequencies can also be obtained by Ritz Method. In the case of orthotropic plates the strain energy is given by equation given below [22]:

$$U_{d\max} = \frac{1}{2}\int_0^a \int_0^b [D_{11}(\frac{\partial^2 w_0}{\partial x^2})^2 + 2D_{12}\frac{\partial^2 w_0}{\partial x^2}\frac{\partial^2 w_0}{\partial y^2} + D_{22}(\frac{\partial^2 w_0}{\partial y^2})^2 + 4D_{66}(\frac{\partial^2 w_0}{\partial x \partial y})^2]dxdy \tag{4.22}$$

At the same time, the maximum kinetic energy is then written as follow [19]:

$$T_{\max} = \frac{1}{2}\int_0^a \int_0^b \rho h\omega^2 {w_0}^2 dxdy \tag{4.23}$$

In Figure 4.3, by considering the resin pocket in the tapered composite plate configuration, we can see that the top side of resin pocket (1) has a taper angle $-\alpha$ and the bottom side is without taper angle. Therefore the thickness of resin pocket (1) can achieved using equation (4.16). Similarly, for arbitrary resin pocket (n), if the coordinate points in x direction are c_n in left side and d_n in right side, the maximum kinetic energy can be written as follow:

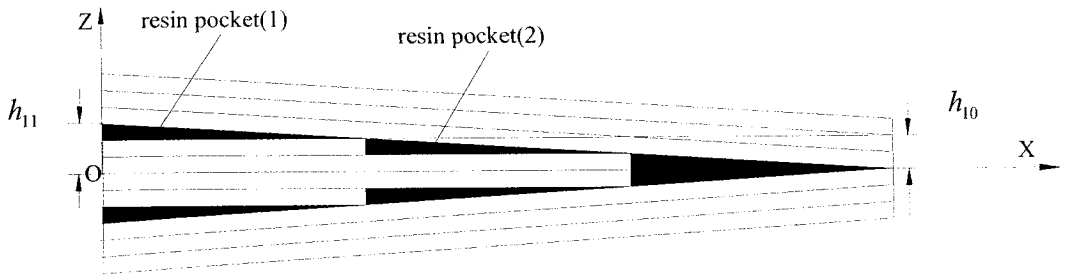

Figure 4.3 Resin pocket inside the tapered composite plate configuration

$$T_{\max} = \frac{1}{2}\int_0^b \int_0^a \rho h\omega^2 w_0{}^2 dxdy - \sum_1^n \frac{1}{2}\int_0^b \int_{c_n}^{d_n} (\rho - \rho_r) h_n' \omega^2 w_0{}^2 dxdy \tag{4.24}$$

In the absence of transverse loads, the maximum potential energy function reduces to the value expressed as follow:

$$U_{d\max} - T_{\max} = \frac{1}{2}\int_0^a \int_0^b \{[D_{11}(\frac{\partial^2 w_0}{\partial x^2})^2 + 2D_{12}\frac{\partial^2 w_0}{\partial x^2}\frac{\partial^2 w_0}{\partial y^2} + D_{22}(\frac{\partial^2 w_0}{\partial y^2})^2 + 4D_{66}(\frac{\partial^2 w_0}{\partial x \partial y})^2]$$

$$- \rho h\omega^2 w_0{}^2\} dxdy + \sum_1^n \frac{1}{2}\int_0^b \int_{c_n}^{d_n} (\rho - \rho_r) h_n' \omega^2 w_0{}^2 dxdy \tag{4.25}$$

The approximate solution to the displacement function $w_0(x, y)$ is sought in the usual form of a double series:

$$w_0(x,y) = \sum_{m=1}^{M}\sum_{n=1}^{N} A_{mn} X_m(x) Y_n(y) \tag{4.26}$$

The different displacement functions that correspond to different boundary condition are expressed as follow:

1. When we consider the boundary condition of simple support for four edges of the uniform and tapered composite plates, the shape function can be written as [22]:

$$w_0(x,y) = \sum_{m=1}^{M}\sum_{n=1}^{N} A_{mn} \cdot \sin\frac{m\pi x}{a} \cdot \sin\frac{n\pi y}{b} \tag{4.27}$$

2. When we consider the boundary condition of four edges clamped for the uniform and tapered composite plates, the shape function can be written as [22]:

$$w_0(x,y) = \sum_{m=1}^{M}\sum_{n=1}^{N} A_{mn} \cdot \frac{x^2}{a^2}\left(\frac{x}{a}-1\right)^2\left(\frac{x}{a}\right)^{m-1} \cdot \frac{y^2}{b^2} \cdot \left(\frac{y}{b}-1\right)^2\left(\frac{y}{b}\right)^{m-1} \tag{4.28}$$

3. When we consider the boundary condition of one edge clamped and the other three edges free, the shape function can be written as [54]:

$$w_0(x) = \sum_{n=1}^{N} A_n\left(1-\cos\frac{\pi x(n-1)}{2a}\right) \tag{4.29}$$

The coefficients A_{mn} will be determined by the stationary condition. We can obtain the following equation:

$$\frac{\partial}{\partial A_{mn}}[U_{d\max} - T_{\max}] = 0 \tag{4.30}$$

By substituting equations (4.25) into (4.30) and considering the different displacement functions with respect to different boundary conditions, we can get the eigenvalue equation of ω^2, and it can be written as follow:

$$\frac{\partial}{\partial A_{mn}}\{\frac{1}{2}\int_0^a\int_0^b\{[D_{11}(\frac{\partial^2 w_0}{\partial x^2})^2 + 2D_{12}\frac{\partial^2 w_0}{\partial x^2}\frac{\partial^2 w_0}{\partial y^2} + D_{22}(\frac{\partial^2 w_0}{\partial y^2})^2 + 4D_{66}(\frac{\partial^2 w_0}{\partial x\partial y})^2]dxdy\}$$

$$-\omega^2\frac{\partial}{\partial A_{mn}}\int_0^a\int_0^b \rho h w_0{}^2 dxdy = 0 \tag{4.31}$$

If we choose m = 1, 2, ..., M, and n = 1, 2, ..., N in the shape functions, we can get the following equation about $\frac{\partial U_{d\max}}{\partial A_{mn}}$:

$$\frac{\partial U_{d\max}}{\partial A_{mn}} = \sum_1^N\sum_1^N G_{mn}\cdot A_{mn} \tag{4.32}$$

Similarly, if we choose m = 1, 2, ..., M, and n = 1, 2, ..., N in the shape functions, we can also get the following equation about $\frac{\partial T_{d\max}}{\partial A_{mn}}$:

$$\frac{\partial T_{d\max}}{\partial A_{mn}} = \sum_{1}^{N}\sum_{1}^{M} L_{mn} \cdot A_{mn} \tag{4.33}$$

Hereafter, we can write the equation (4.30) in the following form:

$$\sum_{1}^{N}\sum_{1}^{N} G_{mn} \cdot A_{mn} - \omega^2 \sum_{1}^{N}\sum_{1}^{M} L_{mn} \cdot A_{mn} = 0 \tag{4.34}$$

.

Then, we can reduce the equation (4.34), and express the eigenvalue equation of ω^2 in the following matrix form:

$$[G]\{A_{mn}\} - \omega^2 [L]\{A_{mn}\} = 0 \tag{4.35}$$

For the first two boundary conditions, we set m = n = 2 and m = n = 3 to calculate the free vibration frequencies of different kinds of tapered composite plate configurations. For the third boundary condition, we set n = 9 to compute the frequencies of different kinds of tapered composite plate configurations. We can get the results of free vibration frequencies for 1st mode, 2nd mode, 3rd mode, etc.

The 1st mode, 2nd mode and 3rd mode free vibration frequencies for the plate configurations are given in Figure 4.3. The mode shape is the same as that used in the Finite Element Method.

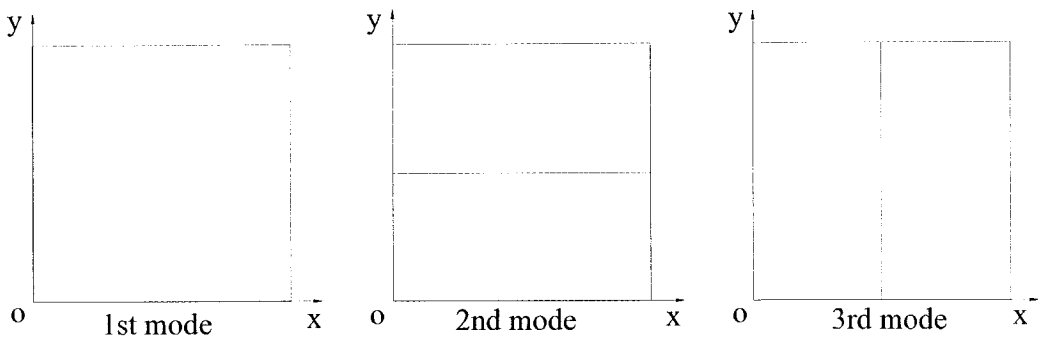

Figure 4.4 The modes of the free vibration of plates

4.4 The Example Calculations for the Free Vibration of the Uniform and Tapered Composite Plate Configurations

In this part, the uniform composite plate and tapered composite plates are considered. By using the results of Chapter 2 and Chapter 3, we calculate the free vibration frequencies using Finite Element Method and Ritz method in the following examples. For the uniform composite configuration, we choose the plate configuration according to the uniform plate configuration in ref. [12], and compare our results of free vibration frequencies with the results in ref. [12]. For the tapered composite plate configurations, the Finite Element Method and Ritz Method are used to calculate the 1^{st} mode, 2^{nd} mode and 3^{rd} mode free vibration frequencies.

4.4.1 Example Calculation for the Uniform Composite Plate

A uniform rectangular laminated plate is made up of the graphite/epoxy material and with symmetric cross-ply arrangement, as shown in Figure 2.6. The laminate is made out of eight identical plies with the following mechanical properties: $E_1 = 134.4 \times 10^9$ Pa ; $E_2 = E_3 = 10.34 \times 10^9$ Pa; $G_{12} = G_{13} = 4.999 \times 10^9$ Pa; $G_{23} = 1.999 \times 10^9$ Pa; $\nu_{12} = \nu_{13} = \nu_{23} = 0.33$; $\rho = 1480$ kg/m^3. The plate has a length $L = 127$ mm and a width $b = 12.7$ mm. Two different plate thicknesses, $h = 1.016$ mm and $h = 10.16$ mm resulting in the two cases of $L/h = 125$ and $L/h = 12.5$, are considered. The uniform plates have configurations $[(90/0)_2]_S$ at the left and right ends respectively (see Figure 2.6).

By using the mechanical behaviors of these two uniform configurations calculated in chapter 2, we use the Finite Element Method to compute their free vibration natural frequencies. The 36-element mesh is taken to calculate the results in this example, and the results have been compared with the results given in ref. [12].

In this example, two types of boundary conditions for these two uniform configurations are studied as follow:

Case 1: one of the short edges fixed and the other three edges free

Case 2: both of the short edges fixed and both of the long edges free

In ref. [12], three kinds of methods are used to calculate the free vibration frequencies, and some experimental results were obtained in this paper. The three methods are: the higher order theory (HOT), the classical laminate plate theory (CLPT), and the first order shear deformation theory (FSDT). We calculate the results using Finite Element Method and based on CLPT. A total of 36 elements were used. We can see all the results of free vibration frequencies in Table 4.1 and Table 4.2.

First, we consider the boundary condition of one of the short edges fixed and other three edges free (Case 1). The natural frequencies for the two uniform composite plates (L/h=125 and L/h=12.5) are calculated using Finite Element Method, and the results are given in Table 4.1.

Table 4.1 The natural frequencies of uniform composite plates with one of the short edges fixed and other three edges free (unit: Hz)

L/h	CLPT [12]	FSDT [12]	Experimental [12]	HOT [12]	FEM (36 elements)
125	82.15	82.12	79.83	82.11	79.01
12.5	820.52	795.09		789.22	790.17

Next, we consider the boundary condition of both of the short edges fixed and both of the long edges free (Case 2). The natural frequencies for the two uniform composite plates (L/h=125 and L/h=12.5) are calculated using Finite Element Method, and the results are given in Table 4.2.

Table 4.2 The natural frequencies of uniform composite plates with both of the short edges fixed and both of the long edges free (unit: Hz)

L/h	CLPT [12]	FSDT [12]	HOT [12]	FEM (36 elements)
125	522.85	521.15	520.72	502.93
12.5	4664.4	4058.6	3885.5	5029.34

From the Table 4.1 and Table 4.2, we can see that the results calculated using Finite Element Method are very close to the results for the uniform plate configuration (L/h=125). For example, for the uniform plate configuration (L/h=125) in Case 1, the experimental result of natural frequency is 79.83(Hz), whereas the result calculated using Finite Element Method is 79.01(Hz), therefore meaning that the present method is efficient for prediction of the natural frequencies for the thin plate configuration. For the uniform plate configuration with L/h=12.5, the result is not as good as that for configuration with L/h=125, because the plate's thickness is large, and therefore the

higher order theory and shear deformation theory must be used to analyze the plate configuration with large thickness.

4.4.2 Example Calculation for the Free Vibration of Tapered Composite Plates

In this part, four different kinds of tapered composite plate configurations, Configuration A, Configuration B, Configuration C, and Configuration D are considered (see Figures 2.7, 2.8, 2.9, and 2.10). Thereafter, we use the Finite Element Method and Ritz Method to calculate the free vibration frequencies of the tapered composite plate configurations. The example is given below and it is the same problem as that of the examples given in Chapter 2 and Chapter 3.

The tapered composite plate configurations are depicted in Figures 2.7, 2.8, 2.9, and 2.10. The laminates are made up of the NCT301 graphite/epoxy material with symmetric cross-ply arrangement. The laminates have twelve plies in the left side and six plies in the right side. For configurations A, B and C, the tapered plates have lay-up configurations $[(0/90)_3]_S$ at the left end and $[0/90/0]_S$ at the right end respectively. For configuration D, the tapered plate has lay-up configurations $[0/resin/90/0/0/90]_S$ at the left end and $[0/90/0]_S$ at the right end respectively. The ply has the following mechanical properties:

$E_1 = 113.9$ GPa, $E_2 = E_3 = 7.9$ GPa, $\nu_{12} = 0.28$, $\nu_{23} = 0.4$, $\nu_{13} = 0.02$,

$G_{12} = 3.1$ GPa, $G_{13} = 3.1$ GPa, $G_{23} = 2.8$ GPa, $\rho = 1480\ kg/m^3$, $h_0 = 0.138$ mm, $\rho = 1480\ kg/m^3$.

The mechanical properties of the epoxy resin are given as:

$E = 3.93$ GPa, $G = 1.034$ GPa, $\nu = 0.37$, $\rho_r = 1200\ kg/m^3$.

The geometric properties of the tapered composite plates are: the length a is 240 mm and the width b is 240 mm, and the thickness changes in x direction from 2.208 mm to 1.104 mm.

By using Finite Element Method and Ritz Method, we calculate the free vibration frequencies of the tapered composite plate configurations under three different boundary conditions.

1. Boundary condition: Four simply supported edges

Under this boundary condition, the three modes of natural frequencies are calculated using Finite Element Method and Ritz Method. The results are shown in Table 4.3, Table 4.4, and Table 4.5, and in Figure 4.5 and Figure 4.6 also, for the four tapered composite plate configurations.

Table 4.3 1st mode natural frequencies of tapered composite plate configurations with four simply supported edges (unit: rad/s)

Taper Configuration	Finite Element Solution			Ritz Solution		
	12 elements	24 elements	36 elements	4-Terms	3-Terms	2-Terms
A	543.9	587.2	596.5	596.0	595.6	589.2
B	543.9	580.2	589.3	588.4	587.5	581.5
C	549.1	590.9	599.9	595.3	594.7	588.4
D	521.2	563.8	577.1	576.8	575.4	569.6

In table 4.3, we can see that the results of 36 elements and 24 elements using finite element method are much closer, and the results of 3 terms and 4 terms using Ritz method are also much closer. Therefore, the 36 elements result for finite element method and 3 terms results for Ritz method are used as the converged results to be compared below.

Table 4.4 2nd mode natural frequencies of tapered composite plate configurations with four simply supported edges (unit: rad/s)

Taper Configuration	Finite Element Solution (36 elements)	Ritz Solution (3 terms)
A	1425.1	1423.5
B	1415.1	1412.4
C	1468.6	1448.9
D	1397.1	1396.1

Table 4.5 3rd mode natural frequencies of tapered composite plate configurations with four simply supported edges (unit: rad/s)

Taper Configuration	Finite Element Solution (36 elements)	Ritz Solution (3 terms)
A	1832.8	1820.7
B	1844.1	1805.6
C	1848.4	1799.3
D	1822.2	1770.1

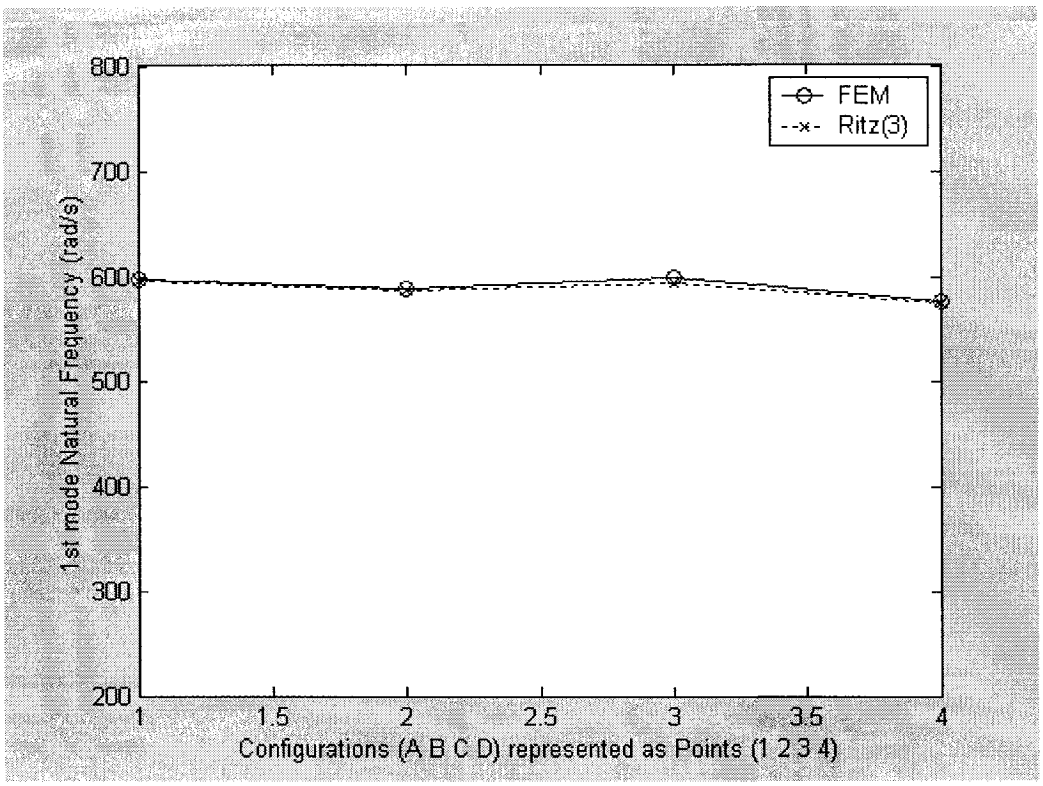

Figure 4.5 1st mode natural frequencies of tapered composite plates with four edges simply supported calculated using Finite Element and Ritz Methods

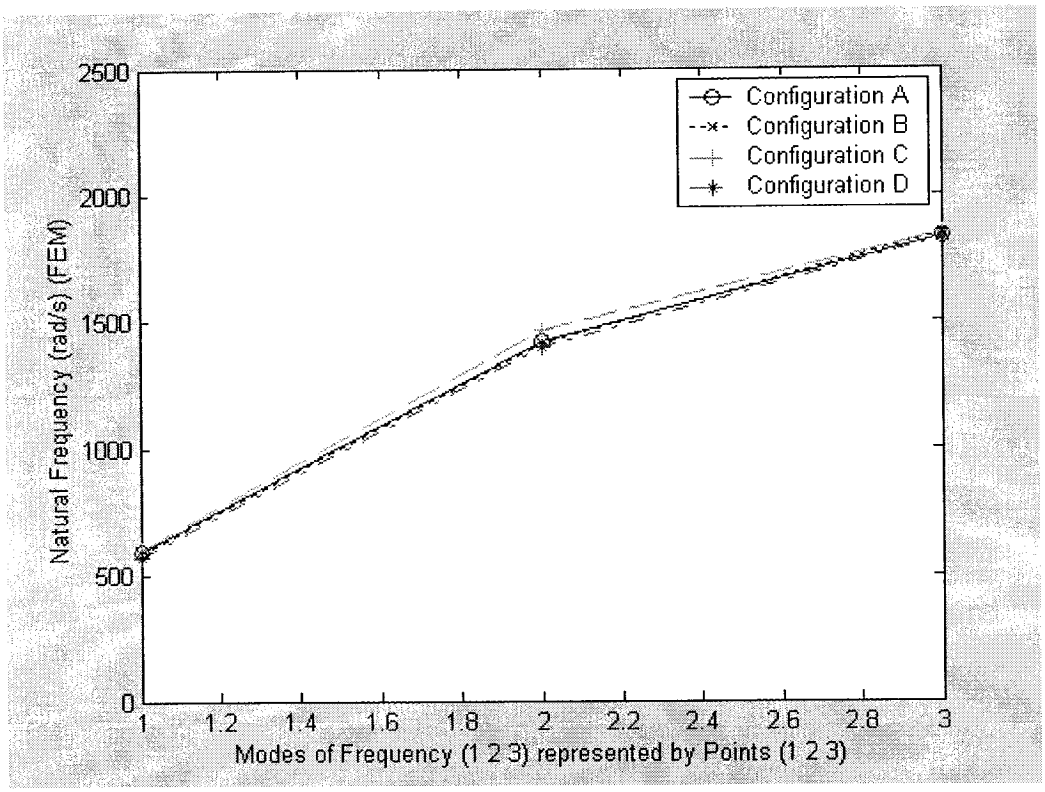

Figure 4.6 The natural frequencies of three modes of tapered composite plate configurations with four edges simply supported calculated using FEM

In Figure 4.5, the graphs show that the 1st mode natural frequencies of the four tapered composite plate configurations calculated using Finite Element Method are very close to the results calculated using Ritz Method. From the Table 4.4 and Table 4.5, it can be seen that the Finite Element Method and Ritz Method also have much closer results for the 2nd and 3rd mode natural frequencies.

In Figure 4.6, we can see that Taper Configuration C has the highest natural frequencies in all the three modes, whereas Taper Configuration D has the lowest

natural frequencies in all the three modes. The natural frequencies of Taper Configuration A and Taper Configuration B have the natural frequencies between the other two configurations. The same trend has been observed in the results obtained using Ritz Method.

2. Boundary condition: Four clamped plate edges

Under this boundary condition, the three modes of natural frequencies are calculated using Finite Element Method and Ritz Method. The results are shown in Table 4.6, Table 4.7, and Table 4.8, and in Figure 4.7 and Figure 4.8 also, for the four tapered composite plate configurations.

Table 4.6 1st mode natural frequencies of tapered composite plate configurations with four clamped plate edges (unit: rad/s)

Taper Configuration	Finite Element Solution (36 elements)	Ritz Solution (3 terms)
A	1292.7	1280.8
B	1283.7	1269.9
C	1301.3	1282.1
D	1249.6	1241.5

Table 4.7 2nd mode natural frequencies of tapered composite plate configurations with four clamped plate edges (unit: rad/s)

Taper Configuration	Finite Element Solution (36 elements)	Ritz Solution (3 terms)
A	2274.5	2312.3
B	2262.7	2297.1
C	2327.8	2342.6
D	2235.1	2278.6

Table 4.8 3rd mode natural frequencies of tapered composite plate configurations with four clamped plate edges (unit: rad/s)

Taper Configuration	Finite Element Solution (36 elements)	Ritz Solution (3 terms)
A	2773.8	3298.1
B	2793.8	3397.1
C	2796.6	3268.9
D	2744.9	3268.8

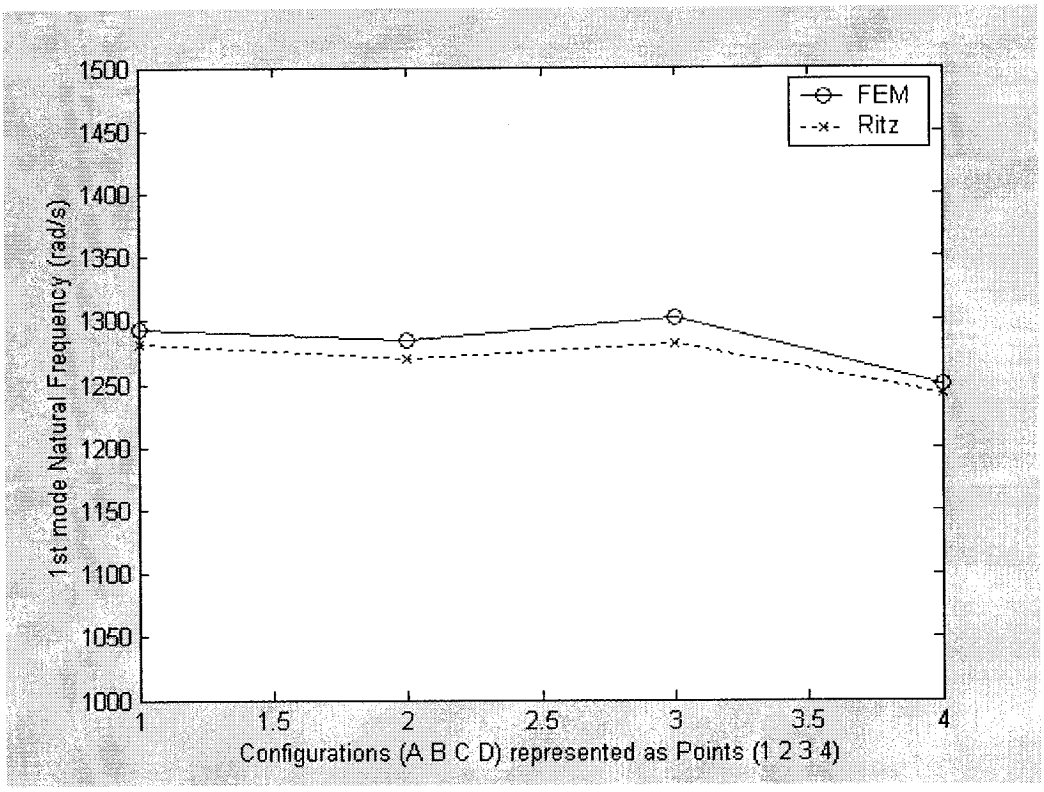

Figure 4.7 1st mode natural frequencies of tapered composite plate configurations with four clamped edges calculated using Finite Element and Ritz Methods

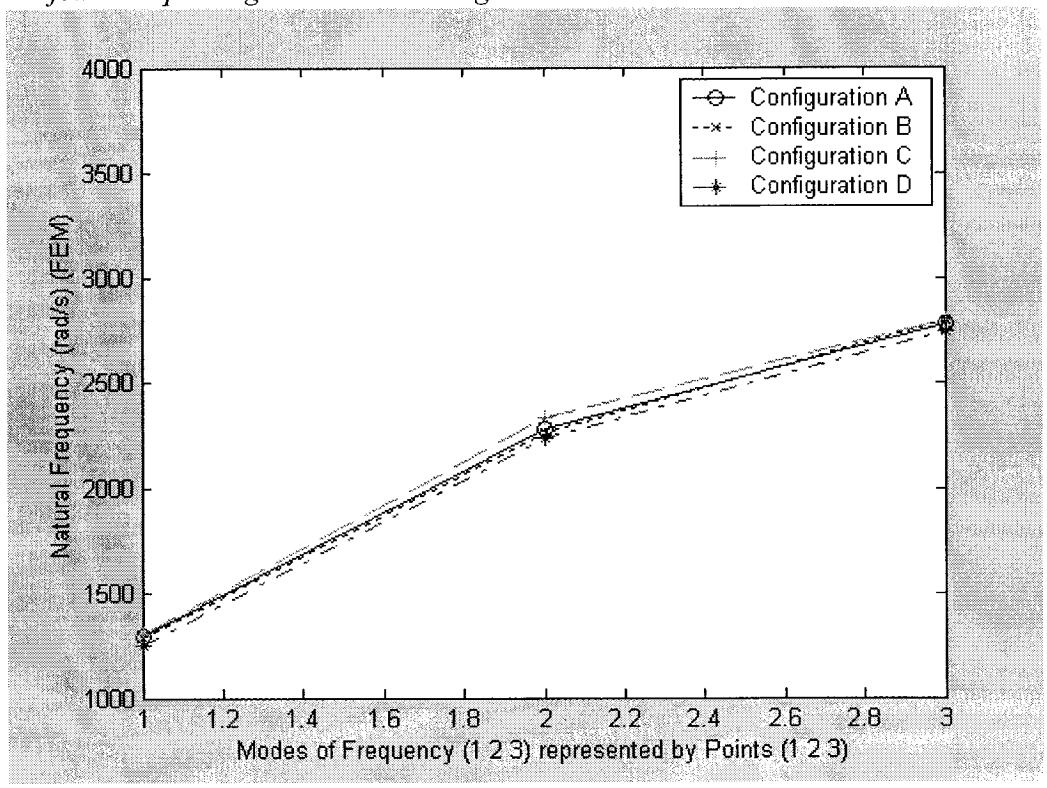

Figure 4.8 Three natural frequencies of all tapered composite plate configurations with four clamped edges calculated using FEM

In Figure 4.7, the graphs show that the 1st mode natural frequencies of the four tapered composite plate configurations calculated using Finite Element Method are very close to the results calculated using Ritz Method. From the Table 4.7 and Table 4.8, it can be observed that the Finite Element Method and Ritz Method have closer results for the 2nd mode natural frequencies, but the results for 3rd mode natural frequencies have some differences.

In Figure 4.8, we can see that Taper Configuration C has the highest natural frequencies in all the three modes, whereas Taper Configuration D has the lowest natural frequencies in all the three modes. The natural frequencies of Taper Configuration A and Taper Configuration B have the natural frequencies between the other two configurations. The same trend has been observed in the results obtained using Ritz Method.

3. Boundary condition: One edge clamped and three edges free

Under this boundary condition, the two modes of natural frequencies are calculated using Finite Element Method and Ritz Method. The results are shown in Table 4.9 and Table 4.10, and in Figure 4.9 and Figure 4.10 also, for the four tapered composite plate configurations.

Table 4.9 1st mode natural frequencies of tapered composite plate configurations with one clamped edge and three free edges (unit: rad/s)

Taper Configuration	Finite Element Solution (36 elements)	Ritz Solution (9 terms)
A	234.4	228.2
B	245.5	232.0
C	242.9	229.6
D	234.6	221.7

Table 4.10 2nd mode natural frequencies of tapered composite plate configurations with one clamped edge and three free edges (unit: rad/s)

Taper Configuration	Finite Element Solution (36 elements)	Ritz Solution (9 terms)
A	1141.0	1127.8
B	1148.0	848.9
C	1149.9	848.5
D	1112.3	826.2

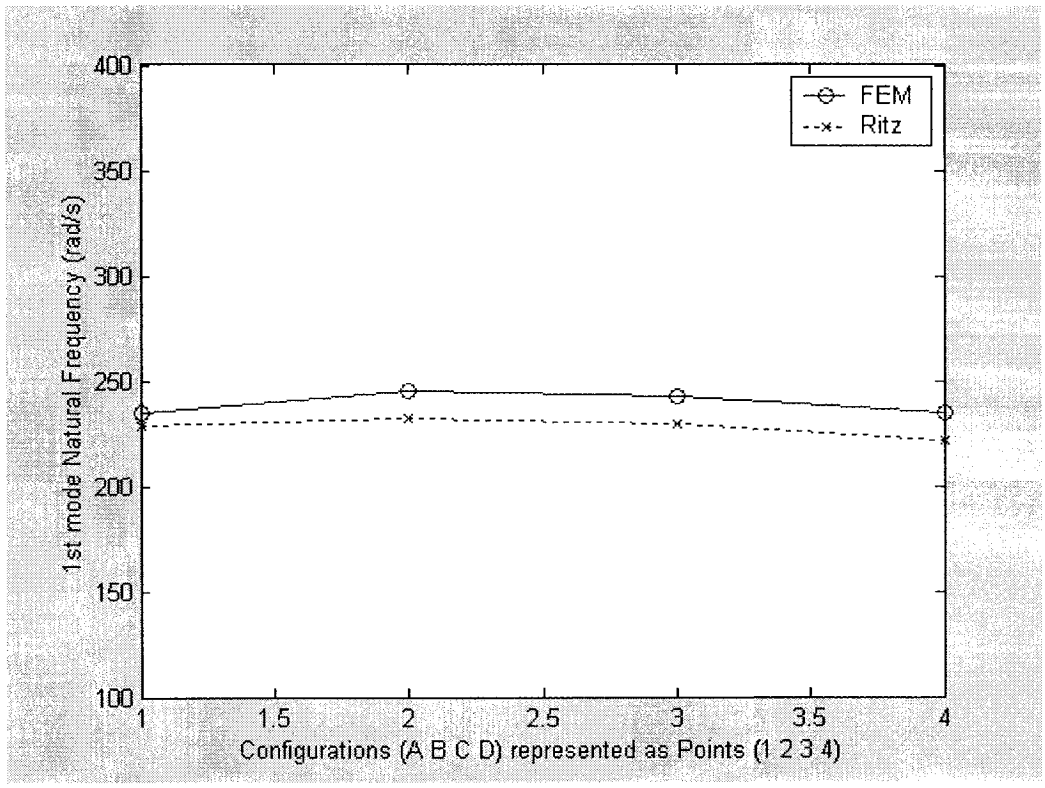

Figure 4.9 1st mode natural frequencies of tapered composite plates with one clamped edge and three free edges calculated using Finite Element and Ritz Methods

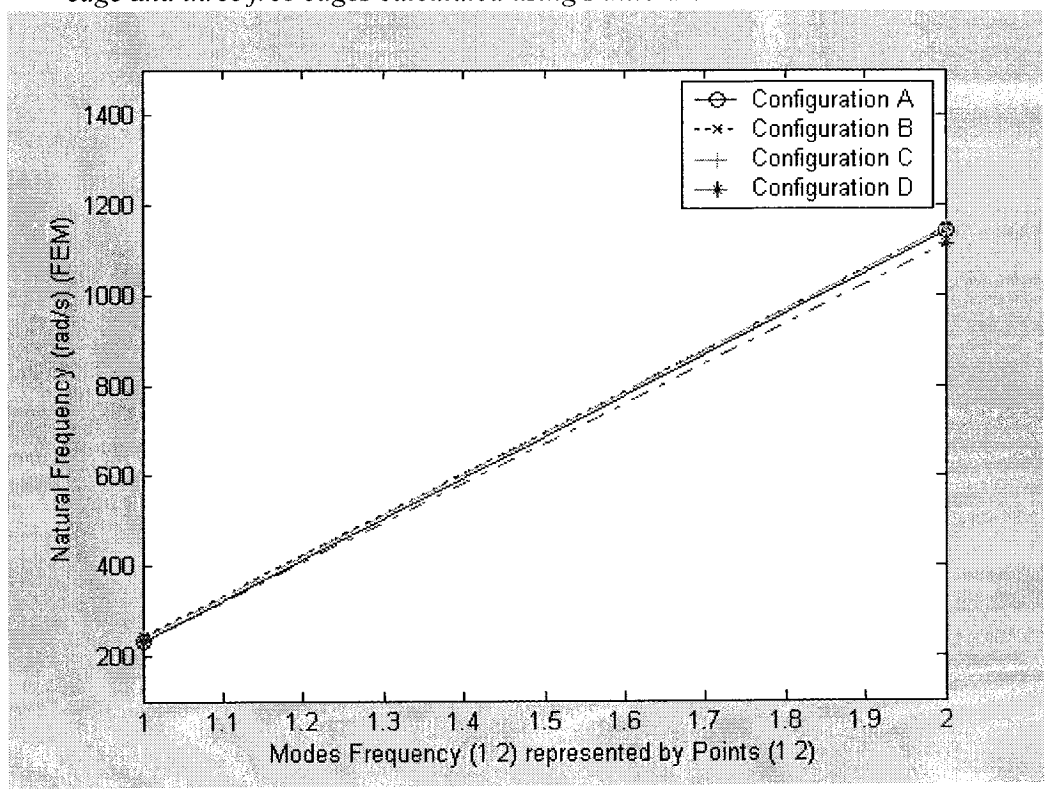

Figure 4.10 The natural frequencies of two modes of all tapered composite plate configurations with one clamped edge and three free edges calculated using FEM

In Figure 4.9, the graphs show that the 1st mode natural frequencies of the four tapered composite plate configurations calculated using Finite Element Method are very close to the results calculated using Ritz Method. From the Table 4.9, results of 2nd mode natural frequencies have some differences using these two methods.

In Figure 4.10, we can see that Taper Configuration B has the highest natural frequencies in both the two modes, whereas Taper Configuration D has the lowest natural frequencies in both the two modes. The natural frequencies of Taper Configuration A and Taper Configuration C have the natural frequencies between the other two configurations. The same trend has been observed in the results obtained using Ritz Method. Here, we can see that the frequencies of the four tapered composite plate configurations are much closer for this kind of boundary condition.

4.5 Conclusion

In this chapter, the uniform composite plate configuration and tapered composite plate configurations are considered. By using the results given in Chapter 2 and Chapter 3, we have calculated the free vibration frequencies for uniform plate configuration and taper configurations using Finite Element Method and Ritz method. For the uniform composite plate configuration, we have chosen the plate configuration according to

the uniform configuration considered in ref. [12]. By comparing our results of free vibration frequencies with the results given in ref [12], we observe that much closer results have been obtained in the present work. For the tapered composite plate configurations, the Finite Element Method and Ritz Method are used to calculate the 1^{st} mode, 2^{nd} mode and 3^{rd} mode free vibration frequencies. The calculation shows that the two methods yield closer results. The calculation and results of this chapter provide a good preparation for the dynamic instability analysis in the following chapter.

Chapter 5

Buckling Analysis of Uniform and Tapered Composite Plates Using Finite Element Method and Ritz Method

5.1 Introduction

Composite plates are widely used in civil, mechanical and aerospace structures. In this chapter, the uniform composite plate configuration and four tapered composite plate configurations are considered. By using the formulation developed in Chapter 3, we calculate the critical buckling loads of the composite plate configurations using Finite Element Method and Ritz Method. We will derive the formulations for calculating buckling loads based on classical laminate theory for Finite Element Method and Ritz Method. By using the results of mechanical behavior of tapered composite plate configurations calculated in Chapter 2 and the stiffness matrices of uniform and tapered composite configurations calculated in Chapter 3, we can obtain the results of critical buckling loads for the uniform and tapered plate configurations. All of the results will be used in instability analysis for different kinds of composite plate configurations in the following chapter.

5.2 Finite Element Buckling Analysis of Uniform and Tapered Composite Plate Configurations

In formulating the plate elements for buckling analysis, the effect of in-plane compressive stresses is included and expressed in the form of incremental stiffness matrix. The potential energy or work done in a plate element due to the in-plane forces can be obtained as follow (see Figure 5.1) [22]:

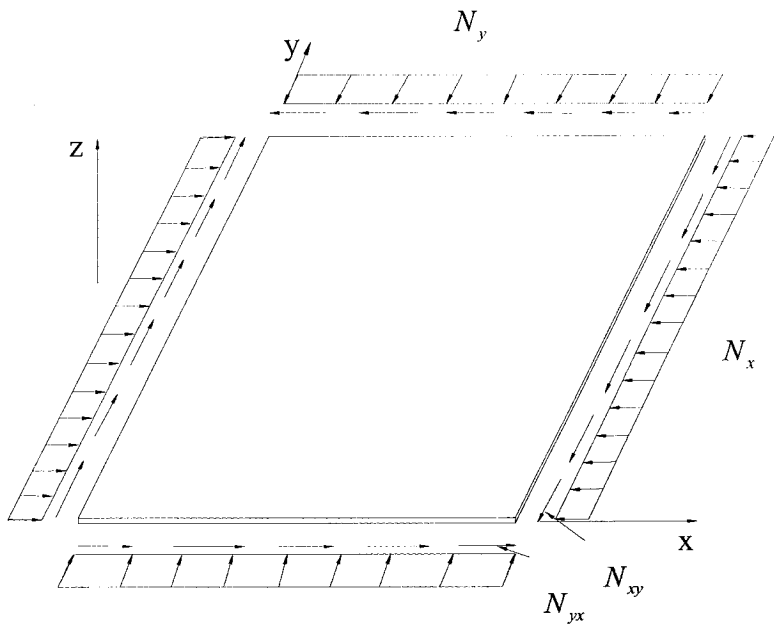

Figure 5.1 In-plane direct and shearing forces on an element

$$W_m = \int\int (N_x \varepsilon'_{xx} + N_y \varepsilon'_{yy} + N_{xy} \gamma'_{xy}) dxdy \tag{5.1}$$

where, ε'_{xx}, ε'_{yy}, and γ'_{xy} are the in-plane strains resulting from the deflection w_0. By considering the thin plate assumption as in Chapter 2, the in-plane strain owed to

transverse displacement can be written in the following form:

$$\varepsilon'_{xx} = \frac{1}{2}(\frac{\partial w_0}{\partial x})^2 \tag{5.2}$$

$$\varepsilon'_{yy} = \frac{1}{2}(\frac{\partial w_0}{\partial y})^2 \tag{5.3}$$

$$\gamma'_{xy} = \frac{\partial w_0}{\partial x}\frac{\partial w_0}{\partial y} \tag{5.4}$$

Therefore, by substituting the equations (5.2), (5.3) and (5.4) into equation (5.1), the potential energy or work done in a plate element due to the in-plane forces can be written as follow [37]:

$$W_m = \frac{1}{2}\int_0^b \int_0^a [N_x(\frac{\partial w_0}{\partial x})^2 + N_y(\frac{\partial w_0}{\partial y})^2 + 2N_{xy}(\frac{\partial w_0}{\partial x})\frac{\partial w_0}{\partial y}]dxdy \tag{5.5}$$

where, $N_x = \sigma_x h$, $N_y = \sigma_y h$, $N_{xy} = \tau_{xy} h$ and σ_x, σ_y, and τ_{xy} are the normal stresses in the x direction and y direction and the shearing stress respectively, as it can be seen in Figure 5.1. The work done in a plate element due to the in-plane forces and transverse loads can be obtained as follow:

$$W = W_f + W_m \tag{5.6}$$

where W_f is the work done due to the transverse loads, W_m is the work done due to

the in-plane forces.

If there are no transverse loads applied to the plate element, the equation of the work done in a plate element can be obtained as follow:

$$W = \frac{1}{2}\int_0^b \int_0^a [N_x(\frac{\partial w_0}{\partial x})^2 + N_y(\frac{\partial w_0}{\partial y})^2 + 2N_{xy}(\frac{\partial w_0}{\partial x})\frac{\partial w_0}{\partial y}]dxdy \tag{5.7}$$

For the plate configurations, the equations of motion can be obtained by use of the Lagrange's equation as follow:

$$\frac{d}{dt}(\frac{\partial T}{\partial \dot{q}_i}) + \frac{\partial (U_d + W)}{\partial q_i} = F_i \tag{5.8}$$

When the potential energy of the equation (5.7) is included in strain energy $U = U_d + W$ of the equation (5.8), the following equation can be obtained:

$$\{F\} = [[k] + [n] - \omega^2[m]]\{q\} \tag{5.9}$$

$\{F\}$: the vector of the nodal forces of the element

$\{q\}$: the vector of nodal displacements of the element

$[k]$: the stiffness matrix of the element

$[m]$: the mass matrix of the element

ω^2 : the eigenvalue

ω : the natural frequency

$[n]$: the incremental stiffness matrix of the element

In the case of static problem, the equation (5.8) can be changed to the following form:

$$\frac{\partial U}{\partial q_i} = \frac{\partial}{\partial q_i}(U_d + W) = F_i \tag{5.10}$$

$$\{F\} = ([k]+[n])\{q\} \tag{5.11}$$

According to the procedure given in the Chapter 3, we can get the stiffness matrix of the element. In the equation (5.9), the matrix $[n]$ is the incremental stiffness matrix, and we can obtain $[n]$ using the following steps:

From the equation (5.7), and considering the equation (4.12) in the chapter 4, we obtain the following equations:

$$(\frac{\partial w_0}{\partial x})^2 = (\sum_{i=1}^{12} \frac{\partial f_i(x,y)}{\partial x} q_i)^2 \tag{5.12}$$

$$(\frac{\partial w_0}{\partial y})^2 = (\sum_{i=1}^{12} \frac{\partial f_i(x,y)}{\partial y} q_i)^2 \tag{5.13}$$

$$(\frac{\partial w_0}{\partial x})\frac{\partial w_0}{\partial y} = (\sum_{i=1}^{12} \frac{\partial f_i(x,y)}{\partial x} q_i)\cdot(\sum_{i=1}^{12} \frac{\partial f_i(x,y)}{\partial y} q_i) \tag{5.14}$$

And then, we can get the following equation forms:

$$\frac{\partial(\frac{\partial w_0}{\partial x})^2}{\partial q_i} = 2\sum_{i=1}^{12}\sum_{j=1}^{12}\frac{\partial f_i(x,y)}{\partial x}\cdot\frac{\partial f_j(x,y)}{\partial x}\cdot q_j \tag{5.15}$$

$$\frac{\partial(\frac{\partial w_0}{\partial y})^2}{\partial q_i} = 2\sum_{i=1}^{12}\sum_{j=1}^{12}\frac{\partial f_i(x,y)}{\partial y}\cdot\frac{\partial f_j(x,y)}{\partial y}\cdot q_j \tag{5.16}$$

$$\frac{\partial[(\frac{\partial w_0}{\partial x})\frac{\partial w_0}{\partial y}]}{\partial q_i} = \sum_{i=1}^{12}\sum_{j=1}^{12}[\frac{\partial f_i(x,y)}{\partial x}\cdot\frac{\partial f_j(x,y)}{\partial y}+\frac{\partial f_i(x,y)}{\partial y}\cdot\frac{\partial f_j(x,y)}{\partial x}]\cdot q_j \tag{5.17}$$

Therefore, one term, $\frac{\partial W}{\partial q_i}$, in the equation (5.10) can be written as follow:

$$\frac{\partial W}{\partial q_i} = \sum_{i=1}^{12}\sum_{j=1}^{12}\int_0^b\int_0^a\{N_x(\frac{\partial f_i}{\partial x})\frac{\partial f_j}{\partial x}+N_y(\frac{\partial f_i}{\partial y})\frac{\partial f_j}{\partial y}+N_{xy}[(\frac{\partial f_i}{\partial x})\frac{\partial f_j}{\partial y}+(\frac{\partial f_i}{\partial y})\frac{\partial f_j}{\partial x}]\}dxdy\cdot q_j \tag{5.18}$$

Hereafter, the incremental stiffness coefficients of the matrix $[n]$ can be obtained by using the following equations:

$$n_{ij} = \int_0^a\int_0^b\left\{N_x(\frac{\partial f_i}{\partial x})\frac{\partial f_j}{\partial x}+N_y(\frac{\partial f_i}{\partial y})\frac{\partial f_j}{\partial y}+N_{xy}[(\frac{\partial f_i}{\partial x})\frac{\partial f_j}{\partial y}+(\frac{\partial f_i}{\partial y})\frac{\partial f_j}{\partial x}]\right\}dxdy \tag{5.19}$$

Thereafter, we can get the incremental stiffness matrix $[n]$ for the 4×4 and 6×6 meshes. After we assemble all the incremental stiffness matrix of every element, we

get the system incremental stiffness matrix $[N]$ of the composite plate structural system. By using the system stiffness matrix $[K]$, the equation of motion for the plates can now be written as:

$$\{P\} = [K]\cdot\{Q\} + [N]\cdot\{Q\} + [M]\cdot\{\ddot{Q}\} = \{[K] + [N] - \omega^2\cdot[M]\}\cdot\{Q\} \tag{5.20}$$

$\{P\}$: the vector of the nodal forces of the structural system

$\{Q\}$: the vector of nodal displacements of the structural system

$[K]$: the stiffness matrix of the structural system

$[M]$: the mass matrix of the structural system

$[N]$: incremental stiffness matrix of the structural system

When there is only in-plane forces applied to the uniform or tapered composite plates, and only the in-plane force in x direction is applied to the plate, the equation can be written:

$$\{0\} = \{[K] + [N]\} \quad \text{or} \quad [K] + N_{xb}[N'] = \{0\} \tag{5.21}$$

N_{xb} : the buckling force

By solving the eigenvalue equation (5.21) above, we can get the critical buckling force (the lowest N_{xb} is the critical buckling load N_{xcr}) N_{xcr} of the composite plate

configuration.

Here, we consider three kinds of boundary conditions: four edges simply supported, four edges clamped and one edge clamped with three edges free. By considering the boundary conditions, it is common and efficient practice to formulate the condensed stiffness matrix $[K]'$ instead of the whole stiffness matrix $[K]$ based on the zero-displacement conditions. Respectively, we can formulate the condensed incremental stiffness matrix $[N]'$ instead of the whole incremental stiffness matrix $[N]$ based on the zero-displacement conditions. By use of the condensed stiffness matrix $[K]'$ and the condensed incremental stiffness matrix $[N]'$ for different boundary conditions, we can get the buckling forces that correspond to different boundary conditions. Finally, we can calculate the buckling forces of 1st mode, 2nd mode and 3rd mode for the uniform composite plate configurations and tapered composite plate configurations.

5.3 Ritz Method Buckling Analysis of Uniform and Tapered Composite Plate Configurations

The analysis of buckling of the uniform and tapered composite plate configurations can also be obtained by Ritz Method. In the case of orthotropic plates the strain

energy is given by equation as follow, when we consider the equation (4.2) of energy in Chapter 4.

In the case of orthotropic plates the strain energy can be reduced as follow:

$$U_d = \frac{1}{2}\int_0^a \int_0^b [D_{11}(\frac{\partial^2 w_0}{\partial x^2})^2 + 2D_{12}\frac{\partial^2 w_0}{\partial x^2}\frac{\partial^2 w_0}{\partial y^2} + D_{22}(\frac{\partial^2 w_0}{\partial y^2})^2 + 4D_{66}(\frac{\partial^2 w_0}{\partial x \partial y})^2]dxdy + C \tag{5.22}$$

The work done in a plate configuration due to the in-plane forces and transverse loads can be obtained as follow:

$$W = W_f + W_m \tag{5.23}$$

where, W_f is the work done due to the transverse loads, and W_m is the work done due to the in-plane forces.

Similarly, the potential energy W_m of the in-plane loads owed to deflection w_0 is written as follow:

$$W_m = -\frac{1}{2}\int\int [N_x(\frac{\partial w_0}{\partial x})^2 + N_y(\frac{\partial w_0}{\partial y})^2 + 2N_{xy}\frac{\partial w_0}{\partial x}\frac{\partial w_0}{\partial y}]dxdy \tag{5.24}$$

If there are no transverse loads applied on the laminated plates, the work can be

expressed as follow:

$$W = W_m$$

Thereafter, the total potential energy is obtained as follow:

$$U = \frac{1}{2}\int_0^a \int_0^b [D_{11}(\frac{\partial^2 w_0}{\partial x^2})^2 + 2D_{12}\frac{\partial^2 w_0}{\partial x^2}\frac{\partial^2 w_0}{\partial y^2} + D_{22}(\frac{\partial^2 w_0}{\partial y^2})^2 + 4D_{66}(\frac{\partial^2 w_0}{\partial x \partial y})^2$$
$$+ N_x(\frac{\partial w_0}{\partial x})^2 + N_y(\frac{\partial w_0}{\partial y})^2 + 2N_{xy}\frac{\partial w_0}{\partial x}\frac{\partial w_0}{\partial y}]dxdy \tag{5.23}$$

By virtue of the principle of the stationary potential energy, we have the equation:

$$\frac{\partial U}{\partial A_{mn}} = \frac{\partial}{\partial A_{mn}}(U_d + W) = 0 \tag{5.24}$$

Here, we consider three kinds of boundary conditions for the tapered composite plate configurations:

1. For the boundary condition of the four edges simply supported of the uniform or tapered composite plate configurations, the shape function can be written as

$$w_0(x,y) = \sum_{m=1}^{M}\sum_{n=1}^{N} A_{mn} \cdot \sin\frac{m\pi x}{a} \cdot \sin\frac{n\pi y}{b} \tag{5.25}$$

2. For the boundary condition of the four edges clamped of the uniform or tapered

composite plate configurations, the shape function can be written as

$$w_0(x,y)=\sum_{m=1}^{M}\sum_{n=1}^{N}A_{mn}\cdot\frac{x^2}{a^2}\left(\frac{x}{a}-1\right)^2\left(\frac{x}{a}\right)^{m-1}\cdot\frac{y^2}{b^2}\cdot\left(\frac{y}{b}-1\right)^2\left(\frac{y}{b}\right)^{m-1} \tag{5.26}$$

3. For the boundary condition of one edge clamped and with the other three edges free, the shape function can be written as:

$$w_0(x)=\sum_{n=1}^{N}A_n(1-\cos\frac{\pi x(n-1)}{2a}) \tag{5.27}$$

We consider only one direction in-plane load N_x. By substituting equation (5.23) into equation (5.24) and considering the different displacement functions corresponding to different boundary conditions, we can get the eigenvalue equation of N_{xcr}, and it can be written as follow:

$$\frac{\partial}{\partial A_{mn}}\{\frac{1}{2}\int_0^a\int_0^b[D_{11}(\frac{\partial^2 w_0}{\partial x^2})^2+2D_{12}\frac{\partial^2 w_0}{\partial x^2}\frac{\partial^2 w_0}{\partial y^2}+D_{22}(\frac{\partial^2 w_0}{\partial y^2})^2+4D_{66}(\frac{\partial^2 w_0}{\partial x\partial y})^2]dxdy\}$$

$$+\frac{\partial}{\partial A_{mn}}\int_0^a\int_0^b N_x(\frac{\partial w_0}{\partial x})^2dxdy=0 \tag{5.28}$$

If we choose m = 1, 2, ..., M, and n = 1, 2, ..., N in the shape functions, we can get the following equation about the $\frac{\partial U_d}{\partial A_{mn}}$:

$$\frac{\partial U_d}{\partial A_{mn}} = \sum_{1}^{N}\sum_{1}^{N} G_{mn} \cdot A_{mn} \tag{5.29}$$

Similarly, if we choose m = 1, 2, ..., M, and n = 1, 2, ..., N in the shape functions, we can get the following equation about the $\frac{\partial W}{\partial A_{mn}}$:

$$\frac{\partial W}{\partial A_{mn}} = \sum_{1}^{N}\sum_{1}^{M} H_{mn} \cdot A_{mn} \tag{5.30}$$

Hereafter, we can write the equation (5.28) in the following form:

$$\sum_{1}^{N}\sum_{1}^{N} G_{mn} \cdot A_{mn} + \sum_{1}^{N}\sum_{1}^{M} H_{mn} \cdot A_{mn} = 0 \tag{5.31}$$

.

Then, we can reduce the equation (5.31), and express the eigenvalue equation of N_{xcr} in the following matrix form:

$$[G]\{A_{mn}\} - N_{xcr}[H]\{A_{mn}\} = 0 \tag{5.32}$$

For the first two boundary conditions, we set m = n = 2 and m = n = 3 to analyze the different kinds of tapered composite plate configurations for the critical buckling loads. For the third boundary condition, we set n = 9 to analyze the different kinds of tapered composite plate configurations. We can get the results of the critical buckling

forces for 1st mode, 2nd mode and 3rd mode.

We can also know the 1st mode, 2nd mode and 3rd mode corresponding to the buckling forces for the plate configurations in Figure 4.3 in Chapter 4. The mode shape is the same as that obtained using Finite Element Method.

5.4 Example Calculations of the Critical Buckling Loads for the Uniform and Tapered Composite Plate Configurations

In this part, the uniform and tapered composite plate configurations are considered. By using the results in Chapter 2 and Chapter 3, we calculate the critical buckling loads for uniform and tapered composite plate configurations using Finite Element Method and Ritz method in the following examples. For the uniform composite configuration, we choose the plate configuration according to the uniform plate configuration given in ref. [12], and compare our results of the critical buckling loads with the results given in ref. [12]. For the tapered composite plate configurations, the Finite Element Method and Ritz Method are used to calculate the 1st mode, 2nd mode and 3rd mode buckling loads.

5.4.1 Example Calculations of Critical Buckling Loads for the Uniform Composite Plates

A uniform rectangular laminated plate is made up of the graphite/epoxy material and with symmetric cross-ply arrangement, as shown in Figure 2.6. The laminate is made of eight identical plies with the following mechanical properties: $E_1 = 134.4 \times 10^9$ Pa; $E_2 = E_3 = 10.34 \times 10^9$ Pa; $G_{12} = G_{13} = 4.999 \times 10^9$ Pa; $G_{23} = 1.999 \times 10^9$ Pa; $\nu_{12} = \nu_{13} = \nu_{23} = 0.33$. The plate has a length $L = 127mm$ and a width $b = 12.7mm$. Two different plate thicknesses, $h = 1.016mm$ and $h = 10.16mm$ resulting in the two cases of $L/h = 125$ and $L/h = 12.5$ are considered. The uniform plates have configurations $[(90/0)_2]_S$ at the left and right ends respectively (Figure 2.6).

By using the equations of mechanical behavior of these two uniform configurations derived in Chapter 2, and using the Finite Element Method, we compute the critical buckling loads. The 36-element mesh is taken to calculate the results in this example, and the results have been compared with the results given in ref. [12].

In this example, two types of boundary conditions for these two uniform configurations are studied as follow:

Case 1: one of the short edges fixed and the other three edges free

Case 2: both of the short edges fixed and both of the long edges free

In ref. [12], three kinds of methods are used to calculate the critical bucking loads. The three methods are: the higher order theory (HOT), the classical laminate plate theory (CLPT), and the first order shear deformation theory (FSDT). We calculate the results using Finite Element Method based on CLPT. A total of 36 elements were used. We can see all the results of free vibration frequencies in Table 5.1 and Table 5.2.

First, we consider the boundary condition of one of the short edges fixed and other three edges free (Case 1). The critical buckling loads for the two uniform composite plates (L/h=125 and L/h=12.5) are calculated using Finite Element Method, and the results are given in Table 5.1.

Table 5.1 The critical buckling loads of uniform composite plates with one of the short edges fixed and other three edges free: (unit: N)

L/h	CLPT [12]	FSDT [12]	HOT [12]	FEM (36 elements)
125	16.43	16.38	16.33	16.37
12.5	16344	15772	15364	16370

Next, we consider the boundary condition of both of the short edges fixed and both of the long edges free (Case 2). The critical buckling loads for the two uniform composite plates (L/h=125 and L/h=12.5) are calculated using Finite Element Method,

and the results are given in Table 5.2.

Table 5.2 The critical buckling loads of uniform composite plates with both of the short edges fixed and both of the long edges free: (unit: N)

L/h	CLPT [12]	FSDT [12]	HOT [12]	FEM (36 elements)
125	261.62	260.11	259.73	262.33
12.5	261623	165644	152179	262336

From the Table 5.1 and Table 5.2, we can see that the results calculated using Finite Element Method are very close to the results for the uniform plate configuration (L/h=125). For example, for the uniform plate configuration (L/h=125) in Case 1, the results of FSDT and HOT are 16.38 (N) and 16.33 (N) respectively, whereas the result calculated using Finite Element Method is 16.37 (N), therefore meaning that the present method is efficient for predicting the critical buckling loads for the thin plate configuration. For the uniform plate configuration with L/h=12.5, the result is not as good as that for configuration with L/h=125, because the plate's thickness is large, and therefore the higher order theory and shear deformation theory must be used to analyze the plate configuration with large thickness.

5.4.2 Example Calculation for the Critical Buckling Loads of Tapered Composite Plates

In this part, four different kinds of tapered composite plate configurations, Configuration A, Configuration B, Configuration C, and Configuration D are considered (see Figures 2.7, 2.8, 2.9, and 2.10). Thereafter, we use the Finite Element Method and Ritz Method to calculate the critical buckling loads of the tapered composite plate configurations. Similarly as it is in chapter 4, the example is given below, and it is the same problem as that of the examples given in chapter 2 and chapter 3.

The tapered composite plate configurations are depicted in Figures 2.7, 2.8, 2.9, and 2.10. The laminates are made up of the NCT301 graphite/epoxy material with symmetric cross-ply arrangement. The laminates have twelve plies in the left side and six plies in the right side. For configurations A, B and C, the tapered plates have lay-up configurations $[(0/90)_3]_S$ at the left end and $[0/90/0]_S$ at the right end respectively. For configuration D, the tapered plate has lay-up configuration $[0/resin/90/0/0/90]_S$ at the left end and $[0/90/0]_S$ at the right end respectively. The ply has the following mechanical properties:

$E_1 = 113.9$ GPa, $E_2 = E_3 = 7.9$ GPa, $\nu_{12} = 0.28$, $\nu_{23} = 0.4$, $\nu_{13} = 0.02$, $G_{12} = 3.1$ GPa, $G_{13} = 3.1$ GPa, $G_{23} = 2.8$ GPa, $\rho = 1480$ kg/m^3, $h_0 = 0.138$ mm.

The mechanical properties of the epoxy resin are given as:

$E = 3.93$ GPa, $G = 1.034$ GPa, $\nu = 0.37$, $\rho_r = 1200\ kg/m^3$.

The geometric properties of the tapered composite plates are: the length a is 240 mm and the width b is 240 mm, and the thickness changes in x direction from 2.208 mm to 1.104 mm.

By using Finite Element Method and Ritz Method, we calculate the critical buckling loads of the tapered composite plate configurations under three different boundary conditions.

1. Boundary condition: Four simply supported edges.

Under this boundary condition, the three modes of the critical buckling loads are calculated using Finite Element Method and Ritz Method. The results are shown in Table 5.3, Table 5.4, and Table 5.5, and in Figure 5.2 and Figure 5.3 also, for the four tapered composite plate configurations.

Table 5.3 1st mode critical buckling loads of tapered composite plate configurations with four simply supported edges (unit: N/m)

Taper Configuration	Finite Element Solution			Ritz Solution		
	12 elements	24 elements	36 elements	4-Terms	3-Terms	2-Terms
A	2560	3386	3496	3305	3320	3358
B	2575	3438	3549	3335	3350	3391
C	2592	3524	3635	3404	3422	3470
D	2539	3213	3373	3192	3255	3274

In table 5.3, we can see that the results of 36 elements and 24 elements using finite element method are much closer, and the results of 3 terms and 4 terms using Ritz method are also much closer. Therefore, the 36 elements result for finite element method and 3 terms results for Ritz method are used as the converged results to be compared below.

Table 5.4 2nd mode critical buckling loads of tapered composite plate configurations with four simply supported edges (unit: N/m)

Taper Configuration	Finite Element Solution (36 elements)	Ritz Solution	
		3 Terms	2 Terms
A	10950.3	10720.3	10432.4
B	10961.1	10811.0	10868.2
C	10969.1	10833.2	10701.7
D	10845.6	10622.6	10268.1

Table 5.5 3rd mode critical buckling loads of tapered composite plate configurations with four simply supported edges (unit: N/m)

Taper Configuration	Finite Element Solution (36 elements)	Ritz Solution (3 Terms)
A	7098.8	8131.51
B	7158.4	8262.7
C	7133.5	8254.6
D	6969.8	7848.4

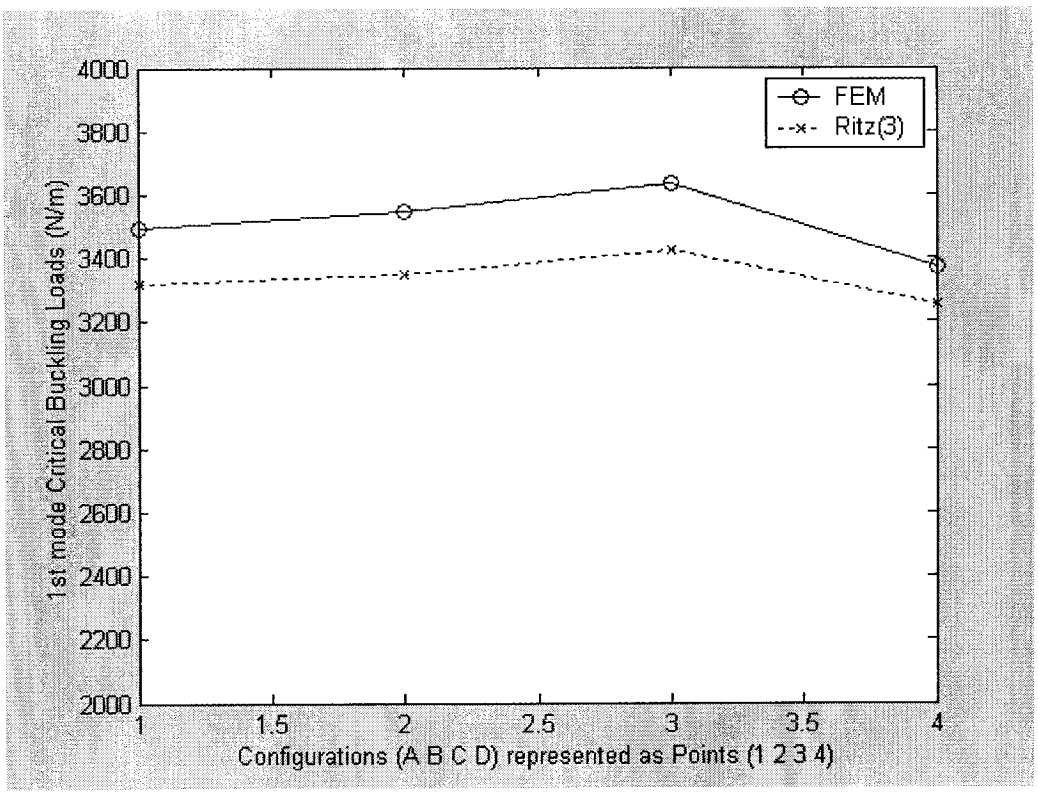

Figure 5.2 1st mode critical buckling loads of tapered composite plates with four edges simply supported calculated using Finite Element and Ritz Methods

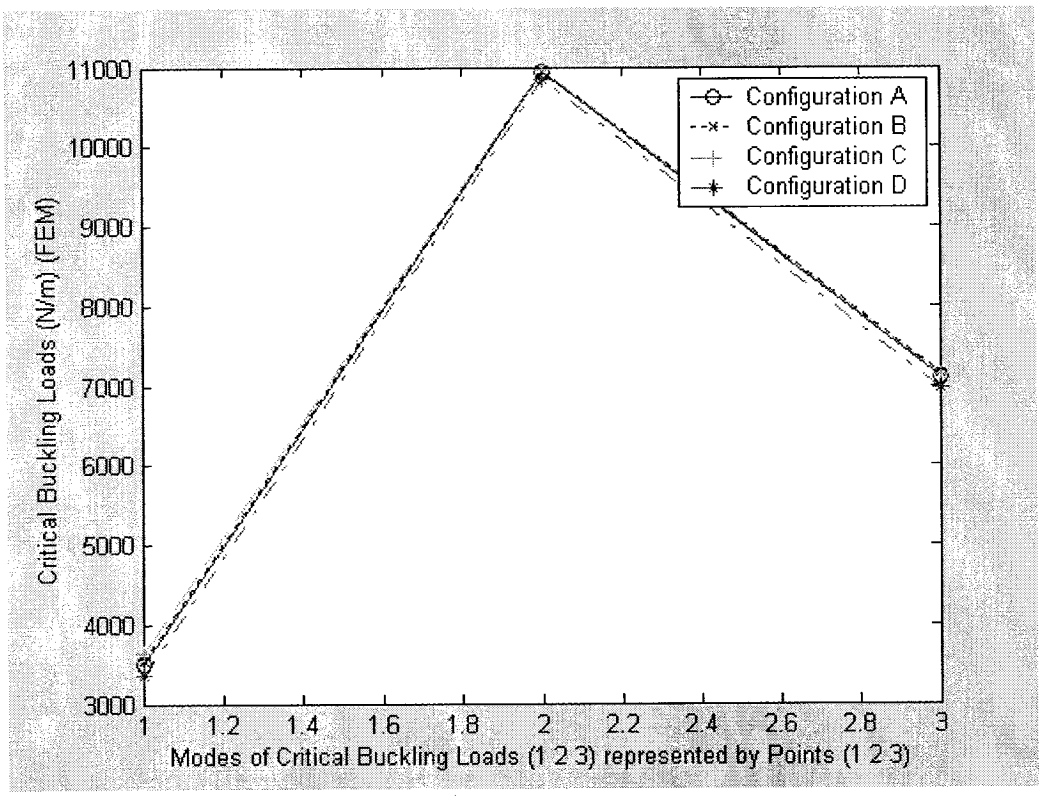

Figure 5.3 The three mode critical buckling loads of tapered composite plate configurations with four edges simply supported calculated using FEM

In Figure 5.2, the graphs show that the 1st mode critical buckling loads of the four tapered composite plate configurations calculated using Finite Element Method are close to the results calculated using Ritz Method. As it can be seen from the Table 5.4, Finite Element Method and Ritz Method also have much closer results for the 2nd mode critical buckling loads. From Table 5.5, 3rd mode critical buckling loads have some differences between the two methods.

In Figure 5.3, we can see that Taper Configuration C has the highest critical buckling loads in all the three modes, whereas Taper Configuration D has the lowest critical buckling loads in all the three modes. The critical buckling loads of Taper Configuration A and Taper Configuration B have the values between the other two configurations. The same trend has been observed in the results obtained using Ritz Method.

2. Boundary condition: Four clamped plate edges.

Under this boundary condition, the three modes of critical buckling loads are calculated using Finite Element Method and Ritz Method. The results are shown in Table 5.6, Table 5.7, and Table 5.8, and in Figure 5.4 and Figure 5.5 also, for the four tapered composite plate configurations.

Table 5.6 1st mode critical buckling loads of tapered composite plate configurations with four clamped plate edges (unit: N/m)

Taper Configuration	Finite Element Solution (36 elements)	Ritz Solution (3 terms)
A	12854	11960
B	13134	12280
C	13383	12430
D	12400	11770

Table 5.7 2nd mode critical buckling loads of tapered composite plate configurations with four clamped plate edges (unit: N/m)

Taper Configuration	Finite Element Solution (36 elements)	Ritz Solution (3 terms)
A	20968.1	22610
B	21017.9	22810
C	21098.4	22940
D	20695.2	22320

Table 5.8 3rd mode critical buckling loads of tapered composite plate configurations with four clamped plate edges (unit: N/m)

Taper Configuration	Finite Element Solution (36 elements)	Ritz Solution (3 terms)
A	14639.4	18660
B	14729.8	18840
C	14725.3	18660
D	14276.8	18620

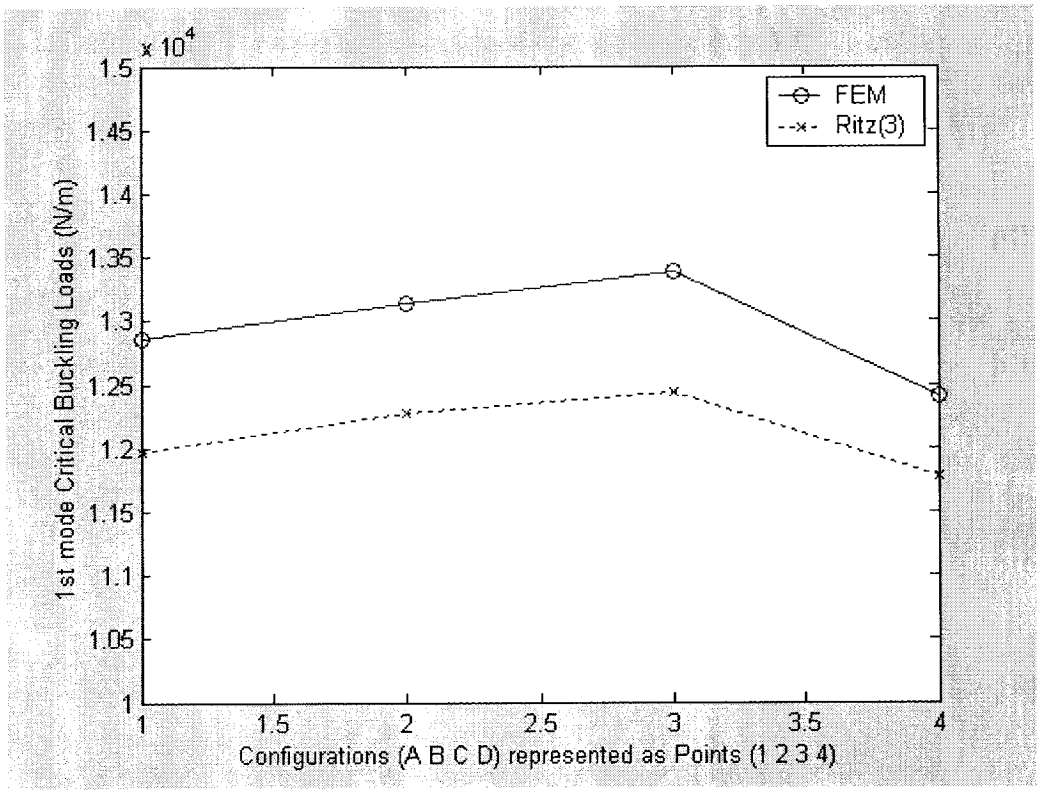

Figure 5.4 1st mode critical buckling loads of tapered composite plates with four edges clamped calculated using Finite Element and Ritz Methods

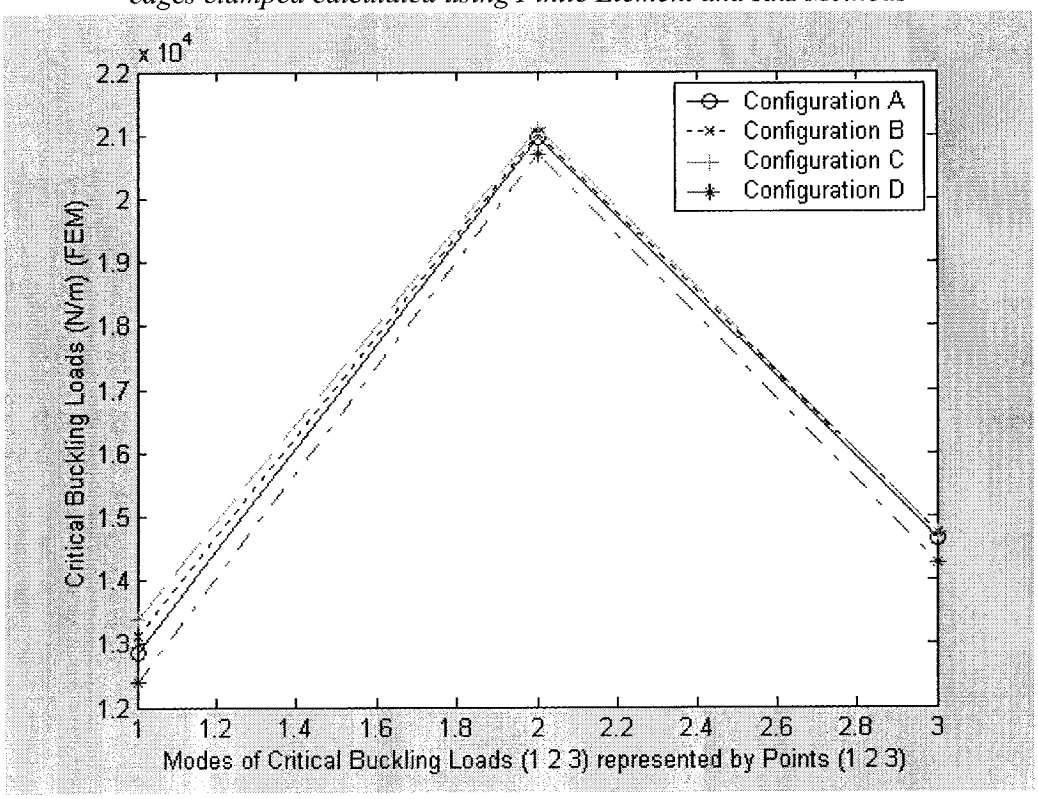

Figure 5.5 The critical buckling loads of three modes of tapered composite plate configurations with four edges clamped calculated using FEM

In Figure 5.4, the graphs show that the 1st mode critical buckling loads of the four tapered composite plate configurations calculated using Finite Element Method are close to the results calculated using Ritz Method. From the Table 5.7 and Table 5.8, it can be seen that the Finite Element Method and Ritz Method have closer results for the 2nd mode critical buckling loads, but the results for 3rd mode critical buckling loads have some differences.

In Figure 5.5, we can see that Taper Configuration C has the highest critical buckling loads in all the three modes, whereas Taper Configuration D has the lowest critical buckling loads in all the three modes. The critical buckling loads of Taper Configuration A and Taper Configuration B have the critical buckling loads between the other two configurations. The same trend has been observed in the results obtained using Ritz Method.

3. Boundary condition: One edge clamped and three edges free

Under this boundary condition, the two modes of critical buckling loads are calculated using Finite Element Method and Ritz Method. The results are shown in Table 5.9 and Table 5.10, and in Figure 5.6 and Figure 5.7 also, for the four tapered composite plate configurations.

Table 5.9 1st mode critical buckling loads of tapered composite plate configurations with one edge clamped and three edges free (unit: N/m)

Taper Configuration	Finite Element Solution (36 elements)	Ritz Solution (9 terms)
A	676.7	676.5
B	694.1	694.1
C	685.9	685.8
D	649.4	649.8

Table 5.10 2nd mode critical buckling loads of tapered composite plate configurations with one edge clamped and three edges free (unit: N/m)

Taper Configuration	Finite Element Solution (36 elements)	Ritz Solution (9 terms)
A	4461.3	4453.3
B	4555.5	4547.0
C	4516.8	4508.4
D	4397.72	4391.21

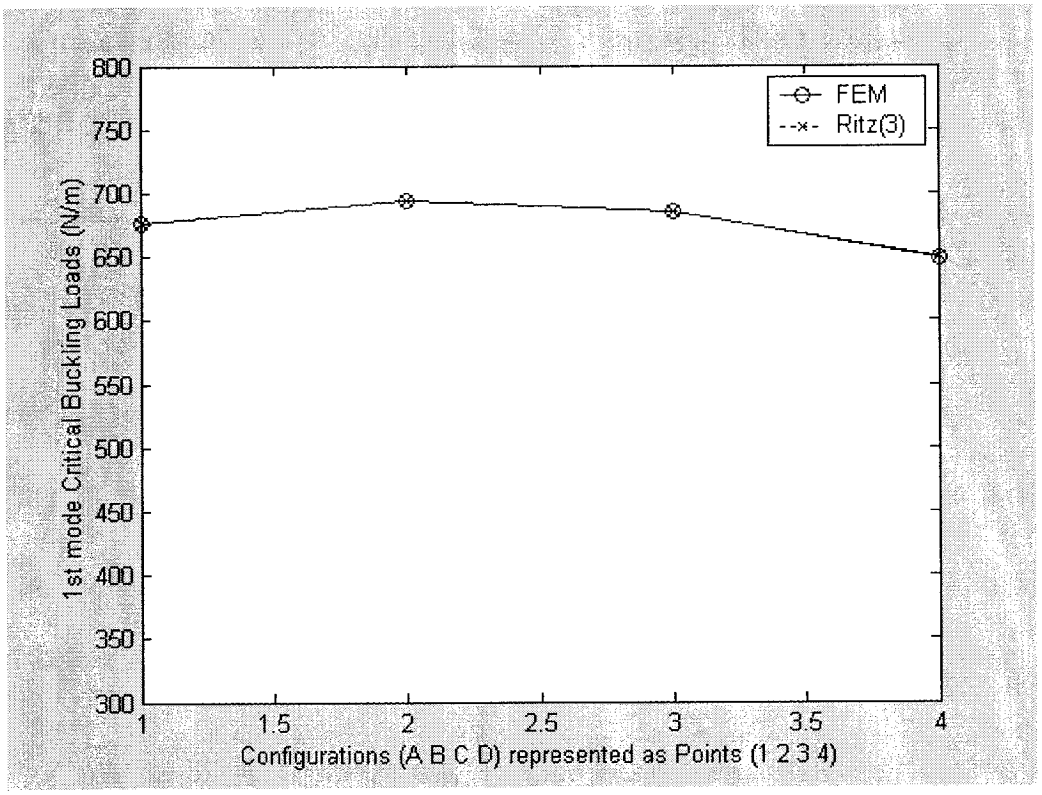

Figure 5.6 1st critical buckling loads of tapered composite plates with one edge clamped and three edges free calculated using Finite Element and Ritz Methods

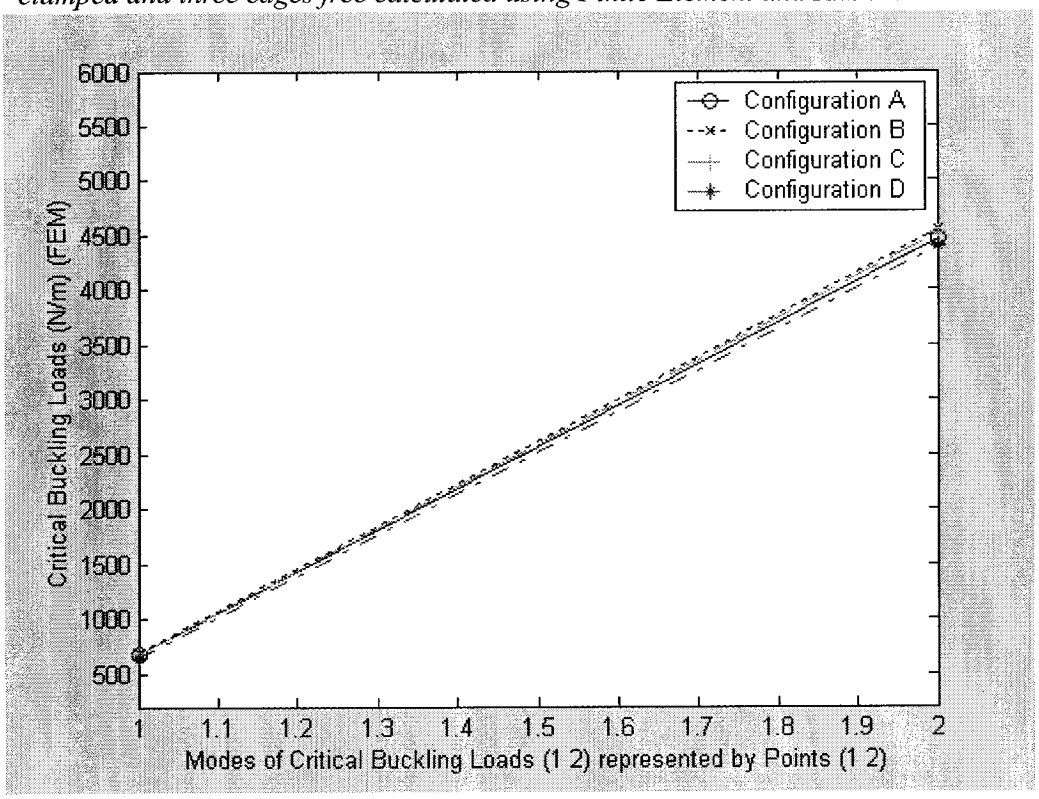

Figure 5.7 The critical buckling loads of two modes of four tapered composite plate configurations with one edges clamped and three edges free calculated using FEM

In Figure 5.6, the graphs show that the 1st mode critical buckling loads of the four tapered composite plate configurations calculated using Finite Element Method are much closer to the results calculated using Ritz Method. From the Table 5.10, it can be seen that the results for 2nd mode critical buckling loads obtained using these two methods are closer.

In Figure 5.7, we can see that Taper Configuration B has the highest critical buckling loads in both the two modes, whereas Taper Configuration D has the lowest critical buckling loads in both the two modes. The critical buckling loads of Taper Configuration A and Taper Configuration C have the critical buckling loads between the other two configurations. The same trend has been observed in the results obtained using Ritz Method. Here, we can see that the critical buckling loads of the four tapered composite plate configurations are much closer for this kind of boundary condition.

5.5 Conclusion

In this chapter, the uniform composite plate configuration and tapered composite plate configurations are considered. By using the results given in Chapter 2 and Chapter 3, we have calculated the critical buckling loads for uniform plate configuration and tapered plate configurations using Finite Element Method and Ritz method. For the

uniform composite plate configuration, we have chosen the plate configuration according to the uniform configuration considered in ref. [12]. By comparing our results of critical buckling loads with the results given in ref. [12], we observe that much close results have been obtained in the present work. For the tapered composite plate configurations, the Finite Element Method and Ritz Method are used to calculate the 1^{st} mode, 2^{nd} mode and 3^{rd} mode critical buckling loads. The calculation shows that the two methods yield close results. The calculation and results of this chapter and Chapter 4 provide a good preparation for the dynamic instability analysis in the following chapter.

Chapter 6

Dynamic Instability Analysis of Uniform and Tapered Composite Plates

6.1 Introduction

Composite plates are widely used in civil, mechanical and aerospace structures. In this chapter, the uniform composite plate configuration and four tapered composite plate configurations are considered. By using the thin plate assumption as in Chapter 3, in this chapter, we calculate the first-order approximation of the first two instability regions for the composite plate configurations using Finite Element Method and Ritz Method. We will derive the formulations based on classical laminate plate theory for analyses using Finite Element Method and Ritz Method. By using the results of mechanical behavior, the stiffness matrix, the mass matrix, and the incremental stiffness matrix of the uniform and tapered composite plate configurations that were calculated in Chapter 2, Chapter 3, Chapter 4, and Chapter 5 respectively, we can determine the instability regions for the uniform and tapered composite plate configurations. The results of instability regions for the uniform composite plate configurations will be compared with the results given in ref. [12].

6.2 Dynamic Instability Analysis of Uniform and Tapered Composite Plate Configurations Using Finite Element Method

In Chapter 3, Chapter 4 and Chapter 5, we have obtained the stiffness matrix $[K]$, the mass matrix $[M]$ and the incremental stiffness matrix $[N]$ for the structural system. Therefore, the equation of motion for the plate can now be written as:

$$\{P\} = [K]\cdot\{Q\} + [N]\cdot\{Q\} + [M]\cdot\{\ddot{Q}\} \tag{6.1}$$

where

$\{P\}$ is the vector of the nodal forces of the structural system,

$\{Q\}$ is the vector of nodal displacements of the structural system,

$[K]$ is the stiffness matrix of the structural system,

$[M]$ is the mass matrix of the structural system,

$[N]$ is incremental stiffness matrix of the structural system,

and overdot denotes differentiation with respect to time.

The governing equation of the plate is obtained by reducing the equation (6.1) in matrix form as follows:

$$[M]\{\ddot{Q}\} + [K]\{Q\} - F_x[N]\{Q\} = \{0\} \tag{6.2}$$

where, F_x is in-plane dynamic buckling loading.

For analyzing the instability of the uniform and tapered composite plates, the plates are subjected to in-plane dynamic buckling loading F_x, and it can be expressed in terms of the critical buckling load N_{cr} as the following form:

$$F_x = \alpha_0 N_{xcr} + \alpha_1 N_{xcr} \cos(\theta t) \tag{6.3}$$

where,

α_0 is the static parameter,

α_1 is the dynamic parameter,

θ is the parametric resonance frequency, and

$\theta / 2\omega$ is the parametric ratio.

By substituting the equation (6.3) for the dynamic buckling loading into the governing equation (6.2), the differential equation for the structural instability can be written as follow:

$$[M]\cdot\{\ddot{Q}\}+[[K]-(\alpha_0+\alpha_1\cdot\cos\theta t)\cdot N_{xcr}\cdot[N]]\cdot\{Q\}=\{0\} \tag{6.4}$$

This Mathieu type equation (6.4) describes the instability behavior of the plate subjected to an in–plane loading which includes a static component and a dynamic component. By solving the generalized eigenvalue problem of this equation, the instability regions can be determined from the boundaries of the stability regions.

Dynamic instability of a structure can be caused by simple parametric resonance with respect to one natural frequency or by combined resonance with respect to two natural frequencies. In this case all dynamic instability regions are separated from dynamic stability regions by periodic solutions with periods $T = 2\pi/\theta$ and $2T = 4\pi/\theta$. The finding of the regions of instability reduces to the determination of conditions under which the differential equation system (6.4) has periodic solutions with period T and $2T$ [1].

To find conditions for the existence of periodic solutions with period $2T$, We seek the solutions of the governing equation (6.4) in the form of a series [1]:

$$\{Q(t)\} = \sum_{k=1,3,5}^{\infty} (\{a_k\} \cdot \sin\frac{k\theta t}{2} + \{b_k\} \cdot \cos\frac{k\theta t}{2}) \tag{6.5}$$

Similarly, to find conditions for the existence of periodic solutions with period T, We seek the solutions of the governing equation (6.4) in the form of a series [1]:

$$\{Q(t)\} = \frac{1}{2}\{b_0\} + \sum_{k=2,4,6}^{\infty} (\{a_k\} \cdot \sin\frac{k\theta t}{2} + \{b_k\} \cdot \cos\frac{k\theta t}{2}) \tag{6.6}$$

where, $\{a_k\}$ and $\{b_k\}$ are vectors which are independent of time. The series is obviously equivalent to the n-term Fourier series for the components of vector $\{Q(t)\}$.

By substituting the series solutions into the governing equation (6.4) and by grouping the sine terms and the cosine terms, two sets of linear algebraic equations in $\{a_k\}$ and $\{b_k\}$ are obtained for each solution.

Hereafter, the determination of the instability regions 1 and 2 can be made by substituting the series solutions into the differential equation and comparing coefficients of $\sin\frac{k\theta t}{2}$ and $\cos\frac{k\theta t}{2}$. For the nontrivial solutions, the resulting determinants must be equal to zero. This leads to the following generalized eigenvalue problems.

For instability Region1 of the composite plate configurations, the boundaries can be obtained using the following equation (see appendix):

$$\begin{vmatrix} [K]-\alpha_0 N_{xcr}[N]\pm\frac{1}{2}\alpha_1 P_{xcr}[N]-\frac{1}{4}\theta^2[M] & -\frac{1}{2}\alpha_1 N_{xcr}[N] & 0 & \cdots\cdots \\ -\frac{1}{2}\alpha_1 N_{xcr}[N] & [K]-\alpha_0 N_{xcr}[N]-\frac{9}{4}\theta^2[M] & -\frac{1}{2}\alpha_1 N_{xcr}[N] & \cdots\cdots \\ 0 & -\frac{1}{2}\alpha_1 N_{xcr}[N] & [K]-\alpha_0 N_{xcr}[N]-\frac{25}{9}\theta^2[M] & \cdots\cdots \\ \cdots\cdots & \cdots\cdots & \cdots\cdots & \cdots\cdots \end{vmatrix} = 0$$

(6.7)

The equation (6.7) determines the two boundaries of the first region of dynamic instability of the uniform and tapered composite plate configurations corresponding to the + and – signs in the term $[K]-\alpha_0 N_{xcr}[N]\pm\frac{1}{2}\alpha_1 N_{xcr}[N]-\frac{1}{4}\theta^2[M]$.

Similarly, for the instability Region2 of the composite plate configurations, the boundaries can be obtained using the following equations (see appendix):

$$\begin{vmatrix} [K]-\alpha_0 N_{xcr}[N]-\theta^2[M] & -\frac{1}{2}\alpha_1 N_{xcr}[N] & 0 & \cdots\cdots \\ -\frac{1}{2}\alpha_1 N_{xcr}[N] & [K]-\alpha_0 N_{xcr}[N]-4\theta^2[M] & -\frac{1}{2}\alpha_1 N_{xcr}[N] & \cdots\cdots \\ 0 & -\frac{1}{2}\alpha_1 N_{xcr}[N] & [K]-\alpha_0 N_{xcr}[N]-9\theta^2[M] & \cdots\cdots \\ \cdots\cdots & \cdots\cdots & \cdots\cdots & \cdots\cdots \end{vmatrix} = 0$$

(6.8)

and

$$\begin{vmatrix} [K]-\alpha_0 N_{xcr}[N] & -\alpha_1 N_{xcr}[N] & 0 & 0 & \cdots \\ -\frac{1}{2}\alpha_1 N_{xcr}[N] & [K]-\alpha_0 N_{xcr}[N]-\theta^2[M] & -\frac{1}{2}\alpha_1 N_{xcr}[N] & 0 & \cdots \\ 0 & -\frac{1}{2}\alpha_1 N_{xcr}[N] & [K]-\alpha_0 N_{xcr}[N]-4\theta^2[M] & -\frac{1}{2}\alpha_1 N_{xcr}[N] & \cdots \\ 0 & 0 & -\frac{1}{2}\alpha_1 N_{xcr}[N] & [K]-\alpha_0 N_{xcr}[N]-9\theta^2[M] & \cdots \\ \cdots & \cdots & \cdots & \cdots & \cdots \end{vmatrix} = 0 \tag{6.9}$$

The two equations (6.8) and (6.9) given above determine the two boundaries of the second region of dynamic instability of the uniform and tapered composite plate configurations.

1. One-term Solution for the Instability Regions for the Composite Plate Configurations

Hereafter, we consider the instability region of one-term solution for the composite plate configurations. The one-term solutions of the governing equation (6.4) can be derived from the equations (6.5) and (6.6), and they can be written as follow:

$$\{Q\} = \{a_1\}\sin(\theta t/2) + \{b_1\}\cos(\theta t/2) \tag{6.10}$$

$$\{Q\} = \frac{1}{2}\{b_0\} + \{a_2\}\sin(\theta t) + \{b_2\}\cos(\theta t) \tag{6.11}$$

By substituting the solutions into the differential equation (6.4) and comparing coefficients of $\sin\frac{k\theta t}{2}$ and $\cos\frac{k\theta t}{2}$, for nontrivial solution, the resulting determinants must be equal to zero. The following generalized eigenvalue problems for 1st Region and 2nd Region are obtained.

For the 1st Instability Region of the uniform and tapered composite plate configurations, by substituting equation (6.10) into the governing equation (6.4), it leads to the following generalized eigenvalue problems.

$$\left|[K] - \alpha_0 N_{xcr}[N] + \frac{1}{2}\alpha_1 N_{xcr}[N] - \frac{1}{4}\theta^2[M]\right| = 0 \tag{6.12}$$

$$\left|[K] - \alpha_0 N_{xcr}[N] - \frac{1}{2}\alpha_1 N_{xcr}[N] - \frac{1}{4}\theta^2[M]\right| = 0 \tag{6.13}$$

Thereafter, we can obtain the upper boundary and lower boundary of the 1st instability region from the two eigenvalue problems given above by equations (6.12) and (6.13).

For the 2nd Instability Region of the uniform and tapered composite plate configurations, by substituting equation (6.11) into the governing equation (6.4), it leads to the following generalized eigenvalue problems.

$$\left|[K]-\alpha_0 N_{xcr}[N]-\theta^2[M]\right|=0 \tag{6.14}$$

$$\begin{vmatrix} [K]-\alpha_0 N_{xcr}[N] & -\alpha_1 N_{xcr}[K] \\ -\frac{1}{2}\alpha_1 N_{xcr}[N] & [K]-\alpha_0 N_{xcr}[N]-\theta^2[M] \end{vmatrix}=0 \tag{6.15}$$

We can also write the equation (6.15) as follow:

$$\begin{vmatrix} [K]-\alpha_0 N_{xcr}[N] & -\alpha_1 N_{xcr}[N] \\ -\frac{1}{2}\alpha_1 N_{xcr}[N] & [K]-\alpha_0 N_{xcr}[N] \end{vmatrix}+\begin{vmatrix} 0 & 0 \\ 0 & [M] \end{vmatrix}\theta^2=0 \tag{6.16}$$

So we can obtain the upper boundary and lower boundary of the 2nd instability region of composite plate configurations from the two eigenvalue problem equations (6.14) and (6.16).

2. Three-term Instability Region for the Composite Plate Configurations

The three-term solutions of the governing equation (6.4) can also be derived from the equations (6.5) and (6.6), and they can be written as follow:

$$\{Q\} = \{a_1\}\sin(\theta t/2) + \{b_1\}\cos(\theta t/2) + \{a_3\}\sin(3\theta t/2) + \{b_3\}\cos(3\theta t) + \{a_5\}\sin(5\theta t/2) + \{b_5\}\cos(5\theta t/2)$$

(6.17)

$$\{Q\} = \frac{1}{2}\{b_0\} + \{a_2\}\sin(\theta t) + \{b_2\}\cos(\theta t) + \{a_4\}\sin(2\theta t) + \{b_4\}\cos(2\theta t) + \{a_6\}\sin(3\theta t) + \{b_6\}\cos(3\theta t)$$

(6.18)

For the 1st Instability Region of the uniform and tapered composite plate configurations, by substituting equation (6.17) into the governing equation (6.4), it leads to the following generalized eigenvalue problem.

$$\begin{vmatrix} [K]-\alpha_0 N_{xcr}[N] \pm \frac{1}{2}\alpha_1 N_{xcr}[N] - \frac{1}{4}\theta^2[M] & -\frac{1}{2}\alpha_1 N_{xcr}[N] & 0 \\ -\frac{1}{2}\alpha_1 N_{xcr}[N] & [K]-\alpha_0 N_{xcr}[N] - \frac{9}{4}\theta^2[M] & -\frac{1}{2}\alpha_1 N_{xcr}[N] \\ 0 & -\frac{1}{2}\alpha_1 N_{xcr}[N] & [K]-\alpha_0 N_{xcr}[N] - \frac{25}{4}\theta^2[M] \end{vmatrix} = 0$$

(6.19)

The eigenvalue problem equation (6.19) expresses the upper boundary and lower boundary of the 1st instability region of the composite plate configurations corresponding to the + and – signs in the term $[K]-\alpha_0 N_{xcr}[N] \pm \frac{1}{2}\alpha_1 N_{xcr}[N] - \frac{1}{4}\theta^2[M]$.

For the 2nd Instability Region of the uniform and tapered composite plate configurations, by substituting equation (6.18) into the governing equation (6.4), it leads to the following generalized eigenvalue problems.

$$\begin{vmatrix} [K]-\alpha_0 N_{xcr}[N]-\theta^2[M] & -\frac{1}{2}\alpha_1 N_{xcr}[N] & 0 \\ -\frac{1}{2}\alpha_1 N_{xcr}[N] & [K]-\alpha_0 N_{xcr}[N]-4\theta^2[M] & -\frac{1}{2}\alpha_1 N_{xcr}[N] \\ 0 & -\frac{1}{2}\alpha_1 N_{xcr}[N] & [K]-\alpha_0 N_{xcr}[N]-9\theta^2[M] \end{vmatrix} = 0 \tag{6.20}$$

and

$$\begin{vmatrix} [K]-\alpha_0 N_{xcr}[N] & -\alpha_1 N_{xcr}[N] & 0 & 0 \\ -\frac{1}{2}\alpha_1 N_{xcr}[N] & [K]-\alpha_0 N_{xcr}[N]-\theta^2[M] & -\frac{1}{2}\alpha_1 N_{xcr}[N] & 0 \\ 0 & -\frac{1}{2}\alpha_1 N_{xcr}[N] & [K]-\alpha_0 N_{xcr}[N]-4\theta^2[M] & -\frac{1}{2}\alpha_1 N_{xcr}[N] \\ 0 & 0 & -\frac{1}{2}\alpha_1 N_{xcr}[N] & [K]-\alpha_0 N_{xcr}[N]-9\theta^2[M] \end{vmatrix} = 0 \tag{6.21}$$

The eigenvalue problems given by equation (6.20) and (6.21) express the upper boundary and lower boundary of the 2nd instability region of the composite plate configurations respectively.

6.3 Dynamic Instability Analysis of Uniform and Tapered Composite Plate Configurations Using Ritz Method

Following the procedures given in Chapter 4 and Chapter 5, we can obtain the strain energy of the composite plate configuration:

$$U = \frac{1}{2} \cdot \int_0^b \int_0^a [D_{11}(\frac{\partial^2 w}{\partial x^2})^2 + D_{22}(\frac{\partial^2 w}{\partial y^2}) + 4D_{66}(\frac{\partial^2 w}{\partial x \partial y}) + 2D_{12}\frac{\partial^2 w}{\partial x^2}\frac{\partial^2 w}{\partial y^2}]dxdy \tag{6.22}$$

The potential (work) of the in–plane forces acting on the composite plate configuration is given by:

$$W = \frac{1}{2}\int_0^b \int_0^a [N_x(\frac{\partial w}{\partial x})^2 + N_y(\frac{\partial w}{\partial y})^2 + 2N_{xy}\frac{\partial w}{\partial x}\frac{\partial w}{\partial y}]dxdy \tag{6.23}$$

The kinetic energy of the composite plate configuration is given by:

$$T = \frac{1}{2}\int\int \rho(\frac{dw}{dt})^2 dxdy \tag{6.24}$$

Therefore, when a composite plate configuration undergoes free vibration, the deflection of the plate has a sinusoidal variation with respect to time t:

$$w = w_0 \cdot \sin \omega t \tag{6.25}$$

Hereafter, the strain energy, the potential (work) and the kinetic energy can be written as follow:

$$U = U_{\max} \cdot \sin^2 \omega t \tag{6.26}$$

$$W = W_{\max} \cdot \sin^2 \omega t \tag{6.27}$$

$$T = \frac{1}{2} \int_0^b \int_0^a \rho (\frac{dw}{dt})^2 dxdy = \frac{1}{2} \omega^2 \sin^2 \omega t \int_0^b \int_0^a \rho {w_0}^2 dxdy \tag{6.28}$$

For the thin plate assumptions given in Chapter 3, the approximate solution of the displacement function $w_0(x, y)$ is sought in the usual form of a double series:

$$w_0(x, y) = \sum_{m=1}^{M} \sum_{n=1}^{N} A_{mn} X_m(x) Y_n(y) \tag{6.29}$$

The different displacement functions that correspond to different boundary conditions are expressed as follow:

1. When we consider the boundary condition of four edges simply supported for the uniform and tapered composite plates, the shape function can be written as:

$$w_0(x,y) = \sum_{m=1}^{M}\sum_{n=1}^{N} A_{mn} \cdot \sin\frac{m\pi x}{a} \cdot \sin\frac{n\pi y}{b} \tag{6.30}$$

2. When we consider the boundary condition of four edges clamped for the uniform and tapered composite plates, the shape function can be written as:

$$w_0(x,y) = \sum_{m=1}^{M}\sum_{n=1}^{N} A_{mn} \cdot \frac{x^2}{a^2}\left(\frac{x}{a}-1\right)^2\left(\frac{x}{a}\right)^{m-1} \cdot \frac{y^2}{b^2}\cdot\left(\frac{y}{b}-1\right)^2\left(\frac{y}{b}\right)^{m-1} \tag{6.31}$$

3. When we consider the boundary condition of one edge clamped and the other three edges free, the shape function can be written as:

$$w_0(x) = \sum_{n=1}^{N} A_n\left(1-\cos\frac{\pi x(n-1)}{2a}\right) \tag{6.32}$$

The coefficients A_{mn} will be determined by the stationary condition. By virtue of the principle of stationary potential energy, the following equations are obtained.

$$\delta(U_{\max} - T_{\max} - W_{\max}) = 0 \tag{6.33}$$

$$\frac{\partial(U_{\max} - T_{\max} - W_{\max})}{\partial A_{mn}} = 0 \tag{6.34}$$

If we choose m = 1, 2, ..., M, and n = 1, 2, ..., N in the shape functions, we can get the following equation for $\frac{\partial U_{\max}}{\partial A_{mn}}$:

$$\frac{\partial U_{\max}}{\partial A_{mn}} = \sum_{1}^{N}\sum_{1}^{N} G_{mn} \cdot A_{mn} \tag{6.35}$$

Similarly, if we choose m = 1, 2, ..., M, and n = 1, 2, ..., N in the shape functions, we can also get the following equation for $\frac{\partial T_{\max}}{\partial A_{mn}}$:

$$\frac{\partial T_{\max}}{\partial A_{mn}} = \sum_{1}^{N}\sum_{1}^{M} L_{mn} \cdot A_{mn} \tag{6.36}$$

And, if we choose m = 1, 2, ..., M, and n = 1, 2, ..., N in the shape functions and the in-plane force is only N_x, we can get the following equation for $\frac{\partial W_{\max}}{\partial A_{mn}}$:

$$\frac{\partial W_{\max}}{\partial A_{mn}} = N_x \sum_{1}^{N} \sum_{1}^{M} H_{mn} \cdot A_{mn} \tag{6.37}$$

Hereafter, we can write the governing equation of the composite plate configurations as in the following form:

$$\sum_{1}^{N} \sum_{1}^{N} G_{mn} \cdot A_{mn} \sum_{1}^{N} \sum_{1}^{M} H_{mn} \cdot A_{mn} + \sum_{1}^{N} \sum_{1}^{M} L_{mn} \cdot \ddot{A}_{mn} = \{0\} \tag{6.38}$$

.

Then, we can reduce the equation (6.38), and express the governing equation (6.38) in the following matrix form:

$$[L] \cdot \{\ddot{A}\} + [G] \cdot \{A\} - N_x [H] \cdot \{A\} = \{0\} \tag{6.39}$$

By considering the dynamic in-plane loading of the composite plate configuration, the load can be expressed as follow:

$$N_x = \alpha_0 N_{xcr} + \alpha_1 N_{xcr} \cos \theta t \tag{6.40}$$

By substituting the equation (6.40) into the differential equation (6.39), the governing equation of the composite plate configuration can be expressed.

$$[L]\{\ddot{A}\}+\{[G]-\alpha_0 N_{xcr}[H]\}\{A\}-(\alpha_1 N_{cr}\cos\theta t)[H]\{A\}=\{0\} \tag{6.41}$$

To find conditions for the existence of periodic solutions with period $2T$, We seek the solutions of the governing equation (6.41) in the form of a series [1]:

$$\{A(t)\}=\sum_{k=1,3,5}^{\infty}(\{a_k\}\cdot\sin\frac{k\theta t}{2}+\{b_k\}\cdot\cos\frac{k\theta t}{2}) \tag{6.42}$$

Similarly, to find conditions for the existence of periodic solutions with period T, We seek the solutions of the governing equation (6.41) in the form of a series [1]:

$$\{A(t)\}=\frac{1}{2}b_0+\sum_{k=2,4,6}^{\infty}(\{a_k\}\cdot\sin\frac{k\theta t}{2}+\{b_k\}\cdot\cos\frac{k\theta t}{2}) \tag{6.43}$$

where, $\{a_k\}$ and $\{b_k\}$ are vectors which are independent of time. The series is obviously equivalent to the n-term Fourier series for the components of vector $A(t)$.

By substituting the series solutions into the governing equation (6.41) and by grouping the sine terms and the cosine terms, two sets of linear algebraic equations in $\{a_k\}$ and $\{b_k\}$ are obtained for each solution.

Determination of the 1st and 2nd instability regions of the composite plate configuration can be made by substituting the series solutions (6.42) and (6.43) into the differential equation (6.41) and comparing coefficients of $\sin\frac{k\theta t}{2}$ and $\cos\frac{k\theta t}{2}$. For nontrivial solution, the resulting determinants must be equal to zero. The following generalized eigenvalue problems for 1st instability region and 2nd instability region are obtained.

Using the procedure similar to that in the Finite Element Method, for the 1st instability region of the composite plate configuration, the boundaries can be obtained by substituting the equation (6.42) into equation (6.41), which results in the following equation:

$$\begin{vmatrix} [G]-\alpha_0 N_{xcr}[H]\pm\frac{1}{2}\alpha_1 P_{xcr}[H]-\frac{1}{4}\theta^2[L] & -\frac{1}{2}\alpha_1 N_{xcr}[H] & 0 & \cdots \\ -\frac{1}{2}\alpha_1 N_{xcr}[H] & [G]-\alpha_0 N_{xcr}[H]-\frac{9}{4}\theta^2[L] & -\frac{1}{2}\alpha_1 N_{xcr}[H] & \cdots \\ 0 & -\frac{1}{2}\alpha_1 N_{xcr}[H] & [G]-\alpha_0 N_{xcr}[H]-\frac{25}{9}\theta^2[L] & \cdots \\ \cdots & \cdots & \cdots & \cdots \end{vmatrix} = 0 \quad (6.44)$$

The equation (6.44) determines the two boundaries of the 1st instability region of dynamic instability of the uniform and tapered composite plate configurations corresponding to the + and – signs in the term $[G]-\alpha_0 N_{xcr}[H]\pm\frac{1}{2}\alpha_1 N_{xcr}[H]-\frac{1}{4}\theta^2[L]$.

Similarly, by substituting the equation (6.43) into the equation (6.41), for the 2nd instability region of the composite plate configuration, the boundaries can be obtained using the following equations:

$$\begin{vmatrix} [G]-\alpha_0 N_{xcr}[H]-\theta^2[L] & -\frac{1}{2}\alpha_1 N_{xcr}[H] & 0 & \cdots\cdots \\ -\frac{1}{2}\alpha_1 N_{xcr}[H] & [G]-\alpha_0 N_{xcr}[H]-4\theta^2[L] & -\frac{1}{2}\alpha_1 N_{xcr}[H] & \cdots\cdots \\ 0 & -\frac{1}{2}\alpha_1 N_{xcr}[H] & [G]-\alpha_0 N_{xcr}[H]-9\theta^2[L] & \cdots\cdots \\ \cdots\cdots & \cdots\cdots & \cdots\cdots & \cdots\cdots \end{vmatrix} = 0 \tag{6.45}$$

and

$$\begin{vmatrix} [G]-\alpha_0 N_{xcr}[H] & -\alpha_1 N_{xcr}[H] & 0 & 0 & \cdots\cdots \\ -\frac{1}{2}\alpha_1 N_{xcr}[H] & [G]-\alpha_0 N_{xcr}[H]-\theta^2[L] & -\frac{1}{2}\alpha_1 N_{xcr}[H] & 0 & \cdots\cdots \\ 0 & -\frac{1}{2}\alpha_1 N_{xcr}[H] & [G]-\alpha_0 N_{xcr}[H]-4\theta^2[L] & -\frac{1}{2}\alpha_1 N_{xcr}[H] & \cdots\cdots \\ 0 & 0 & -\frac{1}{2}\alpha_1 N_{xcr}[H] & [G]-\alpha_0 N_{xcr}[H]-9\theta^2[L] & \cdots\cdots \\ \cdots\cdots & \cdots\cdots & \cdots\cdots & \cdots\cdots & \cdots\cdots \end{vmatrix} = 0 \tag{6.46}$$

These two equations (6.45) and (6.46) determine the two boundaries of the 2nd instability region of dynamic instability of the composite plate configurations respectively.

1. One-term Solution for the Instability Region of the Composite Plates

The one-term solutions of the governing equation (6.41) can be derived from the equations (6.42) and (6.43), and they can be written as follow:

$$\{A\} = \{a_1\}\sin(\theta t/2) + \{b_1\}\cos(\theta t/2) \tag{6.47}$$

$$\{A\} = \frac{1}{2}\{b_0\} + \{a_2\}\sin(\theta t) + \{b_2\}\cos(\theta t) \tag{6.48}$$

By substituting the solutions into the differential equation (6.41) and comparing coefficients of $\sin\frac{k\theta t}{2}$ and $\cos\frac{k\theta t}{2}$, for nontrivial solution, the resulting determinants must be equal to zero. The following generalized eigenvalue problems for 1st instability region and 2nd instability region are obtained.

For the 1st instability region of the uniform and tapered composite plate configurations, by substituting (6.47) into the governing equation (6.41), it leads to the following generalized eigemvalue problems.

$$\left|[G]-\alpha_0 N_{xcr}[H]+\frac{1}{2}\alpha_1 N_{xcr}[H]-\frac{1}{4}\theta^2[L]\right|=0 \tag{6.49}$$

$$\left|[G]-\alpha_0 N_{xcr}[H]-\frac{1}{2}\alpha_1 N_{xcr}[H]-\frac{1}{4}\theta^2[L]\right|=0 \tag{6.50}$$

Thereafter, we can obtain the upper boundary and lower boundary of the 1st instability region from the two eigenvalue problems given by equations (6.49) and (6.50).

For the 2nd instability region of the uniform and tapered composite plate configurations, by substituting (6.48) into the governing equation (6.41), it leads to the following generalized eigenvalue problems.

$$\left|[G]-\alpha_0 N_{xcr}[H]-\theta^2[L]\right|=0 \tag{6.51}$$

$$\begin{vmatrix}[G]-\alpha_0 N_{xcr}[H] & -\alpha_1 N_{xcr}[H] \\ -\frac{1}{2}\alpha_1 N_{xcr}[H] & [G]-\alpha_0 N_{xcr}[H]-\theta^2[L]\end{vmatrix}=0 \tag{6.52}$$

We can also write the equation (6.52) in the following form:

$$\begin{vmatrix}[G]-\alpha_0 N_{xcr}[H] & -\alpha_1 N_{xcr}[H] \\ -\frac{1}{2}\alpha_1 N_{xcr}[H] & [G]-\alpha_0 N_{xcr}[H]\end{vmatrix}+\begin{vmatrix}0 & 0\\ 0 & [L]\end{vmatrix}\theta^2=0 \tag{6.53}$$

We can obtain the upper boundary and lower boundary of the 2nd instability region of composite plate configurations from the two eigenvalue problems given by equations (6.51) and (6.53).

2. Three-term Solution for the Instability Region of the Composite Plate Configurations

Next, the three-term solutions of the governing equation (6.41) can also be derived from the equations (6.42) and (6.43), and they can be written as follow:

$$\{A\} = \{a_1\}\sin(\theta t/2) + \{b_1\}\cos(\theta t/2) + \{a_3\}\sin(3\theta t/2) + \{b_3\}\cos(3\theta t) + \{a_5\}\sin(5\theta t/2) + \{b_5\}\cos(5\theta t/2) \tag{6.54}$$

$$\{A\} = \frac{1}{2}\{b_0\} + \{a_2\}\sin(\theta t) + \{b_2\}\cos(\theta t) + \{a_4\}\sin(2\theta t) + \{b_4\}\cos(2\theta t) + \{a_6\}\sin(3\theta t) + \{b_6\}\cos(3\theta t) \tag{6.55}$$

For the 1st instability region of the uniform and tapered composite plate configurations, by substituting (6.54) into the governing equation (6.41), it leads to the following generalized eigenvalue problem.

$$\begin{vmatrix} [G]-\alpha_0 N_{xcr}[H]\pm\frac{1}{2}\alpha_1 N_{xcr}[H]-\frac{1}{4}\theta^2[L] & -\frac{1}{2}\alpha_1 N_{xcr}[H] & 0 \\ -\frac{1}{2}\alpha_1 N_{xcr}[H] & [G]-\alpha_0 N_{xcr}[H]-\frac{9}{4}\theta^2[L] & -\frac{1}{2}\alpha_1 N_{xcr}[H] \\ 0 & -\frac{1}{2}\alpha_1 N_{xcr}[H] & [G]-\alpha_0 N_{xcr}[H]-\frac{25}{4}\theta^2[L] \end{vmatrix} = 0$$

(6.56)

The eigenvalue problem (6.56) given by equation (6.56) expresses the upper-boundary and lower-boundary of the 1st instability region of the composite plate configurations corresponding to the + and – signs in the term $[G]-\alpha_0 N_{xcr}[H]\pm\frac{1}{2}\alpha_1 N_{xcr}[H]-\frac{1}{4}\theta^2[L]$.

For the 2nd instability region of the uniform and tapered composite plate configurations, by substituting (6.54) into the governing equation (6.41), it leads to the following generalized eigenvalue problems.

$$\begin{vmatrix} [G]-\alpha_0 N_{xcr}[H]-\theta^2[L] & -\frac{1}{2}\alpha_1 N_{xcr}[H] & 0 \\ -\frac{1}{2}\alpha_1 N_{xcr}[H] & [G]-\alpha_0 N_{xcr}[H]-4\theta^2[L] & -\frac{1}{2}\alpha_1 N_{xcr}[H] \\ 0 & -\frac{1}{2}\alpha_1 N_{xcr}[H] & [G]-\alpha_0 N_{xcr}[H]-9\theta^2[L] \end{vmatrix} = 0$$

(6.57)

and

$$\begin{vmatrix} [G]-\alpha_0 N_{xcr}[H] & -\alpha_1 N_{xcr}[H] & 0 & 0 \\ -\frac{1}{2}\alpha_1 N_{xcr}[H] & [G]-\alpha_0 N_{xcr}[H]-\theta^2[L] & -\frac{1}{2}\alpha_1 N_{xcr}[H] & 0 \\ 0 & -\frac{1}{2}\alpha_1 N_{xcr}[H] & [G]-\alpha_0 N_{xcr}[H]-4\theta^2[L] & -\frac{1}{2}\alpha_1 N_{xcr}[H] \\ 0 & 0 & -\frac{1}{2}\alpha_1 N_{xcr}[H] & [G]-\alpha_0 N_{xcr}[H]-9\theta^2[L] \end{vmatrix} = 0$$

(6.58)

The eigenvalue problems given by equations (6.57) and (6.58) express the upper boundary and lower boundary of the 2nd instability region of the composite plate configurations respectively.

6.4 The Example Calculation for the Instability Regions of Uniform and Tapered Composite Plate Configurations

In this section, the uniform composite plate and tapered composite plates are considered. By using the results of Chapter 2, Chapter 3, Chapter 4 and Chapter 5, and the formulation developed in the present Chapter, we calculate the instability regions for uniform and tapered composite plate configurations using Finite Element Method and Ritz method in the following examples. For the uniform composite configuration, we choose the plate configuration considered in ref. [12], and compare our results of the

instability regions with the results given in ref. [12]. For the tapered composite plate configurations, the Finite Element Method and Ritz Method are used to calculate the one-term instability regions and three-term instability regions.

6.4.1 The Example Calculation of Instability Regions for the Uniform Composite Plate

A uniform rectangular laminated plate is made up of the graphite/epoxy material and with symmetric cross-ply arrangement, as shown in Figure 2.6. The laminate is made out of eight identical plies with the following mechanical properties: $E_1 = 134.4 \times 10^9$ Pa ; $E_2 = E_3 = 10.34 \times 10^9$ Pa; $G_{12} = G_{13} = 4.999 \times 10^9$ Pa; $G_{23} = 1.999 \times 10^9$ Pa; $\nu_{12} = \nu_{13} = \nu_{23} = 0.33$; $\rho = 1480\ kg/m^3$. The plate has a length $L = 127$ mm and a width $b = 12.7$ mm. Two different plate thicknesses, $h = 1.016$ mm and $h = 10.16$ mm resulting in the two cases of $L/h = 125$ and $L/h = 12.5$, are considered as in ref. [12]. The uniform plate has configuration $[(90/0)_2]_S$ at the left and right ends respectively (see Figure 2.6).

Based on the results for the mechanical behavior of these two uniform configurations calculated in Chapter 2, we use the Finite Element Method to compute their instability regions. The 36-element mesh is taken to calculate the results in this example, and the results have been compared with the results given in ref. [12].

In this example, two types of boundary conditions for these two uniform configurations are considered as follow:

Case 1: one of the short edges is fixed and the other three edges are free

Case 2: both of the short edges are fixed and both the long edges are free

In ref. [12], the first-order approximation of the first two instability regions for the composite plate are calculated based on the finite element method. The three theories that have been used are: the Higher Order Theory (HOT), the Classical Laminate Plate Theory (CLPT), and the First Order Shear Deformation Theory (FSDT). In this chapter, we calculate the results using Finite Element Method based on CLPT. A total of 36 elements were used. We can see all the results for the first two instability regions for the composite plate in the figures given next.

We consider the boundary condition of one of the short edges being fixed and other three edges being free (Case 1) and the boundary condition of both the short edges being fixed and both the long edges are free (Case 2). The variation of the natural frequency of the plate with the static buckling load and the first-order approximations to the first two instability regions of the composite plates (L/h=125 and L/h=12.5) are calculated using Finite Element Method, and the results are given in Figures 6.1-6.4.

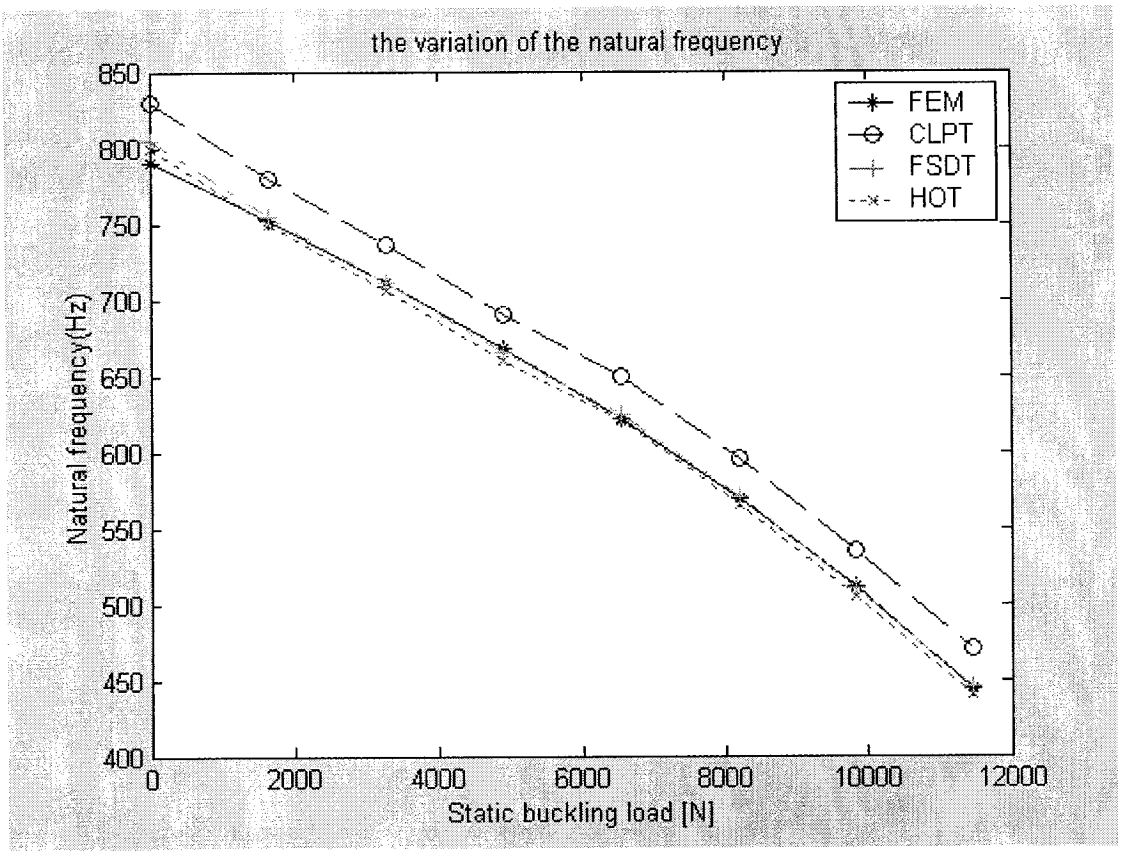

Figure 6.1 The variation of the natural frequency of the uniform composite plate with the static buckling load and with Case 1 boundary condition; L/h=12.5

From Figure 6.1, we can see that the results obtained in the present work using Finite Element Method based on CLPT are very close to the results obtained using Finite Element Method based on FSDT and HOT given in ref. [12]. Therefore, it shows that the present Finite Element Method provides an accurate prediction of the natural frequencies corresponding to different static buckling loads.

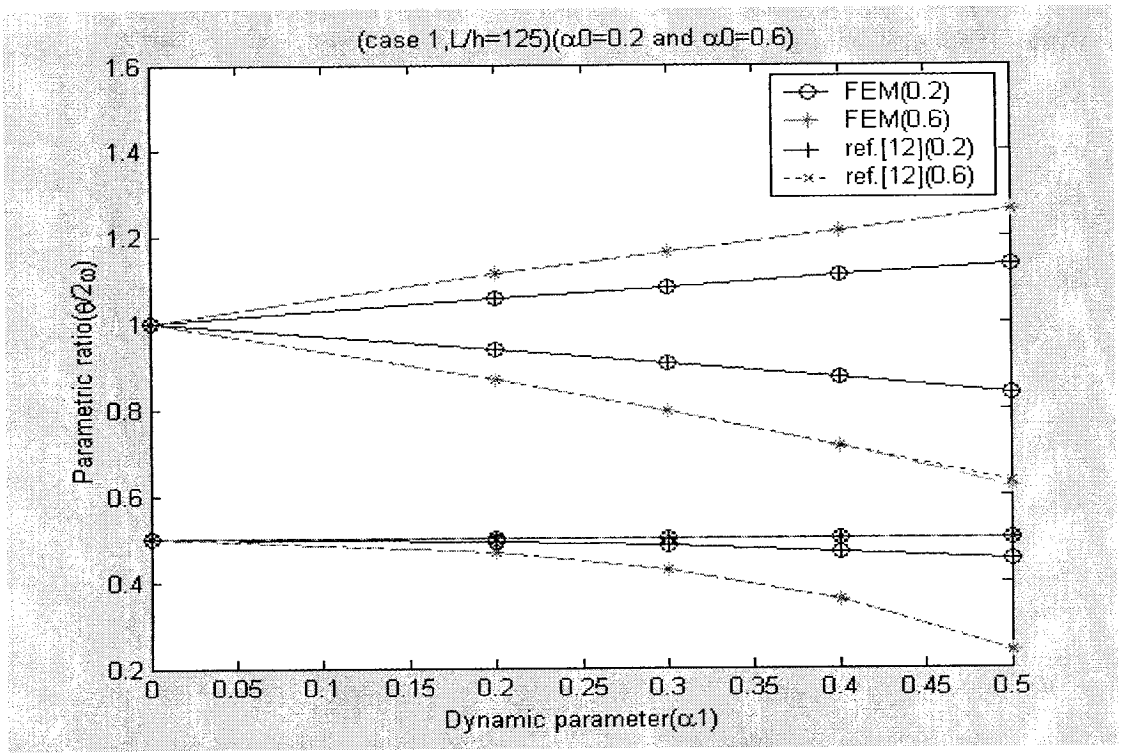

Figure 6.2 The first-order approximation of the first two instability regions for the uniform composite plate with Case 1 boundary condition; L/h=125

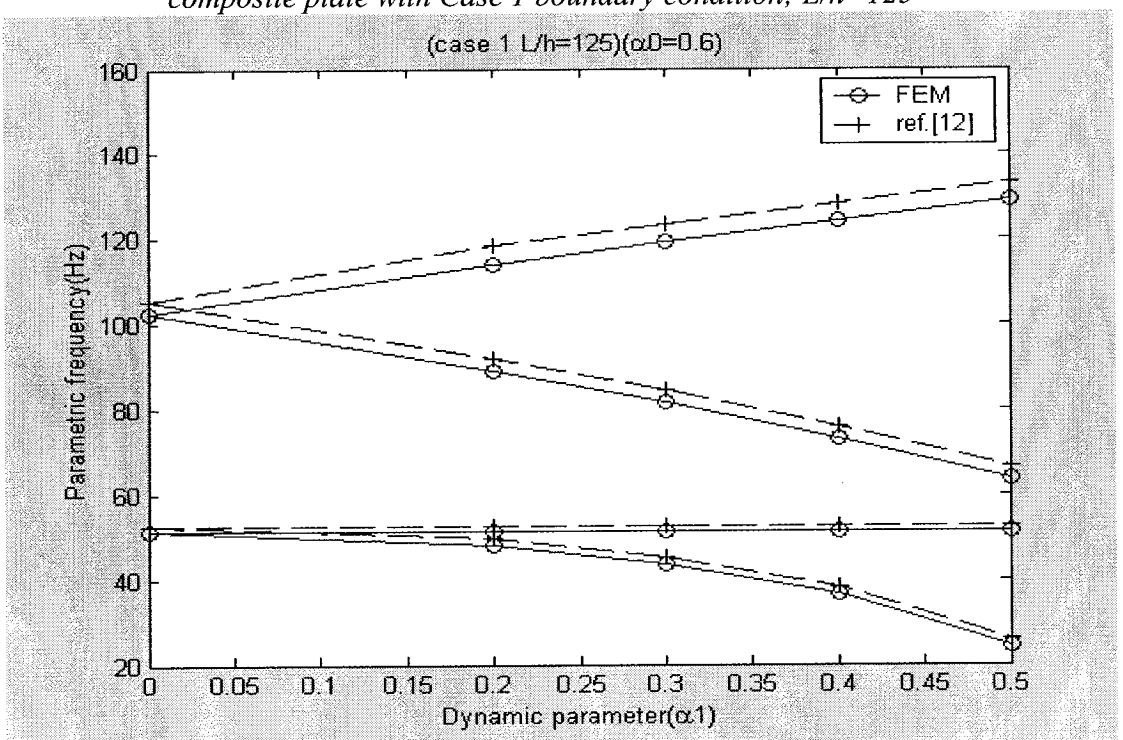

Figure 6.3 Two instability regions of the uniform composite plate calculated using Finite Element Method; Case 1boundary condition; L/h=125

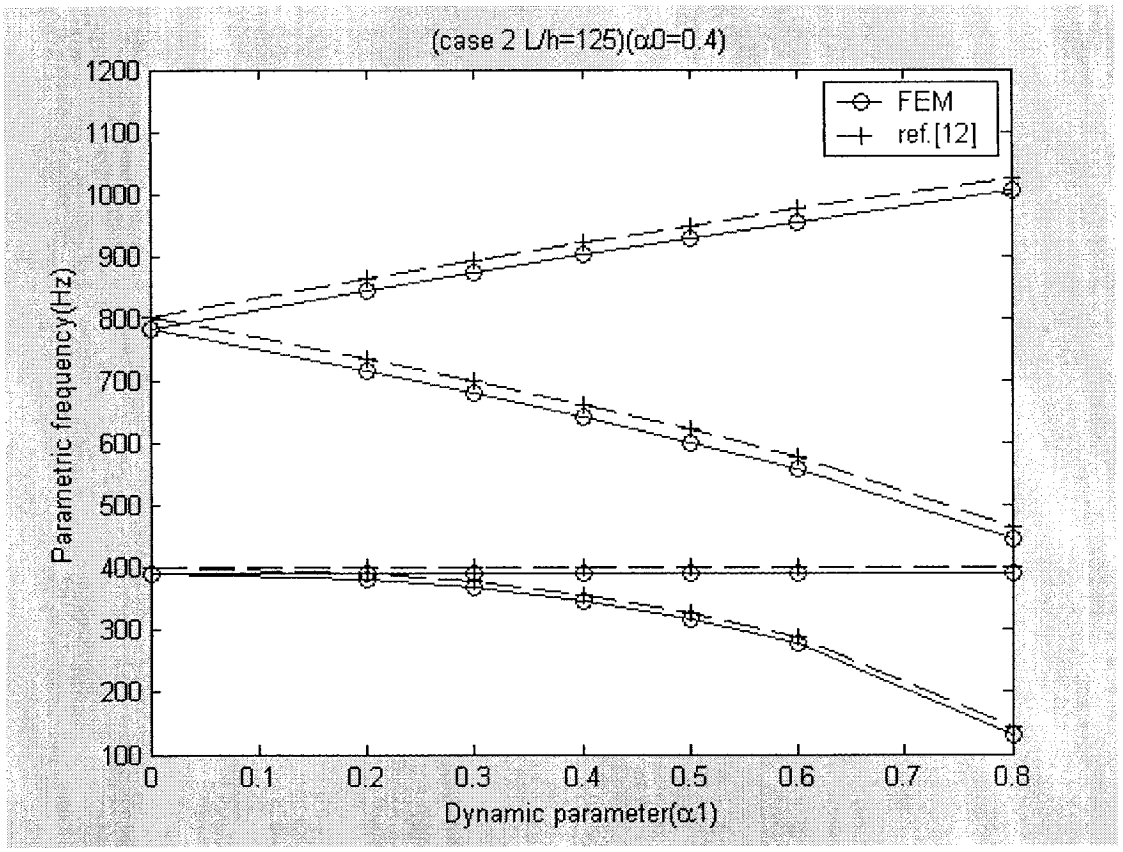

Figure 6.4 Two instability regions of the uniform composite plate calculated using Finite Element Method with Case 2 boundary condition; L/h=125

From Figures 6.2, 6.3 and 6.4, we can see that the results obtained using Finite Element Method are very close to the results given in ref. [12]. Both the results have the same trend of the two instability regions and the width of the instability regions increase with an increase in both static and dynamic loads, as expected. So, it is expected that the present Finite Element Solution will provide accurate results for tapered composite plate configurations in the following example.

6.4.2 Example Calculation of Instability Regions for Tapered Composite Plates

In this section, four different kinds of tapered composite plate configurations, Configuration A, Configuration B, Configuration C, and Configuration D are considered (see Figures 2.7, 2.8, 2.9, and 2.10). We use the Finite Element Method and Ritz Method to calculate the instability regions of the tapered composite plate configurations. The example is given below and it involves the same problem as that of the examples given in Chapter 2, Chapter 3, Chapter 4 and Chapter 5.

The tapered composite plate configurations are depicted in Figures 2.7, 2.8, 2.9, and 2.10. The laminates are made up of the NCT301 graphite/epoxy material with symmetric cross-ply arrangement. The laminates have twelve plies in the left side and six plies in the right side. For configurations A, B and C, the tapered plates have lay-up configurations $[(0/90)_3]_S$ at the left end and $[0/90/0]_S$ at the right end respectively. For configuration D, the tapered plate has lay-up configurations $[0/resin/90/0/0/90]_S$ at the left end and $[0/90/0]_S$ at the right end respectively. The ply has the following mechanical properties: $E_1 = 113.9$ GPa, $E_2 = E_3 = 7.9$ GPa, $\nu_{12} = 0.28$, $\nu_{23} = 0.4$, $\nu_{21} = 0.02$, $G_{12} = 3.1$ GPa, $G_{13} = 3.1$ GPa, $G_{23} = 2.8$ GPa, $\rho = 1480\ kg/m^3$, $h_0 = 0.138$ mm, $\rho = 1480\ kg/m^3$.

The mechanical properties of the epoxy resin are given as:

$E = 3.93$ GPa, $G = 1.034$ GPa, $\nu = 0.37$, $\rho_r = 1200\ kg/m^3$.

The geometric properties of the tapered composite plates are: the length a is 240 mm and the width b is 240 mm, and the thickness changes in x direction from 2.208 mm to 1.104 mm.

By using Finite Element Method and Ritz Method, we calculate the instability regions of the tapered composite plate configurations under three different boundary conditions.

1. The Instability Analysis of Taper Configuration A under Three Kinds of Boundary Conditions:

With four edges simply supported, the variation of the natural frequency with the static buckling load and the two instability regions ($\alpha_0 = 0.2, \alpha_0 = 0.5$, and $\alpha_0 = 0.8$) of the tapered composite plate configuration A are shown in the Figures 6.5-6.8.

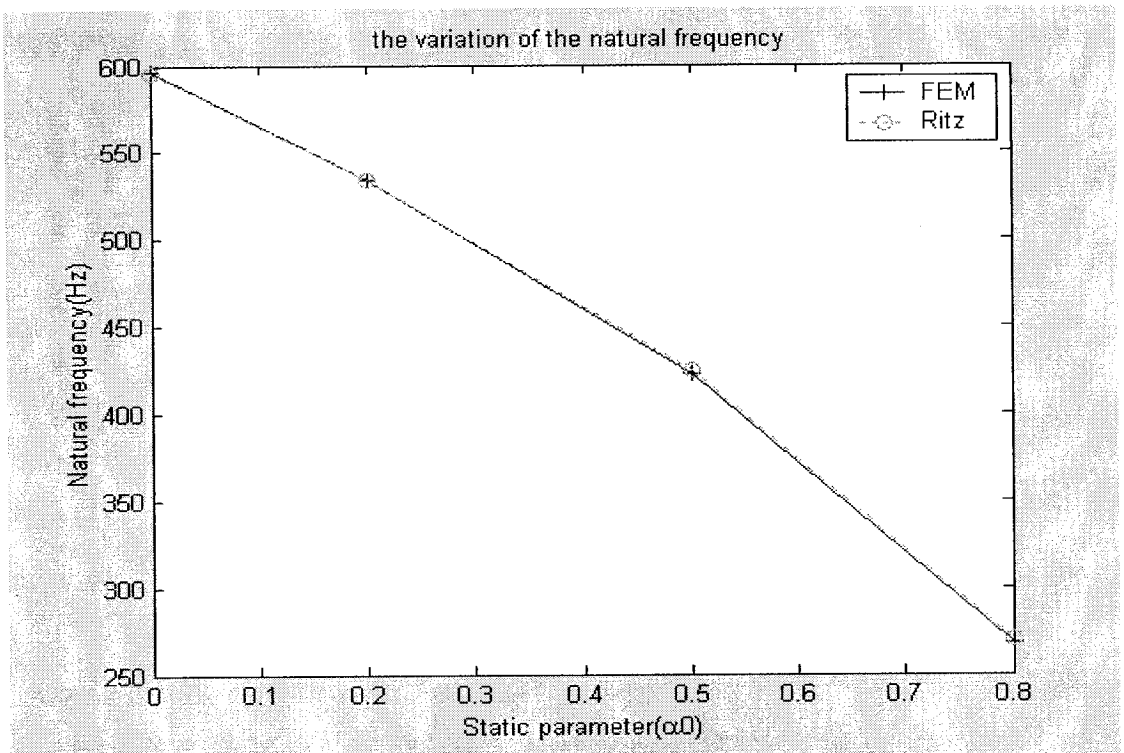

Figure 6.5 The variation of the natural frequency of taper configuration A with the static buckling load; four edges are simply supported

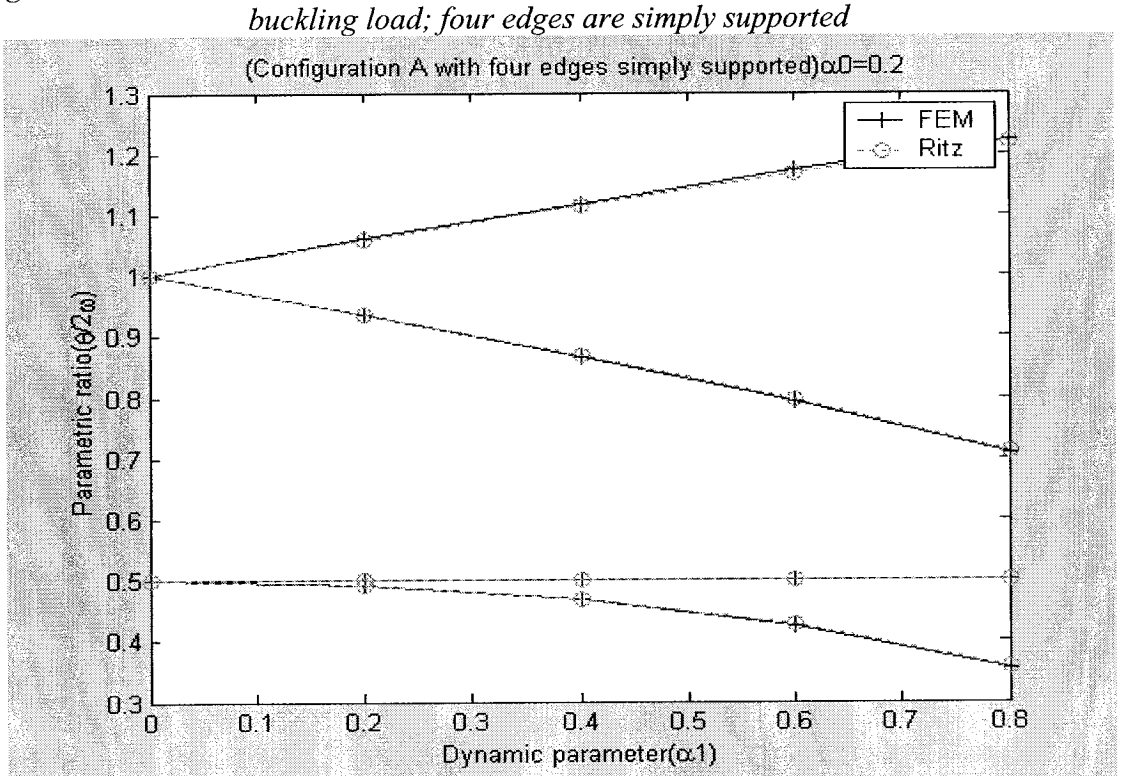

Figure 6.6 Two instability regions of taper configuration A determined using Finite Element Method and Ritz Method; four edges are simply supported ($\alpha_0 = 0.2$)

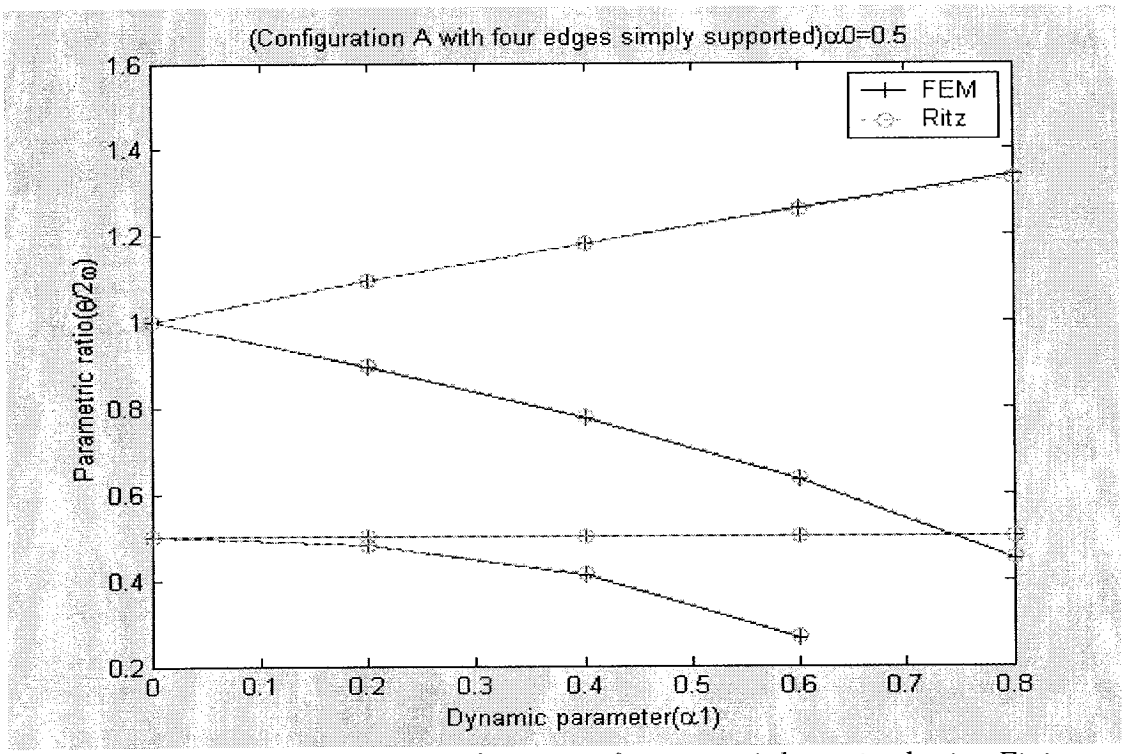

Figure 6.7 Two instability regions of taper configuration A determined using Finite Element Method and Ritz Method; four edges are simply supported ($\alpha_0 = 0.5$)

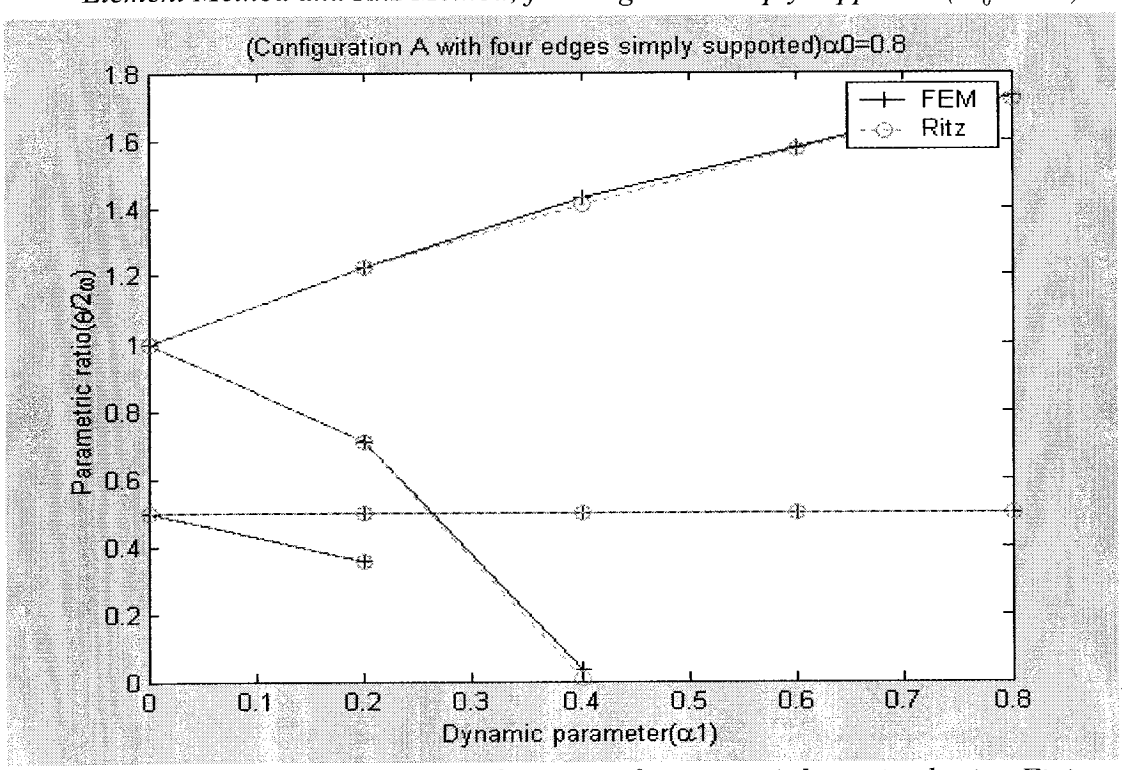

Figure 6.8 Two instability regions of taper configuration A determined using Finite Element Method and Ritz Method; four edges are simply supported ($\alpha_0 = 0.8$)

In Figure 6.5, the graphs show that the natural frequencies decrease as the static buckling loads increase. The variations of natural frequencies of the tapered composite plate configuration A obtained using Finite Element Method and Ritz Method have almost the same form.

From Figures 6.6, 6.7, and 6.8, we can see the two instability regions with different static parameters corresponding to $\alpha_0 = 0.2, \alpha_0 = 0.5$, and $\alpha_0 = 0.8$. The graphs show that the widths of the instability regions increase with an increase in both the static and dynamic loads. The instability regions for tapered composite plate configuration A determined using Finite Element Method are much closer to that obtained using Ritz Method.

Next, considering the boundary condition of four edges clamped, the variation of the natural frequency with the static buckling load and the two instability regions ($\alpha_0 = 0.2, \alpha_0 = 0.5$, and $\alpha_0 = 0.8$) of the tapered composite plate configuration A are determined and shown in the Figures 6.9-6.12.

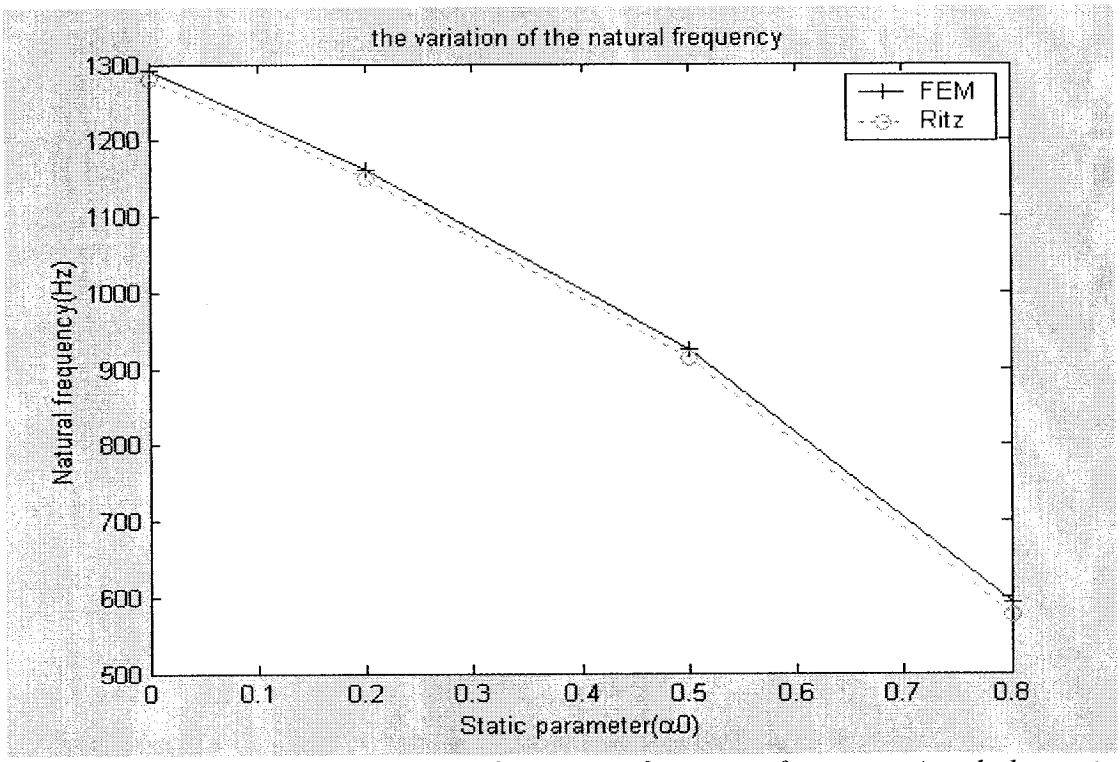

Figure 6.9 The variation of the natural frequency of taper configuration A with the static buckling load; four edges are clamped

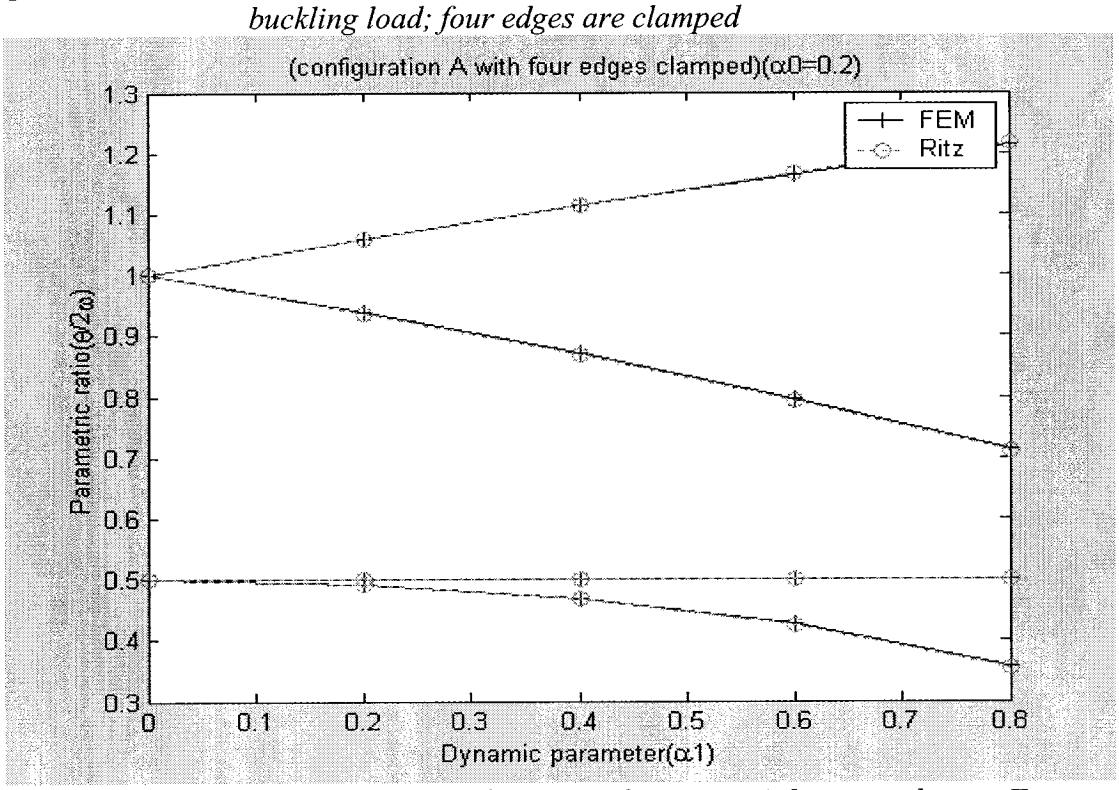

Figure 6.10 Two instability regions of taper configuration A determined using Finite Element Method and Ritz Method; four edges are clamped ($\alpha_0 = 0.2$)

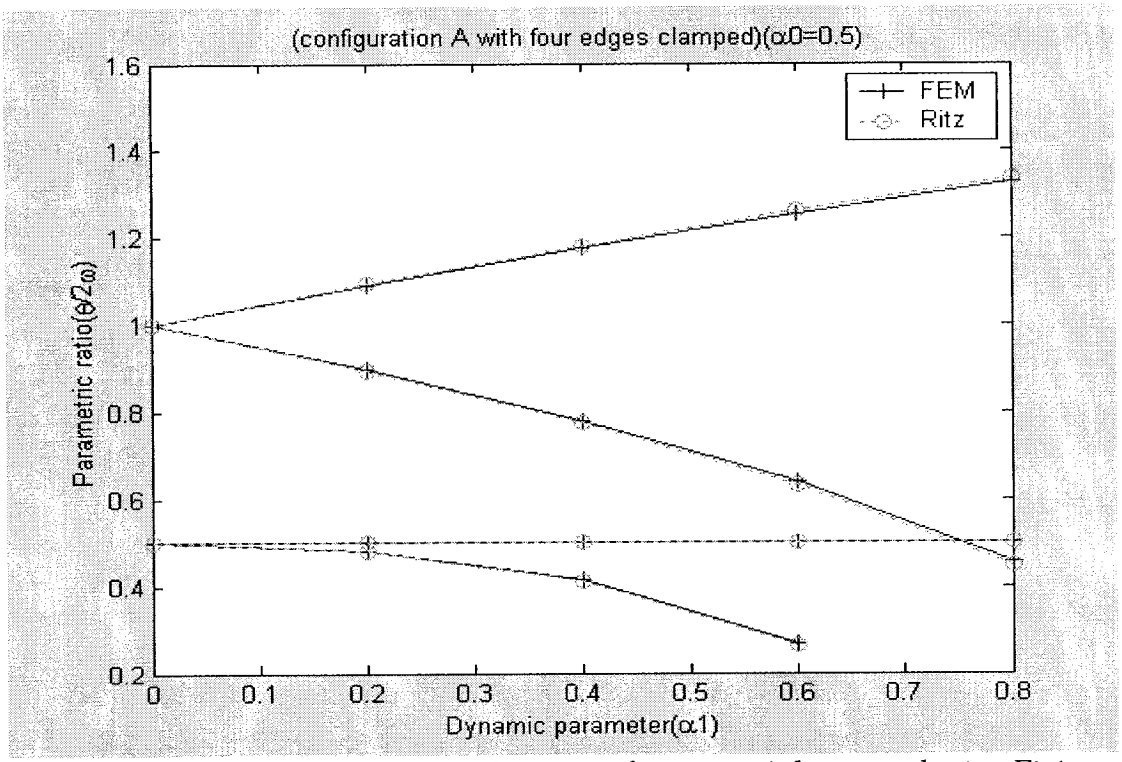

Figure 6.11 Two instability regions of taper configuration A determined using Finite Element Method and Ritz Method; four edges are clamped ($\alpha_0 = 0.5$)

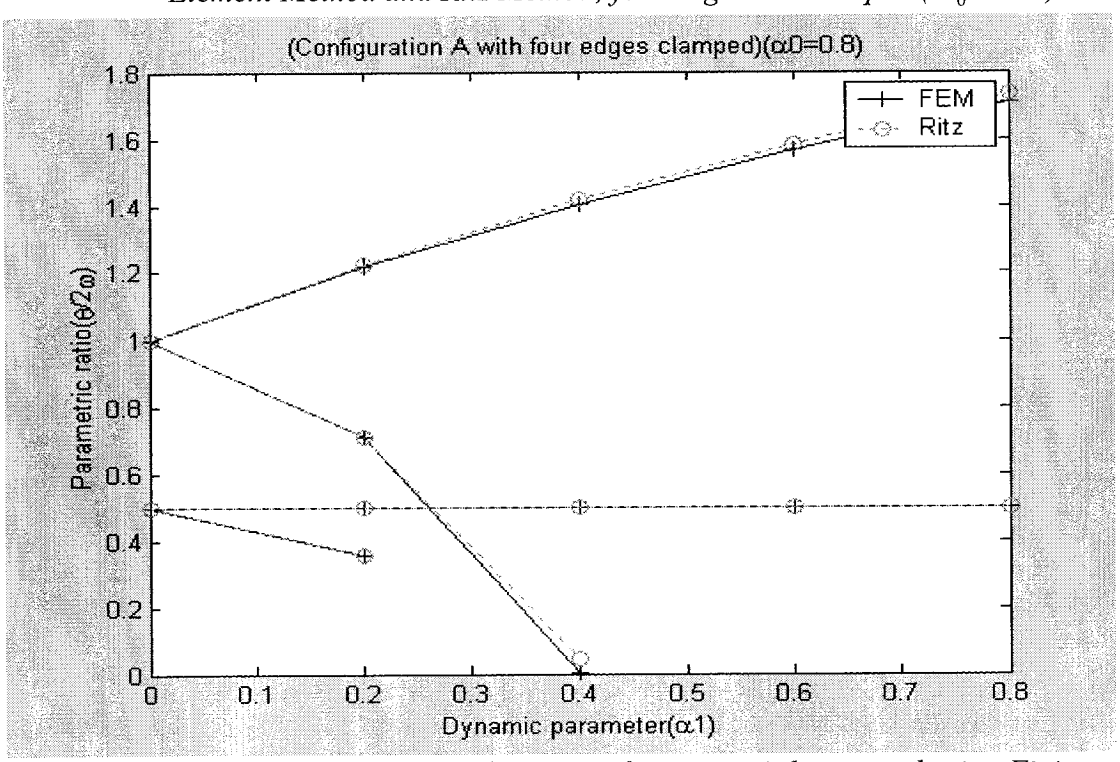

Figure 6.12 Two instability regions of taper configuration A determined using Finite Element Method and Ritz Method; four edges are clamped ($\alpha_0 = 0.8$)

In Figure 6.9, the graphs show that the natural frequencies decrease as the static buckling loads increase. The variations of natural frequencies of the tapered composite plate configuration A obtained using Finite Element Method and Ritz Method have almost the same form.

From Figures 6.10, 6.11, and 6.12, we can see the two instability regions with different static parameters corresponding to $\alpha_0 = 0.2$, $\alpha_0 = 0.5$, and $\alpha_0 = 0.8$. The graphs show that the widths of the instability regions increase with an increase in both the static and dynamic loads. The instability regions for tapered composite plate configuration A with four edges clamped determined using Finite Element Method are very close to that obtained using Ritz Method.

Finally, considering the boundary condition of one edge clamped and other three edges free, the variation of the natural frequency with the static buckling load and the two instability regions ($\alpha_0 = 0.2$, $\alpha_0 = 0.5$, and $\alpha_0 = 0.8$) of the tapered composite plate configuration A are determined and shown in the following Figures 6.13-6.16.

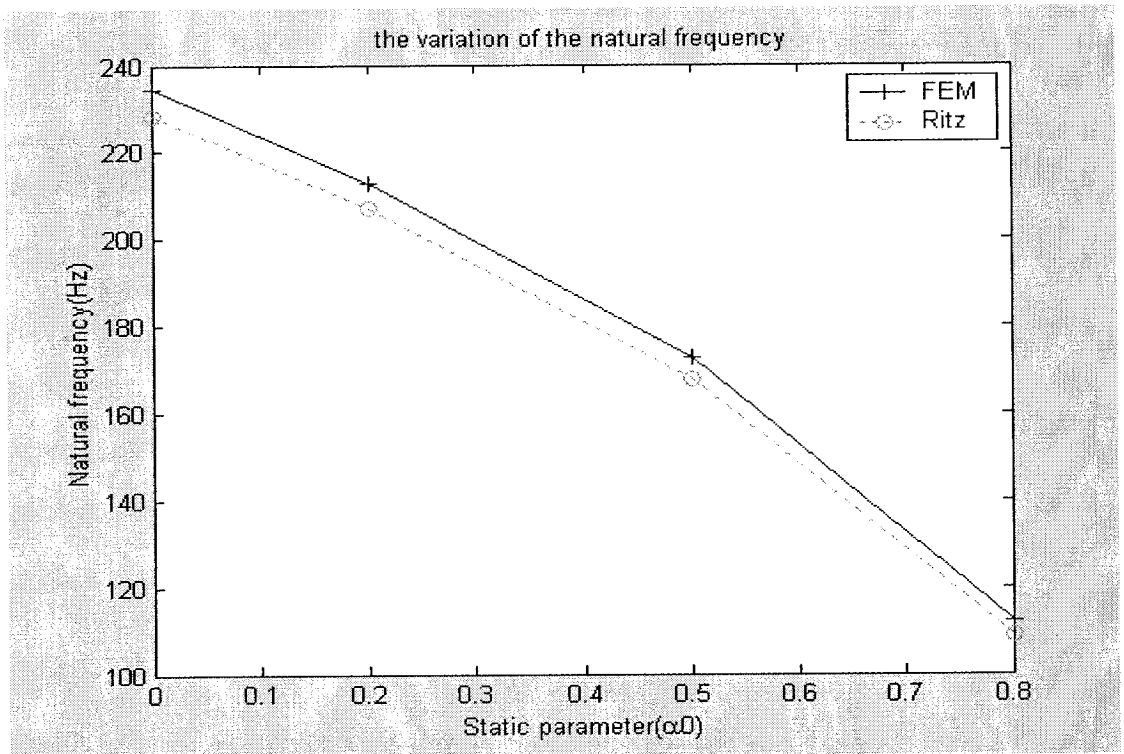

Figure 6.13 The variation of the natural frequency of taper configuration A with the static buckling load; one edge is clamped and other three are edges free

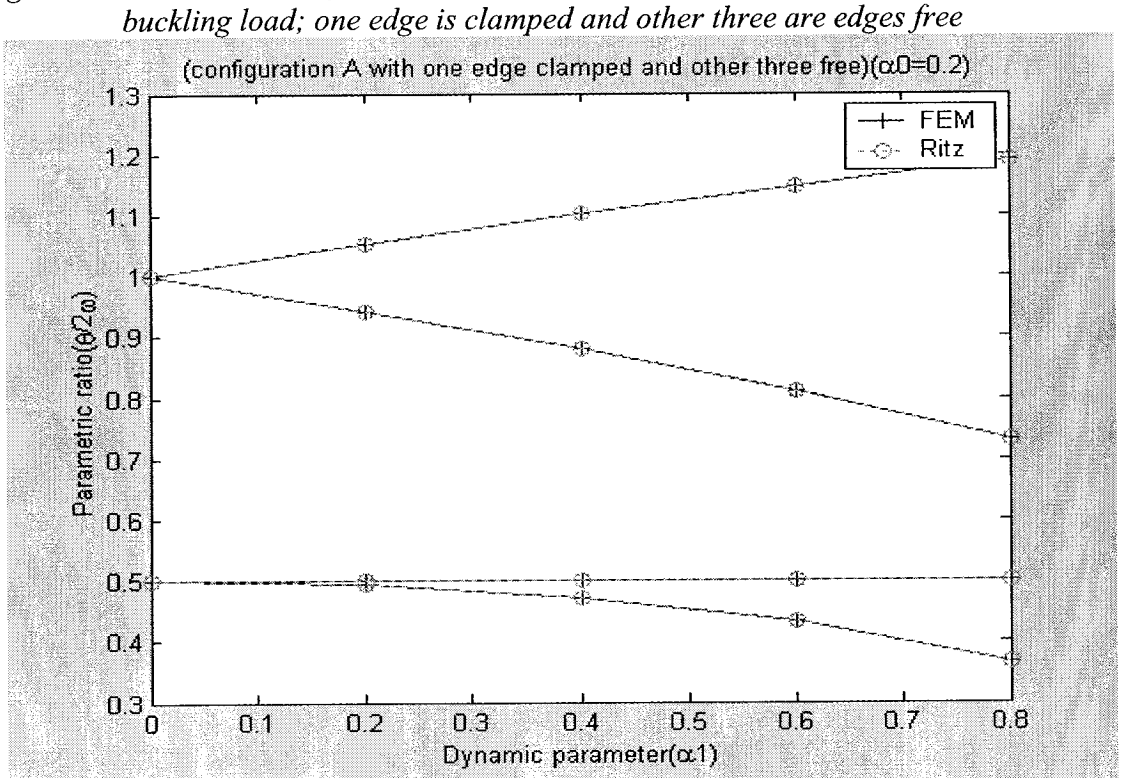

Figure 6.14 Two instability regions of taper configuration A determined using Finite Element Method and Ritz Method; one edge is clamped and other three are edges free ($\alpha_0 = 0.2$)

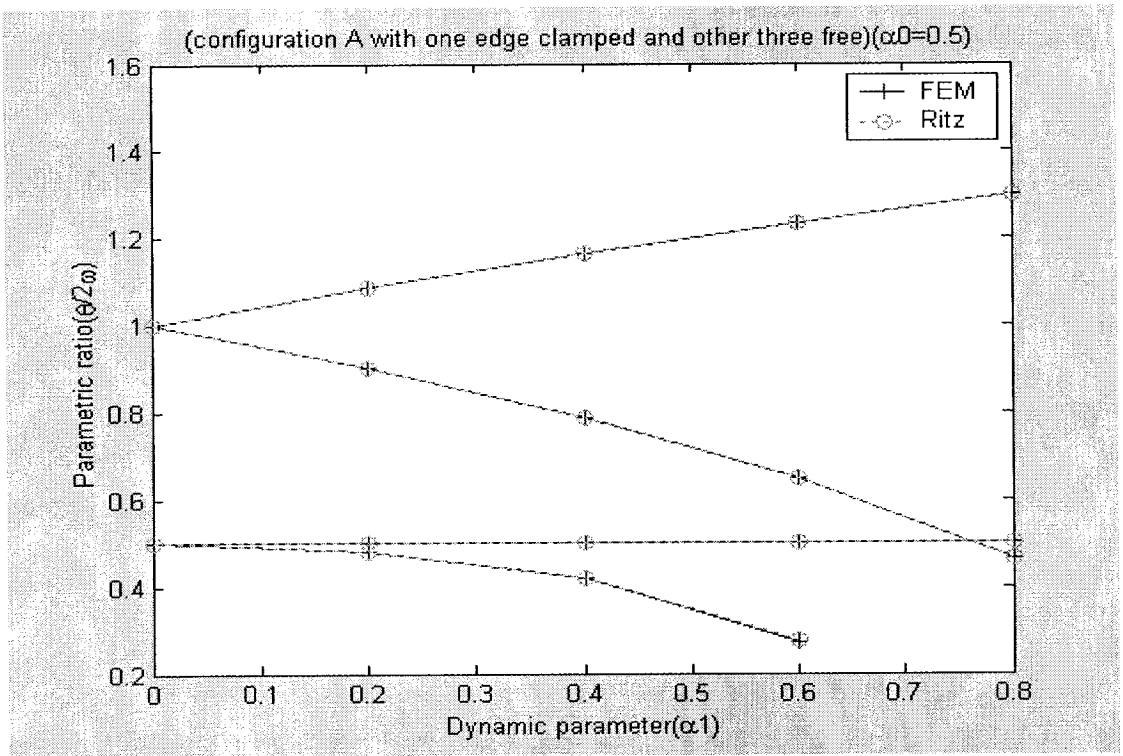

Figure 6.15 Two instability regions of taper configuration A determined using Finite Element Method and Ritz Method; one edge is clamped and other three edges are free ($\alpha_0 = 0.5$)

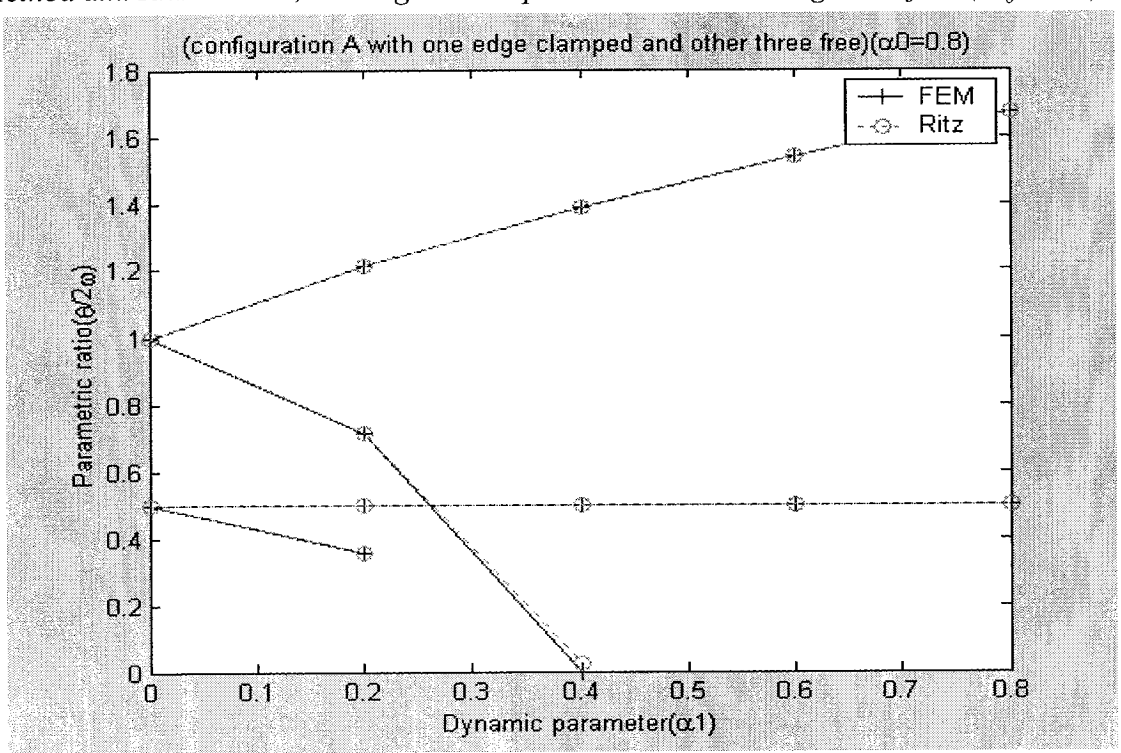

Figure 6.16 Two instability regions of taper configuration A determined using Finite Element Method and Ritz Method; one edge is clamped and other three edges are free ($\alpha_0 = 0.8$)

In Figure 6.13, the graphs show that the natural frequencies decrease as the static buckling loads increase. The variations of natural frequencies of the tapered composite plate configuration A obtained using Finite Element Method and Ritz Method have the same form.

From Figures 6.14, 6.15, and 6.16, we can see the two instability regions with different static parameters corresponding to $\alpha_0 = 0.2, \alpha_0 = 0.5$, and $\alpha_0 = 0.8$. The graphs show that the widths of the instability regions increase with an increase in both the static and dynamic loads. The instability regions for tapered composite plate configuration A under this boundary condition determined using Finite Element Method are much closer to that obtained using Ritz Method.

2. The Instability Analysis of Taper Configuration B under Three Kinds of Boundary Conditions:

With four edges simply supported, the variation of the natural frequency with the static buckling load and the two instability regions ($\alpha_0 = 0.2, \alpha_0 = 0.5$, and $\alpha_0 = 0.8$) of the tapered composite plate configuration B are shown in the Figures 6.17-6.20.

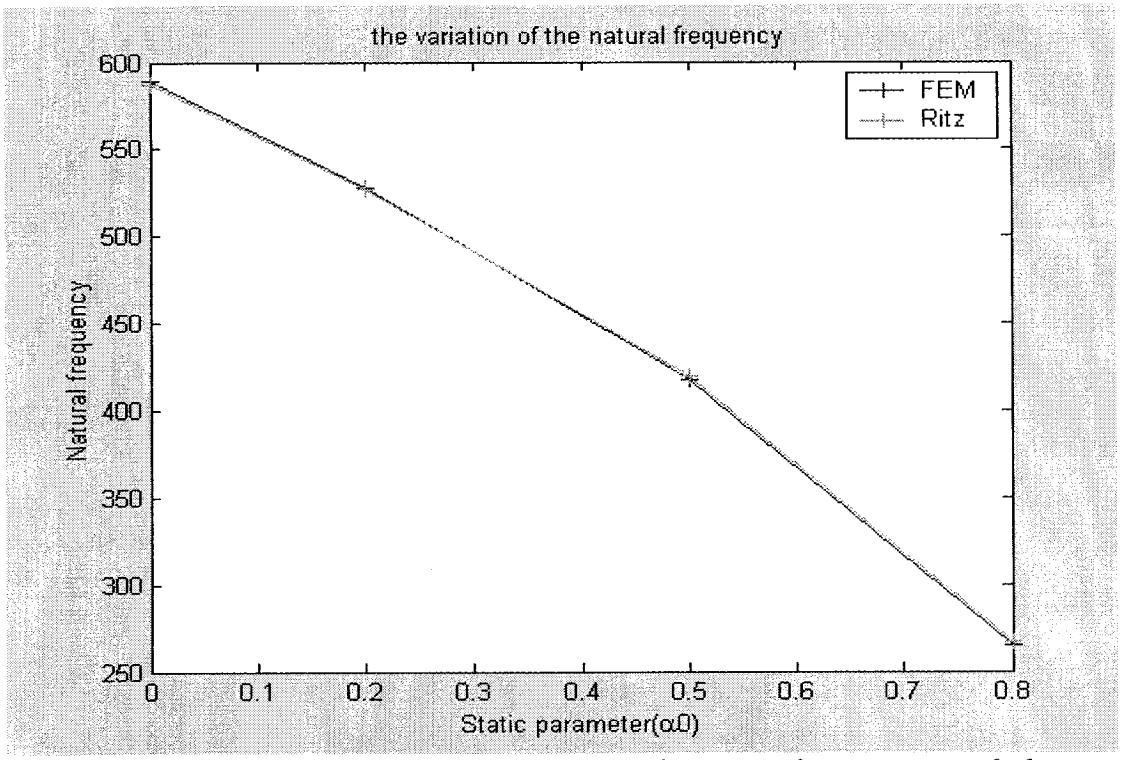

Figure 6.17 The variation of the natural frequency of taper configuration B with the static buckling load; four edges are simply supported

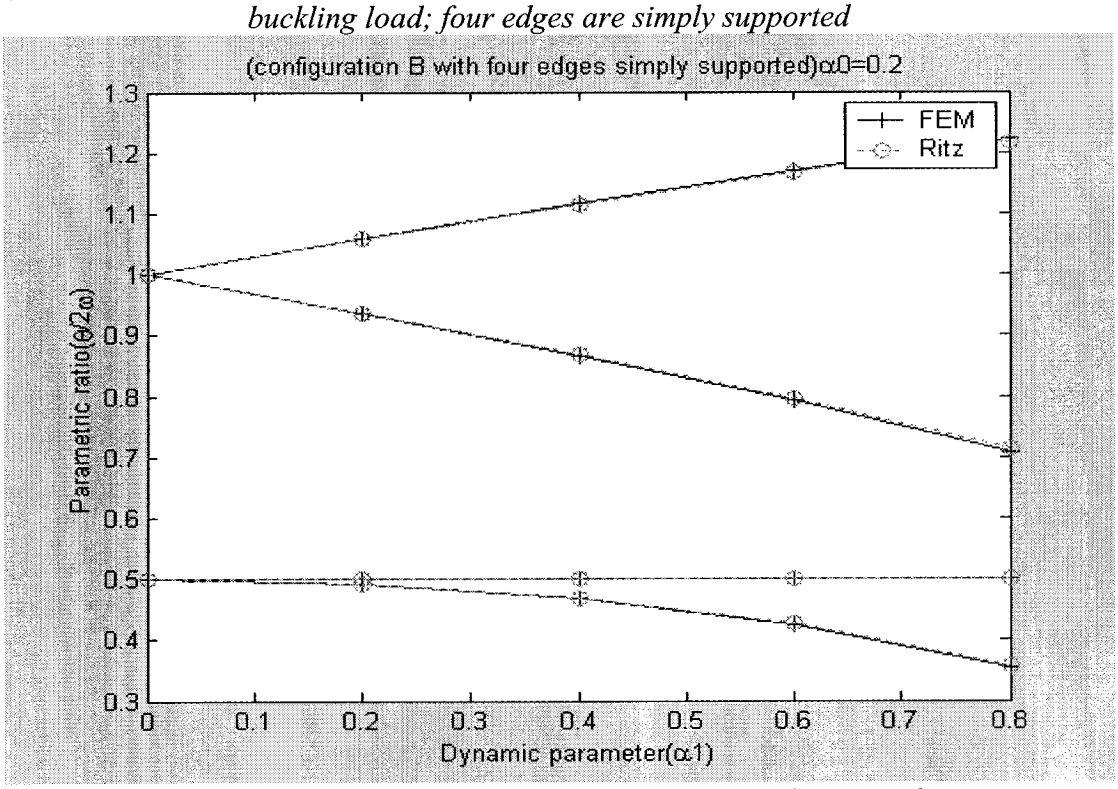

Figure 6.18 Two instability regions of taper configuration B determined using Finite Element Method and Ritz Method; four edges are simply supported ($\alpha_0 = 0.2$)

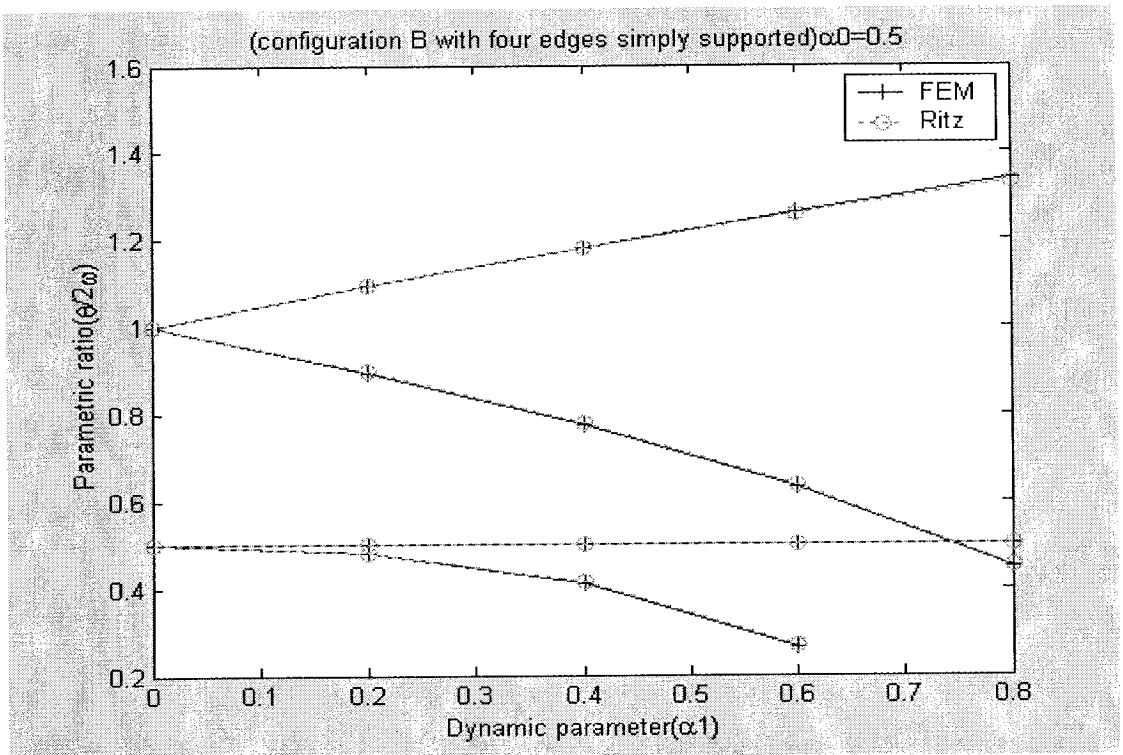

Figure 6.19 Two instability regions of taper configuration B determined using Finite Element Method and Ritz Method; four edges are simply supported ($\alpha_0 = 0.5$)

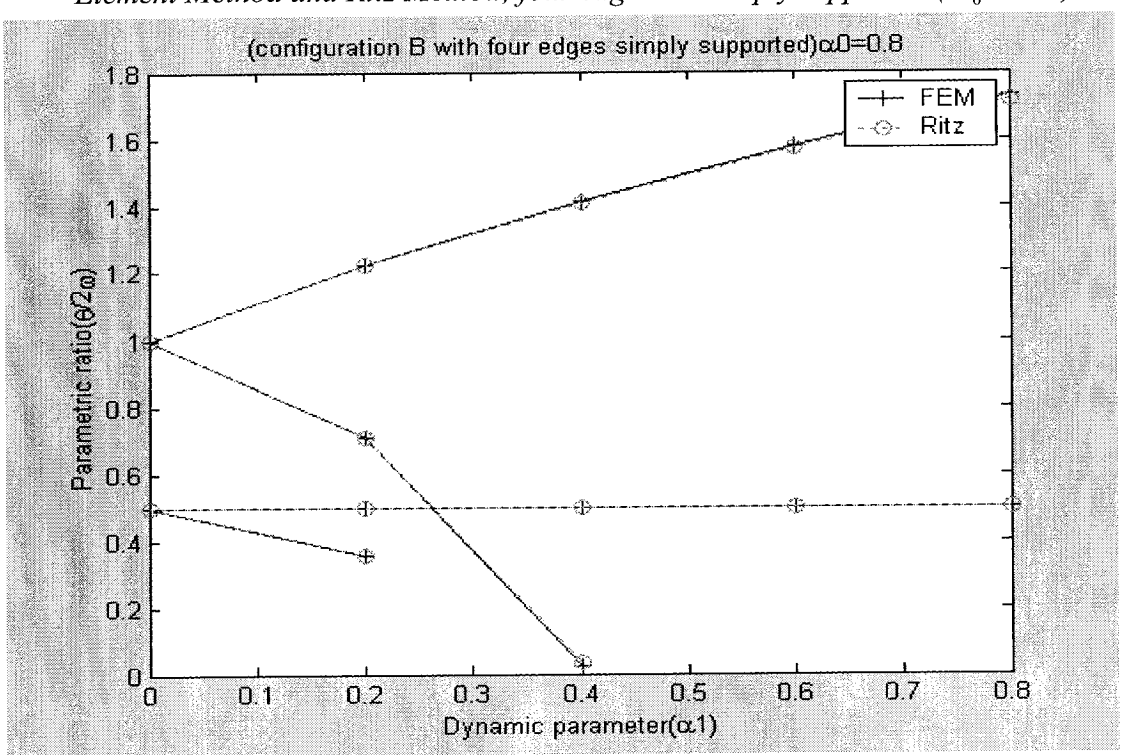

Figure 6.20 Two instability regions of taper configuration B determined using Finite Element Method and Ritz Method; four edges are simply supported ($\alpha_0 = 0.8$)

In Figure 6.17, the graphs show that the natural frequencies decrease as the static buckling loads increase. The variations of natural frequencies of the tapered composite plate configuration B obtained using Finite Element Method and Ritz Method have almost the same form.

From Figures 6.18, 6.19, and 6.20, we can see the two instability regions with different static parameters corresponding to $\alpha_0 = 0.2, \alpha_0 = 0.5$, and $\alpha_0 = 0.8$. The graphs show that the widths of the instability regions increase with an increase in both the static and dynamic loads. The instability regions for tapered composite plate configuration B obtained using Finite Element Method are very close to that obtained using Ritz Method.

Next, considering the boundary condition of four edges clamped, the variation of the natural frequency with the static buckling load and the two instability regions ($\alpha_0 = 0.2, \alpha_0 = 0.5$, and $\alpha_0 = 0.8$) of the tapered composite plate configuration B are determined and shown in the Figures 6.21-6.24.

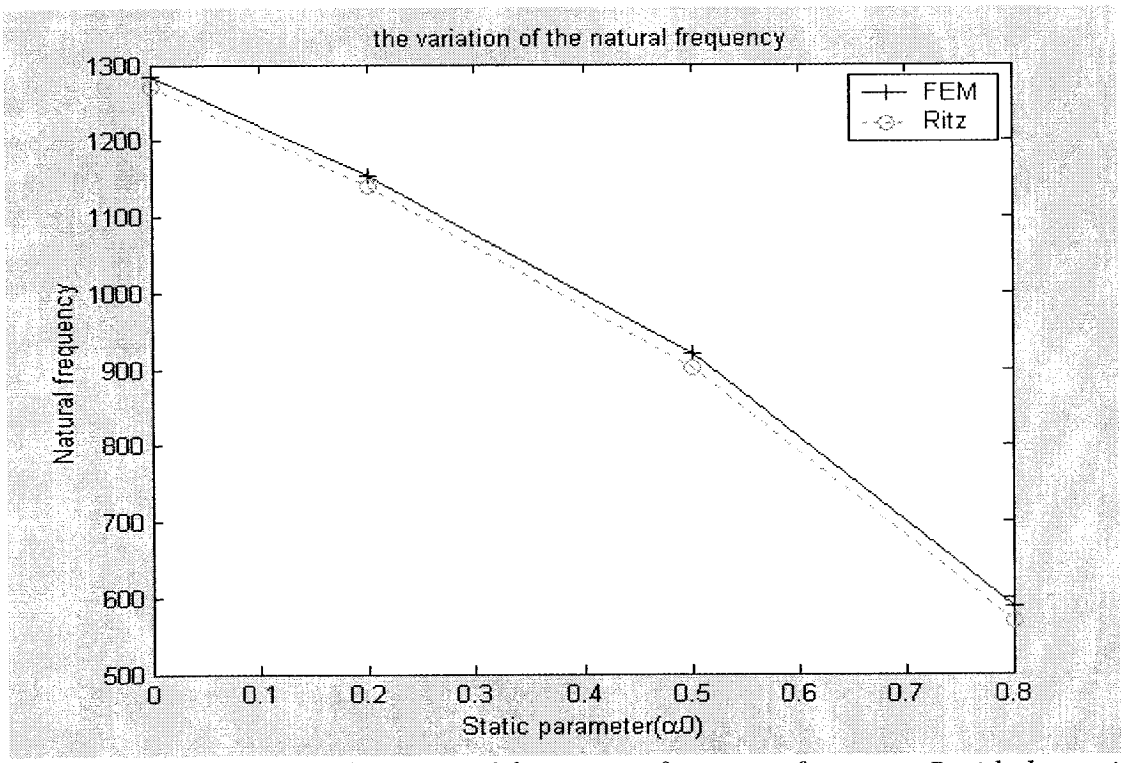

Figure 6.21 The variation of the natural frequency of taper configuration B with the static buckling load; four edges are clamped

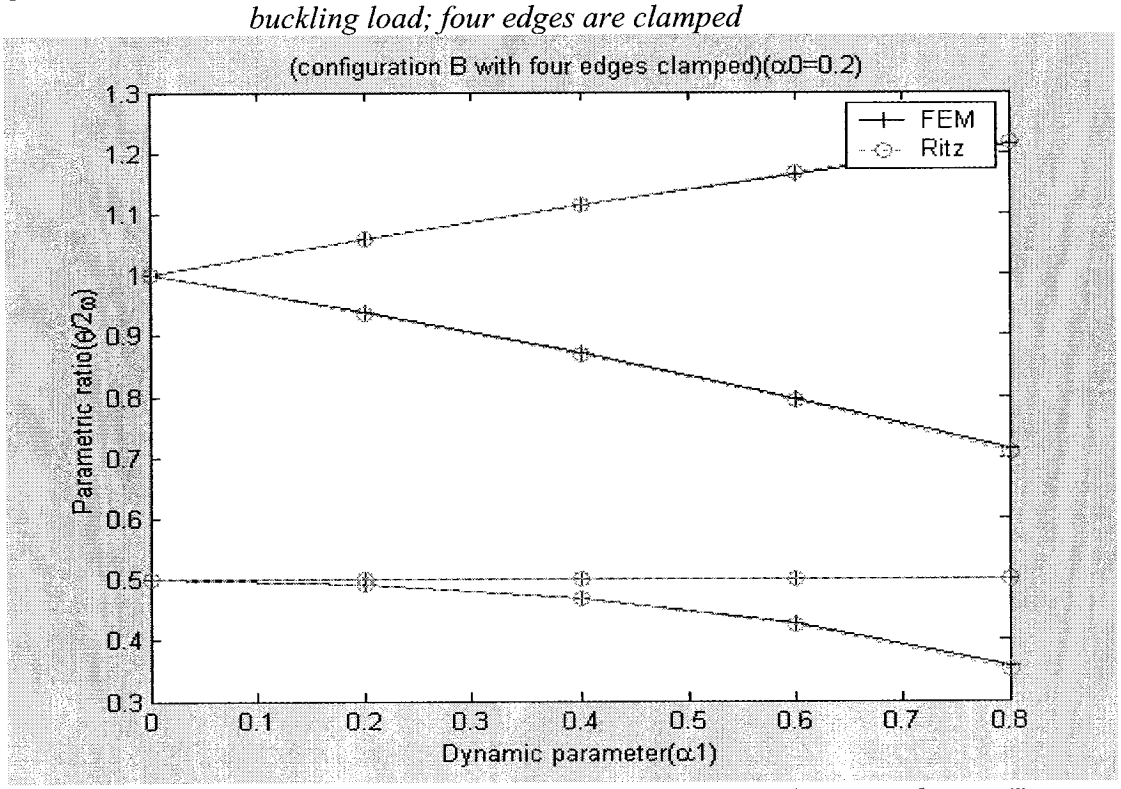

Figure 6.22 Two instability regions of taper configuration B determined using Finite Element Method and Ritz Method; four edges are clamped ($\alpha_0 = 0.2$)

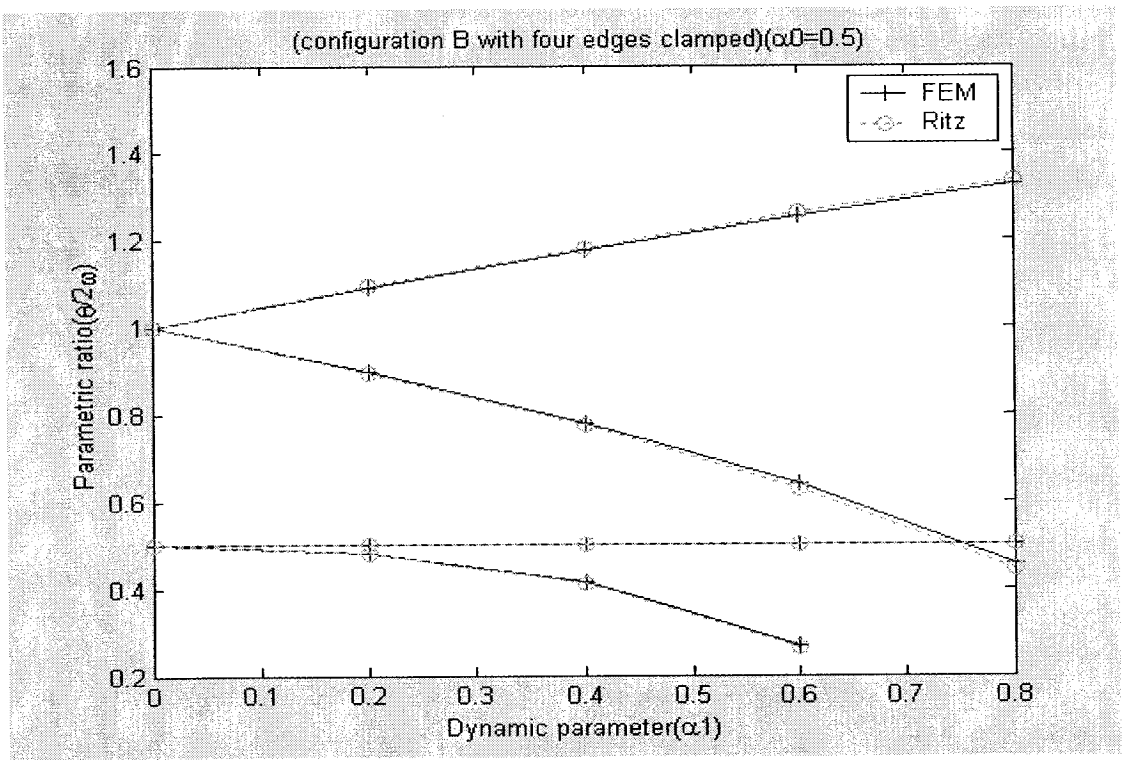

Figure 6.23 Two instability regions of taper configuration B determined using Finite Element Method and Ritz Method; four edges are clamped ($\alpha_0 = 0.5$)

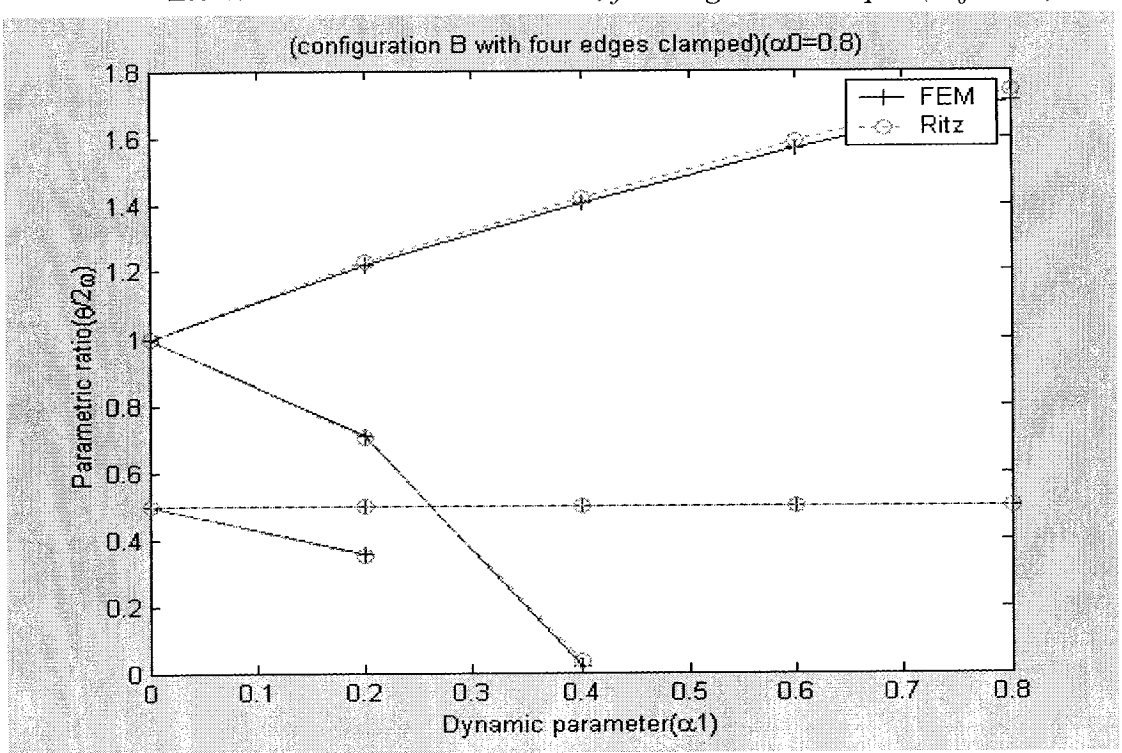

Figure 6.24 Two instability regions of taper configuration B determined using Finite Element Method and Ritz Method; four edges are clamped ($\alpha_0 = 0.8$)

In Figure 6.21, the graphs show that the natural frequencies decrease as the static buckling loads increase. The variations of natural frequencies of the tapered composite plate configuration B obtained using Finite Element Method and Ritz Method have almost the same form.

From Figures 6.22, 6.23, and 6.24, we can see the two instability regions with different static parameters corresponding to $\alpha_0 = 0.2, \alpha_0 = 0.5$, and $\alpha_0 = 0.8$. The graphs show that the widths of the instability regions increase with an increase in both the static and dynamic loads. The instability regions for tapered composite plate configuration B determined using Finite Element Method are very close to that obtained using Ritz Method.

Finally, considering the boundary condition of one edge clamped and other three edges free, the variation of the natural frequency with the static buckling load and the two instability regions ($\alpha_0 = 0.2, \alpha_0 = 0.5$, and $\alpha_0 = 0.8$) of the tapered composite plate configuration B are determined and shown in the Figures 6.25-6.28.

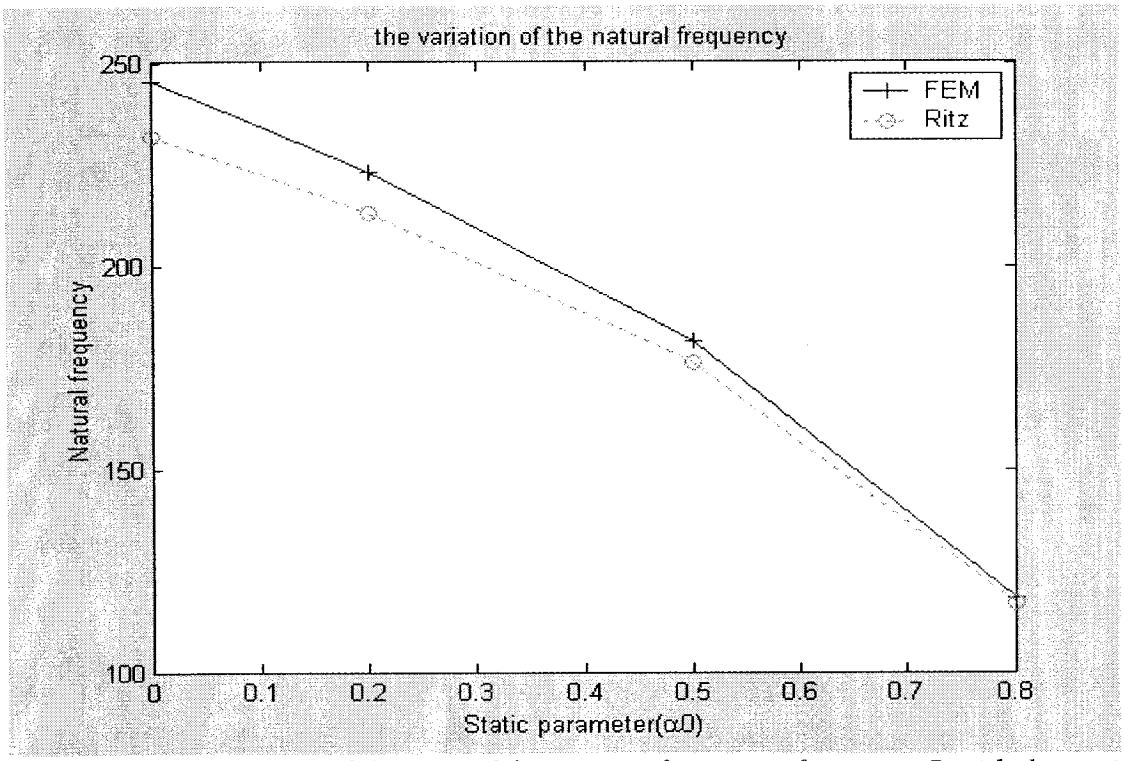

Figure 6.25 The variation of the natural frequency of taper configuration B with the static buckling load; one edge is clamped and other three edges are free

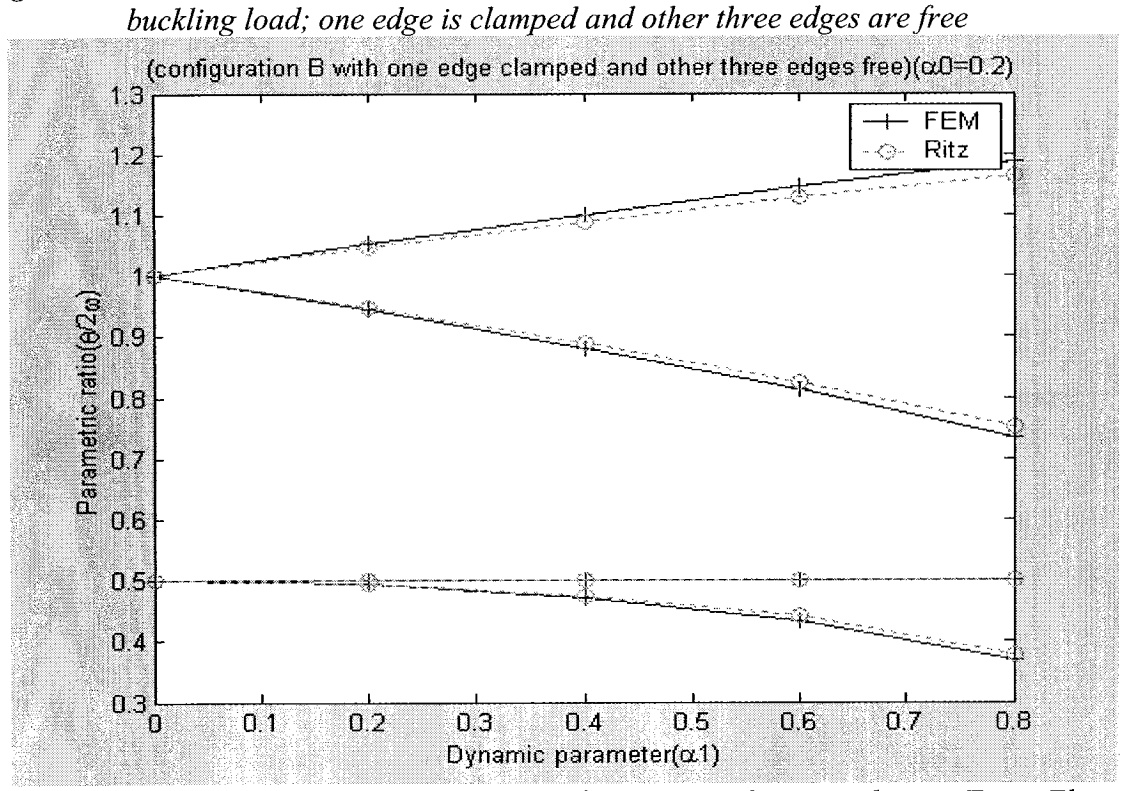

Figure 6.26 Two instability regions of taper configuration B determined using Finite Element Method and Ritz Method; one edge is clamped and other three edges are free ($\alpha_0 = 0.2$)

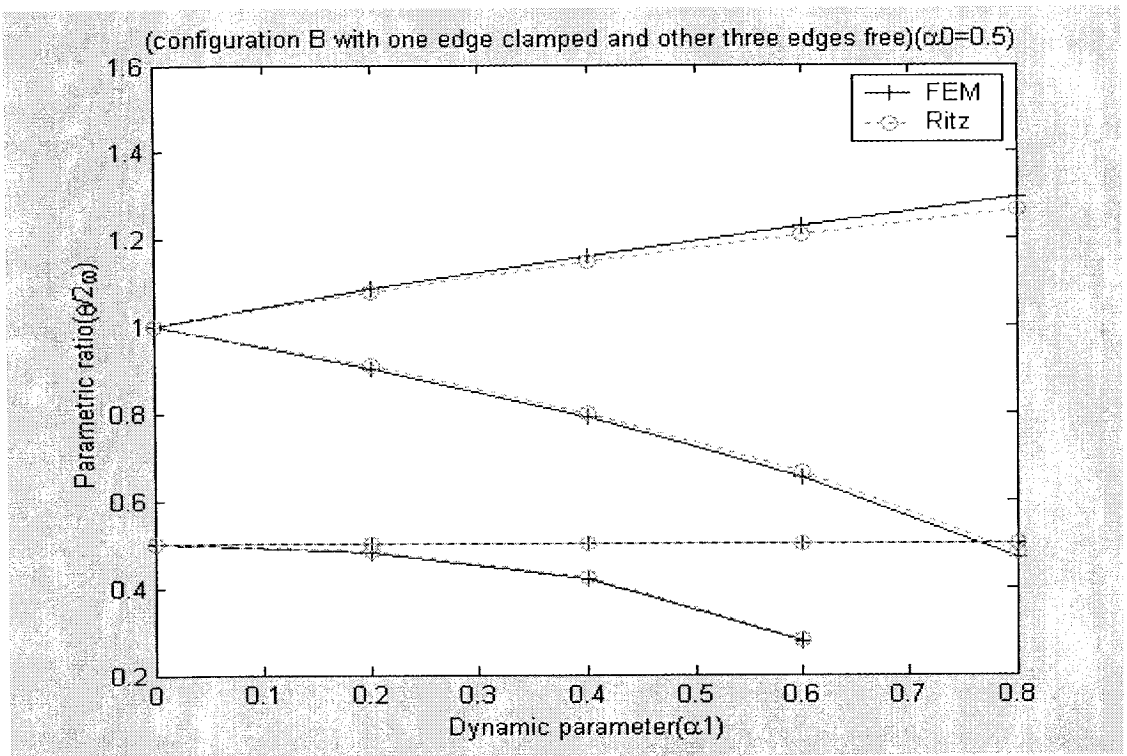

Figure 6.27 Two instability regions of taper configuration B determined using Finite Element Method and Ritz Method; one edge is clamped and other three edges are free ($\alpha_0 = 0.5$)

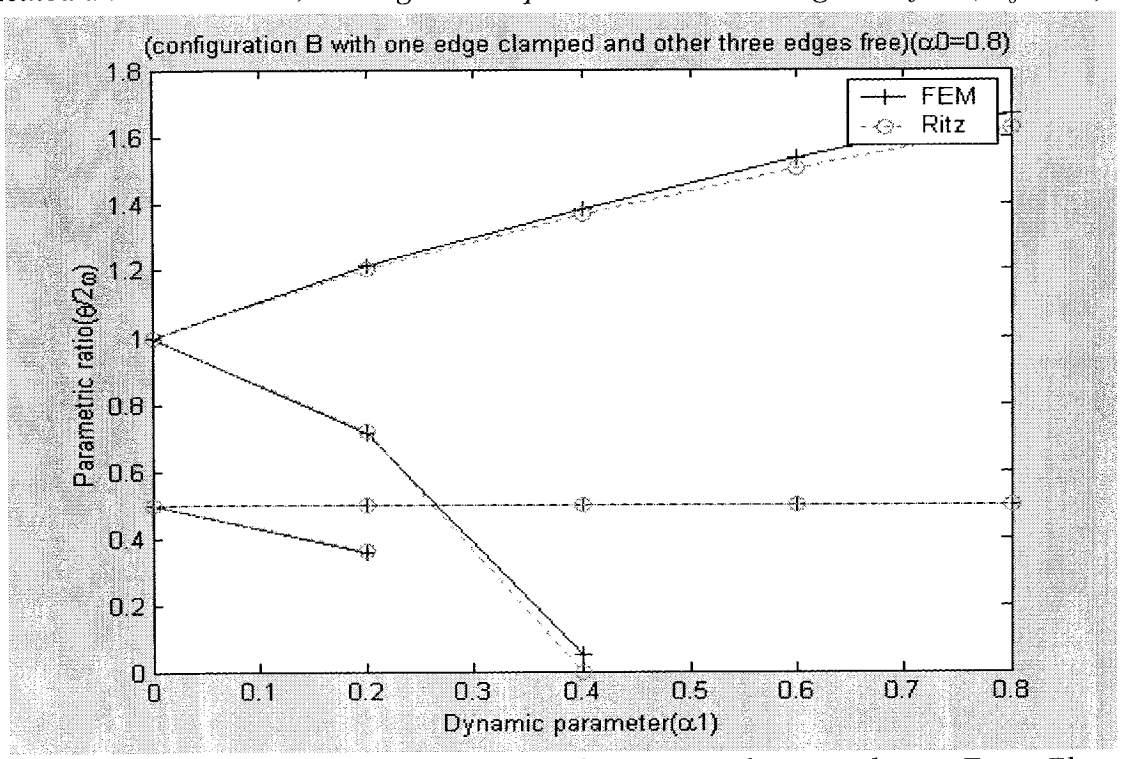

Figure 6.28 Two instability regions of taper configuration B determined using Finite Element Method and Ritz Method; one edge is clamped and other three edges are free ($\alpha_0 = 0.8$)

In Figure 6.25, the graphs show that the natural frequencies decrease as the static buckling loads increase. The variations of natural frequencies of the tapered composite plate configuration B obtained using Finite Element Method and Ritz Method have close form.

From Figures 6.26, 6.27, and 6.28, we can see the two instability regions with different static parameters corresponding to $\alpha_0 = 0.2, \alpha_0 = 0.5$, and $\alpha_0 = 0.8$. The graphs show that the widths of the instability regions increase with an increase in both the static and dynamic loads. The instability regions for tapered composite plate configuration B determined using Finite Element Method are very close to that obtained using Ritz Method.

3. The Instability Analysis of Taper Configuration C under Three Kinds of Boundary Conditions:

With four edges simply supported, the variation of the natural frequency with the static buckling load and the two instability regions ($\alpha_0 = 0.2, \alpha_0 = 0.5$, and $\alpha_0 = 0.8$) of the tapered composite plate configuration C are shown in the Figures 6.29-6.32.

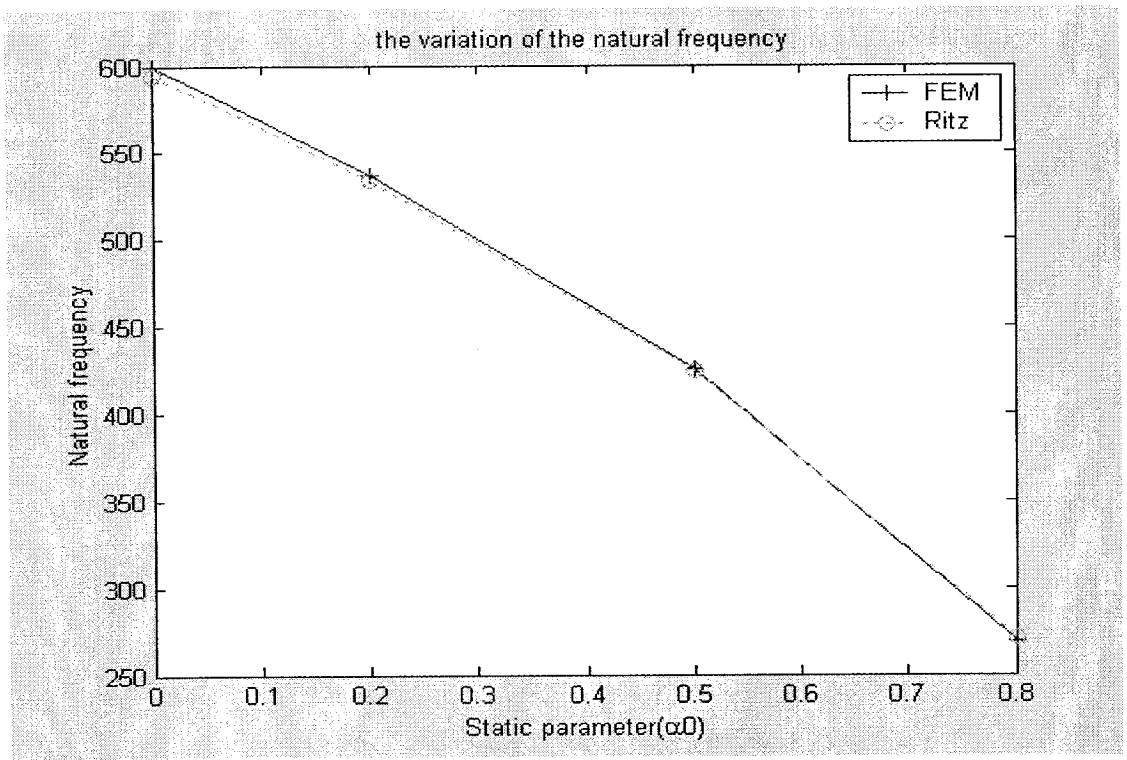

Figure 6.29 The variation of the natural frequency of taper configuration C with the static buckling load; four edges are simply supported

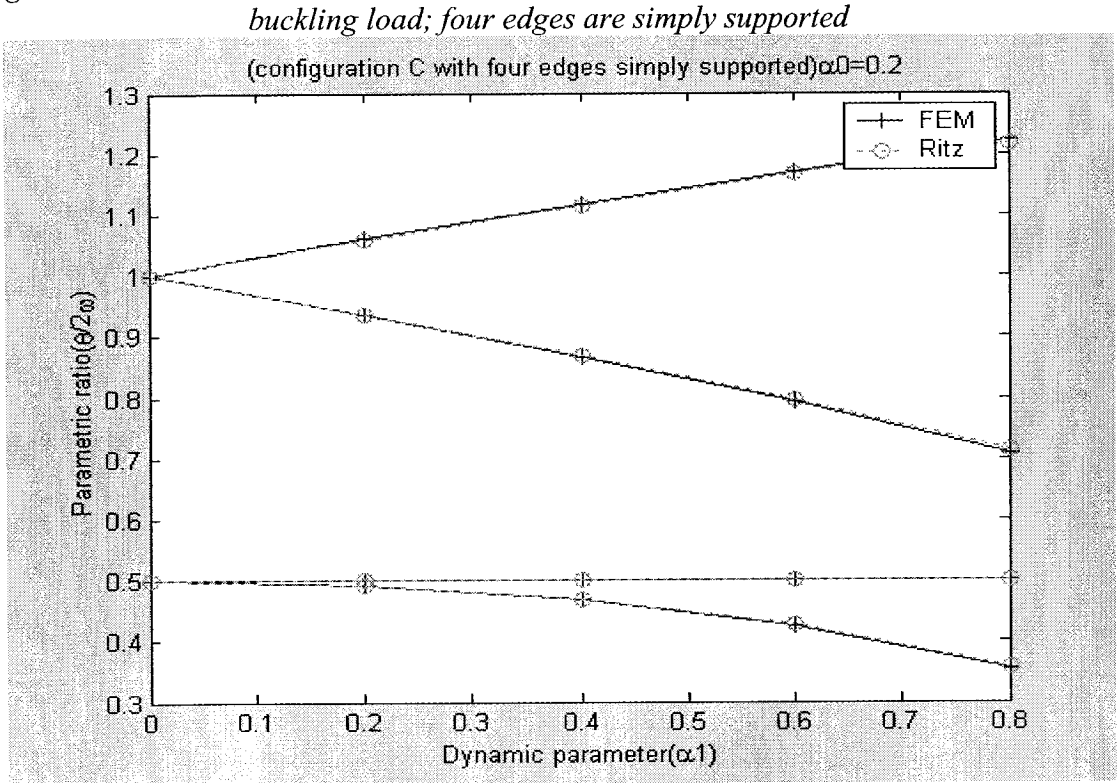

Figure 6.30 Two instability regions of taper configuration C determined using Finite Element Method and Ritz Method; four edges are simply supported ($\alpha_0 = 0.2$)

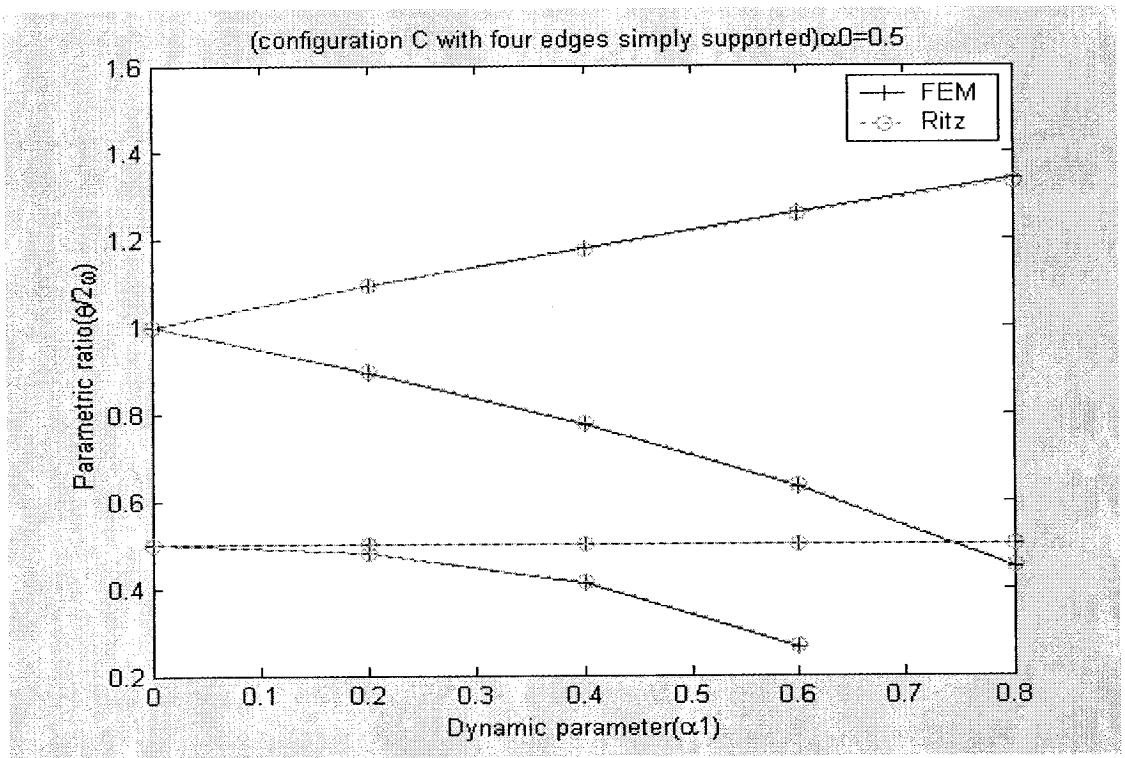

Figure 6.31 Two instability regions of taper configuration C determined using Finite Element Method and Ritz Method; four edges are simply supported ($\alpha_0 = 0.5$)

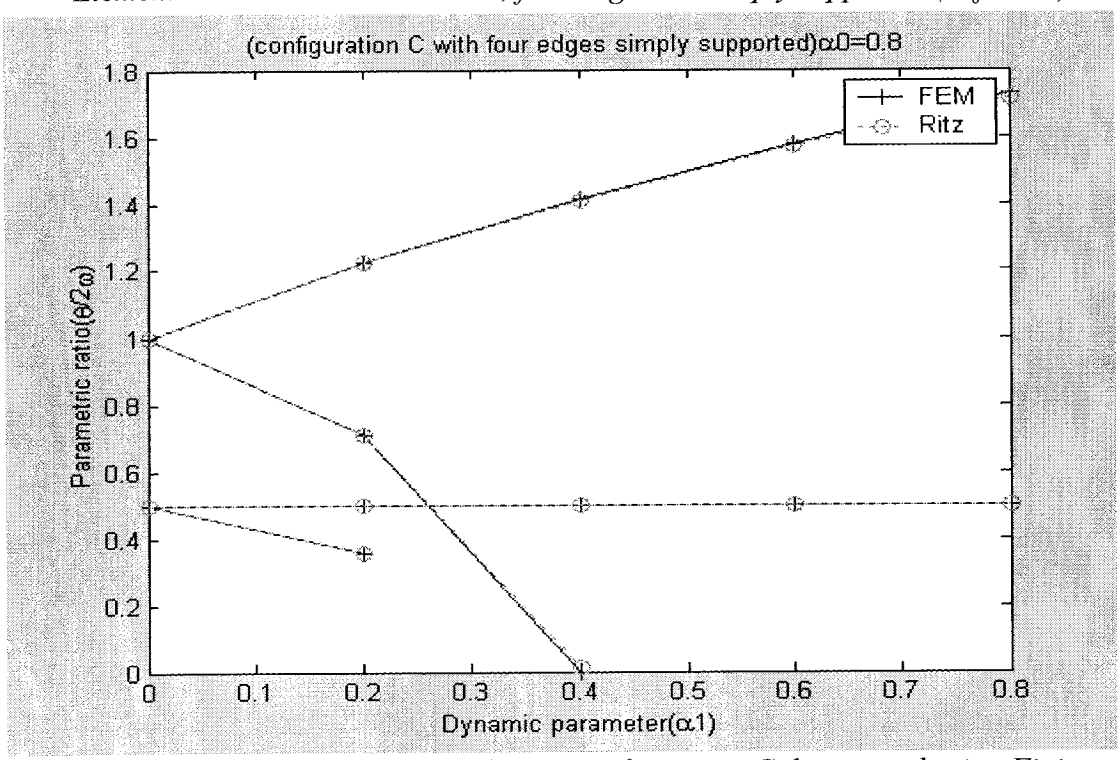

Figure 6.32 Two instability regions of taper configuration C determined using Finite Element Method and Ritz Method; four edges are simply supported ($\alpha_0 = 0.8$)

In Figure 6.29, the graphs show that the natural frequencies decrease as the static buckling loads increase. The variations of natural frequencies of the tapered composite plate configuration C obtained using Finite Element Method and Ritz Method have almost the same form.

From Figures 6.30, 6.31, and 6.32, we can see the two instability regions with different static parameters corresponding to $\alpha_0 = 0.2, \alpha_0 = 0.5$, and $\alpha_0 = 0.8$. The graphs show that the widths of the instability regions increase with an increase in both the static and dynamic loads. The instability regions for tapered composite plate configuration C determined using Finite Element Method are very close to that obtained using Ritz Method.

Next, considering the boundary condition of four edges clamped, the variation of the natural frequency with the static buckling load and the two instability regions ($\alpha_0 = 0.2, \alpha_0 = 0.5$, and $\alpha_0 = 0.8$) of the tapered composite plate configuration C are determined and shown in the Figures 6.33-6.36.

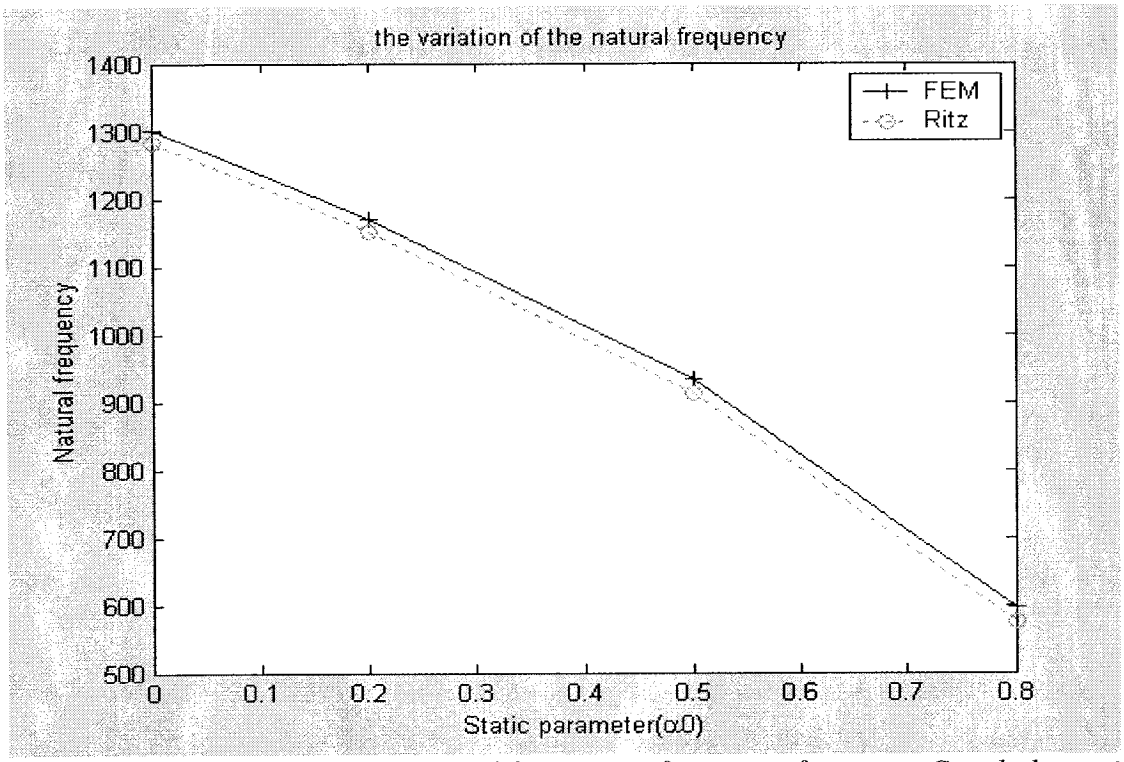

Figure 6.33 The variation of the natural frequency of taper configuration C with the static buckling load; four edges are clamped

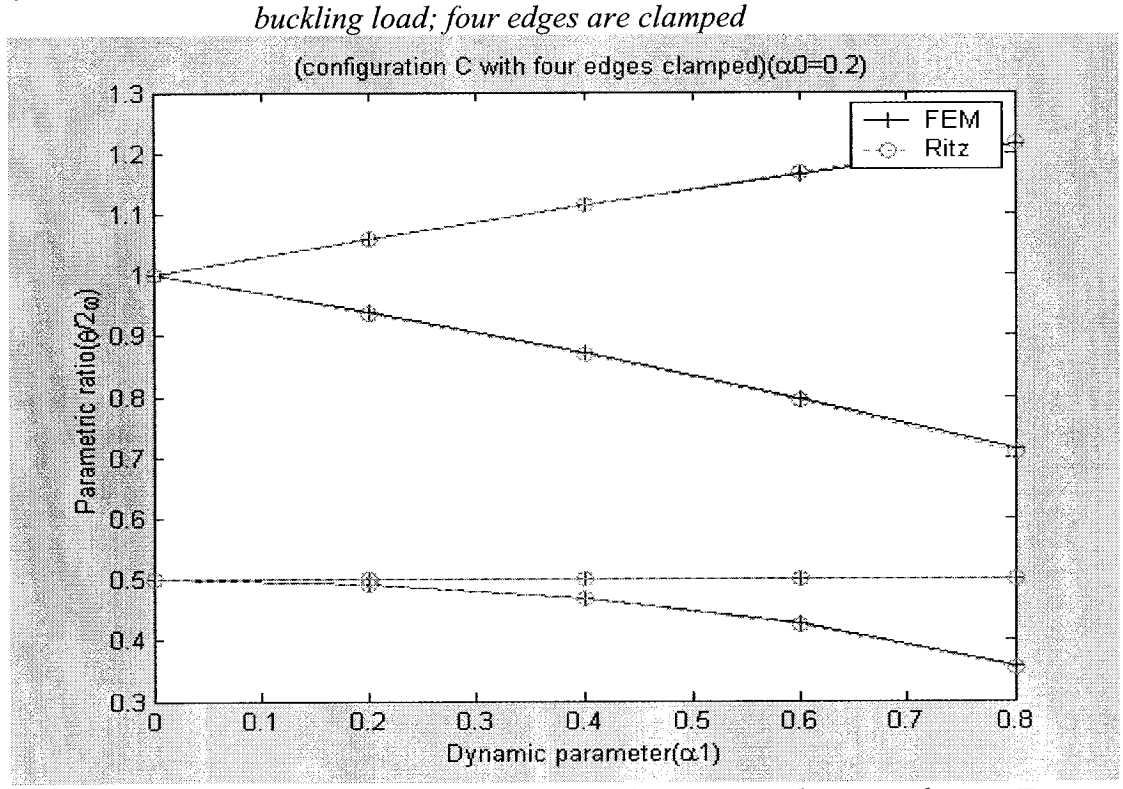

Figure 6.34 Two instability regions of taper configuration C determined using Finite Element Method and Ritz Method; four edges are clamped ($\alpha_0 = 0.2$)

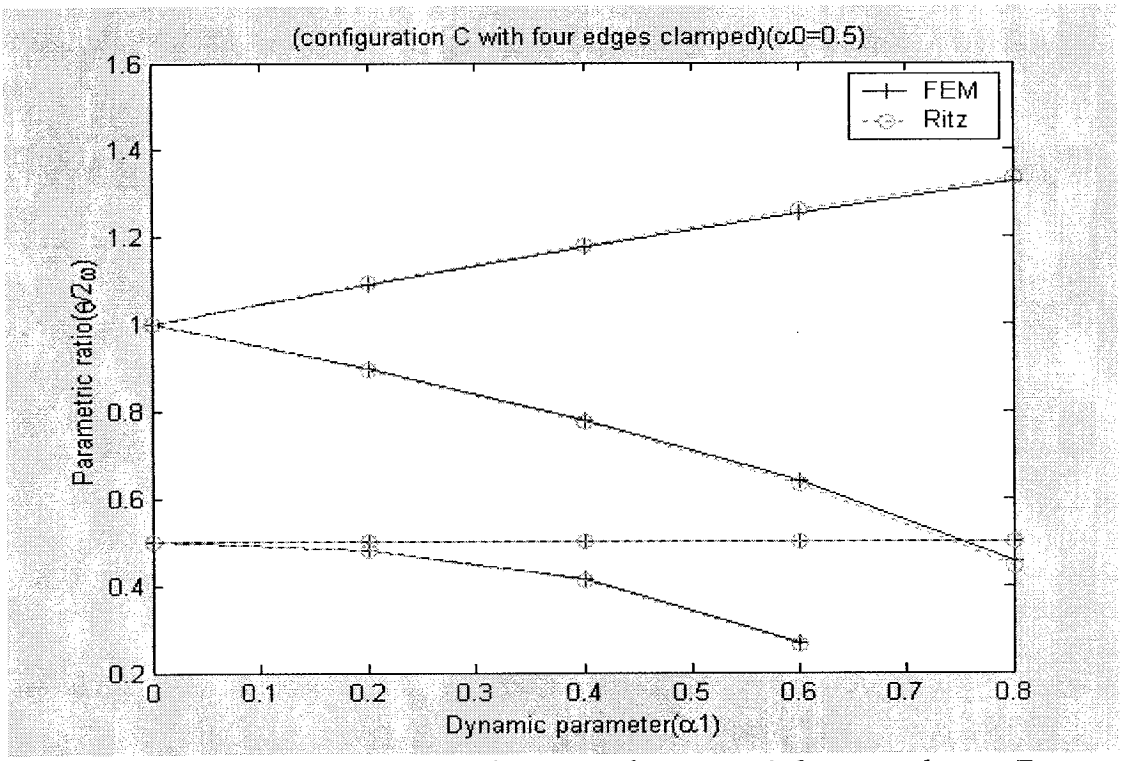

Figure 6.35 Two instability regions of taper configuration C determined using Finite Element Method and Ritz Method; four edges are clamped ($\alpha_0 = 0.5$)

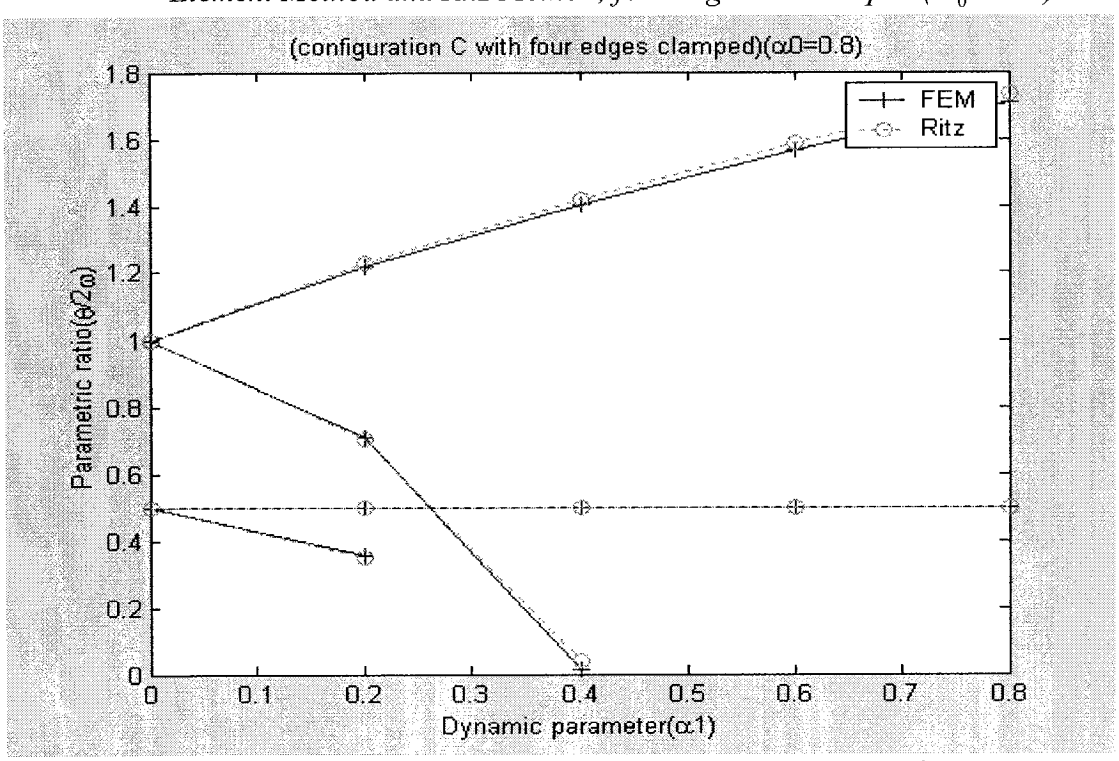

Figure 6.36 Two instability regions of taper configuration C determined using Finite Element Method and Ritz Method; four edges are clamped ($\alpha_0 = 0.8$)

In Figure 6.33, the graphs show that the natural frequencies decrease as the static buckling loads increase. The variations of natural frequencies of the tapered composite plate configuration C obtained using Finite Element Method and Ritz Method have almost the same form.

From Figures 6.34, 6.35, and 6.36, we can see the two instability regions with different static parameters corresponding to $\alpha_0 = 0.2, \alpha_0 = 0.5$, and $\alpha_0 = 0.8$. The graphs show that the widths of the instability regions increase with an increase in both the static and dynamic loads. The instability regions for tapered composite plate configuration C determined using Finite Element Method are very close to that obtained using Ritz Method.

Finally, considering the boundary condition of one edge clamped and other three edges free, the variation of the natural frequency with the static buckling load and the two instability regions ($\alpha_0 = 0.2, \alpha_0 = 0.5$, and $\alpha_0 = 0.8$) of the tapered composite plate configuration C are determined and shown in the Figures 6.37-6.40.

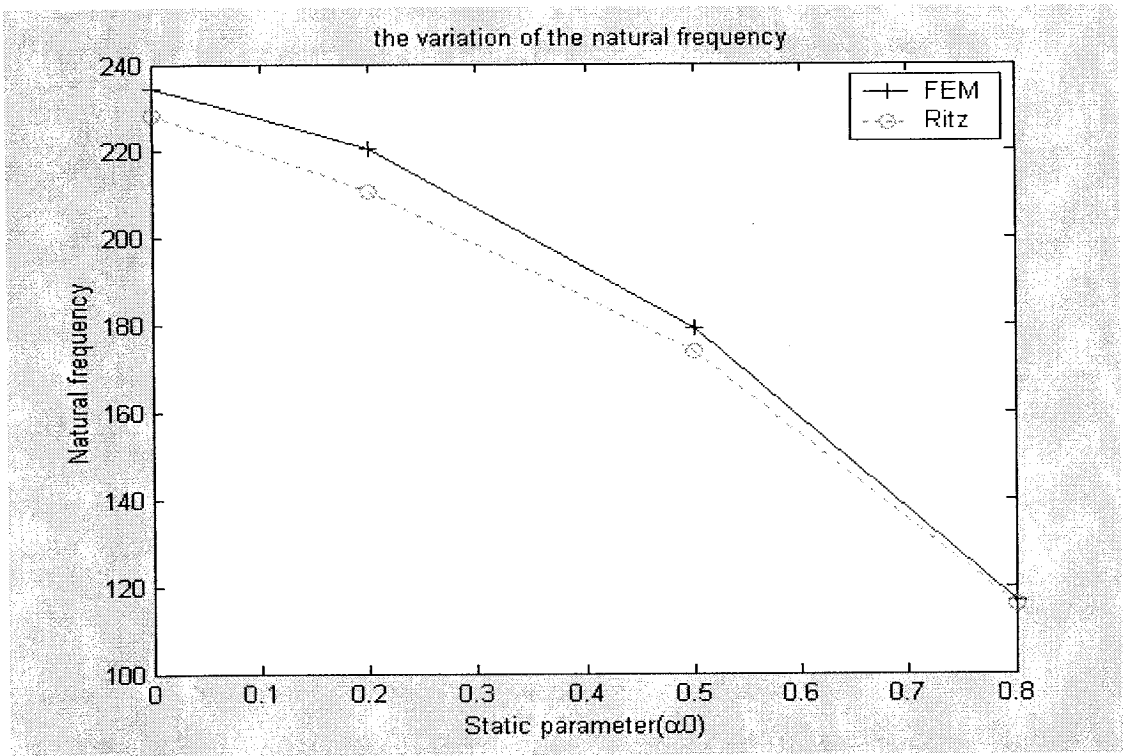

Figure 6.37 The variation of the natural frequency of taper configuration C with the static buckling load; one edge is clamped and other three edges are free

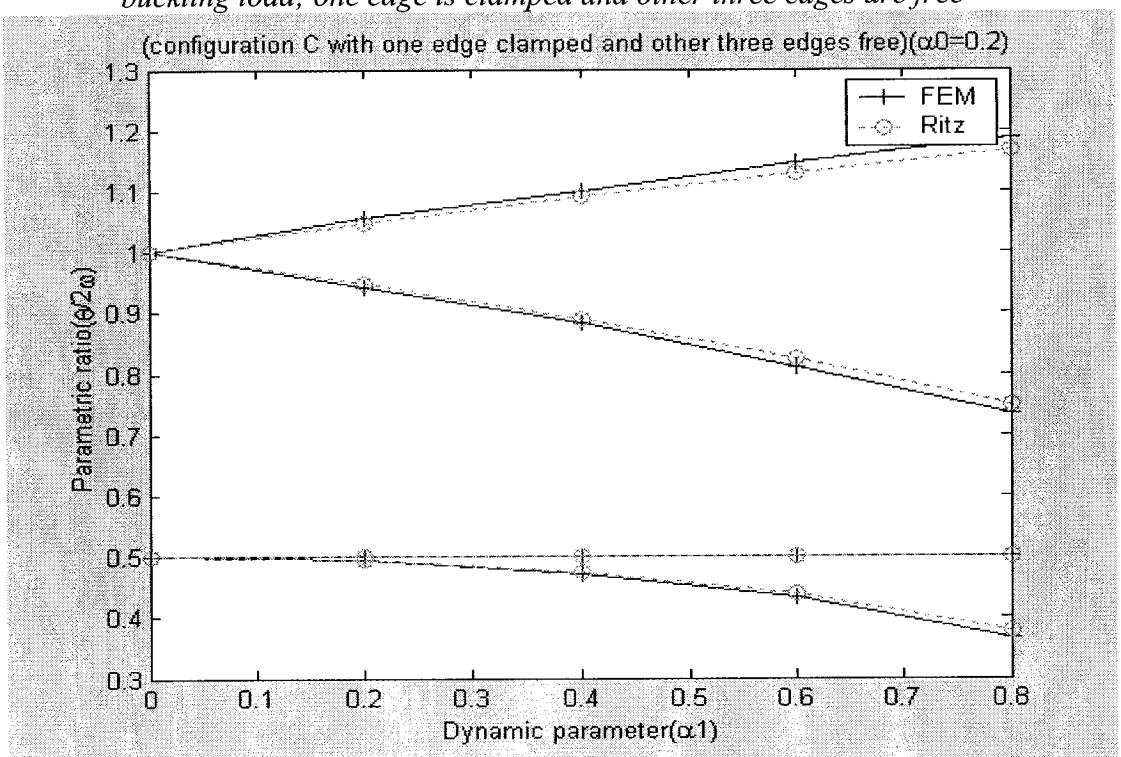

Figure 6.38 Two instability regions of taper configuration C determined using Finite Element Method and Ritz Method; one edge is clamped and other three edges are free ($\alpha_0 = 0.2$)

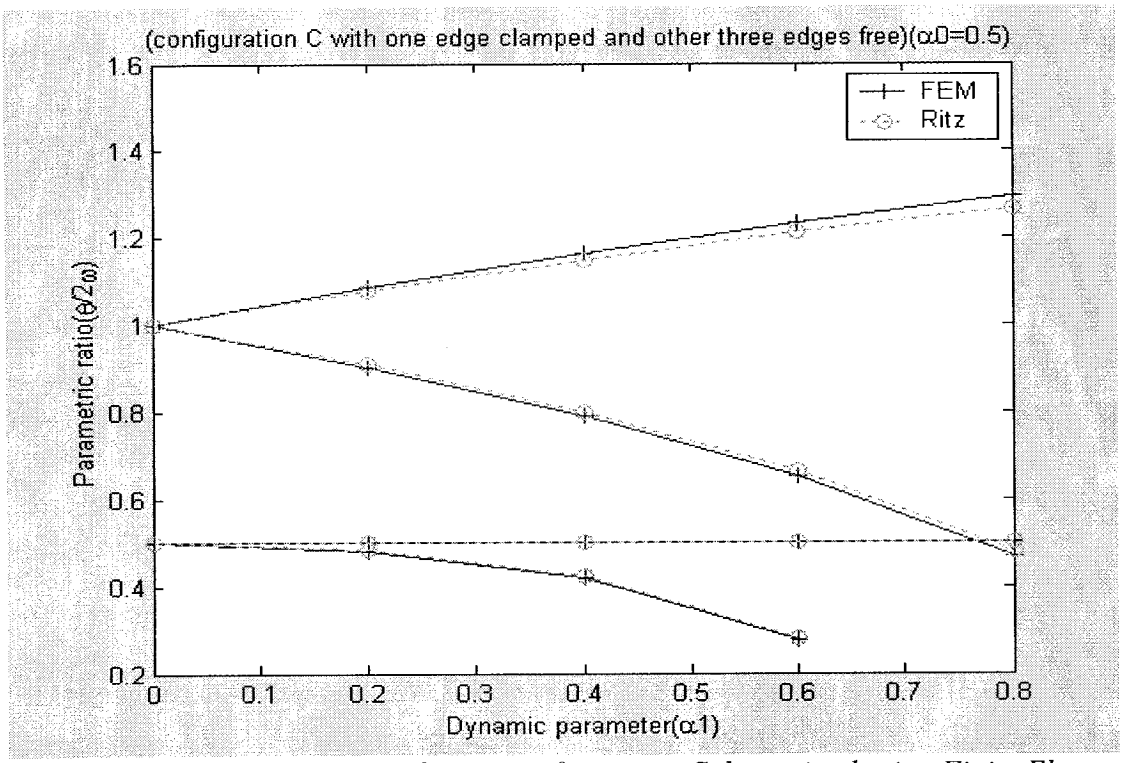

Figure 6.39 Two instability regions of taper configuration C determined using Finite Element Method and Ritz Method; one edge is clamped and other three edges are free ($\alpha_0 = 0.5$)

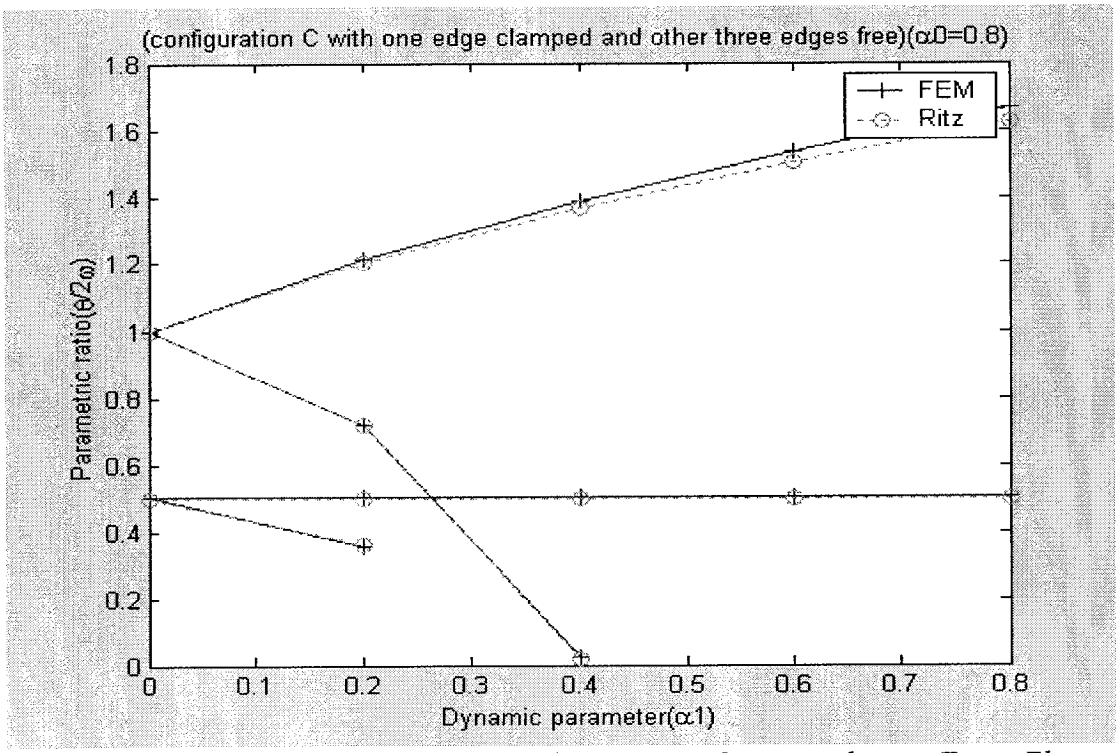

Figure 6.40 Two instability regions of taper configuration C determined using Finite Element Method and Ritz Method; one edge is clamped and other three edges are free ($\alpha_0 = 0.8$)

In Figure 6.37, the graphs show that the natural frequencies decrease as the static buckling loads increase. The variations of natural frequencies of the tapered composite plate configuration C obtained using Finite Element Method and Ritz Method have almost the same form.

From Figures 6.38, 6.39, and 6.40, we can see the two instability regions with different static parameters corresponding to $\alpha_0 = 0.2, \alpha_0 = 0.5$, and $\alpha_0 = 0.8$. The graphs show that the widths of the instability regions increase with an increase in both the static and dynamic loads. The instability regions for tapered composite plate configuration C obtained using Finite Element Method are much closer to that obtained using Ritz Method.

4. The Instability Analysis of Taper Configuration D under Three Kinds of Boundary Conditions:

With four edges simply supported, the variation of the natural frequency with the static buckling load and the two instability regions ($\alpha_0 = 0.2, \alpha_0 = 0.5$, and $\alpha_0 = 0.8$) of the tapered composite plate configuration D are shown in the Figures 6.41-6.44.

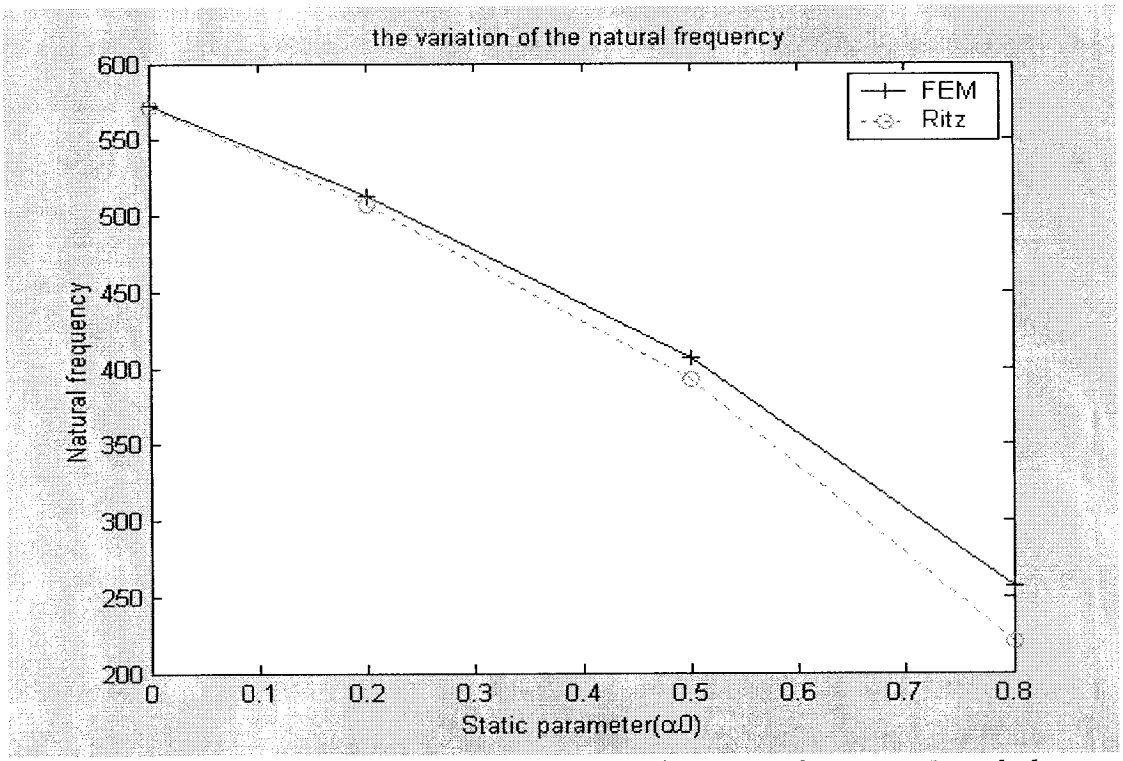

Figure 6.41 The variation of the natural frequency of taper configuration D with the static buckling load; four edges are simply supported

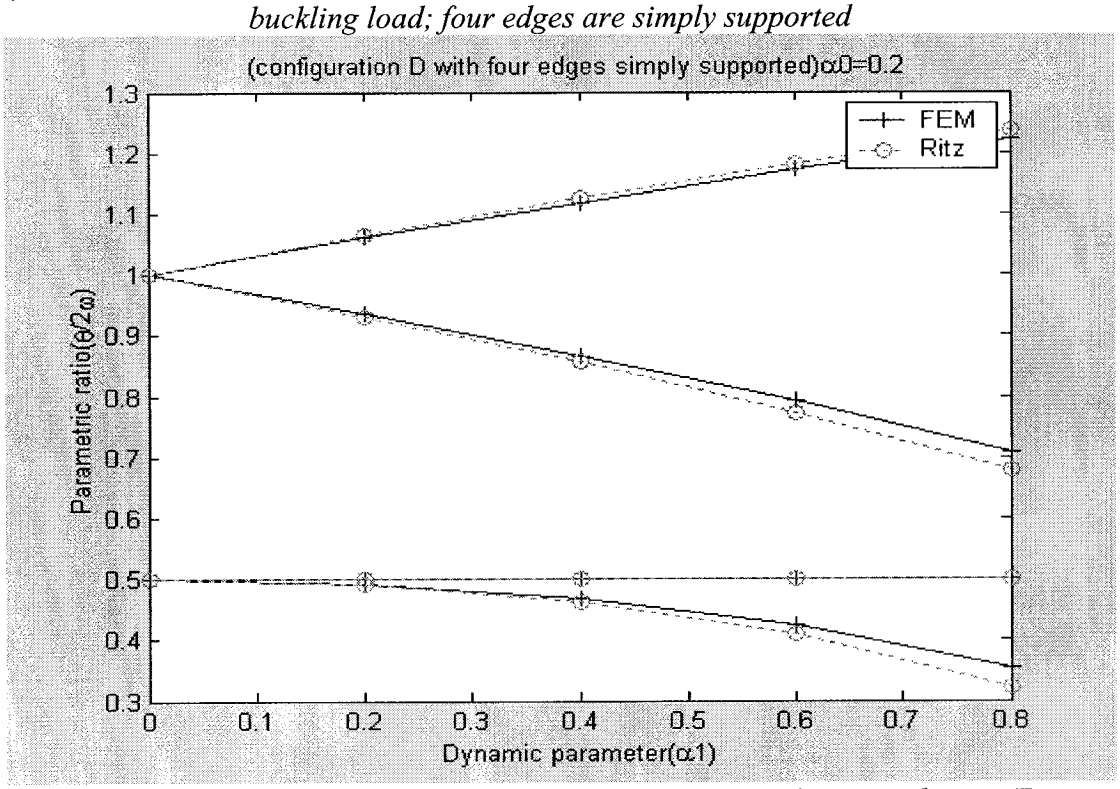

Figure 6.42 Two instability regions of taper configuration D determined using Finite Element Method and Ritz Method; four edges are simply supported ($\alpha_0 = 0.2$)

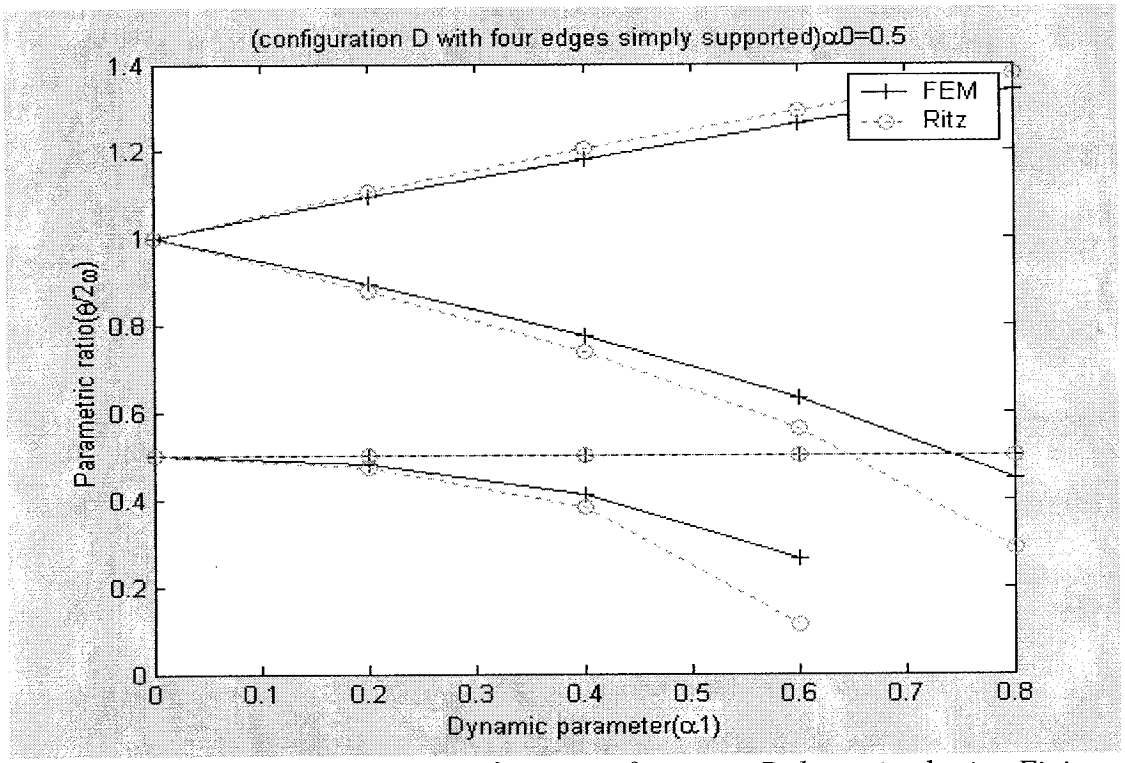

Figure 6.43 Two instability regions of taper configuration D determined using Finite Element Method and Ritz Method; four edges are simply supported ($\alpha_0 = 0.5$)

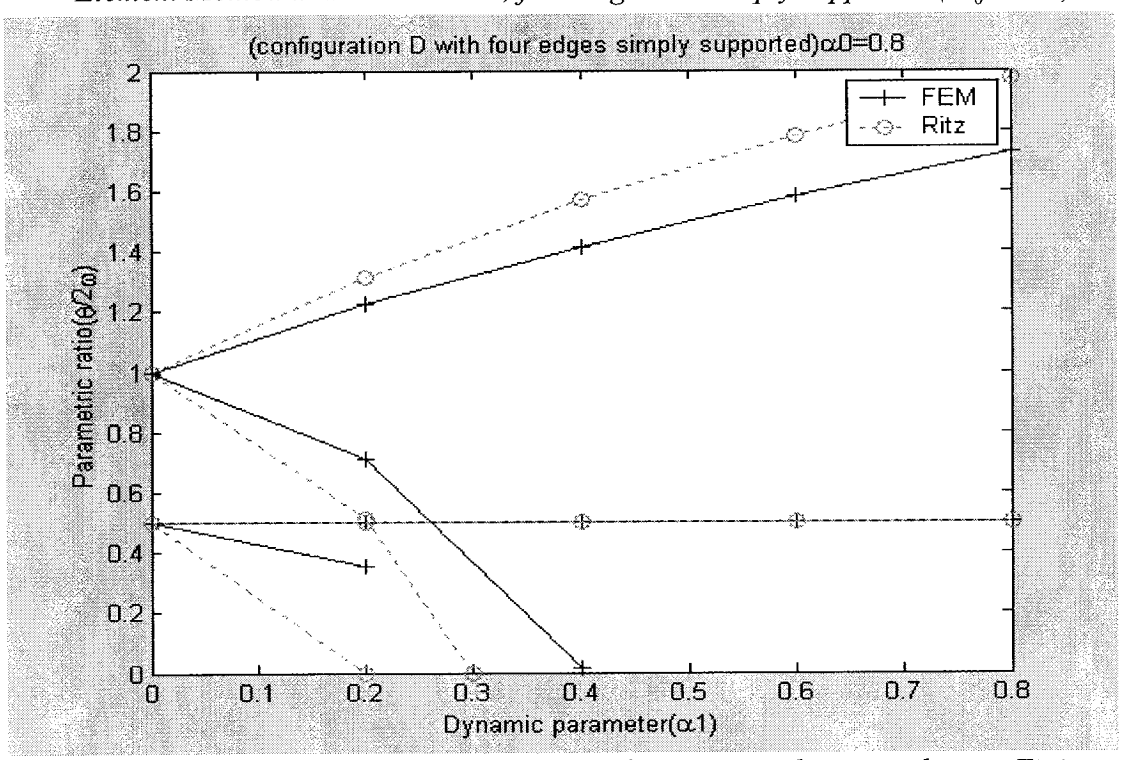

Figure 6.44 Two instability regions of taper configuration D determined using Finite Element Method and Ritz Method; four edges are simply supported ($\alpha_0 = 0.8$)

In Figure 6.41, the graphs show that the natural frequencies decrease as the static buckling loads increase. The variations of natural frequencies of the tapered composite plate configuration D obtained using Finite Element Method and Ritz Method have almost the same form.

From Figures 6.42, 6.43, and 6.44, we can see the two instability regions with different static parameters corresponding to $\alpha_0 = 0.2, \alpha_0 = 0.5$, and $\alpha_0 = 0.8$. The graphs show that the widths of the instability regions increase with an increase in both the static and dynamic loads. The instability regions for tapered composite plate configuration D obtained using Finite Element Method have more difference with that obtained using Ritz Method when the static parameters have large values.

Next, considering the boundary condition of four edges clamped, the variation of the natural frequency with the static buckling load and the two instability regions ($\alpha_0 = 0.2, \alpha_0 = 0.5$, and $\alpha_0 = 0.8$) of the tapered composite plate configuration D are determined and shown in the Figures 6.45-6.48.

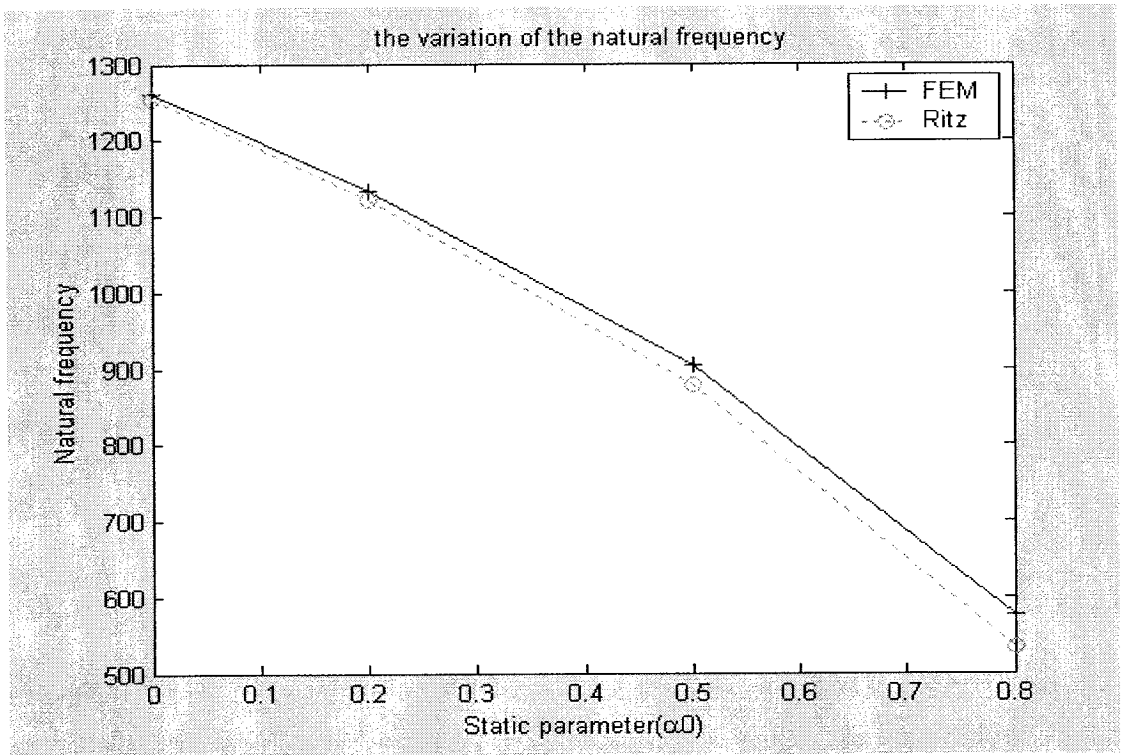

Figure 6.45 The variation of the natural frequency of taper configuration D with the static buckling load; four edges are clamped

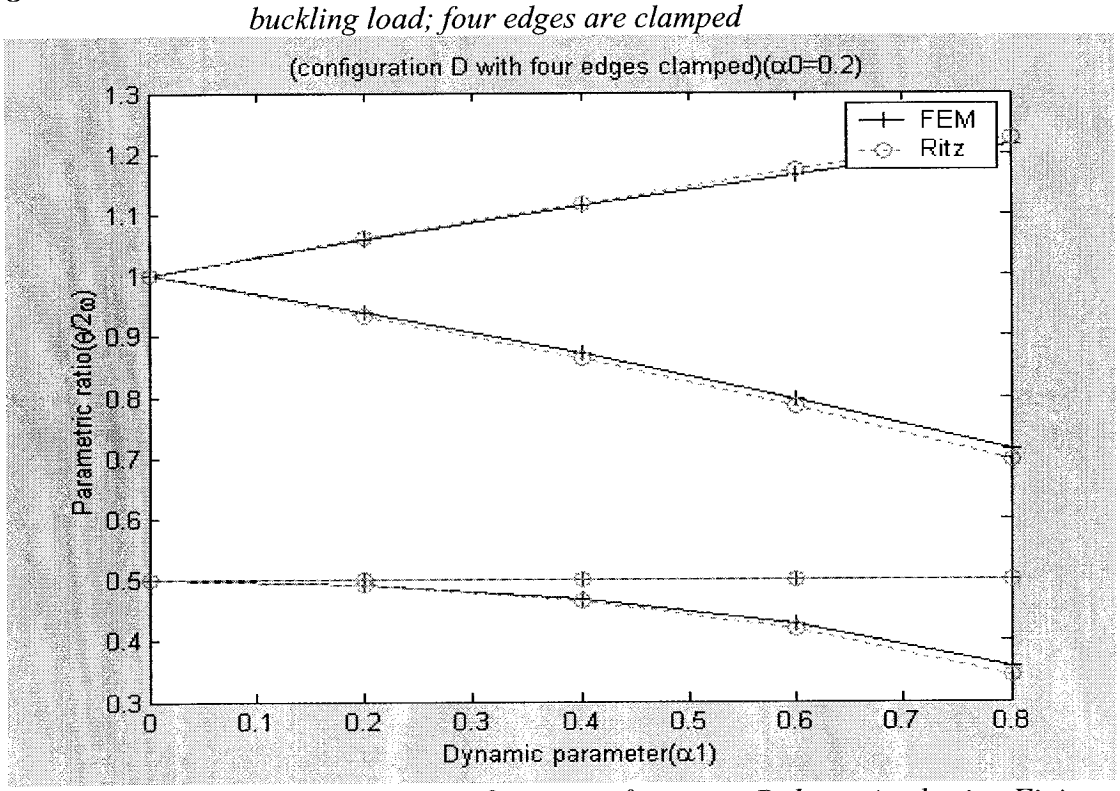

Figure 6.46 Two instability regions of taper configuration D determined using Finite Element Method and Ritz Method; four edges are clamped ($\alpha_0 = 0.2$)

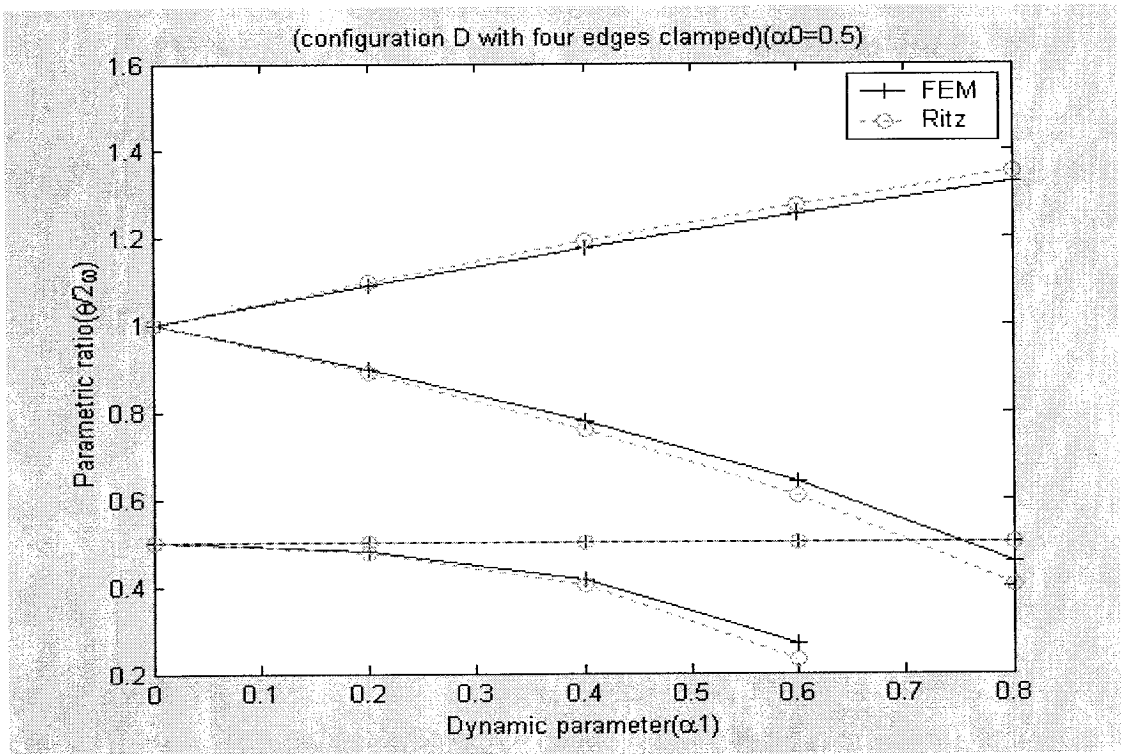

Figure 6.47 Two instability regions of taper configuration D determined using Finite Element Method and Ritz Method; four edges are clamped ($\alpha_0 = 0.5$)

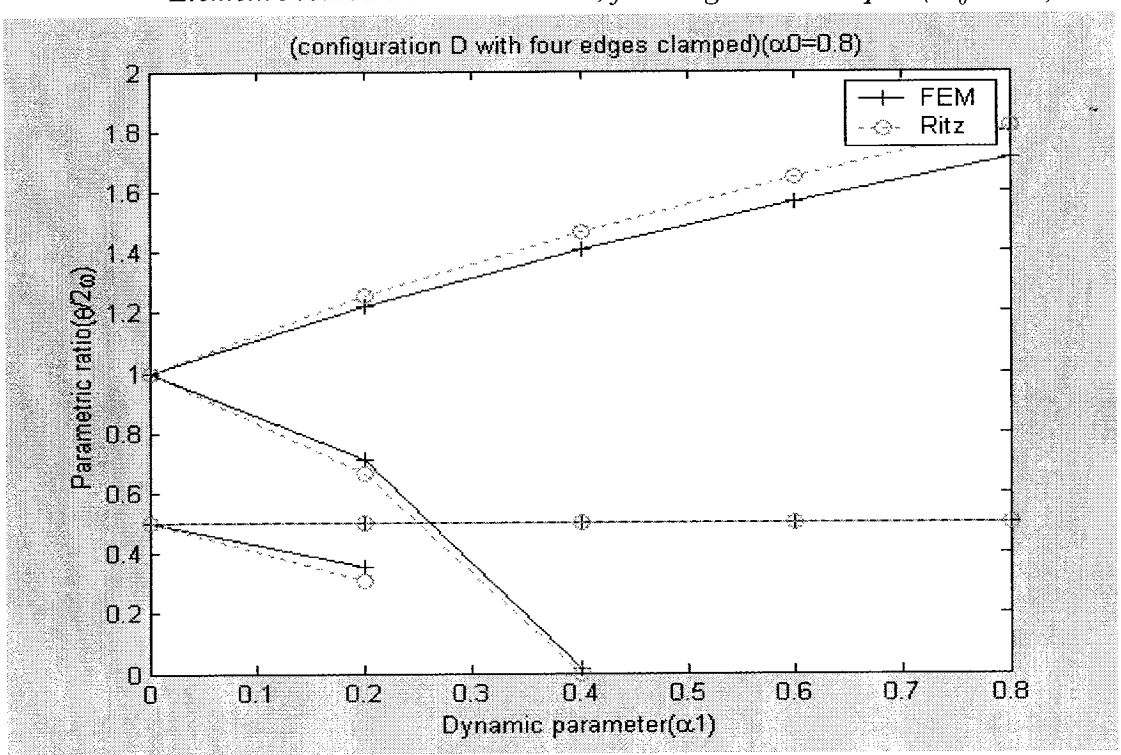

Figure 6.48 Two instability regions of taper configuration D determined using Finite Element Method and Ritz Method; four edges are clamped ($\alpha_0 = 0.8$)

In Figure 6.45, the graphs show that the natural frequencies decrease as the static buckling loads increase. The variations of natural frequencies of the tapered composite plate configuration D obtained using Finite Element Method and Ritz Method have almost the same form.

From Figures 6.46, 6.47, and 6.48, we can see the two instability regions with different static parameters corresponding to $\alpha_0 = 0.2, \alpha_0 = 0.5$, and $\alpha_0 = 0.8$. The graphs show that the widths of the instability regions increase with an increase in both the static and dynamic loads. The instability regions for tapered composite plate configuration D obtained using Finite Element Method are much close to that obtained using Ritz Method.

Finally, considering the boundary condition of one edge clamped and other three edges free, the variation of the natural frequency with the static buckling load and the two instability regions ($\alpha_0 = 0.2, \alpha_0 = 0.5$, and $\alpha_0 = 0.8$) of the tapered composite plate configuration D are determined and shown in the Figures 6.49-6.52.

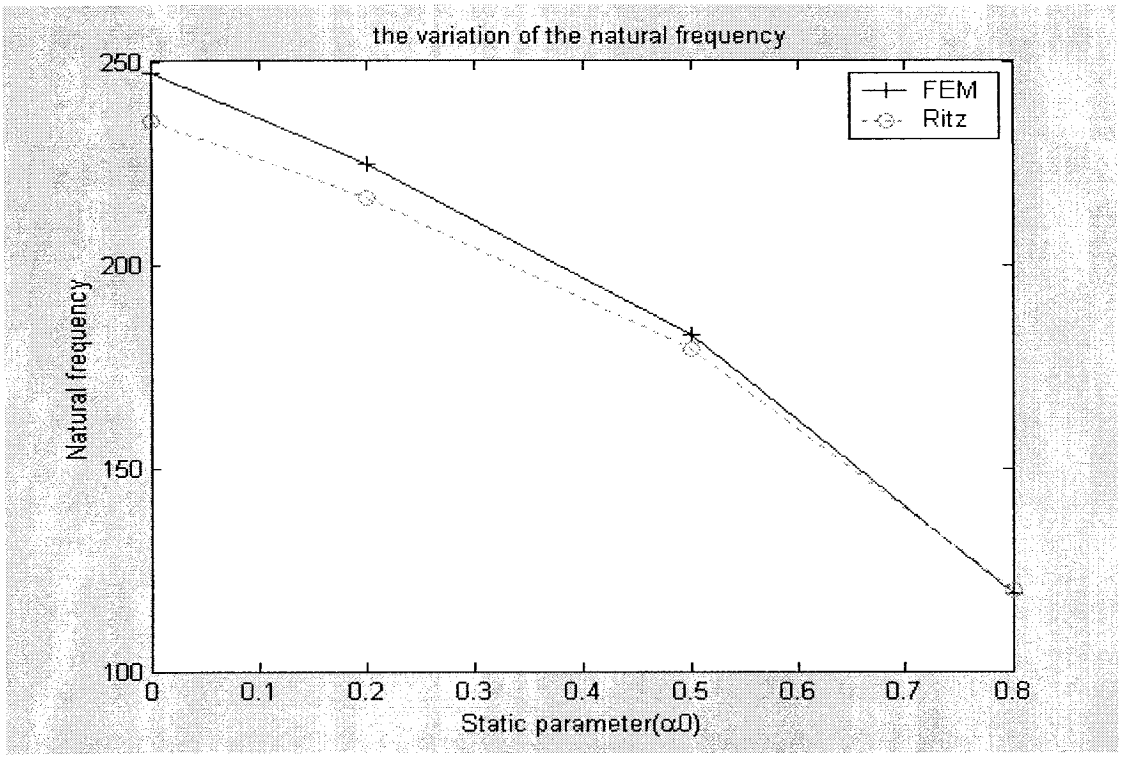

Figure 6.49 The variation of the natural frequency of taper configuration D with the static buckling load; one edge is clamped and other three edges are free

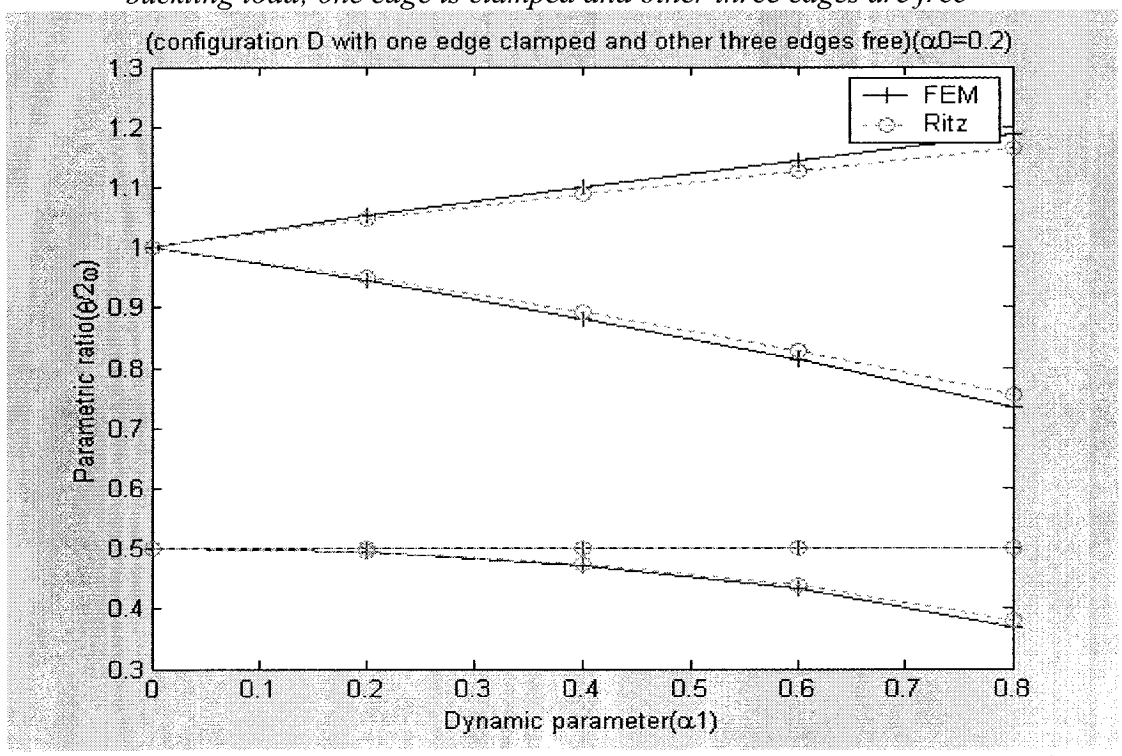

Figure 6.50 Two instability regions of taper configuration D determined using Finite Element Method and Ritz Method; one edge is clamped and other three edges are free ($\alpha_0 = 0.2$)

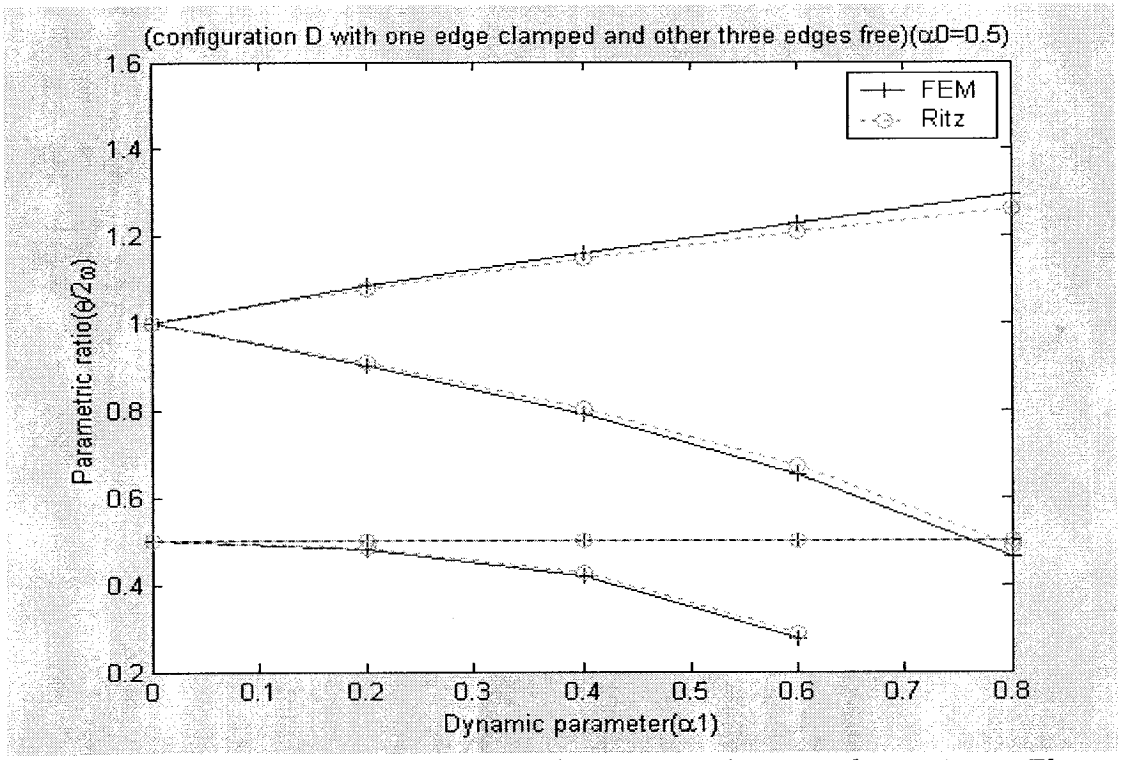

Figure 6.51 Two instability regions of taper configuration D determined using Finite Element Method and Ritz Method; one edge is clamped and other three edges are free ($\alpha_0 = 0.5$)

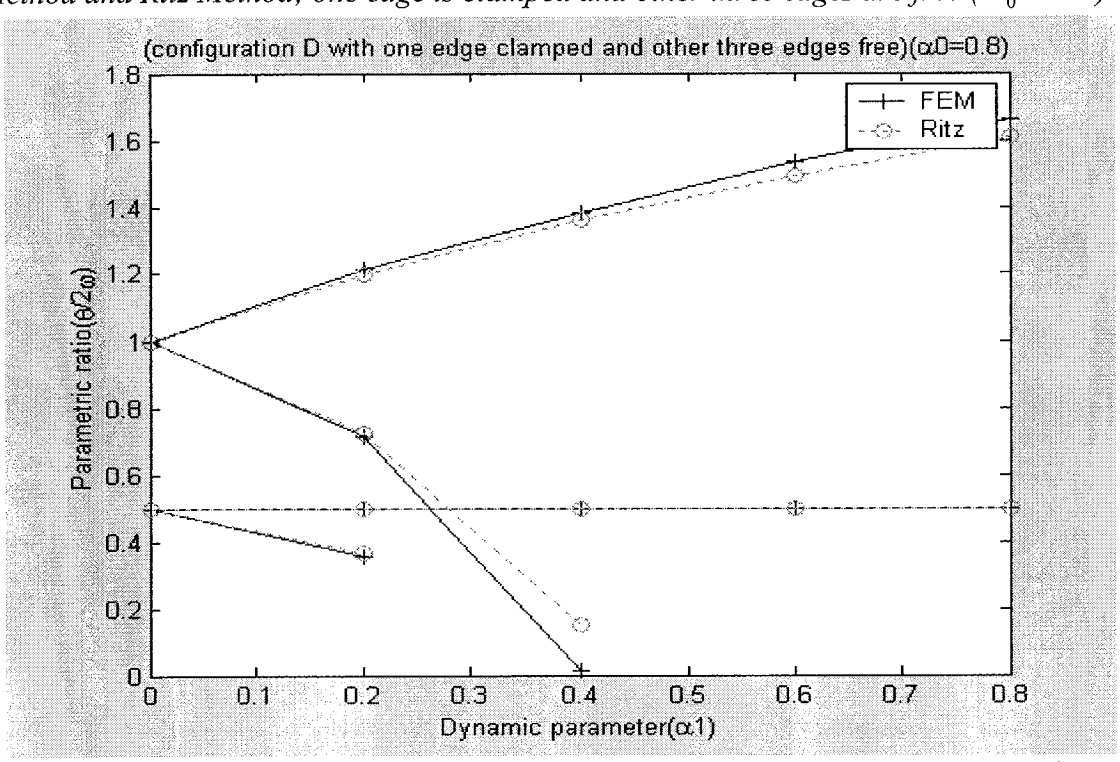

Figure 6.52 Two instability regions of taper configuration D determined using Finite Element Method and Ritz Method; one edge is clamped and other three edges are free ($\alpha_0 = 0.8$)

In Figure 6.49, the graphs show that the natural frequencies decrease as the static buckling loads increase. The variations of natural frequencies of the tapered composite plate configuration D obtained using Finite Element Method and Ritz Method have much close form.

From Figures 6.50, 6.51, and 6.52, we can see the two instability regions with different static parameters corresponding to $\alpha_0 = 0.2, \alpha_0 = 0.5$, and $\alpha_0 = 0.8$. The graphs show that the widths of the instability regions increase with an increase in both the static and dynamic loads. The instability regions for tapered composite plate configuration D obtained using Finite Element Method are very close to that obtained using Ritz Method.

5. The analysis of two instability regions of different tapered composite plate configurations.

By using the results for the instability regions of four tapered composite configurations calculated using Finite Element Method, we compare the two instability regions of the four taper configurations that have three boundary conditions corresponding to four edges simply supported, four edges clamped, and one edge clamped and other three edges free. The static parameter α_0 is 0.2.

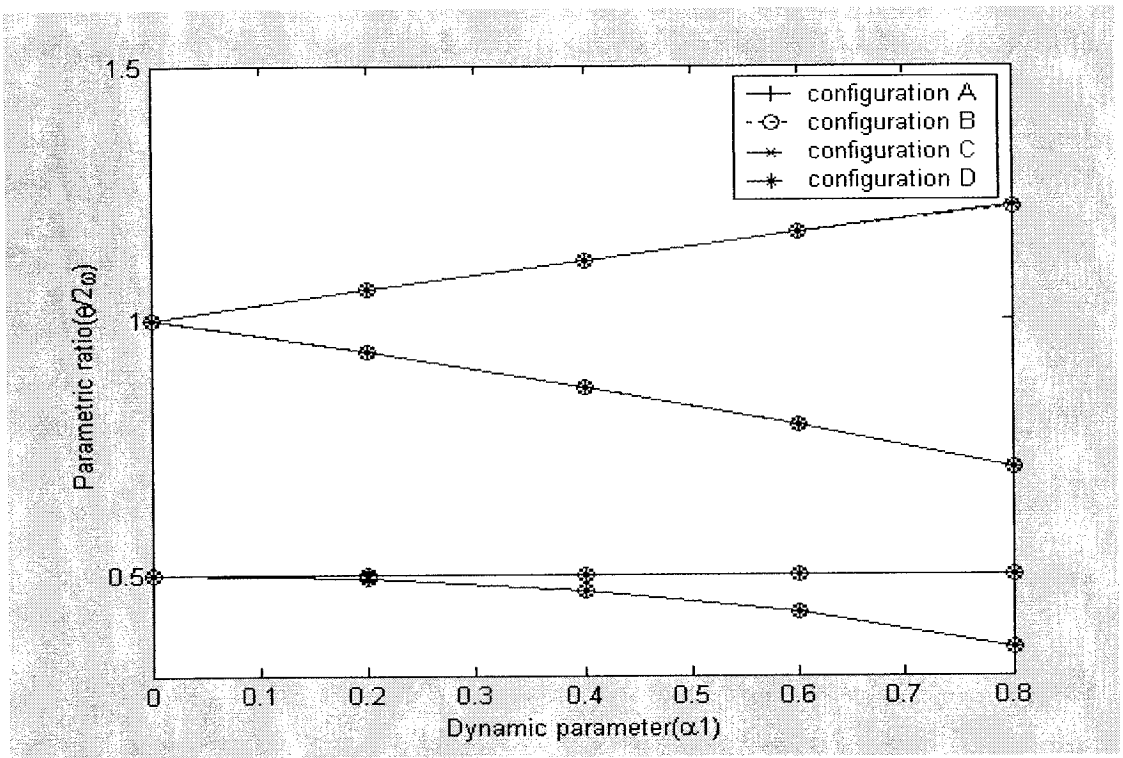

Figure 6.53 Two instability regions of the four tapered composite plate configurations with four edges simply supported determined using Finite Element Method; $\alpha_0 = 0.2$

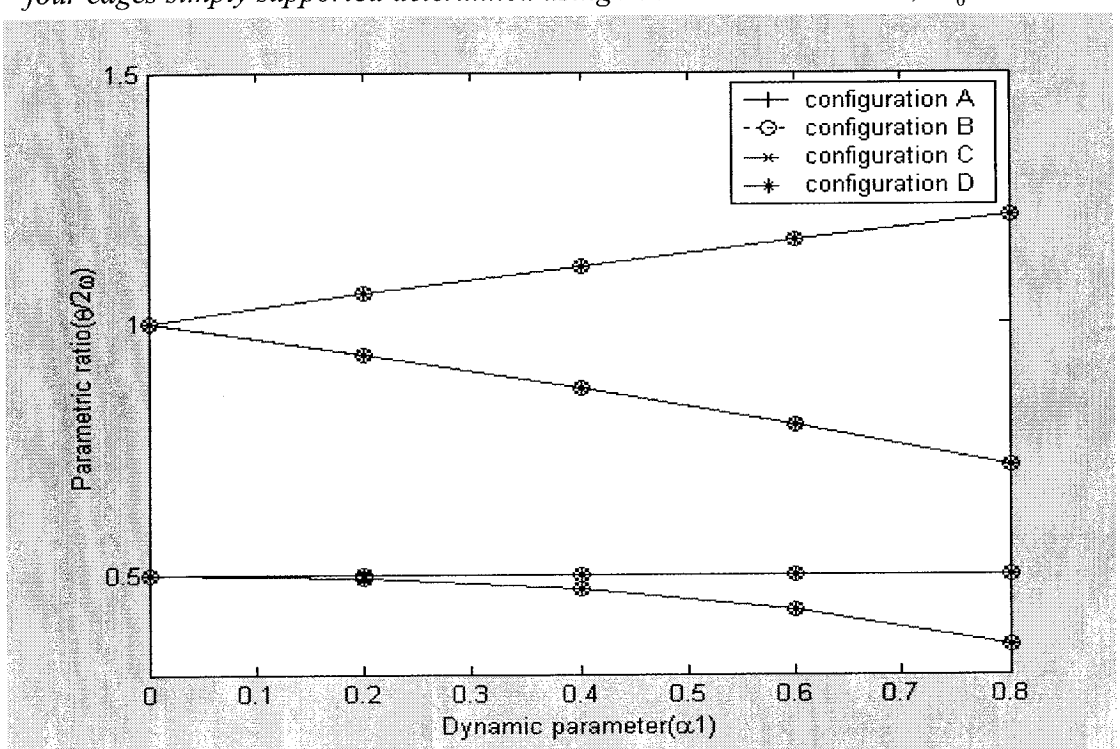

Figure 6.54 Two instability regions of the four tapered composite plate configurations with four edges clamped determined using Finite Element Method; $\alpha_0 = 0.2$

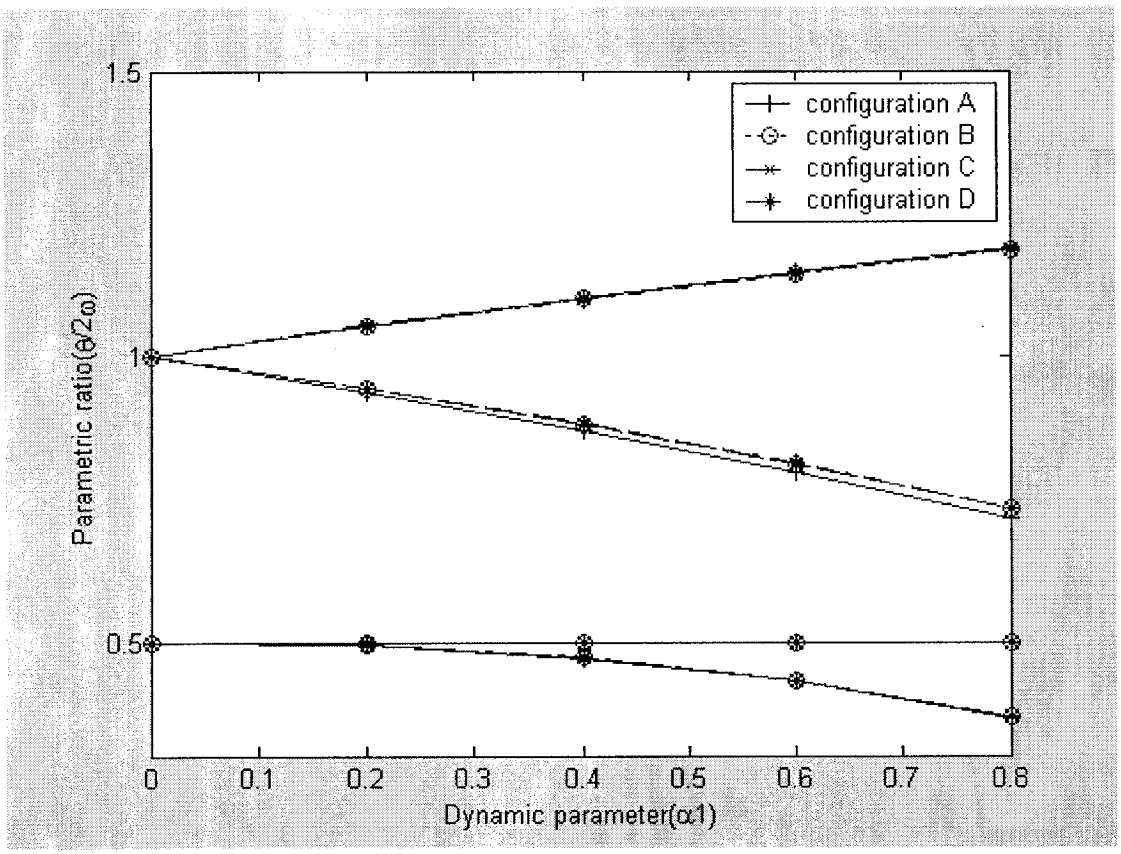

Figure 6.55 Two instability regions of the four tapered composite plate configurations with one edge clamped and other three edges free determined using Finite Element Method; $\alpha_0 = 0.2$

In Figure 6.53, the graphs show that the two instability regions of the four tapered composite plate configurations A, B, C, and D with four edges simply supported are almost the same. Therefore, there is not too much difference in the instability regions of the four different tapered composite plate configurations.

Similarly, in Figure 6.54, the graphs show that the two instability regions of the four tapered composite plate configurations A, B, C, and D with four edges clamped are

almost the same. So, with the change of the taper configuration, the instability regions do not change too much.

In Figure 6.55, the instability regions of the four tapered composite plate configurations A, B, C, and D with one edge clamped and other three edges free are shown. Configurations B, C, and D have instability regions that are too close, and configuration A has a wider region than the other three configurations due to the large resin content (at a single location) in configuration A.

6.5 Conclusion

In this chapter, the uniform composite plate configuration and tapered composite plate configurations are considered. By using the results given in Chapter 2, Chapter 3, Chapter 4 and Chapter 5, we have calculated the instability regions for uniform plate configuration and tapered plate configurations using Finite Element Method and Ritz method. For the uniform composite plate configuration, we have chosen the plate configuration according to the uniform configuration considered in ref. [12]. By comparing our results of instability region with the results given in ref. [12], we observe that much closer results have been obtained in the present work. For the tapered composite plate configurations, the Finite Element Method and Ritz Method are used to calculate the 1^{st} instability region and 2^{nd} instability region. The calculation shows that the two methods yield results that are very close. The calculation results of this chapter

and that of the last two chapters provide an accurate prediction of the dynamic instability regions for tapered composite plate configurations.

Chapter 7

Conclusions and future work

In the present thesis, the finite element method and Ritz method have been used for vibration, buckling and instability analyses of uniform and tapered composite plates with and without in-plane forces. The effects on the laminate stiffness of the composite plates caused by the taper angle have been considered. Different configurations of tapered plates, Configurations A, B, C, and D, have been investigated. The study of the vibration, buckling and instability has been developed based on classical laminated plate theory.

The taper angle of composite plate changes not only the geometric properties but also the stiffness of the oblique plies. Consequently, the mechanical behavior of tapered composite plate differs from that of uniform plate. The effect on the ply stiffness can be small if the taper angle is very small. When the taper angle of the plate increases, this influence is not negligible.

Considering the effect of taper angle, the constitutive equations of motion of

tapered composite plate with and without in-plane forces have been derived. Then, based on these differential equations, the Finite Element Method and Ritz method have been applied considering four tapered composite plate configurations. Thereafter, the vibration, buckling and instability analyses are conducted using theses two methods.

The finite element model for the plate structure considers element with four nodes and three degrees of freedom per node, so as to satisfy the geometric boundary conditions. It was shown that this kind of finite element model for plates based on classical laminated plate theory is easy to use for calculation, and the results are accurate especially for the thin uniform and tapered composite plate configurations.

The Ritz method used in the thesis is based on classical laminated plate theory, and the different shape functions of the plates corresponding to different boundary conditions are used in the calculation. The accurate results of vibration, buckling and instability analysis are obtained using Ritz method. Hereafter, the results have been compared with that of finite element method, and the results are much closer. It may be noted that the accuracy of the Ritz method depends on: 1. the chosen approximate functions for deflections and their suitability for specific boundary conditions, and 2. the number of terms used. On the other hand, the finite element solution does not suffer from this limitation. Therefore, the finite element solution would be more accurate.

For the calculation program, symbolic and numerical computations have been done using MATLAB® software. At the end of each formulation of vibration, buckling

and instability analyses, appropriate problems have been solved and the results are validated with the solutions given in some references if available. In the analysis of vibration, buckling and instability, comparisons between the results obtained using Ritz method and finite element method have been achieved in all the problems.

The parametric study is carried out for the tapered composite plates with and without in-plane forces to see the effects of various changes in the laminate parameters on the vibration, buckling and instability of the laminates. These changes include the change in the boundary conditions, and the change in the laminate configuration for the tapered composite plates. For the instability analysis, the static in-plane forces and the dynamic in-plane forces are all changed for obtaining different instability regions. The work done in the present thesis has provided some conclusions on the results obtained using the finite element method and the Ritz method, and the design of the tapered composite plates. The important and principal conclusions are:

- The accuracy can be obtained more efficiently and rapidly by increasing the number of the elements of the finite element mesh based on CLPT, and the results for thin laminates will be much closer to that of finite element method based on FSDT and HOT given in the ref. [12].
- The natural frequencies and the critical buckling loads determined using the current approach for the uniform composite plates are in good agreement with that obtained in ref. [12]. For tapered composite plate configurations, excellent correlation is observed between the natural frequencies and critical

buckling loads calculated using finite element method and the corresponding results obtained using Ritz method.

- The finite element solution based on CLPT predicts results for the natural frequencies and the critical buckling loads that are much closer to that given in ref. [12] for two types of boundary conditions. The deviations increase with plate thickness due to increased transverse shear effects.
- The width of the instability region of the uniform and tapered composite plate configurations increases with an increase in both, static and dynamic loads, as expected. Deviations also increase with plate thickness.
- Among the tapered plates designed using Configurations A, B, C and D, Configuration D is the least-stiff configuration and Configuration C is the stiffest configuration. This is because the kept and dropped plies are same and the dropped resin pockets in Configuration C are closer to the mid-plane whereas in Configuration D they are farthest from mid-plane. As for the instability regions of the four configurations, the differences among them are much smaller.

The study on the instability of the tapered composite plate with and without in-plane forces can be continued in the future based on the following recommendations:

1. The finite element method and Ritz method presented in this thesis can be extended for the analysis of the instability of different types of tapered composite plate structures based on SDPT and HOT.

2. The effect of damping can be considered in the analysis of vibrations and instability of tapered composite plate configurations.
3. The study in this thesis can be applied to design optimization of tapered composite plate configurations.
4. The effects of random material properties and loading can be included in the dynamic instability analysis.

References

[1] Bolotin, V. V., *The Dynamic Stability of Elastic Systems*, 1964, Holden-Day, INC., San Francisco, London, Amsterdam.

[2] Hutt, J. M. and Salam, A. E., "Dynamic stability of plates by finite elements", *Journal of Engineering Mechanics*, Div. 97, 1971, pp. 879-899.

[3] Krajcinovic, D. and Herrmann, G., "Numerical solutions of the dynamic stability problem", *International Journal of Numerical Methods in Engineering*, Vol. 2, 1970, pp. 551-561.

[4] Duffield, R. C. and Willems, N., "Parametric resonance of stiffened rectangular plates", *Journal of Applied Mechanics*, Vol. 39, 1972, pp. 217-226.

[5] Duffield, R. C. and Willems, N., "Parametric resonance of skew stiffened rectangular plates", *Journal of Applied Mechanics*, Vol. 40, 1973, pp. 439-444.

[6] Tani, J. and Nakamura, T., "Dynamic stability of annular plates under periodic radial loads", *The Journal of the Acoustical Society of America*, Vol. 64, 1978, pp. 827-831.

[7] Birman, V., "Dynamic stability of unsymmetrically rectangular laminated plates", *Mechanics Research Communications*, Vol. 12, 1985, pp. 81-86.

[8] Srinivasan, R. S. and Chellapandi, P., "Dynamic stability of rectangular laminated composite plates", *Computers and Structures*, Vol. 24, 1986, pp. 233-238.

[9] Bert, C. W. and Birman, V., "Dynamic stability of shear deformable anti-symmetric angle-ply plates", *International Journal of Solids and Structures*, Vol.

23, 1987, pp.1053-1061.

[10] Chen, L. W. and Yang, J. Y., "Dynamic stability of laminated composite plates by the finite element method", *Computers and Structures*, Vol. 36, 1990, pp. 845-851.

[11] Moorthy, J., Reddy, J. N., and Plaut, R.H., "Parametric instability of laminated composite plates with transverse shear deformation", *International Journal of Solids and Structures*, Vol. 26, 1990, pp. 801-811.

[12] Aditi, C. and Adrian, G., "Dynamic instability of composite laminates using higher order theory", *Computers and Structures*, Vol. 77, 2000, pp. 453-460.

[13] Wang, S. and Dawe, D. J., "Dynamic instability of composite laminated rectangular plates and primatic structures", *Computer Methods in Applied Mechanics and Engineering*, Vol. 191, 2002, pp. 1791-1826.

[14] Nigam, A. K., "Vibration Analysis of Composite Beams using Hierarchical Finite Element Method", *M.A.Sc. Thesis*, 2002, Concordia University.

[15] Zabihollah, A., "Vibration and Buckling Analysis of Tapered Composite Beams Using Conventional and Advanced Finite Element Formulations", *M.A.Sc. Thesis*, 2003, Concordia University.

[16] Chen L., "Free Vibration Analysis of Tapered Composite Beams Using Hierarchical Finite Element Method", *M.A.Sc. Thesis*, 2004, Concordia University.

[17] Reddy, J.N., *Mechanics of Laminated Composite Plates – Theory and Analysis*, 1997, CRC Press, U.S.A.

[18] Whitney, J. M., *Structural Analysis of Laminated Anisotropic Plates*, 1987, Technomic Publishing Company, Lancaster, Pa.

[19] Noor, A. K., "Free Vibration of Multilayered Composite Plates", *AIAA Journal*, Vol. 11, 1973, pp. 1038-1039.

[20] Khedeir, A. A. and Reddy, J. N., "Free Vibration of Cross-ply Laminated Beams with Arbitrary Boundary Conditions", *International Journal of Engineering Science*, Vol. 32 (12), 1994, pp. 1971-1980.

[21] Khedeir, A. A. and Reddy, J. N., "Buckling and Vibration of Laminated Composite Plates using Various Plate Theories", *AIAA Journal*, Vol. 27, 1989, pp. 1808-1817.

[22] Bertholet, J. M., *Composite Materials – Mechanical Behavior and Structural Analysis*, 1999, Springer Verlag, New York.

[23] Kollar, L. P. and Springer, G. S., *Mechanics of Composite Structures*, 2003, Cambridge University Press, Cambridge.

[24]Reddy, J.N., *An Introduction to the Finite Element Method*, 1993, McGraw-Hill, New York.

[25] Zienkiewicz, O. C., *The Finite Element Method*, 2000, Oxford, Boston: Butterworth-Heinemann.

[26] Cook, R.D., Malkus, D. S. and Plesha, M. E., *Concepts and Applications of Finite Element Analysis*, 2002, Wiley Publishing Company, New York.

[27] Nickel, R. and Secor, G., "Convergence of Consistently Derived Timoshenko Beam Finite Elements", *International Journal of Numerical Methods in Engineering*, Vol. 5, 1972, pp. 243-253.

[28] Dawe, D. J., "A Finite Element for the Vibration Analysis of Timoshenko

Beams", *Journal of Sound and Vibration*, Vol.60 (1), 1978, pp. 11-20.

[29] To, C. W. S., "Higher Order Tapered Beam Finite Element for Vibration Analysis", *Journal of Sound and Vibration*, Vol. 63 (1), 1979, pp. 33-50.

[30] Thomas, J. L. and Dokumaci, E., "Improved Finite Element for Vibration Analysis of Tapered Beams", *Aeronautical Quarterly*, Vol. 24, 1973, pp. 39-46.

[31] Thomas, J. and Abbas, A. H., "Finite Element Model for Dynamic Analysis of Timoshenko Beam", *Journal of Sound and Vibration*, Vol. 41 (3), 1975, pp. 291-299.

[32] Cleghorn, W. L. and Tabarrok, B., "Finite Element Formulation of a Tapered Timoshenko Beam for Free Vibration Analysis", *Journal of Sound and Vibration*, Vol.152 (3), 1997, pp. 461-470.

[33] Shi, G., Lam, K. Y. and Tay, T. E., "On Efficient Finite Element Modeling of Composite Beams and Plates Using Higher Order Theories and an Accurate Composite Beam Element", *Composite Structures,* Vol. 41(2), 1998, pp. 159-165.

[34] Ramtekkar, G. S., Desai, Y. M., and Shah, A. H., "Natural Vibration of Laminated Composite Beams by using Mixed Finite Element Modeling", *Journal of Sound and Vibration*, Vol. 257(4), 2002,pp. 635-651.

[35] Rao, S. R., and Ganesan, N., "Dynamic Response of Tapered Composite Beams Using Higher Order Shear Deformation Theory", *Journal of Sound and Vibration*, Vol.187 (5), 1995, pp. 737-756.

[36] Hyer, M.W., *Stress analysis of fiber-reinforced composite materials*, 1998, WCB McGraw-Hill, Boston.

[37] Yang, T. Y., *Finite Element Structural Analysis*, 1986, Prentice-Hall, Inc.

Englewood Cliffs, N.J.

[38] Reddy, J. N., *Mechanics of laminated composite plates and shells: theory and analysis*, 2004, CRC Press, Boca Raton, FL ; London.

[39] Chen, T. Y. and Chen, B. Z., *Marine Structural Mechanics*, 1984, Defense Industry Press, China

[40] Szilard, R., *Theory and Analysis of Plates*, 1974, Prentice-Hall, Inc., Englewood Cliffs, N.J.

Appendix

Derivation of equation for the boundaries of instability region [1]

The governing equation of the plate is obtained in matrix form as follows:

$$[M]\{\ddot{Q}\}+[K]\{Q\}-F_x[N]\{Q\}=\{0\} \tag{A.1}$$

where

$\{Q\}$ is the vector of nodal displacements of the structural system,

$[K]$ is the stiffness matrix of the structural system,

$[M]$ is the mass matrix of the structural system,

$[N]$ is the incremental stiffness matrix of the structural system, and

F_x is the in-plane dynamic buckling loading

F_x can be expressed in terms of the critical buckling load N_{xcr} as the following form:

$$F_x=\alpha_0 N_{xcr}+\alpha_1 N_{xcr}\cos(\theta t) \tag{A.2}$$

where

α_0 is the static parameter,

α_1 is the dynamic parameter,

θ is the parametric resonance frequency, and

$\theta / 2\omega$ is the parametric ratio

By substituting the dynamic buckling load (A.2) into the governing equation (A.1), the differential equation system of the structural instability can be written as follow:

$$[M]\cdot\{\ddot{Q}\}+([K]-(\alpha_0+\alpha_1\cdot\cos\theta t)\cdot N_{xcr}\cdot[N])\cdot\{Q\}=\{0\} \tag{A.3}$$

This Mathieu type equation (A.3) describes the instability behavior of the plate subjected to an in–plane loading which includes static and dynamic components. By solving the generalized eigenvalue problem of this equation, the instability regions can be determined from the boundaries of the stability.

To find conditions for the existence of periodic solutions with period $2T$, we seek the solutions of the governing equation in the form of a series [1]:

$$\{Q(t)\}=\sum_{k=1,3,5}^{\infty}(\{a_k\}\cdot\sin\frac{k\theta t}{2}+\{b_k\}\cdot\cos\frac{k\theta t}{2}) \tag{A.4}$$

Similarly, to find conditions for the existence of periodic solutions with period T, we seek the solutions of the governing equation in the form of a series [1]:

$$\{Q(t)\} = \frac{1}{2}\{b_0\} + \sum_{k=2,4,6}^{\infty} (\{a_k\} \cdot \sin\frac{k\theta t}{2} + \{b_k\} \cdot \cos\frac{k\theta t}{2}) \tag{A.5}$$

Therefore, we consider 3-term boundaries of instability regions.

1. The first instability region boundary, $k = 5$

The equation (A.4) can be reduced to the following form:

$$Q(t) = \{a_1\}\sin\frac{\theta t}{2} + \{b_1\}\cos\frac{\theta t}{2} + \{a_3\}\sin\frac{3\theta t}{2} + \{b_3\}\cos\frac{3\theta t}{2} + \{a_5\}\sin\frac{5\theta t}{2} + \{b_5\}\cos\frac{5\theta t}{2} \tag{A.6}$$

Hereafter, we can obtain the following equation:

$$\begin{aligned}\ddot{Q}(t) = &-\frac{\theta^2}{4}\{a_1\}\sin\frac{\theta t}{2} - \frac{\theta^2}{4}\{b_1\}\cos\frac{\theta t}{2} - \frac{9\theta^2}{4}\{a_3\}\sin\frac{3\theta t}{2} - \frac{9\theta^2}{4}\{b_3\}\cos\frac{3\theta t}{2} \\ &- \frac{25\theta^2}{4}\{a_5\}\sin\frac{5\theta t}{2} - \frac{25\theta^2}{4}\{b_5\}\cos\frac{5\theta t}{2}\end{aligned} \tag{A.7}$$

By substituting the equations (A.6) and (A.7) into the governing equation (A.3), the differential equation system of the structural instability can be written as follow:

$$\begin{aligned}&[M]\cdot[-\frac{\theta^2}{4}\{a_1\}\sin\frac{\theta t}{2} - \frac{\theta^2}{4}\{b_1\}\cos\frac{\theta t}{2} - \frac{9\theta^2}{4}\{a_3\}\sin\frac{3\theta t}{2} - \frac{9\theta^2}{4}\{b_3\}\cos\frac{3\theta t}{2} \\ &- \frac{25\theta^2}{4}\{a_5\}\sin\frac{5\theta t}{2} - \frac{25\theta^2}{4}\{b_5\}\cos\frac{5\theta t}{2}] + [[K] - (\alpha_0 + \alpha_1 \cdot \cos\theta t)\cdot N_{xcr}\cdot[N]]\cdot \\ &[\{a_1\}\sin\frac{\theta t}{2} + \{b_1\}\cos\frac{\theta t}{2} + \{a_3\}\sin\frac{3\theta t}{2} + \{b_3\}\cos\frac{3\theta t}{2} + \{a_5\}\sin\frac{5\theta t}{2} + \{b_5\}\cos\frac{5\theta t}{2}] \\ &= \{0\}\end{aligned} \tag{A.8}$$

For comparing coefficients of $\sin\frac{\theta t}{2}$, $\sin\frac{3\theta t}{2}$, $\sin\frac{5\theta t}{2}$, $\cos\frac{\theta t}{2}$, $\cos\frac{3\theta t}{2}$ and $\cos\frac{5\theta t}{2}$ etc, we can use the following formulae.

$$\sin\frac{\theta t}{2}\cos\theta t = \frac{1}{2}\sin\frac{3\theta t}{2} - \frac{1}{2}\sin\frac{\theta t}{2} \tag{A.9}$$

$$\cos\frac{\theta t}{2}\cos\theta t = \frac{1}{2}\cos\frac{3\theta t}{2} + \frac{1}{2}\cos\frac{\theta t}{2} \tag{A.10}$$

$$\sin\frac{3\theta t}{2}\cos\theta t = \frac{1}{2}\sin\frac{5\theta t}{2} + \frac{1}{2}\sin\frac{\theta t}{2} \tag{A.11}$$

$$\cos\frac{3\theta t}{2}\cos\theta t = \frac{1}{2}\cos\frac{5\theta t}{2} + \frac{1}{2}\cos\frac{\theta t}{2} \tag{A.12}$$

$$\sin\frac{5\theta t}{2}\cos\theta t = \frac{1}{2}\sin\frac{7\theta t}{2} + \frac{1}{2}\sin\frac{3\theta t}{2} \tag{A.13}$$

$$\cos\frac{5\theta t}{2}\cos\theta t = \frac{1}{2}\cos\frac{7\theta t}{2} + \frac{1}{2}\cos\frac{3\theta t}{2} \tag{A.14}$$

By using equations (A.9)-(A.14) in the governing equation (A.8), we can obtain the coefficients of $\sin\frac{\theta t}{2}$, $\sin\frac{3\theta t}{2}$, $\sin\frac{5\theta t}{2}$, $\cos\frac{\theta t}{2}$, $\cos\frac{3\theta t}{2}$ and $\cos\frac{5\theta t}{2}$ respectively.

The coefficient of $\sin\frac{\theta t}{2}$ can be written as follow:

$$-\frac{\theta^2}{4}[M]\cdot\{a_1\}+([K]-\alpha_0 N_{xcr}[N])\cdot\{a_1\}+\frac{1}{2}\alpha_1 N_{xcr}[N]\cdot\{a_1\}-\frac{1}{2}\alpha_1 N_{xcr}[N]\{a_3\}$$

The coefficient of $\sin\frac{3\theta t}{2}$ can be written as follow:

$$-\frac{9\theta^2}{4}[M]\cdot\{a_3\}+([K]-\alpha_0 N_{xcr}[N])\cdot\{a_3\}-\frac{1}{2}\alpha_1 N_{xcr}[N]\cdot\{a_1\}-\frac{1}{2}\alpha_1 N_{xcr}[N]\{a_5\}$$

The coefficient of $\sin\frac{5\theta t}{2}$ can be written as follow:

$$-\frac{25\theta^2}{4}[M]\cdot\{a_5\}+([K]-\alpha_0 N_{xcr}[N])\cdot\{a_5\}-\frac{1}{2}\alpha_1 N_{xcr}[N]\cdot\{a_3\}$$

The coefficient of $\cos\frac{\theta t}{2}$ can be written as follow:

$$-\frac{\theta^2}{4}[M]\cdot\{b_1\}+([K]-\alpha_0 N_{xcr}[N])\cdot\{b_1\}-\frac{1}{2}\alpha_1 N_{xcr}[N]\cdot\{b_1\}-\frac{1}{2}\alpha_1 N_{xcr}[N]\{b_3\}$$

The coefficient of $\cos\frac{3\theta t}{2}$ can be written as follow:

$$-\frac{9\theta^2}{4}[M]\cdot\{b_3\}+([K]-\alpha_0 N_{xcr}[N])\cdot\{b_3\}-\frac{1}{2}\alpha_1 N_{xcr}[N]\cdot\{b_1\}-\frac{1}{2}\alpha_1 N_{xcr}[N]\{b_5\}$$

The coefficient of $\cos\frac{5\theta t}{2}$ can be written as follow:

$$-\frac{25\theta^2}{4}[M]\cdot\{b_5\}+([K]-\alpha_0 N_{xcr}[N])\cdot\{b_5\}-\frac{1}{2}\alpha_1 N_{xcr}[N]\cdot\{b_3\}$$

Thereafter, according to the governing equation (A.8), the following equations are obtained.

$$\begin{cases} -\frac{\theta^2}{4}[M]\cdot\{a_1\}+([K]-\alpha_0 N_{xcr}[N])\cdot\{a_1\}+\frac{1}{2}\alpha_1 N_{xcr}[N]\cdot\{a_1\}-\frac{1}{2}\alpha_1 N_{xcr}[N]\cdot\{a_3\}=\{0\} \\ -\frac{9\theta}{4}[M]\cdot\{a_3\}+([K]-\alpha_0 N_{xcr}[N])\cdot\{a_3\}-\frac{1}{2}\alpha_1 N_{xcr}[N]\cdot\{a_1\}-\frac{1}{2}\alpha_1 N_{xcr}[N]\cdot\{a_5\}=\{0\} \\ -\frac{25\theta^2}{4}[M]\cdot\{a_5\}+([K]-\alpha_0 N_{xcr}[N])\cdot\{a_5\}-\frac{1}{2}\alpha_1 N_{xcr}[N]\cdot\{a_3\}=\{0\} \end{cases}$$

(A.15)

$$\begin{cases} -\frac{\theta^2}{4}[M]\cdot\{b_1\}+([K]-\alpha_0 N_{xcr}[N])\cdot\{b_1\}-\frac{1}{2}\alpha_1 N_{xcr}[N]\cdot\{b_1\}-\frac{1}{2}\alpha_1 N_{xcr}[N]\cdot\{b_3\}=\{0\} \\ -\frac{9\theta}{4}[M]\cdot\{b_3\}+([K]-\alpha_0 N_{xcr}[N])\cdot\{b_3\}-\frac{1}{2}\alpha_1 N_{xcr}[N]\cdot\{b_1\}-\frac{1}{2}\alpha_1 N_{xcr}[N]\cdot\{b_5\}=\{0\} \\ -\frac{25\theta^2}{4}[M]\cdot\{b_5\}+([K]-\alpha_0 N_{xcr}[N])\cdot\{b_5\}-\frac{1}{2}\alpha_1 N_{xcr}[N]\cdot\{b_3\}=\{0\} \end{cases}$$

(A.16)

For nontrivial solutions, the resulting determinants must be zero. Equations (A.15) and (A.16) lead to the following generalized eigenvalue problems:

$$\begin{vmatrix} [K]-\alpha_0 N_{xcr}[N]\pm\frac{1}{2}\alpha_1 N_{xcr}[N]-\frac{1}{4}\theta^2[M] & -\frac{1}{2}\alpha_1 N_{xcr}[N] & 0 \\ -\frac{1}{2}\alpha_1 N_{xcr}[N] & [K]-\alpha_0 N_{xcr}[N]-\frac{9}{4}\theta^2[M] & -\frac{1}{2}\alpha_1 N_{xcr}[N] \\ 0 & -\frac{1}{2}\alpha_1 N_{xcr}[N] & [K]-\alpha_0 N_{xcr}[N]-\frac{25}{4}\theta^2[M] \end{vmatrix} = 0 \tag{A.17}$$

The equation (A.17) determines the two boundaries of the first region of dynamic instability of the uniform and tapered composite plate configurations corresponding to the + and – signs in the term $[K]-\alpha_0 N_{xcr}[N]\pm\frac{1}{2}\alpha_1 N_{xcr}[N]-\frac{1}{4}\theta^2[M]$.

.

2. The second instability region boundary, $k = 6$

The equation (A.5) can be reduced to the following form:

$$Q(t)=\frac{1}{2}\{b_0\}+\{a_2\}\sin\theta t+\{b_2\}\cos\theta t+\{a_4\}\sin 2\theta t+\{b_4\}\cos 2\theta t+\{a_6\}\sin 3\theta t+\{b_6\}\cos 3\theta t \tag{A.18}$$

Hereafter, we can obtain the following equation:

$$\ddot{Q}(t)=-\theta^2\cdot\{a_2\}\sin\theta t-\theta^2\cdot\{b_2\}\cos\theta t-4\theta^2\cdot\{a_4\}\sin 2\theta t-4\theta^2\cdot\{b_4\}\cos 2\theta t -9\theta^2\cdot\{a_6\}\sin 3\theta t-9\theta^2\cdot\{b_6\}\cos 3\theta t \tag{A.19}$$

By substituting the equations (A.18) and (A.19) into the governing equation (A.3), the

differential equation system of the structural instability can be written as follow:

$$[M]\cdot[-\theta^2\{a_2\}\sin\theta t-\theta^2\{b_2\}\cos\theta t-4\theta^2\{a_4\}\sin 2\theta t-4\theta^2\{b_4\}\cos 2\theta t$$
$$-9\theta^2\{a_6\}\sin 3\theta t-9\theta^2\{b_6\}\cos 3\theta t]+[[K]-(\alpha_0+\alpha_1\cdot\cos\theta t)\cdot N_{xcr}\cdot[N]]\cdot$$
$$[\frac{1}{2}\{b_0\}+\{a_2\}\sin\theta t+\{b_2\}\cos\theta t+\{a_4\}\sin 2\theta t+\{b_4\}\cos 2\theta t+\{a_6\}\sin 3\theta t+\{b_6\}\cos 3\theta t]$$
$$=\{0\} \tag{A.20}$$

For comparing coefficients of $\sin\theta t$, $\sin 2\theta t$, $\sin 3\theta t$, $\cos\theta t$, $\cos 2\theta t$ and $\cos 3\theta t$ etc, we can use the following formulae.

$$\sin\theta t\cdot\cos\theta t=\frac{1}{2}\sin 2\theta t \tag{A.21}$$

$$\cos\theta t\cdot\cos\theta t=\frac{1}{2}\cos 2\theta t+\frac{1}{2} \tag{A.22}$$

$$\sin 2\theta t\cdot\cos\theta t=\frac{1}{2}\sin 3\theta t+\frac{1}{2}\sin\theta t \tag{A.23}$$

$$\cos 2\theta t\cdot\cos\theta t=\frac{1}{2}\cos 3\theta t+\frac{1}{2}\cos\theta t \tag{A.24}$$

$$\sin 3\theta t\cdot\cos\theta t=\frac{1}{2}\sin 4\theta t+\frac{1}{2}\sin 2\theta t \tag{A.25}$$

$$\cos 3\theta t\cdot\cos\theta t=\frac{1}{2}\cos 4\theta t+\frac{1}{2}\cos 2\theta t \tag{A.26}$$

By using equations (A.21)-(A.26) in the governing equation (A.20), we can obtain the coefficients of $\sin\theta t$, $\sin 2\theta t$, $\sin 3\theta t$, $\cos\theta t$, $\cos 2\theta t$ and $\cos 3\theta t$ respectively.

The coefficient of $\sin\theta t$ can be written as follow:

$$-\theta^2[M]\cdot\{a_2\}+([K]-\alpha_0 N_{xcr}[N])\{a_2\}-\frac{1}{2}\alpha_1 N_{xcr}[N]\cdot\{a_4\}$$

The coefficient of $\sin 2\theta t$ can be written as follow:

$$-4\theta^2[M]\cdot\{a_4\}+([K]-\alpha_0 N_{xcr}[N])\{a_4\}-\frac{1}{2}\alpha_1 N_{xcr}[N]\cdot\{a_2\}-\frac{1}{2}\alpha_1 N_{xcr}[N]\cdot\{a_6\}$$

The coefficient of $\sin 3\theta t$ can be written as follow:

$$-9\theta^2[M]\cdot\{a_6\}+([K]-\alpha_0 N_{xcr}[N])\{a_6\}-\frac{1}{2}\alpha_1 N_{xcr}[N]\cdot\{a_4\}$$

The coefficient of 1 can be written as follow:

$$\frac{1}{2}([K]-\alpha_0 N_{xcr}[N])\{b_0\}-\frac{1}{2}\alpha_1 N_{xcr}[N]\cdot\{b_2\}$$

The coefficient of $\cos\theta t$ can be written as follow:

$$-\theta^2[M]\cdot\{b_2\}+([K]-\alpha_0 N_{xcr}[N])\{b_2\}-\frac{1}{2}\alpha_1 N_{xcr}[N]\cdot\{b_0\}-\frac{1}{2}\alpha_1 N_{xcr}[N]\cdot\{b_4\}$$

The coefficient of $\cos 2\theta t$ can be written as follow:

$$-4\theta^2[M]\cdot\{b_4\}+([K]-\alpha_0 N_{xcr}[N])\{b_4\}-\frac{1}{2}\alpha_1 N_{xcr}[N]\cdot\{b_2\}-\frac{1}{2}\alpha_1 N_{xcr}[N]\cdot\{b_6\}$$

The coefficient of $\cos 3\theta t$ can be written as follow:

$$-9\theta^2[M]\cdot\{b_6\}+([K]-\alpha_0 N_{xcr}[N])\{b_6\}-\frac{1}{2}\alpha_1 N_{xcr}[N]\cdot\{b_4\}$$

Thereafter, according to the governing equation (A.20), the following equations are obtained.

$$\begin{cases} [-\theta^2[M]+([K]-\alpha_0 N_{xcr}[N])]\cdot\{a_2\}-\frac{1}{2}\alpha_1 N_{xcr}[N]\cdot\{a_4\}=\{0\} \\ -\frac{1}{2}\alpha_1 N_{xcr}[N]\cdot\{a_2\}+[-4\theta^2[M]+([K]-\alpha_0 N_{xcr}[N])\cdot\{a_4\}-\frac{1}{2}\alpha_1 N_{xcr}[N]\cdot\{a_6\}=\{0\} \\ -\frac{1}{2}\alpha_1 N_{xcr}[N]\cdot\{a_4\}+[-9\theta^2[M]+([K]-\alpha_0 N_{xcr}[N])\{a_6\}=\{0\} \end{cases}$$

(A.27)

$$\begin{cases} \frac{1}{2}([K]-\alpha_0 N_{xcr}[N])\cdot\{b_0\}-\frac{1}{2}\alpha_1 N_{xcr}[N]\cdot\{b_2\}=\{0\} \\ -\frac{1}{2}\alpha_1 N_{xcr}[N]\cdot\{b_0\}+[-\theta^2[M]+([K]-\alpha_0 N_{xcr}[N])]\cdot\{b_2\}-\frac{1}{2}\alpha_1 N_{xcr}[N]\cdot\{b_4\}=\{0\} \\ -\frac{1}{2}\alpha_1 N_{xcr}[N]\cdot\{b_2\}+[-4\theta^2[M]+([K]-\alpha_0 N_{xcr}[N])]\cdot\{b_4\}-\frac{1}{2}\alpha_1 N_{xcr}[N]\cdot\{b_6\}=\{0\} \\ -\frac{1}{2}\alpha_1 N_{xcr}[N]\cdot\{b_4\}+[-9\theta^2[M]+([K]-\alpha_0 N_{xcr}[N])]\cdot\{b_6\}=\{0\} \end{cases}$$

(A.28)

For nontrivial solutions, the resulting determinants must be zero. Equations (A.27) and (A.28) lead to the following generalized eigenvalue problems:

$$\begin{vmatrix} [K]-\alpha_0 N_{xcr}[N]-\theta^2[M] & -\frac{1}{2}\alpha_1 N_{xcr}[N] & 0 \\ -\frac{1}{2}\alpha_1 N_{xcr}[N] & [K]-\alpha_0 N_{xcr}[N]-4\theta^2[M] & -\frac{1}{2}\alpha_1 N_{xcr}[N] \\ 0 & -\frac{1}{2}\alpha_1 N_{xcr}[N] & [K]-\alpha_0 N_{xcr}[N]-9\theta^2[M] \end{vmatrix} = 0$$

(A.29)

$$\begin{vmatrix} [K]-\alpha_0 N_{xcr}[N] & -\alpha_1 N_{xcr}[N] & 0 & 0 \\ -\frac{1}{2}\alpha_1 N_{xcr}[N] & [K]-\alpha_0 N_{xcr}[N]-\theta^2[M] & -\frac{1}{2}\alpha_1 N_{xcr}[N] & 0 \\ 0 & -\frac{1}{2}\alpha_1 N_{xcr}[N] & [K]-\alpha_0 N_{xcr}[N]-4\theta^2[M] & -\frac{1}{2}\alpha_1 N_{xcr}[N] \\ 0 & 0 & -\frac{1}{2}\alpha_1 N_{xcr}[N] & [K]-\alpha_0 N_{xcr}[N]-9\theta^2[M] \end{vmatrix} = 0$$

(A.30)

The equations (A.29) and (A.30) determine the two boundaries of the second region of dynamic instability of the uniform and tapered composite plate configurations.

By using similar steps as given above, we can obtain the instability regions of other terms for uniform and tapered composite plate configurations.